PETROLOGY AND GEOCHEMISTRY OF INTRA-BACK ARC BASALTS FROM THE ARGENTINE ANDES

by

ALBERTO EDGARDO SAAL

B.S. Geology, Universidad de Córdoba, Argentina
(1985)
Ph.D. Geology, Universidad de Córdoba, Argentina
(1993)

Submitted to the Department of
Earth, Atmospheric and Planetary Sciences
in Partial Fulfillment of the Requirements
for the Degree of

Master of Sciences in Geochemistry

at the
Massachusetts Institute of Technology
August 1994

Signature of Author_____
Department of Earth, Atmospheric and Planetary Sciences
August, 1994

Certified by_____
Frederick A. Frey
Thesis Supervisor

Accepted by_____
Thomas Jordan
Chairman, Departmental Committee on Graduate Students

to Eliana

PETROLOGY AND GEOCHEMISTRY OF INTRA-BACK ARC BASALTS FROM THE ARGENTINE ANDES

by Alberto Edgardo Saal

Submitted to the Department of Earth, Atmospheric and Planetary Sciences in partial fulfillment of the requirements for the degree of

Master of Sciences in Geochemistry

at the
Massachusetts Institute of Technology
August, 1994

ABSTRACT

Understanding the origin and evolution of arc magmatism is necessary to quantify the processes involved in crustal recycling, addition of mantle material to the crust and incorporation of oceanic lithosphere into the mantle at convergent plate boundaries. This dissertation adds to this understanding by investigating the major, trace element and the isotopic compositions of alkaline basalts erupted at varying distances (50-250 km), behind the Andean volcanic front between 35°-37°S. The study of these primitive alkaline basalts erupted through distinct terranes of different ages (Precambrian to late Paleozoic), provides the information necessary to evaluate the relative role of crustal contamination and varying mantle source composition in the generation of the volcanic front lavas.

The composition of the volcanic front and back-arc lavas indicates that although crustal contamination cannot be ruled out, this process does not easily account for the compositional variation in the most primitive lavas from the volcanic front and the across arc geochemical variation. In contrast, for lavas ranging in age from Pleistocene to Prehistoric, the across arc variation in major element composition and the correlation between Pb isotopic ratios and incompatible element ratios such as Ba/Nb, could be explained by decreasing the degree of melting and the flux of fluid coming from the slab, and increasing depth of magma segregation toward the back arc. Although, progressive depletion of the mantle source coupled with increasing fluid flux toward the volcanic front may have played an important role in the chemistry of lavas across the arc, this model cannot explain the variations in Nb, Zr, Ti, Y, P and Ce abundances and ratios. These geochemical characteristics could result from 1) an heterogeneous mantle source, or 2) different fluid/melt-mantle interaction across the arc.

In each of the volcanic fields behind the volcanic front, there is a temporal variation in the composition of the alkaline lavas from the Pliocene to the Prehistoric. In general, the temporal trend is defined by a transitional change from hypersthene normative lavas, with a low concentration of incompatible elements, a strong arc geochemical signature and high Sr, Pb and low Nd isotopic ratios to younger nepheline normative lavas with higher concentration of incompatible elements, a weaker arc geochemical signature, and lower Sr, Pb and higher Nd isotopic ratios. The late Pliocene-early Pleistocene temporal variation in the back arc lavas from arc geochemical signature to a weak arc geochemical signature could be related to small variations in the conditions of subduction (rate and/or angle of subduction) of the Nazca plate.

Thesis Supervisor: Dr. Frederick A. Frey
Professor of Geochemistry

TABLE OF CONTENTS

Abstract	iii
Table of Contents	iv
List of Tables	vi
List of Figures	vii
Acknowledgements	x
I. Introduction	1
II. Geologic Setting	3
1. Alkaline Magmatism Behind the Volcanic Front	5
III. Sampling	7
IV. Analytical Methods	8
V. Results	9
1. Petrography	9
2. Alteration and Crystal Sorting	12
3. Major and Compatible Trace Elements	14
4. Incompatible Trace Elements	17
5. Isotopic Composition	18
6. Variation Across the Arc	18
7. Temporal Geochemical Trend	21
VI. Discussion	23
1. The Role of Crystal Fractionation	23
2. The Hypersthene Normative Lavas	25
3. The Importance of Crustal Contamination	27
1. Nevado Group II: Different Mantle Source or Crustally Contaminated Lavas?	28
2. The Geochemical Signature of the Magmatism in the SVZ; Slab or Lower Crustal Imput?	30
4. What is the Cause of the Across Arc Geochemical Trend?	32
5. Temporal Geochemical Variations in the Alkaline Basalts	36
6. Multiple Versus Single, and Depleted Versus Enriched Mantle Source	38
1. Nevado Group I Lavas. Arc-Back Arc Transition?. Evidence for Temporal Changes in the Conditions of Melting and in the Mantle Source Composition	42

7. Changing the "Slab Component Flux" with Time 43
VII Conclusions 47
References 50

LIST OF TABLES

Table 1, Accuracy and Precision Evaluation 64

Table 2, Modal Analyses of Alkaline Basalts 65

Table 3, Alteration and Crystal Sorting 67

Table 4, Chemical Composition of the Alkaline Basalts 79

Table 5, Isotopic Composition of the Alkaline Basalts 97

Table 6, Mass Balance Calculation for the Hypersthene Normative Lavas from Buta Ranquil 98

LIST OF FIGURES

Figure 1, Tectonic Setting of Western South America 102
Figure 2, Map Showing the Outcrop of Pliocene-Quaternary and Older Units of the Patagonian Plateau Lavas in Southernmost South America 103
Figure 3, Map of the Andean Region from 35°-37° S Showing the Differents Pliocene-Quaternary Volcanics Fields 104
Figure 4, Main Cratonic and Allochtonous Terranes of Southern South America 105
Figure 5, Geology of the San Rafael Block 106
Figure 6, Geology of the Nevado Volcanic Field Western Sector 107
Figure 7, Geology of The Los Volcanes, Llancanelo and Buta Ranquil Volcanic Fields 108
Figure 8, Olivine Modal Proportion vs. Ni and MgO contents 109
Figure 9, Plagioclase and Clinopyroxene Modal Proportion vs. Al_2O_3/CaO and Sr 110
Figure 10, Compositional Variation between Flow, Bomb and Pyroclastic Material 111
Figure 11, SiO_2 vs K_2O Diagram for the Alkaline Basalts 112
Figure 12, Total Alkalis vs. SiO_2 113
Figure 13, Major Element vs MgO Variation Diagram 114
Figure 14, Al2O3/CaO, Ni and Cr vs. MgO Variation Diagram 116
Figure 15, SiO_2 vs K_2O Diagram for the the Eastern Stratovolcanoes and Volcanic Front lavas 117
Figure 16, MgO, Ti, and CaO vs. V Diagram 118
Figure 17, Projection of Alkaline Basalts onto the Planes Cpx-NE-Ol and Cpx-Ol-Plag, following the Algorithms of Sack et al. (1987) 119
Figure 18, Primitive Mantle Normalized Abundance Pattern for Alkaline Basalts 121
Figure 19, Primitive Mantle Normalized Abundance Pattern for Alkaline Basalts which have Quartz Xenocryst 122
Figure 20, $^{143}Nd/^{144}Nd$ vs. $^{87}Sr/^{86}Sr$ Diagram for the Alkaline Basalts 123

Figure 21, $^{207}Pb/^{204}Pb$ and $^{208}Pb/^{204}Pb$ vs. $^{206}Pb/^{204}Pb$ Diagram for the Alkaline Basalts 124
Figure 22, $^{208}Pb/^{204}Pb$ vs. $^{207}Pb/^{204}Pb$ Diagram for the Alkaline Basalts 125
Figure 23, $^{143}Nd/^{144}Nd$ and $^{87}Sr/^{86}Sr$ vs $^{206}Pb/^{204}Pb$ Diagram for the Alkaline Basalts 126
Figure 24, Major Element vs MgO Variation Diagram, Arc Back-Arc Comparison 127
Figure 25, Cr and Ni vs. MgO and Ti and CaO vs V Diagrams, Arc Back-Arc Comparison 128
Figure 26, Incompatible Element-MgO Variation Diagram, Arc Back-Arc Comparison 129
Figure 27 a, b, c, Incompatible Trace Element vs. Ce Variation Diagram, Arc Back-Arc Comparison, Transparency Indicate Primitive Lavas (MgO>7%) 130
Figure 28 a, b, c, Trace Incompatible Element Ratios vs. Ce Variation Diagram, Arc Back-Arc Comparison 136
Figure 29 Ba/Nb vs. Ti, K/Rb vs. Rb, P/Ce vs. Ce and Ce/Y vs. Zr Variation Diagrams, Arc Back-Arc Comparison 139
Figure 30, $^{143}Nd/^{144}Nd$ vs. $^{87}Sr/^{86}Sr$ Diagram, Arc Back-Arc Comparison 140
Figure 31, $^{207}Pb/^{204}Pb$ vs. $^{206}Pb/^{204}Pb$ Diagram, Arc Back-Arc Comparison 141
Figure 32, $^{208}Pb/^{204}Pb$ vs. $^{206}Pb/^{204}Pb$ Diagram, Arc Back-Arc Comparison 142
Figure 33, $^{208}Pb/^{204}Pb$ vs. $^{207}Pb/^{204}Pb$ Diagram, Arc Back-Arc Comparison 143
Figure 34, Sr, Pb and Nd Isotopic Composition vs. Longitude 144
Figure 35, Primitive Mantle Normalized Diagram, Isotopic Composition and Temporal Variations in The Los Volcanes Area Lavas 145
Figure 36, SiO2, K, K/Ce and Rb/Sr vs $^{87}Sr/^{86}Sr$ Diagrams 146
Figure 37, Ba/Nb and Ba/Ce vs. Isotopic Composition Diagram 147
Figure 38, Temporal Compositional Variation in the Las Vacas and the Las Yeguas Cinder Cones 148

Figure 39, Primitive Mantle Normalized Diagram for Nevado Area Basalts, Temporal Variations 149
Figure 40, Primitive Mantle Normalized Diagram, Isotopic Composition and Temporal Variations in The Nevado Area Lavas 150
Figure 41, Primitive Mantle Normalized Diagram for Pleistocene Lavas in the Los Volcanes Area 151
Figure 42, Primitive Mantle Normalized Diagram, Isotopic Composition and Temporal Variations in Llancanelo Area Lavas 152
Figure 43, Primitive Mantle Normalized Diagram, Isotopic Composition and Temporal Variations in Buta Ranquil Area Lavas 153
Figure 44, Projection of Primitive Alkaline Basalts onto the Planes Ol-Qz-Jd+CaTs, following the Algorithms of Green (1970) 154
Figure 45, Mass Balance Calculation to Explain the Hypersthene Normative Basalts from Buta Ranquil as Mixture between the Ne-normative Lavas and Basaltic Andesites from Tromen Vn. 155
Figure 46, Ti/Zr vs. Nb/Y and Ce/Nb vs. Ce/Y Diagrams for Lavas with Mg# > 60, Volcanic Front-Nevado Lavas Comparison 156
Figure 47, K/Ba vs K/Nb and Ba/Nb Diagrams for Primitive Lavas (MgO > 7%), Arc Back-Arc Comparison 157
Figure 48, K/Ba and Zr/Nb versus Ti Diagrams for Primitive Lavas (MgO >7%), Arc Back-Arc Comparison 158
Figure 49, Ti/Nb and Nb/Y vs. Mg# Diagrams for Primitive Lavas (MgO >7%), Volcanic Front-Nevado Lavas Comparison 159
Figure 50, Ba/Nb vs. Nb, Zr and Ti Diagrams for Primitive Lavas (MgO >7%), Arc Back-Arc Comparison 160
Figure 51, Primitive Mantle Normalized Diagram for Nevado Group I Lavas 161
Figure 52, Ti/Nb vs. Ce/Y and Ce/Y vs. Zr Diagrams for Primitive Lavas (MgO >7%), Volcanic Front-Nevado Lavas Comparison 162
Figure 53, Volcanic Arc Melt Flux Normalized by Length Scale as a Function of the Subduction Angle and Dimensionless Percolation Velocity 163
Figure 54, Fluid and Matrix Streamlines Calculated for the Andes Subduction Zone at Latitude 36^{o} S. 164

ACKNOWLEDGEMENTS

First and foremost I gratefully acknowledge Fred Frey, not only for all the geochemistry I learned from him, which is inevitable, but also for the hope he gave me. Hope that a person can face daily life without changing his ideals, objectives and his endless good will.

I am indebted to several other excellent scientists and exceptional persons. Nobu Shimizu, Stan Hart, Tim Grove, Sam Bowring, and Peter Kelemen have enlightened me with stimulating discussion on petrology and geochemistry. I have benefited immensely from their knowledge and experience. Thanks also to Mike Rhodes for allowing access to the XRF lab (University of Massachusetts, Amherst) and to Sam Bowring for permitting the isotope analysis in his lab. Thanks to Pillalamarri Ila, for teaching me the secrets of Neutron Activation and for her friendship, to Alan Brandon, who provided a challenging perspective supporting crustal contamination and to Drew Coleman and Pete Dawson for their help in the analytical techniques.

Thanks to my dearest friends Eiichi Takazawa, Huai-Jen Yang, Tom Wagner and Glenn Gaetani, for the continuing support, their invaluable help and friendship.

I also would like to thank Carlos Rapela, and Beatriz Coira for their support, and especially Leopoldo Lopez Escobar whose unconditional help brought me to MIT. I acknowledge Daniel Delpino and Adriana Bermudez whose valuable geologic information made the geochemical interpretation possible. Thanks to Bill Shaw and Rafael Katzman for their help in the geodynamic model, and to Rosie Hegg and Cynthia Hanes for their patience and help during administrative work.

Last, but of the utmost importance, thanks to my parents, Adela and Rafael, for their love and encouragement. Finally, to Eliana, my wife and dearest friend. I am indebted to Eliana for her time, care and love during all these years, sharing our dreams and lives wherever in the world they took us.

I. INTRODUCTION

The understanding of the origin and evolution of arc magmas is a fundamental issue to solve because it will provide information about crustal recycling, addition of mantle material to the crust and incorporation of oceanic lithosphere into the mantle at a convergent plate boundary. Although understanding of arc magmatism has increased remarkably in the last decade, there is no consensus concerning the relative roles of the different magmatic sources like mantle wedge, subducted oceanic lithosphere (including basalts and the overlying sediments), and the lithosphere immediately under the arc (lithospheric mantle and crust), or the role of the various magmatic processes involved like crystal fractionation, magma and/or source mixing, assimilation and contamination. Solutions to these problems are not simple and no simple generalized model is adequate to explain the large range in major, trace elements and isotopic composition of different arc magmas.

One of the best examples of continental arc magmatism is the Andean volcanic chain, formed at the active convergent margin of the South-American continental plate and the subducting Nazca oceanic plate. In the Andes, recent volcanic activity occurs in four zones: The Northern Volcanic Zone (6^{o}N-8^{o}S); the Central Volcanic Zone (16^{o}S-28^{o}S); the Southern Volcanic Zone (33^{o}S-46^{o}S), and the Austral Volcanic Zone (49^{o}S-55^{o}S), with intervening regions characterized by volcanic quiescence (Figure 1). Jordan et al. (1983) showed that the tectonic segmentation of the Andes coincides with segmentation of the subducted Nazca plate. The Southern Volcanic Zone (SVZ) is bounded by volcanic gaps that correlate with features of the subducting slab. The northern boundary coincides with the shallow dipping of the Benioff zone and the impingement of the Juan Fernandez Ridge on the Chile trench (Barazangi and Isacks, 1976; Bevis and Isacks 1984, Kay et al. 1987). The southern gap is defined by the intersection of the active Chile rise triple junction with the Chile trench (Herron et al. 1981). Moreover, Tormey et al. (1991) based not only on geologic and geophysical data but also on different geochemical regimes divided the SVZ in three areas: the Northern SVZ (33^{o}S-34.5^{o}S); the Transitional SVZ (34.5^{o}S-37^{o}S) and the Southern SVZ (37^{o}S-42^{o}S).

The SVZ has been the subject of numerous geochemical and petrological studies of lavas erupted on or near the volcanic front (Lopez Escobar and Frey, 1976; Lopez Escobar et al., 1977, 1981; Frey et al., 1984; Hildreth et al., 1984; Hickey et al., 1986; Hildreth and Moorbath, 1988; Gerlach et al., 1988; Davidson et al., 1988; Futa and Stern, 1988; Hickey-Vargas et al. 1989; Hickey-Vargas,1992 Tormey et al., 1989, 1991, 1992; Ferguson et al., 1992; Hildreth and Drake, 1992, McMillan et al., 1989, among others).

Although, the absence of primitive basalts (Mg# $\approx$ 70) in the SVZ is a major obstacle in assessing the relative importance of mantle sources to Andean lavas, several different models have

been used to explain the geochemical characteristics of the magmatic arc in the SVZ. Hildreth and Moorbath (1988) postulated a process of mixing assimilation storage and homogenization (MASH) in the lower crust as responsible for controlling compositional variations along the SVZ. In contrast, Stern (1991b) presented a model of source-region contamination. Tormey et al. (1991) proposed that the variation along arc, principally north and south of 37°S, reflects lavas evolving dominantly by higher pressure crystallization in the northern area with accompanying contamination by a lower crust composed of a young arc derived garnet granulite. In contrast, in the southern area lavas evolved by low pressure crystallization with insignificant crustal contamination. Hickey et al. (1986), in a transect across the arc, consider that the west to east variation in the composition of the basaltic lavas was caused either by lower degree of mantle melting because of the smaller contribution of fluids from the slab or greater input from a thicker subcontinental lithosphere to the east.

Along all the SVZ (from 34° to 46° S) Quaternary volcanic activity, arc and back arc volcanism, occurs in a broad belt, 300-500 Km wide (Figure 2). It is defined in the west by the volcanic front of the Andean orogenic belt, and in the east by the alkaline basalts erupted from small, scattered and fissure-aligned cinder cones which form the Patagonian plateau lavas (Skew and Stern, 1979; Ramos et al. 1982; Rapela et al. 1988; among others).

Based on the west-to-east transition from sub-alkaline orogenic arc to alkaline back arc plateau basalts, the SVZ can be divided into two areas: 1) south of 39°S, where the volcanic front and the back arc form two spatially and compositionally different volcanic association. 2) Between 34.5°S-39°S, where no simple spatial or compositional division separates orogenic arc and back arc regions (Muñoz et al. 1987; Muñoz and Stern, 1988, 1989; Stern et al. 1990), (Figure 2). In this northern region Stern et al., (1990) found that the alkaline back arc basalts are interspersed with arc stratovolcanoes, and that they have isotopic and some trace element characteristics which are intermediate between the volcanic front lavas and the more southerly alkaline basalts which are not interspersed with arc stratovolcanoes.

In this work we focus on the alkaline basalts erupted between 35°S-37°S. The reasons for this choice are:

1) The primitive characteristic of the alkali basalts (up to 12% MgO, Ni 200 ppm, Cr 500 ppm) relative to lavas erupted on the volcanic front (Bermudez and Delpino, 1989).

2) The possibility, based on very few data, that some of the geochemical and isotopic characteristic of the relatively primitive back arc lavas are similar to lavas erupted on the volcanic front at this latitude (Muñoz and Stern, 1988, 1989; Stern et al. 1990).

3) The volcanic front at this latitude is being studied in detail (Dungan et al, (1992); Tormey et al., 1994).

4) This area includes recently erupted alkali basalts at varying distances, 300-500 km, from

the trench.

The general objective of this research is to characterize these alkaline basalts, and to compare their geochemical and petrologic characteristics with lavas erupted on the volcanic front at 35°S-37°S. A specific objective is to determine if there is a correlation between the arc geochemical signature (high abundance ratios of alkaline and alkaline earth elements relative to LREE and HFSE) and distance from the trench. Such information, along with the primitive character of the alkali basalts, and their isotopic characteristics will help in evaluating the relative role of crustal contamination and mantle source composition in the generation of the volcanic front lavas.

II. GEOLOGIC SETTING

The area studied (35°-37° S) is defined to the north by the absence of alkaline volcanism east of the volcanic front (Muñoz and Stern; 1988; Muñoz et al., 1989; Tormey et al., 1991). The southern boundary is delineated by the intersection of the projection of the Mocha Fracture Zone with the volcanic front (Swift and Carr, 1974; Herron, 1981; Hildreth and Moorbath, 1988; Tormey et al., 1991). The continental crust in this area increases in thickness from 30-35 km at 37° S to 60 km at 35° S (Hildreth and Moorbath, 1988).

In this region the Nazca plate subducts eastward with a dip of 20°-30° (Stauder, 1973; Barazangi and Isacks, 1976; Hanus and Vanek, 1978; Bevis and Isacks, 1984, Cahill and Isacks, 1992) and with a convergence rate of 9-11 cm/yr (Minster and Jordan, 1978). The age of the subducting oceanic lithosphere is about 40 My (Herron, 1981; Hildreth and Moorbath, 1988; Tormey et al., 1991). The absence of a major accretionary prism east of the trench, the position of the Quaternary volcanic front eastward of the Jurassic magmatic arc and the seaward strike of the Jurassic magmatic arc indicate sediment subduction and erosion of the over riding continental plate (Plafker, 1972; Hussong et al., 1976; Kulm et al., 1977; Scholl et al., 1977; Drake et al., 1982; Hildreth and Moorbath, 1988; Stern, 1991b; Tormey et al., 1991).

The Cenozoic magmatic arc between 35°-37° erupted mainly in four physiographic provinces: Principal Cordillera; San Rafael Block; Los Huarpes and Payenia Depressions and Alvear Sub-Basin (Figure 3). The first two areas are fault-bounded uplifted regions separated by the intervening tectonically depressed areas (Los Huarpes and Payenia).

The Alvear Sub-Basin is the eastern section of the area considered in this study. It consists of Precambrian metamorphic basement (K/Ar age of 605 My.) unconformably overlain by lower Paleozoic marine to continental sediments (Criado-Roque, 1979). During Permo-Triassic times a thick succession of felsic volcanic rocks related with the Gondwana magmatism (Choiyoi Group) was deposited in the basin. The main body of the basin contains Triassic to

Cenozoic continental sediments. The basin is bounded on the west by the San Rafael Block and Nevado fault (Bermudez & Delpino, 1989) (Figure 3). The San Rafael block shows a similar stratigraphy but the Triassic to Cenozoic continental sediments are absent (Criado Roque & Ibañez, 1979).

The Llancanelo fault defines the boundary between the San Rafael Block to the east and the Los Huarpes and Payenia Depression to the west (Polansky, 1954; Bermudez & Delpino, 1989) (Figure 3). There is no information about the basement of this depressed area.

The Principal Cordillera and Los Huarpes-Payenia depression are in contact along the Rio Grande fault (Yrigoyen, 1979) (figure 3). In the Principal Cordillera, basement older than Permian does not outcrop, the oldest rocks are the Choiyoi Group (Permo-Triassic). Mesozoic continental and marine sediments overlay the Choiyoi, and finally the Cenozoic is characterized by the volcanic and sedimentary sequence accumulated during Andean orogenesis (Drake, 1976; Yrigoyen, 1979; Lopez Escobar and Frey, 1976; Drake et al., 1982; Hildreth and Moorbath, 1988; Tormey et al., 1991). Because the Paleozoic geological features change abruptly across the Colorado river (Turner and Baldis, 1979), the basement under the Principal Cordillera and Los Huarpes-Payenia depressions cannot be inferred from areas that outcrop to the south of Colorado river (Neuquinian Basin, Northern Patagonia) (Figure 4). Apparently the Paleozoic evolution of Patagonia (territory south of Colorado river) was independent from the rest of the continent (Rapela and Kay, 1988; Ramos, 1984).

To the north, the Principal Cordillera is limited by the Frontal Cordillera, a Paleozoic to Triassic orogen where metamorphic rocks of Devonian or older age are rare (Caminos, 1979; Ramos et al., 1986). In the tectonic reconstruction of Ramos et al., 1986 and Ramos, 1988 (figure 4), the Frontal Cordillera is an allochtonous block (Chilenia terrane in Figure 4). forming the basement of the Principal Cordillera and the Los Huarpes-Payenia depression. In any case, based on the reconstruction of Ramos, (1988), this Paleozoic basement (Chilenia terrane) is different from that of the San Rafael Block and Alvear Sub-Basin of Precambrian age, which are associated with either the Precordillera displaced terrane or Pampean terrane (Figure 4).

Cenozoic Andean magmatism in this area occurred over a large region extending from 250 to 500 km from the Chile trench. The magmatism can be divided into three zones (Figures 2 and 3):

1) Volcanic Front: Late-Quaternary stratovolcanoes, simple or compound, and/or calderas built on the Principal Cordillera which have erupted subalkaline associations of basalt, andesite, dacite and in some cases rhyolites (Lopez Escobar and Frey, 1976; Lopez Escobar et al., 1977, 1981; Frey et al., 1984; Hildreth et al., 1984; Stern et al., 1984a and b; Hickey et al., 1986; Hildreth and Moorbath, 1988; Davidson et al., 1988; Stern, 1991b; Tormey et al., 1989,

1991, 1994; Ferguson et al., 1992; Hildreth and Drake, 1992, McMillan et al., 1989, among others).

2) Eastern Stratovolcanoes and Calderas, situated behind the front, erupted on Principal Cordillera (Domuyo, Tromen); on the San Rafael Block (Nevado, Pelado, Plateado) and on the intervening Los Huarpes-Payenia Depression (Payun Matrú). Previous geologic studies show that Tromen, Domuyo (both Quaternary), Pelado and Plateado (both Miocene) are mainly built of andesites of subalkaline composition similar to the volcanic front (Llambias et al., 1978; 1982; Bermudez, 1991; Bermudez and Delpino 1989). The Nevado volcano (Pliocene) consists of high K_2O calc-alkaline lavas (with a range in SiO_2 from $\approx$ 49 to $\approx$ 64 %wt) (Bermudez, 1991; Bermudez and Delpino 1989). In contrast Payun Matrú volcano, erupted in a tectonically depressed area (Payenia), is dominantly trachyte and trachyandesite of alkaline composition (Llambias, 1966). Llambias et al. (1982), considered that this variation in composition which correlates with the structural level of basement (block or depression) reflects volcanism under different tectonic conditions.

3) Alkaline basalts (Pliocene-Quaternary), which constitute large volcanic fields of cinder cones, which are scattered or aligned along fractures.

Pre-Pliocene compression may have played a significant role in creating the structure of uplifted blocks and intervening depressions that is typical for this area (Muñoz et al. 1989). The last phase of compression in the Principal Cordillera ended in the late-Miocene (Charrier and Vicent, 1972). South of 34^o there is no evidence of post-Miocene compression (Jordan et al, 1983). On the contrary, Muñoz et al. 1989, Muñoz and Stern 1989, Bermudez and Delpino 1989 consider the existence of a intra arc extensional event between 35^o and 39^o S since the early Pleistocene. In contrast, Ramos (per.com. 1993) maintains that there is no structural or geophysical evidence in favor of intra-arc extension, but that extensional fractures and transcompressional basins are the result of the subduction related east-west compression (Denwey and Lamb, 1992).

II.1. ALKALINE MAGMATISM BEHIND THE VOLCANIC FRONT

Voluminous Pliocene-Quaternary alkaline basaltic eruptions occurred in a back-arc position between the 35^o-37^o S., forming The Andino-Cuyana Volcanic Province (Bermudez & Delpino, 1987). The basalts cover an area of approximately of 13500 km^2 (Bermudez & Delpino, 1989). Based on the geologic work of Bermudez & Delpino (1987, 1989) it is possible to divide the volcanic province in four volcanic fields:

a) The Nevado volcanic field is built of more than 160 cinder cones erupted on the San Rafael Block and the western margin of Alvear Sub-Basin (Figure 5 and 6), at distances of 125

to 250 km from the volcanic front. This field includes three aligned strato volcanoes Nevado-Plateado-Pelado (Sierra del Nevado) (Bermudez, 1991). In all cases, the alkaline basalt eruptions are aligned along northwestern striking faults and/or fractures, some of these structures extend for 30 to 70 km (Figure 6).

b) The Llancanelo volcanic field consists of approximately 60 cinder cones erupted in the Los Huarpes Depression, approximately 75 to 125 km from the volcanic front (Figure 7). They are scattered or aligned along east-west fractures (Bermudez & Delpino, 1989).

c) The Los Volcanes volcanic field is the western sector of a large volcanic field that surrounds the Payun Matru caldera (Figure 7). It contains approximately 30 scattered cinder cones located at 60 to 150 km from the volcanic front in the Payenia depression. In the eastern sector (not sampled), the eruptions were controlled by east-west fractures, with characteristics of fissure-related volcanism (Bermudez & Delpino, 1989).

d) The Buta Ranquil volcanic field consists of three independent relatively small eruptive centers: Barranca volcano; Cochiquito volcano; Buta Ranquil volcano (figure 7). This field is, limited to the west by the Tromen stratovolcano, located on the eastern boundary of the Principal Cordillera at 100 km from the volcanic front.

Several types of volcanic structures exist in these volcanic fields. For example, the Nevado area includes scattered simple pyroclastic monogenetic cones, composite cones with multiple lava flows and pyroclastic layers, multiple cones extending along fractures and fissure related eruptions (Bermudez & Delpino, 1989).

The temporal order of eruptions is very difficult to assess due to the lack of geochronological dates and stratigraphic control. Nevertheless, there are some composite cones in the Nevado area, e.g., Las Vacas and Las Yeguas (figure 6), with multiple flows, that can be used to evaluate temporal variations. Also, morphology, degree of erosion of monogenetic cones, formation of soil covering the flows and the overlapping of flows from different cones are used in defining relative age.

The Nevado volcanic field is characterized by morphologically old and highly eroded cones. K/Ar ages of 1.8 My (Bermudez, 1987) and 1.7 +/- 0.4 My (Muñoz et al., 1989) agree with the geologic work of Bermudez and Delpino (1987, 1989) who divide lavas in this region into two age groups, Late Pliocene-Early Pleistocene and Pleistocene.

In contrast, the Llancanelo Volcanic Field contains uneroded cones and has relatively young K/Ar ages of 0.4 +/- 0.2 My, 0.5 +/- 0.2 My and 0 +/- 0.1 My with normal magnetic polarity (Valencio et al., 1986); thus, they are Late Pleistocene to Early Holocene in age, but in this area there are also older (Plio-Pleistocene) basalts.

On the basis of stratigraphic ages from Bermudez & Delpino (1989), and K/Ar dates ranging from 0.2 to 0.5 My with normal polarity (Valencio et al., 1986), the range of age

assigned to Los Volcanes Volcanic Field is from Early Pleistocene to Late Holocene.

Barrancas Volcano is morphologically the oldest, and most strongly eroded volcanic cone that was studied. It has a K/Ar age of 3.2+/-1 My, Pliocene, (Valencio et al., 1986). Buta Ranquil and Cochiquito are morphologically younger than Barrancas, with one K/Ar age on Buta Ranquil of 0.3 +/- 0.2, Late Pleistocene, (Valencio et al., 1986). The same age is inferred for Cochiquito (Bermudez & Delpino, 1989).

III. SAMPLING

The sampling focussed on the four Volcanic Fields of the Andino-Cuyana Volcanic Province (Bermudez & Delpino, 1989). These fields, Nevado, Llancanelo, Los Volcanes and Buta Ranquil areas are located at different distances from the volcanic front (Figure 3). They include lavas of varying age that erupted through different crustal sections. Our objective is to determine and to understand the geochemical variability within and between these fields, and to use these results to characterize the mantle wedge above the subducting Nazca plate. The samples collected also enable evaluation of the compositional variability along and between specific fractures e.g., NW-SE fractures in Nevado area versus E-W fractures in Llancanelo and Los Volcanes areas.

We sampled the Nevado volcanic field (43 samples), because it represents the most easterly volcanism erupted through the Precambrian basement during the late Pliocene-early Pleistocene and Pleistocene ages (Figures 5 and 6). Samples are from small monogenetic cinder cones, moderate size cones aligned along NW-SE fractures and from multiple flows in individual cones. The samples collected enable evaluation of compositional variability at a single cone (Las Vacas and Las Yeguas).

Sampling of the Llancanelo volcanic field (12 samples), is important because it consists of younger basalts, (Late Pleistocene-Early Holocene) erupted along E-W fractures closer to the volcanic front on the Los Huarpes Depression (Paleozoic Basement ?) (Figure 7).

Los Volcanes volcanic field (43 samples) is the best place to evaluate geochemical variations with eruption age, because the basalts from this area include the largest age range, from Early Pleistocene to Prehistoric. Moreover, this field is adjacent to the alkaline Payun Matrú volcano (Llambias et al., 1982), and these lavas may aid in understanding why this volcano differs from calc-alkaline volcanoes to the east and west. In this area multiple samples were taken from a single flow in order to evaluate intraflow variations. In addition, adjacent pyroclastics and bombs were collected and analyzed.

The Buta Ranquil volcanic field (12 samples) is southwest of the Los Volcanes field and these alkaline basalts erupted close to the Tromen strato-volcanoe.

IV. ANALYTICAL METHODS

Samples were broken by hammer into small chips using a plastic cover to avoid contamination. The chips with filled vesicles (secondary minerals) were removed and the remaining chips were cleaned in an ultrasonic bath with distilled water and ground to a fine powder in a agate shatterbox for three minutes.

Bulk rock major element compositions were determined in duplicate by X-ray fluorescence (XRF) analysis of fused glasses using an automated Siemens XRF analyzer at the University of Massachusetts, Amherst, following the techniques reported by Rhodes (1983). Abundances of Rb, Sr, Ba, Cr, V, Ni, Zn, Ga, Y, Zr and Nb was determined by XRF analysis of duplicate pressed powder discs at the University of Massachusetts, Amherst. Major and trace element precision estimates are one standard deviation in percent based on the duplicate analyses of all the alkaline basalts (table 1). The maximun standard deviation are quite large for samples with very low trace element abundance. For example Ni and Cr, where the standard deviation reaches 20% at 9 ppm. Data (50 analyses) for USGS standard rock BHVO-1 were obtained concurrently with the analyses of the alkaline basalts. The mean value from these analyses and consensus literature values with one standard deviation (Gladney and Roelandts, 1988) are reported in table 1.

Sr, Nd and Pb isotopic compositions on twelve samples were determined at MIT. Sr, Nd and Pb were separated by conventional ion exchange techniques: two stage dissolution ($HF+HNO_3$ and HCl) in teflon beakers on a hotplate. Separate aliquots for Sr, Nd and Pb were redissolved in 3.5 N HNO_3, 3N HCl and 1.1 N HBr, respectively, in preparation for column chemistry. Sr was separated using a Sr-specific resin (Sr spec^R) on a teflon microcolumn (D.S. Coleman pers. com. 1993). The REE fraction was collected using standard cation chromatography. Sm and Nd were separated on an HDEHP-on-teflon column following techniques of White and Patchett, (1984). Pb was separated using standard HBr techniques. The samples were analyzed, on single Ta filaments for Sr, triple and single Re filaments for Nd and Pb respectively, on a VG Sector 54 thermal ionization mass spectrometer. Sr and Nd were analyzed in dynamic multicollector mode and Pb was analyzed in static multicollector mode. $^{87}Sr/^{86}Sr$ ratios were corrected for mass fractionation by normalizing to $^{88}Sr/^{86}Sr= 0.1194$, assuming exponential fractionation. Replicated measurements of standard NBS-987 yield an average of 0.7102410 +/- 0.000009 (2s, n=35). $^{143}Nd/^{144}Nd$ ratios were corrected for mass fractionation by normalizing to $^{146}Nd/^{144}Nd= 0.7219$ (exponential fractionation correction). Measurement of the standards La Jolla Nd and AMES Nd yielded values of 0.511847+/-0.000010 (2s, n=25) and 0.511906+/-0.000010 (2s, n=41) respectively. Pb analyses were corrected 0.12%/amu for fractionation determined from replicate analyses of NBS-SRM-981. Error for Pb analyses is 0.05%/amu (ie. 0.10% for $^{206}Pb/^{204}Pb$, 0.15% for $^{207}Pb/^{204}Pb$ and 0.20% for $^{208}Pb/^{204}Pb$)

due to uncertainty in fractionation correction. Internal precision (standard deviation of all measurements during one run for each sample) for all analyses reported here is better than the external reproducibility (standard deviation of the all the results obtained for the standard sample) with the exception of $^{208}Pb/^{204}Pb$ which has internal precision of 0.40%.

V. RESULTS

V.1. PETROGRAPHY

Modal analyses were performed by point-counting standard thin sections with 500 to 1000 points per section (table 2).

Nevado Volcanic Field:

Lavas from Nevado volcanic field are porphyritic basalts. Based on different groundmass textures and phenocrysts there are two distinctive groups:

a) One group is characterized by intergranular texture and rarely intersertal (0.2 - 0.7 mm). They contain olivine (3.4 - 1 mm) as the dominant phenocryst phase (10 - 15%). In some cases, it is accompanied by lesser amounts (up to 8%) of Ca-rich clinopyroxene (1 mm) or by plagioclase (1 mm) (up to 4%). Glomerocrysts of olivine or clinopyroxene with plagioclase occur in a few lavas. Basalts from Las Vacas cone (sample 18-9 to 18-13), belong to this group, but they have lower amounts of olivine (5-12%). Samples from Lomas de Mondaca (sample19-1,2,4), La Montura (sample 66-83) and Negro South (sample 6-110384) cones represent a subgroup. They have the same intergranular texture, but in this case clinopyroxene is the dominant phenocryst phase (up to 17%) followed by plagioclase (phenocryst up to 2% or microphenocryst up to 8%) and olivine (up to 10%). In this subgroup the groundmass and phenocryst have similar size, 0.7 mm and 1-2 mm respectively. Glomerocrysts of olivine-clinopyroxene and plagioclase-clinopyroxene are common.

b) The second group, erupted principally in the eastern sector of the Nevado volcanic field close to Punta del Agua (samples 16-1,2), is characterized by a subophitic texture with a coarse-grained matrix (1.4 - 0.7mm). This group has low contents of olivine as the only phenocryst (7 - 9%) ranging between 1.7 to 2 mm, and the coarse matrix is rich in clinopyroxene and plagioclase. In the western sector of Nevado Vn. only lava from Borbaran cinder cone shows this texture (sample 19-7).

The change between the two principal groups is gradational, with samples that share the features of both groups. Also, in both groups olivine and clinopyroxene are euhedral to subhedral single crystals or they form glomerocrysts with plagioclase. Some olivines have embayed margins

suggesting reaction with the melt, in other cases they show skeletal growth. Magnetite to titano-magnetite occurs as euhedral crystal to ameboid groundmass shapes. Sometimes it is present as inclusions in olivine, suggesting hydrous and or relative oxidizing conditions (Gust and Perfit, 1987). In the samples with subophitic texture the clinopyroxene always is reddish-brown indicating a Ti-rich composition. One sample (sample 19-2) contains segregation vesicles, which are filled with dark, partly glassy segregation material. They are inferred to be frozen residual liquid rich in K_2O, TiO_2 and P_2O_5, (Anderson et al., 1984).

In both groups, there is evidence of crustal contamination. A single xenocryst of quartz occurs in thin sections of seven samples (16-1,2 in the subophitic group and 18-7; 19-8; 27-150384; 83-66; 6-110384 in the intergranular group). These quartz crystals are resorbed, and most are surrounded by a corona of small clinopyroxene crystals oriented in a radial direction (ocellar texture).

Some samples from the group of lavas with intergranular texture (18-1,2,3,4,10; 19-1,2,3,4,5,10,11; 27-150384) contain evidence of magma mingling. These samples have two different matrixes with sharp contacts at the microscopic scale, usually one has intersertal texture, and is strongly vesicular, and very different from the intergranular host matrix. In Lomas de Mondaca lavas (which is characterized by clinopyroxene as dominant phenocryst) there are basaltic inclusions with olivine phenocrysts (sample 19-1). In contrast to the petrographic result, we did not find any geochemical evidence of mingling in these samples.

Finally, the lavas appear fresh in both hand specimen and thin sections. Nearly all phenocrysts are unaltered, except for olivine which in some samples has rims of iddingsite. The groundmasses are also unaltered, except for calcite in the groundmass and vesicles of a few samples. The order of crystallization in lavas from Nevado Volcanic Field, determined by petrography and modal analysis, is near liquidus olivine followed by clinopyroxene and plagioclase. However, in lavas from Lomas de Mondaca, La Montura and Negro South, olivine, clinopyroxene and plagioclase crystallized almost simultaneously.

Llancanelo Volcanic Field:

The lavas from this area and Nevado area have similar petrographic characteristics. One group (samples 21-5, 6) is characterized by a fine groundmass (0.2 mm) with intergranular texture where olivine phenocrysts (2.4 mm) reach up to 10% in abundance. The other group (samples 21-1, 2, 3, 4, 8) has a coarse groundmass (0.7 -1 mm) with subophitic texture, where olivine (<6%, except sample 21-4 up to 10%) is the only phenocryst (1.7 - 3.4 mm). These Llancanelo lavas do not contain iddingsite, or other secondary mineral or segregation vesicles. Also, one sample contains a quartz xenocryst (sample 6-21).

Los Volcanes Volcanic Field:

Lavas from this volcanic field are porphyritic basalts. Based on the groundmass texture and

the phenocrysts, it is possible to separate them into three main groups, although, the changes between the distinctive types are transitional with samples sharing characteristics of more than one textural group:

a) Coarse grain (0.5 to 1mm) groundmass with subophitic texture and olivine as the only phenocryst, similar to that seen in some Nevado and Llancanelo lavas.

b) Strongly porphyritic basalts, with large differences in the size between the intergranular matrix (0.2 mm) and phenocrysts (3.4 -1.4 mm). Plagioclase and olivine are the dominant phenocryst phases.

c) Groundmass with the matrix crystal ranging in size from 0.2 to 0.5 mm. Plagioclase (1.7 - 2.4 up to 5 mm) is the dominant phenocryst phase (5 - 20%), accompanied by olivine (5 - 10%) and in less proportion clinopyroxene (<5%). This group commonly contains glomerocrysts of plagioclase, plagioclase-olivine, and plagioclase-clinopyroxene. Within this group there is a subgroup of samples with intersertal texture (from hyaline to cryptocrystalline). For example, strongly vesicular samples taken from scorial vent and some bombs. Also, two types of plagioclase phenocrysts occur in these lavas:

1) Euhedral to subhedral laths with complex zoning and several stages of growth defined by bands of very small melt inclusions. Some plagioclases have embayed margins indicating reaction with the groundmass. Also, several plagioclases have abrupt thin clear rims with the cores having a sieve like resorption texture with crudely oriented inclusions of glass or groundmass in a fine-mesh-like arrangement. This plagioclase type is common in the volcanic front lavas (Lopez Escobar and Frey, 1976; Frey et al., 1984; Hildreth et al., 1984; Stern et al., 1984a and b; Hildreth and Moorbath, 1988; Tormey et al., 1993; Ferguson et al., 1992; Hildreth and Drake, 1992, among others)

2) The other type of plagioclase phenocryst is characterized by small single euhedral laths free of inclusions.

In one sample from the Los Volcanes area there is a xenolith (1 cm diameter) of hornblendic tonalite (5-22). Also, segregated vesicles are more frequent in Los Volcanes lavas (25-10; 26-2) than in basalts from other volcanic fields. There are no alteration or secondary minerals in lavas from this area.

Buta Ranquil Volcanic Field

This area contains three independent volcanoes Cochiquito, Barrancas and Buta Ranquil. Cochiquito samples are characterized by basalts with porphyritic texture, with a matrix where the crystals have a gradational change in size (0.2 to 0.5 mm) and olivine (10 - 12%) is the only phenocryst (0.7 - 1.7 mm). Lavas from Buta Ranquil have a phenocryst assemblage similar to group (c) of the Los Volcanes lavas; i.e. plagioclase (10 - 18%)-clinopyroxene (1 - 7%)-olivine (2 - 8%), in a groundmass with 0.2 to 0.5 mm crystals. In both volcanoes the lavas are inferred to be

Late Pleistocene to Early Holocene age. Barrancas lavas are porphyritic basalts with olivine as the only phenocryst (15%) in a intergranular matrix. These lavas have a Pliocene age.

It is important to note that the different textural groups roughly correlate with the stratigraphic age (Table 2). The lavas with intergranular texture and olivine as the only phenocrysts are inferred to be Plio-Pleistocene. Lavas with intergranular texture with clinopyroxene as the most abundant phenocryst or lavas with subophitic texture and olivine as the only phenocryst phase are inferred to be of Pleistocene to early Holocene age. The porphyritic basalts with olivine-plagioclase as phenocryst phase, with large differences in the size between the intergranular matrix and phenocrysts or the lavas with plagioclase as the most abundant phenocryst in a groundmass where the crystals in the matrix have a gradational change in size are inferred to be early Holocene to Prehistoric in age.

V.2. ALTERATION AND CRYSTAL SORTING

In order to determine the compositional variability of an individual flow, we collected four samples each from two different flows: the "El Escorial" flow and the "Santa Maria" flow, in the Los Volcanes area. The purpose is to evaluate if one sample is representative of the composition of a lava flow. Also, this type of evaluation shows how intraflow compositional variation may be caused by late-stage alteration, crystal sorting during emplacement of the flow and varying extents of crustal assimilation. In both flows, samples were collected at varying distances from the vent: In the "El Escorial" samples 23-2 and 23-3, are massive and vesicular respectively, taken at 5 km, sample 23-1 at 7 km and sample 24-7 at 12 km from the vent. In the "Santa Maria" flow sample 24-3 is a glassy sample taken directly from the vent, sample 24-5 at 1 km and 24-1(B) and 24-1(A), are massive and vesicular respectively, collected at 5 km from the vent.

In table 3 the mean, standard deviation and standard error are compared with the analytical error (from duplicate XRF analyses) in order to determine the compositional variability in a single flow. We evaluate the variation in major and trace element abundance and trace element abundance ratios that we use in following chapters.

In the massive samples from the "El Escorial" flow (samples 23-1,2 and 24-7), Cr, Ni and MgO display the largest difference, and Rb, K_2O, Ba, Zr, Nb and Ce show smaller but significant differences. Also the sample that displays lower concentration of compatible elements has the higher abundance of incompatible element (sample 24-7). Abundance of Cr, Ni and MgO decrease and incompatible elements increase with distance from the vent. These variations in the "El Escorial flow" could be explained by olivine sorting (less than 4%) during flow emplacement. However, no important change in olivine phenocryst proportion was observed in the thin sections (table 2). It is important to consider that the precision of point counting results for 500 to 1000

points on samples with 10% olivine phenocrysts give an error between +/- 2 to 3% olivine (Van der Plas and Tobi, 1967), which is similar to the estimated olivine sorting. Also, we compare the composition of the vesicular sample (23-3) with two massive samples: one sampled at the same position as the vesicular sample (23-2) and the other sampled far from the vent (24-7). The vesicular sample is within the compositional range of the massive samples. Interestingly, the vesicular sample is compositionally distinct from the massive sample collected at the same position (23-2), but very similar to the sample taken far from the vent (24-7). This evidence is consistent with olivine sorting, because the vesicular sample is from the margin of the flow and its inferred lower olivine content may reflect vertical olivine segregation within the flow. The variation in trace element abundance ratios, i.e., Ba/Nb, Ce/Nb, Ce/Y, Rb/Ba, Ba/Ce, Rb/Ce are smaller than the range in analytical error, with the exception of Zr/Nb and K/Rb ratios.

In the Santa Maria flow, the massive (24-5; 24-1B) and vesicular (24-1A) samples are significantly different only in Ni and MgO (Table 3) with the vesicular sample displaying the lowest abundance of these elements. Rb, Ba, K, Zr, Nb, Ce abundances show no significant variations between these samples. Also, we compare the glassy sample taken directly from the vent (24-3) with the mean composition of Santa Maria flow calculated using samples 24-1B, 24-1A, 24-5. The glassy sample has higher concentrations of Ni, Cr and MgO with no significant variation in incompatible elements (except Rb) compared to the mean composition of Santa Maria flow. In all the samples the modal analyses do not show important differences in mineral proportion (Table 2). The variation in trace element abundance ratios, Ba/Nb, Zr/Nb, Ce/Nb, Ce/Y, Ba/Ce, Rb/Ce are smaller than the range in analytical error, and the range of Rb/Ba and K/Rb ratios are sligtly greater than analytical error.

Table 3 shows that in the "El Escorial" and "Santa Maria" flows the variation of mobile elements (Rb, K_2O and Ba) positively correlates with the less mobile elements (Zr and Nb), proving that the variation is not a product of alteration.

In order to evaluate if phenocryst accumulation was an important process controlling the compositional variation among all the samples, we looked for correlation between composition, modal abundance and phenocryst proportion (figure 8 and 9). Abundance of MgO and Ni are positively correlated with the abundance of olivine (figure 8), but samples with olivine proportion close to 15% range in Ni from 100 to 320 ppm. Also, samples with olivine as the only phenocryst phase range widely in MgO and Ni (figure 8). In contrast, abundances of Sr and Al_2O_3/CaO ratios are not correlated with the modal proportions of plagioclase and clinopyroxene (figure 9).

In the C° Las Bombas we sampled one flow (23-4), two bombs (23-9,10) and pyroclastic material (23-11*) and in C° Santa Maria, in addition to four flow samples, we collected one bomb (4-24) in order to compare compositional variations between the different extrusive material. In Las Bombas there are no significant compositional differences between the bombs, and only Ni

and Cr are slightly higher in the pyroclasts than in the bombs (Figure10, Table 3). In contrast, the lava flow has higher concentrations of CaO, MgO, Fe_2O_3*, Ni, Cr and lower K_2O, Na_2O, SiO_2, Rb, Ba, Zr, Nb, indicating that the bombs and pyroclastic sample represent more evolved compositions than the lava flow (Figure 10, Table 3). However, the Santa Maria bomb is compositionally similar to the Santa Maria flow. Incompatible element abundance ratios do not vary beween bomb and flow from the Santa Maria cone, but there are differences between the flow and bomb (mean) composition at C° Las Bombas in Rb/Ba, Rb/Ce and K/Rb (Table 3).

In order to determine compositional variations produced by alteration, two samples from the same flow west of C° Las Chinches (Nevado area) were studied. One sample with calcite in vesicles and as small veins is more altered (15-7) than the other (15-8). The altered sample has lower MgO, K_2O, Rb contents, higher CaO and Sr abundances, probably caused by calcite, with significant differences in ratios involving these elements. The differences in the abundances and abundance ratios involving these elements between altered and less altered sample range between 8 to 30 times the analytical standard error.

In summary, based on petrography and compositions, we conclude that the compositions of most samples were not affected by post-extrusion processes. Also, there is no evidence for plagioclase or clinopyroxene accumulation, but some lavas show small amount of olivine sorting ($\approx$ <4%) during flow emplacement. In rare samples the prescence of calcite has caused significant changes in abundance ratios involving alkali metals, but not in ratios involving Ba, Ce, Nb, Zr and Y.

V.3. MAJOR AND COMPATIBLE TRACE ELEMENTS

Major element compositions and normative mineral proportions of the samples are in Table 4. In the classification scheme of Peccerillo & Taylor, 1976, (Figure 11), most of the rocks are medium K_2O basalts (45 - 52 wt % SiO_2), the major exception is a basaltic andesite sample from Barrancas (53.9 wt % SiO_2). All the samples plot within the alkalic field on the total alkalis-silica diagram (Figure 12) (Macdonald and Katsura 1964). It is interesting also to note that, although, lavas from the eastern stratovolcanoes like Payun Matru, Nevado, Tromen and Plateado-Pelado show important differences in K_2O (Figure 15), this difference in K_2O was not observed in the alkaline basalts associated with the different stratovolcanoes (Figure 11).

Almost all the basalts (126 samples) are nepheline normative (0.1-12%); only 12 samples are hypersthene normative (0.66-15% wt), i.e. Buta Ranquil (27-1, 2, 3, BR15), El Manzano (22-4) and Barrancas (VM11, VM13, 26-10) erupted on the Principal Cordillera and from the Nevado area (16-4, 5 from C° Nevado, 16-6 from C° Los Tordillos, 46 from C° Pelado and 11-040484 from C° Negro NE) erupted on the San Rafael Block. $Fe^{+3}/(Fe^{+3}+Fe^{+2})$ ratios have not been

determined analytically and a value of 0.1 has been assumed. Therefore, normative composition and Mg#=(Mg/Mg+Fe^{+2}) were calculated based on the atomic ratio with $Fe^{+3}/(Fe^{+3}+Fe^{+2})$= 0.1. Lavas that have hypersthene in the CIPW norm are characterized by lower CaO, TiO_2, P_2O_5 and higher SiO_2 and Al_2O_3/CaO ratios compared with the other samples at the same MgO content (Figures 13 and 14). One important characteristic of these basalts is that either they erupted close to the eastern stratovolcanoes (i.e., sample 16-4,5,6 are close to Nevado Vn.; 46 and 11-040484 are next to C° Pelado and Plateado respectively and the samples from Buta Ranquil 27-1,2,3 are adjacent to Tromen Vn.) or they are older rocks, i.e., Barrancas Vn. (Pliocene) (Figure 5, 6 and 7).

Lavas from different volcanic fields range widely in MgO content: from 12.5 to 6 wt % in the Nevado area, from 10 to 6 wt % in Los Volcanes and Llancanelo areas. Lavas from Barrancas Vn. vary from 10 to 3.5 wt %, and lavas from Buta Ranquil Vn. and Cochiquito Vn. exhibit the smallest range in MgO, from 8 to 6 wt % (Table 4, Figure 13).

On a major element-MgO variation diagram (Figure 13), SiO_2, Al_2O_3, Na_2O, K_2O and TiO_2 content increase and Fe_2O_3* slightly decreases with decreasing MgO. CaO decreases in lavas from Buta Ranquil area, it is constant in basalts from Llancanelo areas, and it first increases from 9.5% to 11% and then decreases to 7% in lavas from Los Volcanes area. The samples from Nevado area show dispersion in CaO content, with lavas characterized by intragranular texture with clinopyroxene as the dominant phenocryst phase and lavas with subophitic texture (i.e., 16-1,2 from Punta del Agua; 19-1,2,4 from Lomas de Mondaca; 19-7 from C° Borbaran; 2-170484 from Pto. La Suiza; 83-66 C° La Montura; 83-62 C° El Masuco), having higher CaO content (from 11 up to 12.7%) than the other lavas from this area (<11%).

It is important to notice that lavas with quartz xenocrysts do not show differences in major element composition with respect to the other samples, in fact, the most primitive sample (27-150384) has quartz xenocryst (Figures 13 and 14). The exception are samples 16-1 and 16-2 (from Punta del Agua), which have quartz xenocrysts, and they are compositionally different from the rest of the samples from the Nevado area, with higher CaO, Fe_2O_3, TiO_2, Na_2O, K_2O, and lower Al_2O_3 and MgO (Figures 13 and 14).

Al_2O_3/CaO ratio correlates negatively with MgO, except for Nevado area lavas that do not change in Al_2O_3/CaO ratios as MgO decreases. Nevado lavas characterized by intragranular texture with clinopyroxene as the dominant phenocryst phase and subophitic texture lavas clearly have lower Al_2O_3/CaO, a result of higher CaO contents. Also, it is interesting to point out that lavas with quartz xenocrysts that have different composition in major elements (16-1 and 16-2) also have low Al_2O_3/CaO ratios, which is opposite to what is expected by crustal contamination (Figure 14).

MgO (12.5 to 4%) correlates with Ni (300 to 25 ppm) and Cr (500 to 0 ppm) contents

(except for samples 16-1, 2; 46; 2-170484; 8-16) (Figure 14), with Nevado area basalts ranging to the highest abundances of Ni, Cr, and MgO. Abundance of V does not correlate with MgO or TiO_2 but it positively correlates with CaO (Figure 16).

On the projection olivine (OL)- clinopyroxene (CPX)- nepheline (NE)- plagioclase (PLAG) diagrams (calculated with the algorithm of Sack et al., 1987), the alkaline basalts lie between Olivine + Ca-rich Pyroxene + Plagioclase cotectic (fO_2 - QFM) at 1 atmosphere obtained by Sack et al. (1987) and the Olivine + Orthopyroxene + Ca-rich pyroxene + Spinel saturated liquidus ranging in pressure from 0.8 to 3 GPa reported by Stolper (1980), Takahashi and Kushiro (1983) and Fuji and Scarfe (1985) (Figure 17).

Samples from Nevado area plot in groups concordant with their petrographic characteristics: one group lies closer to the Ol+Cpx+Opx+Sp cotectic, these samples have petrographically intergranular texture and olivine as the dominant phenocrysts. The samples from C° Las Vacas that have lower amounts of olivine phenocryst plot closer to Olivine + Ca-rich pyroxene + Plagioclase cotectic. The last group characterized by lavas with intergranular texture and Ca-rich pyroxene as the dominant phenocryst and lavas with subophitic texture plot closer to the Olivine + Ca-rich pyroxene + Plagioclase cotectic and could indicate the same cotectic at pressure higher than 1 atmosphere. Although samples 16-1 and 16-2 belong to the last group, they display major element compositions different from the rest of the samples from Nevado area (Figure 13), and also they are the only two samples that plot on the Olivine + Ca-rich pyroxene + Plagioclase cotectic at 1 atm (Figure 17). The basalts with normative hypersthene plot across the olivine basalt thermal divide toward SiO_2 saturation, thereby indicating their tholeiitic affinity.

Several criteria have been proposed for distinguishing primitive basaltic magma equilibrated with mantle peridotite: Mg# of 0.68-0.75 for up to 30% melting (Frey et al, 1978), FeO*/MgO <1 (Tatsumi et al., 1983) and high Ni content (235-400 ppm) (Sato, 1977). Although there are several samples from Nevado area that share at least two of the criteria for primitive lavas only four samples (20-1,2 from C° Negro; 19-6 from C° El Leon; and 27-150384 from Lomas de Mondaca) have Mg# of 0.68 to 0.71, Ni of 255 to 318 ppm and FeO*/MgO of 0.79 to 0.93 indicating the primitive characteristic of these basalts (Table 1). In these samples the modal proportion of olivine is between 12 to 15%. Other samples with similar amounts of olivine have Ni content as low as 100 ppm (Figure 8). The high pressure experimental data from Stolper (1980), Takahashi and Kushiro (1983), and Fuji and Scarfe (1985) are useful in assessing potentially primitive composition. The primitive samples from Nevado area have ratios of normative Olivine/Ca-rich pyroxene and Olivine/Nepheline consistent with Ol+Opx+Cpx+Sp+Liquid cotectic (Figure 17).

V.4. INCOMPATIBLE TRACE ELEMENTS

Trace element concentrations are listed in Table 4. Selected analyses, to cover all the compositional spectrum, are shown in primitive mantle normalized abundance diagrams (Figure 18). Composition for MORB, EMORB, OIB (Sun and McDonough, 1989) and continental volcanic arc basalt (Planchon Vn., from Tormey et al.,1994) are also shown for comparison. Usually, alkaline lavas from the back arc in different magmatic arcs have patterns resembling those of OIB, for example, the alkaline lavas from the Japan Sea (Nakamura et al, 1989), or from the northwestern Mexican volcanic belt (Verma and Nelson, 1989; Luhr et al., 1989). In contrast, in our case the alkaline lavas have patterns that do not match with that of OIB, but they share characteristics of OIB and volcanic arc basalts (such as Planchon Vn. lavas). In the normalized diagram, the arc lava pattern is clearly different from OIB and MORB in that arc lavas have positive anomalies of Ba and Sr and the negative anomalies of Nb and Ti with respect to the adjacent elements with similar compatibility. Although absolute abundance of incompatible elements can be strongly affected by processes such as partial melting and crystal fractionation, abundance ratios of these elements are less sensitive to these processes, (with the exception for very small degree of melting, e.g., F<< D); thus they provide clues to the composition of the magmatic source. Kay (1977,1980), Perfit et al.(1980), Nakamura et al. (1985), Gill (1986), Arculus and Powell (1986), and Hickey et al. (1986) have shown that arc related magmas are characterized by high ratios of alkaline and alkaline earth elements to LREE and HFSE.

Lavas from Los Volcanes, Llancanelo, Cochiquito Vn., one sample from Barrancas Vn. (26-10), two samples from Buta Ranquil (27-4 and BR-16) and six samples from Nevado area (from now on Nevado Group II: 16-1,2 form Punta del Agua; 18-4 and 50-83, both samples from the youngest flow in Las Yeguas cone; 18-8 from the youngest flow in Las Vacas cone; 19-7 from C° Borbaran) have relatively small negative anomalies of Nb and Ti and small positive anomalies of Ba and Sr in the normalized diagram. Moreover, specially in the case of Los Volcanes basalts the incompatible element abundance ratios are similar to those of oceanic island basalts. In contrast, Group I lavas from Nevado area, Buta Ranquil Vn. (27-1, 2, 3, 6) and Barrancas Vn. (26-11, 12) have a normalized pattern that resembles those of the volcanic arc basalts (Planchon Vn.); for example, the depletion in Nb and Ti and enrichment in Ba and Sr, typical of arc lavas, also occurs in these alkaline basalts.

The lavas with hypersthene normative (tholeiitic affinities), in the case of Barrancas and Buta Ranquil volcanoes, have higher abundances of all incompatible elements, except Ti and Y, compared to nepheline basalts at the same volcano (Figure 18). Also, it is important to notice that for Buta Ranquil the range in MgO for nepheline lavas (6.99 to 7.87 wt%) is not very different from that of the hypersthene normative basalts (6.10 to 6.92 wt%), but for Barrancas nepheline

normative lavas the content in MgO is higher (10 wt%) than the hypersthene normative basalt (3 wt% in 26-10). In contrast, the hypersthene normative lavas from Nevado area have the same (46; 11-40484) or lower (16-4, 5, 6) incompatible element contents than the normative nepheline lavas at the same MgO content (8 wt%).

It is also important to point out that the samples from Nevado Group I with quartz xenocrysts do not show different incompatible element contents with respect to the other lavas from the same group (Figure 19). Sample 16-1 and 16-2 (MgO ≈ 6 to 7 wt%), which have quartz xenocryst have a slightly higher incompatible element contents than the other samples from Group II (MgO ≈ 9 to 10 wt%), but in this case, the difference in incompatible element contents could be explained by the different degree of differentiation of the samples (Figure 18).

V.5. ISOTOPIC COMPOSITION

Twelve samples were analyzed for $^{87}Sr/^{86}Sr$, $^{143}Nd/^{144}Nd$, $^{206}Pb/^{204}Pb$, $^{207}Pb/^{204}Pb$ and $^{208}Pb/^{204}Pb$ isotope ratios (Table 5). The Sr isotope composition of the alkaline basalts ranges from 0.703769 to 0.704208. A similar range of Sr isotopic composition of alkaline basalts in the region between 34°-39° S (0.70350 to 0.70445) was obtained by Muñoz et al, (1989) and Stern et al. (1990), on six and five samples respectively. The Nd isotope ratios range from 0.512743 to 0.512829, and they correlate negatively with $^{87}Sr/^{86}Sr$ ratios with all the points plotting in the mantle array (Figure 20). The Pb isotopic ratios vary from 18.310 to 18.594 for $^{206}Pb/^{204}Pb$, from 15.554 to 15.607 for $^{207}Pb/^{204}Pb$, from 38.184 to 38.418 for $^{208}Pb/^{204}Pb$. The samples have higher $^{207}Pb/^{204}Pb$ and $^{208}Pb/^{204}Pb$ at a given $^{206}Pb/^{204}Pb$ ratios than MORB reference line (NHRL) and the field of Nazca metallic sediments (Hart, 1984; Hickey et al., 1986) (Figure 21). Also the alkaline lavas have higher $^{207}Pb/^{204}Pb$ at a given $^{208}Pb/^{204}Pb$ than OIB (Figure 22). No correlation was found between Sr or Nd and Pb isotopic ratios (Figure 23).

Among these twelve basalts only samples 16-1 (from Punta del Agua) and 18-7 (from the Las Yeguas cone) have quartz xenocrysts in thin section. These basalts have lower Sr and Pb and higher Nd isotopic ratios than other samples from the same area (Table 5), which is opposite to what would be expected from crustal contamination.

V.6. VARIATION ACROSS THE ARC

The volcanic front basalts and basaltic andesites (up to 56 SiO_2 wt%), and back-arc basalts display different major and compatible trace element abundance at the same MgO content. The volcanic front lavas have lower $Fe_2O_3^*$, TiO_2, P_2O_5, CaO, higher SiO_2 and similar Al_2O_3 than those from the back arc (Figure 24). Also, the volcanic front lavas range to lower compatible trace

element concentration than the back arc basalts (Figure 25). On the contrary, the samples with normative hypersthene in the back arc area have major and compatible trace element composition similar to that of the volcanic front lavas (Figure 24 and 25). The V content of volcanic front lavas, like the back arc basalts, correlates with CaO content but it does not correlate with Ti (Figure 25).

Although incompatible element abundance-MgO variation diagram shows considerable scatter for back arc lavas, Figure 26 demonstrates that in general, back arc basalts are more enriched in all incompatible elements, especially Nb, with respect to MgO than the volcanic front rocks. The difference between volcanic front and back arc lavas are evident in incompatible element abundances and ratios. Figure 27 shows incompatible element abundance versus Ce for the volcanic front and the different volcanic fields behind it, with Nevado area lavas considered as the two previously defined groups (Groups I and II). The abundance ranges for Rb, Ba, K, Zr and Y, in general overlap in the volcanic front and the back arc lavas, but Nb, Ti and P are lower in the volcanic front samples. Sr versus Ce clearly shows that Sr and Ce are equally incompatible in the back arc lavas, but Sr is more compatible in the volcanic front rocks (Figure 27 a, b, c). The same figures are also shown on transparency for lavas with MgO content higher than 7 wt%, and in this way, we separate the effect of fractionation. The most primitive from the volcanic front lavas range to higher K and Rb and lower Y contents at the same Ce abundance than lavas from the back arc basalts. Comparing primitive and evolved lavas the behavior of Sr in the volcanic front lavas is easily explained by plagioclase fractionation (Figure 27 transparency).

Abundance ratios of incompatible elements vary between volcanic front and back arc basalts and between the different volcanic fields. Ratios of K/Nb, Ce/Nb and Zr/Nb are systematically higher in the volcanic front rocks than in the back arc lavas. Also these ratios are higher in Nevado and Buta Ranquil lavas, (with the exception of Nevado group II, 16-1,2; 18-4,8; 50-83; 19-7) than in Los Volcanes and Llancanelo basalts (Figure 28a).

K/Ba, Rb/Ba, K/Ce and Rb/Ce ratios in the volcanic front lavas are either higher or similar to the back arc lavas. In this case lavas from Nevado and Llancanelo area have lower ratios than basalts from Los Volcanes and Buta Ranquil (Figure 28b). On the other hand, Ba/Ce ratios are higher in Nevado area than the volcanic front and the other back arc lavas (Figure 28b).

Ti/Ce and Nb/Ce ratios are lower in the volcanic front lavas than in the back-arc basalts, but Zr/Ce ratios are similar in lavas from both areas (Figure 28c). Also Buta Ranquil and Nevado area lavas display lower Ti/Ce and Nb/Ce ratios than Los Volcanes and Llancanelo basalts. Buta Ranquil samples have similar to higher Zr/Ce ratios than the samples from the other volcanic fields and Nevado area lavas have the lowest Zr/Ce ratios (Figure 28c).

K/Rb versus Rb, Ba/Nb versus Ti and Ce/Y versus Zr diagrams show that the volcanic front lavas range to compositions similar to Nevado basalts, both areas displaying lower K/Rb and

higher Ba/Nb and Ce/Y ratios than Los Volcanes area (Figure 29).

The range in Ce/Y ratios is slightly lower in the volcanic front lavas (1.36-3) than the basalts from the different volcanic fields (1-3.20). Also, in the volcanic front lavas abundance of Y and Ce are equally variable (factor of two), but in the back arc lavas Ce abundance vary three times and Y 1.5 times (Figure 29, Table 4). It is important to notice that at Zr content ≈ 125 ppm the volcanic front lavas and Nevado lavas have a strong increase in Ce/Y ratios (a factor of 2.5) with a small change in Zr (a factor of 1.5). In contrast, in Los Volcanes lavas Ce/Y have a small enrichment (a factor of 2) with a big change in Zr (a factor of 2.5), (Figure 29).

P/Ce ratios are higher in the back arc basalts than volcanic front lavas, but hypersthene normative samples from Buta Ranquil, Barrancas, and Nevado area have P/Ce ratios equivalent to that of the volcanic front (Figure 29).

As mentioned before, although absolute abundance of incompatible elements can be strongly affected by processes such as partial melting and crystal fractionation, abundance ratios of elements with similar global partition coefficient (i.e., K and Rb) generally remain constant during the early stage of such process, (with the exception for very small degree of melting, e.g., F<< D), and they thus provide clues to the composition of the magmatic source. In figure 28 and 29 the respective abundance ratio for primitive mantle is indicated in each diagram, and it is evident that the alkaline lavas have abundance ratios of incompatible element with similar global partition coefficient closer to primitive mantle ratios than volcanic front lavas.

The lavas from the volcanic front between 35° to 41° S range in $^{87}Sr/^{86}Sr$ ratios from 0.703670 to 0.704270 and there is no systematic change of this ratio along strike. In contrast, the volcanic front lavas have $^{143}Nd/^{144}Nd$ ratios lower in the 35°-37° S than in the region 37°-41° S (Figure 30). The alkaline basalts erupted behind the front show the same along strike isotopic trend as the volcanic front. For example, $^{87}Sr/^{86}Sr$ ratios are similar from 35°-39° S, but back arc lavas from 35°-37° S have lower $^{143}Nd/^{144}Nd$ than back arc lavas from 38°-39° S. Although the Sr and Nd isotopic ratios in the alkaline basalts are similar to volcanic front lavas at a similar latitude, the lead isotopic ratios in the alkaline basalts range to lower ratios than the volcanic front (Figure 31, 32, 33). Los Volcanes basalts range to lower Pb isotopic ratios, and they also range to lower $^{143}Nd/^{144}Nd$ ratios than Nevado basalts (Figure 34). Incompatible element abundances show, in general, no good correlations with isotopic data. Only in the Los Volcanes area the four samples analyzed for isotopic ratios display negative correlation between incompatible element abundance and $^{87}Sr/^{86}Sr$, $^{208}Pb/^{204}Pb$ ratios, a positive correlation with $^{143}Nd/^{144}Nd$ ratios, and no correlation with MgO content (Figure 35). Also, there is no correlation between $^{87}Sr/^{86}Sr$ and SiO_2, K, Rb/Sr, or K/Ce (Figure 36). In contrast, the Ba/Nb and Ba/Ce ratios display slight positive correlation with $^{87}Sr/^{86}Sr$ or $^{208}Pb/^{204}Pb$ and negative correlation with $^{143}Nd/^{144}Nd$ ratios, with the Nevado and Buta Ranquil area lavas as a group and Los Volcanes and Llancanelo

area basalts as another group, (sample 16-1 from Nevado area is anomalous, figure 37).

V.7. TEMPORAL GEOCHEMICAL TREND

A temporal geochemical trend is very difficult to assess due to the lack of geochronological dates and stratigraphic control. Nevertheless, there are some composite cones in Nevado area, e.g., Las Vacas and Las Yeguas (Figure 6), with multiple flows that can be used to evaluate temporal variations. Also, morphology, degree of erosion of monogenetic cones, formation of soil covering the flows and the overlapping of flows from different cones are used in defining relative age.

The maximun age interval in the Nevado area is from late Pliocene to Pleistocene. The Nevado hypersthene normative lavas 16-4, 5, 6 (Plio-early Pleistocene) have not only the lowest abundances of incompatible elements in this area (except for Ti and Y) at similar MgO content (MgO from 7.87 to 8.25 wt% compared to a range from 6 to 12.5 for Nevado Group I), but also they have high Ba/Nb ratios (Figure 39c). Nevado Group I lavas are younger than the hypesthene normative lavas, with an assigned age late Pliocene-early Pleistocene. Group I lavas are nepheline normative with high abundance of incompatible elements and high Ba/Nb abundance ratios (Figure 39b).

Four flows were sampled at the composite cones Las Vacas and Las Yeguas. Figure 38 shows that in both cases the incompatible element abundance and their ratios do not display significant variation between the older three flows, but the youngest flow in both volcanoes has lower Ba, Sr, Ce and higher Nb. MgO, Ni, Cr are also higher in the youngest flow. To avoid the effects of fractional crystallization the abundance ratios of incompatible elements were also compared between the flows. The youngest flow in both composite cones has the lowest Ba/Nb ratio (40 to 50% lower). This evidence suggests that the lavas from Nevado area that have low Ba/Nb ratios (Group II= 16-1,2; 18-4,8; 50-83; 19-7) represent younger flows, e.g., Pleistocene? (Figure 39a). The four samples analysed for isotopic ratios from the Nevado area do not show correlation between isotopic composition and relative age, (Figure 40). Nevertheless, the only sample analysed from Group II, (16-1) of Pleistocene age, ranges to low Ba/Nb ratios and to low Pb and Sr and high Nd isotopic ratios respect to the other three samples from Group I (Figures 40 and 37). Although geochronologic dates are necessary to certify a temporal correlation, in Nevado area we observe a change from hypersthene normative to nepheline normative lavas with younger age. This change represents an increase in incompatible element abundance from hypersthene normative to Group I nepheline normative basalts and a decrease in the arc signature (Ba/Nb) from the hypersthene normative and Group I lavas to Group II basalts (Figure 39).

The Los Volcanes area represents a range in age from Pleistocene to Prehistoric. These

basalts display a slight correlation (considering two groups Pleistocene and Holocene) between age and incompatible element abundance. Older lavas have lower incompatible element abundance (ranging from 6.33 to 8.33 wt% MgO) compared to the younger basalts (ranging from 5.80 to 7.60 wt% MgO) (Figure 35 and 41). Also, the incompatible element contents are negatively correlated with Sr isotope ratios and $^{208}Pb/^{204}Pb$ ratios and positively correlated with Nd isotopic ratios. Therefore, the youngest lavas have higher abundances of incompatible elements, lower $^{87}Sr/^{86}Sr$, higher $^{143}Nd/^{144}Nd$ and lower $^{208}Pb/^{204}Pb$. Also the basalts from Pleistocene to early Holocene ages range to higher Ba/Nb ratios than the younger Holocene to Prehistoric lavas (Figure 35).

In the Llancanelo area the basalts represent two different ages Plio-Pleistocene and late Pleistocene-early Holocene. Only two samples (21-7 and 21-1) have been analysed for isotopic ratios (one of each age), the older sample has higher Sr and Pb and lower Nd isotopic ratios and higher Ba/Nb ratios than the younger one (Figure 42). In this case, the youngest sample with lower MgO content (5.71 wt%) also has lower abundance of incompatible elements; this is unlike the mentioned trend for Los Volcanes lavas. All samples from Los Volcanes and Llancanelo are nepheline normative, but in this area there are older (Miocene?) hypersthene normative basalts (Bermudez, 1987). Therefore, there is a temporal change from hypersthene normative lavas to nepheline normative lavas, similar to the trend observed in the Nevado lavas.

Although Buta Ranquil Vn. is considered of late Pleistocene-early Holocene age, its samples range widely in incompatible element abundance without a large change in MgO (from 6.10 to 7.87 wt%) between the different flows. Another difference at this volcano is that the hypersthene normative samples (27-1,2,3) have higher abundances of incompatible element than the nepheline normative lavas (Figure 43). In contrast with other areas, the youngest Buta Ranquil lavas have lower incompatible element abundances, but as in the other volcanic fields Ba/Nb ratios are lowest in the youngest flows. The two samples analyzed for isotope ratios represent the range in age and they show the same trend as the other areas. Older flows have higher Sr and Pb isotopic ratios and higher Ba/Nb ratios than younger flow (Figure 43).

An important result is that there are no systematic changes in incompatible element abundance, abundance ratios and isotopic composition with the distance to the trench (Figure 27, 28, 29 and 34): Nevado area basalts are at the greatest distance from the trench, but they are more similar in composition to the volcanic front lavas than Los Volcanes area lavas, which outcrop closer to the volcanic front. There are, however, systematic changes in major element composition, incompatible element abundances, isotopic ratios and Ba/Nb ratios with stratigraphic age in the Los Volcanes area (the area that has the largest range in age from early Pleistocene to Prehistoric). The other volcanic fields represent a smaller interval of time and the systematic change with time observed in their lavas is not as well defined as in Los Volcanes area basalts, or

they present additional complexities like in the case of Nevado Group I.

VI. DISCUSSION

VI.1. THE ROLE OF CRYSTAL FRACTIONATION

Possible fractionating minerals are the phenocryst phases in the alkaline basalts: olivine, clinopyroxene, plagioclase and magnetite or titano-magnetite. The change in slope on the MgO variation diagram are consistent with a major role for mineral/melt fractionation (Figures 13, 14 and 16). Thus, the increasing SiO_2, the decreasing Ni, and slightly decreasing of FeO with decreasing MgO content would require fractionation of olivine. The increase of Al_2O_3/CaO ratios with decreasing MgO and the good correlation of Sr versus Ce in the alkaline lavas indicate that the clinopyroxene/plagioclase ratio of fractionating phases was high, with the exception of Nevado lavas, whose constant Al_2O_3/CaO ratios indicates a lower clinopyroxene/plagioclase ratio (Figures 13,14,16 and 27c). This is specially true for the Nevado samples with intergranular texture and clinopyroxene as the dominant phenocryst and the samples with subophitic texture, which have the lowest Al_2O_3/CaO ratios (Figure 14); the lack of correlation between Al2O3/CaO abundance ratios and modal proportions of clinopyroxene demostrates that there is no clinopyroxene accumulation in these samples (Figure 9). Also, some evolved lavas from the Los Volcanes area have a tendency for Sr to decrease as Ce increases, indicating fractionation of plagioclase (compare Figure 27c with transparency). The slight decrease in FeO, the increasing of TiO_2 with decreasing MgO, and the lack of correlation between V and MgO or TiO_2 suggests that fractionation of magnetite or titano-magnetite was not significant. In contrast, the correlation between V and CaO indicates that clinopyroxene was an important phase controlling V concentration in the melt (Figures 13 and 16), an inference that is consistent with the partition coefficient of V in clinopyroxene, which ranges from 3.1 to 4.0 in alkaline basalts (Hart and Dunn, 1993).

On the projection Olivine (OL) - Clinopyroxene (CPX) - Nepheline (NE) - Plagioclase (PLAG) diagrams (calculated with the algorithm of Sack et al., 1987), the alkaline basalts lavas lie between Olivine + Ca-rich pyroxene + Plagioclase cotectic (fO_2 = QFM) at 1 atmosphere for alkaline composition, obtained experimentally in anhydrous condition by Sack et al. (1987), and the Olivine + Orthopyroxene + Ca-rich Pyroxene + Spinel saturated liquidus at pressures ranging from 0.8 to 3 GPa in anhydrous conditions reported by Stolper (1980), Takahashi and Kushiro (1983) and Fuji and Scarfe (1985). The result indicates pressures of crystallization higher than one atmosphere for the alkaline lavas (Figure 17). This is concordant with the increase of Al_2O_3/CaO with decrease of MgO, and the strong correlation of Sr with Ce, which indicates that clinopyroxene

was a more important fractionating phase than plagioclase suggesting high pressure crystallization in anhydrous conditions (Gust and Perfit, 1987). In contrast, most of these lavas have plagioclase-rich phenocryst assemblages, with the exception of some samples that show olivine as the main phenocryst followed by plagioclase in small quantities (Table 2). This difference between petrography and chemistry suggests that at shallow level (lower pressure) the observed plagioclase-rich phenocryst assemblage crystallized, but it did not fractionate.

Samples from the Nevado area plot in groups concordant with their petrographic characteristics: 1) Several samples including the labeled "primitive group" are close to the Ol + Cpx + Opx + Sp cotectic, these samples have intergranular texture and olivine as the dominant phenocryst. Comparison of these primitive basalts with isobaric partial melt compositions obtained experimentally by Falloon and Green (1988) indicates pressure of 1.5 to 2 Gpa (Figure 44). All the high pressure experimental data (Stolper, 1980; Takahashi and Kushiro, 1983; Fuji and Scarfe, 1985 and Falloon and Green, 1988) shows that, at constant temperature, as pressure increases liquids saturated with Ol+Opx+Cpx+Sp become increasingly nepheline normative and Ca-rich pyroxene saturated as well. In contrast, temperature has the opposite effect of pressure (Sack et al., 1987). 2) The samples from C° Las Vacas that exhibit intergranular texture but lesser amounts of olivine phenocrysts plot closer to Olivine+Ca-rich pyroxene+Plagioclase cotectic indicating olivine fractionation from the first group. 3) The samples with intergranular texture and Ca-rich pyroxene as the dominant phenocryst and lavas with subophitic texture (cpx-rich group in Figure 17) plot between the two cotectics, suggesting olivine and small amounts of clinopyroxene fractionation. In all the cases this is in agreement with the observed variation in major and compatible element abundances. In this cpx-rich group, there is also a contrast between the mineral assemblage in thin section and the compositional trends. For example, lavas with clinopyroxene as the dominant phenocryst followed by plagioclase have constant Al_2O_3/CaO ratios with decreasing MgO, which is consistent with only fractionation of olivine; possibly in these magmas low pressure crystallization of clinopyroxene and plagioclase occurred without fractionation. Also, the observed variation in Nevado basalts could be the integrated result of polybaric crystallization during magma ascent (O'Donnell and Presnall, 1980; Sack et al, 1987) rather than crystallization at single depth.

Water is an important variable that modifies the proportion, composition and order of crystallization of the different phases. For example, an increase of water content in basaltic magma delays the crystallization of plagioclase and increases its CaO content (Baker and Eggler, 1983; Presnall et al, 1978; Sisson and Grove 1993). Water also delays the crystallization of silicate minerals promoting the early crystallization of Cr-spinel and magnetite (Sisson and Grove 1993 a, b), and it allows the crystallization of clinopyroxene at lower pressure (Gaetani and Grove 1993). The lack of hydrous minerals like amphibole suggest low water contents in the alkaline basalt

magmas. Cawthorn and O'Hara (1976) and Cawthorn (1976) show that not only water but Na_2O content in melts exerts a major control on the stability of amphibole in the system CMAS-Na_2O-H_2O at H_2O-pressure of 5 kb, in CMAS-Na_2O-H_2O system, hydrous basalt would require at least 3% Na_2O to crystallize hornblende. The experimental work of Sisson and Grove (1993) in high alumina basalts (to which they add NaOH to create a nepheline normative composition) at H_2O-pressure 2 kb (6% = saturated in H_2O) shows that hornblende will crystallize at Na_2O content between 4 and 5%. The studied alkaline basalts have no amphibole present and most of the samples range between 3 to 4% in Na_2O. Therefore, although the amount of water in the basalts cannot be precisely estimated, we suggest that the alkaline basaltic magmas were not saturated in water.

VI.2. THE HYPERSTHENE NORMATIVE LAVAS

The lavas that have hypersthene in the CIPW norm (Table 4), samples from the Nevado and Buta Ranquil areas, are characterized by lower CaO, TiO_2, P_2O_5, and V abundances, lower P/Ce ratios, higher SiO_2 content and higher Al_2O_3/CaO ratios than the nepheline normative lavas at the same MgO content (Figures 13, 14, 16 and 29). The hypersthene normative samples plot across the olivine basalt thermal divide toward the SiO_2 saturation field in the projection of Olivine-Clinopyroxene-Nepheline from Plagioclase, indicating their tholeiitic affinity (Figure 17). Also, these lavas in Nevado area have similar (46; 11-40484) or lower (16-4, 5, 6) incompatible element contents than the nepheline normative basalts at the same MgO content (Figure 39). The large differences in abundances of incompatible elements (factor of up to 5), indicate that the nepheline normative lavas and the hypersthene normative lavas are not genetically related by mixing the nepheline lavas with more evolved lavas and/or crustal contamination. This suggests that the difference between these lava types may be related to the melting process. Also, as we mentioned before, the experimental data indicates that the nepheline normative lavas represent melts generated at higher pressure than the hypersthene normative lavas.

In contrast, in the Buta Ranquil area, the Buta Ranquil volcano erupted hypersthene normative basalts with higher incompatible element contents than nepheline normative samples with similar MgO content. Therefore, the variation in major and incompatible element contents, could be explained by crustal contamination or mixing with more evolved lavas. For example, the major and incompatible element composition of the hypersthene lavas from Buta Ranquil Vn. could be explained by mixing between the nepheline basalts and the basaltic andesite erupted very close to Buta Ranquil from the calcalkaline stratovolcanoe Tromen. Table 6 and Figure 45 show the results of the mass balance calculation between the nepheline normative lavas of Buta Ranquil (27-4; BR16-81) and the calcalkaline basaltic andesites of Tromen (27-5; 27-7) to obtain the

hypersthene normative lavas in Buta Ranquil (27-1; 27-2; 27-3). The calculation used the major elements to obtain the proportion of each component in the mixture and the goodness of fit is evaluated by the sum of the squares of the residuals. In all the cases this sum is less than 1 (0.09 to 0.86), with MgO and Al_2O_3 having the biggest residuals. The "allowed residual" shows how large the residual could be if we propagate the errors in the fitting parameters and in the analytical determinations. For example, the mass balance equation is

$$C^i_m +/-\partial^i_m = [(C^i_a+/-\partial^i_a)*(P_a+/-\partial P_a) + (C^i_b+/-\partial^i_b)*(P^b+/-\partial P_b)]$$

where C^i_m, C^i_a and C^i_b are the concentration of the i element in the hypersthene normative basalt, in the nepheline normative basalt and in the basaltic andesite, respectively; Pa and Pb are the fitting parameters for the nepheline normative lavas and the basaltic andesite; ∂^i_a, ∂^i_b, ∂P_a and ∂P_b are the standard errors in the analytical determinations and in the fitting parameters for the nepheline normative basalt and the basaltic andesite respectively. The allowed residual (∂^i_m) is the result of propagating the standard errors in the fitting parameters and in the analytical determinations (Snedecor and Cochram, 1979)

$$\partial^i_m = [(C^i_a*\partial P_a + P_a*\partial^i_a + \partial^i_a*\partial P_a) +(C^i_b*\partial P_b + P_b*\partial^i_b+ \partial^i_b*\partial P_b)]$$

The fitting parameters obtained from the major element calculations were used to estimate trace elements abundance. It is clear that the biggest differences from comparing the residuals with the allowed residuals for trace elements come from Sr, Ni and Cr. The differences observed in MgO, Ni, Cr and Al_2O_3 and Sr indicate clearly that segregation of crystal phases like olivine and plagioclase were also important (fractional crystallization or accumulation). Petrographic evidence of mixing are the two different types of plagioclase phenocrysts in the hypersthene lavas: One type, euhedral to subhedral laths with complex zoning and several stages of growth defined by bands of very small melt inclusions. Some plagioclases have embayed margins indicating reaction with the groundmass. Also, several plagioclases have abrupt thin clear rims with the cores having a sieve like resorption texture with crudely oriented inclusions of glass or groundmass in a fine-mesh-like arrangement. This plagioclase type is common in the Tromen strato volcano lavas. The other type of plagioclase phenocryst is characterized by small single euhedral laths free of inclusions, typical of those in the nepheline normative lavas. It is important to mention that the Hy-normative lavas from Nevado are different from the Hy-normative lavas from Buta Ranquil. There is neither geochemical, nor petrographic evidence for mixing with more evolved lavas in Nevado Hy-normative basalts. In contrast, although we found similar petrographic evidences of mixing in some Ne-normative lavas from the Los Volcanes area (two different types of plagioclase), we did

not find geochemical evidence of mixing in those samples; perhaps the explanation is that we do not have enough geochemical information about the evolved lavas from Payun Matru strato-volcanoe.

Finally, in the case of the hypersthene normative lavas from the Barrancas volcano in the Buta Ranquil area, which are more evolved basalts (3% MgO) than the nepheline lavas (10% MgO) at the same volcano, there is no consistent data for inferring whether melting, crystal fractionation, mixing and/or crustal contamination was responsible for the generation of hypersthene normative samples.

Based on the geologic and geochemical data, there are two important points to state about the hypersthene normative basalts:

1) The hypersthene normative basalts erupted near the eastern stratovolcanoes; i.e., samples 16-4, 5 and 6 in Nevado area were sampled at a large distance (≈ 20 Km) from Nevado volcano (Figure 5), but they correspond to flows which erupted from the Nevado Vn. (Delpino, per. com., 1992). This evidence suggests that the hypersthene normative lavas are closely associated with the stratovolcanoes; and 2) In the Nevado area the oldest group of lavas (Plio-Pleistocene), includes hypersthene and nepheline normative basalts; however, hypersthene normative lavas are absent in younger groups. Moreover, although in the Los Volcanes and Llancanelo areas there are no hypersthene normative lavas in the age range considered here (Pliocene-Prehistoric), there are hypersthene normative lavas assigned to the Miocene (Bermudez, 1987). Thus, there is an important temporal trend from hypersthene normative to nepheline normative lavas with decreasing age, thereby implying a change with time in the condition of melting. Based on anhydrous experimental data, the formation of hypersthene normative lavas requires lower pressure of melting (Stolper, 1980; Takahashi and Kushiro, 1983; Fuji and Scarfe, 1985; Kinzler and Grove, 1992 a and b).

VI.3. THE IMPORTANCE OF CRUSTAL CONTAMINATION

The presence of quartz xenocrysts provides evidence of crustal contamination in some lavas from Nevado area (16-1,2; 18-7; 19-8; 27-150384; 83-66; 6-110384). Field evidence indicates that the quartz may be from quartzites exposed at the level of extrusion (Delpino per. com., 1993). It is important to determine the geochemical effect of this contamination process. Most of the lavas with quartz xenocrysts cannot be distinguished from other Nevado basalts in their major or trace element composition (Figures 13 14 and 19). The exceptions are the samples 16-1 and 16-2, collected from the same flow close to the locality of Punta del Agua (Figure 5). Relative to other lavas from the Nevado region, these two samples have similar SiO_2 content, higher Na_2O, K_2O, CaO, Fe_2O_3*, TiO_2, Cr and Ni, and lower Al_2O_3, V, Al_2O_3/CaO ratios at the same MgO content

(Figure 13 and 14). Also, these samples have incompatible element contents and abundance ratios different from other lavas from Nevado area. Specifically, samples 16-1 and 2 have similar Sr, Rb, Ba, and P but range to higher K, Nb, Zr and Ti, and lower Y abundances at the same Ce content. Therefore, samples 16-1 and 16-2 have higher K/Ba and lower (LILE, LREE)/HFSE ratios than other Nevado lavas (Figure 27 a,b,c and 28 a,b,c). The lower Al_2O_3, similar SiO_2, Rb and Sr and the higher Fe_2O_3*, TiO_2, Zr, Nb, Ni, Cr of samples 16-1 and 16-2 are not easily explained by either bulk or selective crustal contamination of Nevado basalts. For example, high SiO_2, Rb, Nb, Zr and low TiO_2, Ni and Cr are expected in crustally contaminated lavas. Moreover, if we assume that these samples are crustally contaminated, crustal contamination diminishes the typically high LILE/HFSE ratios that are characteristic of arc magmatism (e.g., Ba/Nb). Hildreth and Moorbath (1988, Figure 14) argued that crustal contamination explains the inverse correlation between Ba/Nb and $^{87}Sr/^{86}Sr$ ratios observed in the volcanic front lavas of the Southern Volcanic Zone. Sample 16-1 however, has low Sr and Pb and high Nd isotopic ratios with respect to the other Nevado lavas (Figure 37). In fact, the two quartz xenocryst-bearing samples from the Nevado area analyzed for isotopic ratios have the lowest $^{87}Sr/^{86}Sr$, $^{208}Pb/^{204}Pb$ and the highest $^{143}Nd/^{144}Nd$ in this area (Figure 37). Based on this evidence, crustal contamination in samples 16-1 and 16-2, which contain quartz xenocrysts, is not an obvious explanation for their atypical geochemical characteristics.

VI.3.1. Nevado Group II: Different mantle source or crustally contaminated lavas?

Sample 18-4 and 50-83 from the youngest flow in Las Yeguas cone; 18-8 from the youngest flow in Las Vacas cone and 19-7 from C° Borbaran have chemical characteristics similar to samples 16-1 and 16-2; therefore, we group these samples as Nevado Group II. Nevado Group II lavas have primitive mantle normalized patterns similar to Los Volcanes, Llancanelo and Cochiquito lavas; i.e., they have a lower arc signature, as measured by low LILE/(HFSE, and LREE) or by low LREE/HFSE (Figure 18, 28 a,c and 29). The only sample from Nevado Group II analyzed for isotopes, sample 16-1 has isotopic ratios similar to Los Volcanes lavas and also plots closer to the area defined by Los Volcanes-Llancanelo lavas than the area defined by Nevado-Buta Ranquil lavas in the correlation between isotopes and Ba/Nb, Ba/Ce ratios (Figure 37). The change in composition between Nevado Group I and Group II samples represents a change in composition with time. The sampling of 4 lavas flow in two strato-cones, Las Vacas Vn. and Las Yeguas Vn., shows that the youngest flow in both volcanoes has the geochemical characteristics described for Nevado Group II, which is compositionally different from the older flows, (Figure 38). Relative to Group I Nevado lavas, Group II basalts range to higher K_2O, Fe_2O_3*, Ti, Zr,

Nb content, and K/Ba abundance ratios, and to lower Al_2O_3, Y and (LILE, and LREE)/HFSE ratios (Figure 13, which only shows samples 16-1 and 16-2, transparency in figure 27, figures 28 a,b,c, and 29). Also, Group II lavas are characterized by constant Ti/Zr, variable Nb/Y, a low arc signature; i.e., Ce/Nb (Figure 46) and relatively low Sr, Pb and high Nd isotopic ratios. They differ from Nevado Group I lavas which have comparatively constant Nb/Y, variable Ti/Zr, high arc signature and high Sr, Pb and low Nd isotopic ratios (Figures 18, 28, 29, 37 and 46). These differences in major, trace element abundance and isotopic composition between Nevado Group I and Group II primitive lavas (MgO > 7%) cannot be explained by crystal fractionation or different degree of melting from a common mantle source. For example, these processes will not produce the different isotopic composition between Group I and Group II or the variation in incompatible element abundance ratios with very similar bulk partition coefficient (e.g., Ba/Nb, K/Ba, Ce/Nb, Ba/Ce) without assuming unreasonably low extent of melting (bulk partition coefficient >> extent of melting). Moreover, as mentioned before for samples 16-1 and 16-2 (Group II) the compositional differences between these two groups cannot be explained by crustal contamination. For example, if Group II lavas are the result of contamination of Group I lavas with partial melts generated in the lower crust (hypothesis proposed by Hildreth and Moorbath, 1988, to explain the volcanic front and across arc geochemical variation), we can explain Group II lavas having lower Ba/Nb and Ce/Nb ratios, higher K/Ba and a more variable Nb/Y abundance ratios than Group I lavas, but we cannot explain their higher Ti content, the similar Ce/Y, and the constant Ti/Zr abundance ratios compared to those from Group I lavas, or the correlation between Ba/Nb or Ba/Ce and Sr, Pb and Nd isotopic ratios (Figures 18, 28, 29, 37 and 46). Therefore, these geochemical variations reflect a change in source composition rather than crustal contamination.

In order to test the "two source" hypothesis, a batch melting model (Shaw, 1970) was evaluated to explain the Ti/Zr and Nb/Y variation within Group I and Group II primitive lavas. The assumptions in the model are: 1) as a first approximation, we consider that both mantle sources have compositions similar to primitive mantle. This assumption is based on the incompatible trace element abundance ratios (comparing elements with similar partition coefficient), such as Ce/Nb (Figure 28 a), which in both group of lavas is similar to those ratios in the primitive mantle. Although the trace element abundance ratios indicate two mantle sources with similar extent of depletion, the distinct isotopic ratios between both group of lavas indicate the existence of two different mantle sources, 2) the slab component, which has a strong influence on LILE/HFSE abundance ratios, did not modify the abundance of Nb, Zr, Ti, Y, and 3) the two mantle sources have different mineralogy. The suggested difference in mineralogy is based on the constant Ti/Zr at variable Nb/Y ratios, the low Al_2O_3 and Y contents in Group II lavas compared with the variable Ti/Zr ratios with small variation in Nb/Y and high Al_2O_3 and Y content in Group I lavas (Figure 27, transparency, and figure 46). A low extent of melting of a garnet-bearing mantle source would

generate basalts with almost constant Ti/Zr ratios, variable Nb/Y and low concentration of Al_2O_3 and Y compared to melts formed by low extent of melting of a spinel-bearing mantle. The mineral proportions for the primitive mantle and the melting raction in the case of spinel peridotite were taken from Kinzler and Grove (1992 a, b). Because we assume a similar trace element mantle composition for both group of lavas, we used the initial spinel peridotite mineral proportions modified to garnet peridotite based on the breakdown reaction from Hauri, (1992).

$$Mg_2SiO_4 + Ca_{.6}Mg_{2.4}Al_2Si_3O_{12} = 1.4\ Mg_2Si_2O_6 + 0.6\ CaMgSi_2O_6 + MgAl_2O_4$$
(olivine) (garnet) (opx) (cpx) (spinel)

In this case, the melting reaction was taken from Kinzler, (1992). The model fits the data reasonably well for Nevado Group II (Figure 46). Therefore, Group II lavas could be explained by melting of a primitive mantle source with low arc signature and garnet as a residual phase. However, for Group I lavas, the samples with low Nb/Y and high Ti/Zr abundance ratios, also have low Mg#, which is inconsistent with the composition of lavas generated by progressive melting from a mantle source (Figure 46). Therefore, a more complex process is required to explain the geochemical variation within Group I lavas.

VI.3.2. The geochemical signature of the magmatism in the SVZ; slab or lower crustal imput?

Is the mantle signature of the SVZ magmas masked by contamination with melts from the lower continental crust as the magmas rise through it? Hildreth and Moorbath, (1988, 1991) proposed that in a continental arc many of the geochemical characteristics of volcanic front lavas are controlled by processes of mixing, assimilation, storage and homogenization in partially molten zones in the lower crust. There has been debate about the geochemical characteristics that reflect mantle sources and processes, and those that reflect crustal processes (Lopez Escobar and Frey, 1976; Lopez Escobar et al., 1977, 1981; Frey et al., 1984; Hildreth et al., 1984; Hickey et al., 1986; Hildreth and Moorbath, 1988; Gerlach et al., 1988; Davidson et al., 1988; Futa and Stern, 1988; Hickey-Vargas et al. 1989; Hickey-Vargas,1992; Tormey et al., 1989, 1991, 1992; Ferguson et al., 1992; Hildreth and Drake, 1992, McMillan et al., 1989, among others). These studies of volcanic front lavas have not unambiguously distinguished between these possibilities. However, alkaline basalts erupted for distances up to 500 km from the trench can be used to evaluate the role of lower crust contamination because they include high MgO lavas with a strong arc signature that ascended through different accreted terranes of distinct ages.

The alkaline basalts in the SVZ differ from oceanic basalts; Do these geochemical differences

reflect contamination by continental lower crust? Hofmann and White (1982) showed that in oceanic basalts Rb/Ba ratios are nearly constant (≈0.090), but that K/Rb and K/Ba vary widely depending on the incompatible element concentration. As incompatible element abundances increase in oceanic basalts, K/Rb ranges from ≈2000 to ≈380 and K/Ba from ≈177 to ≈35. In the SVZ alkaline basalts, the K/Rb ratios range from 250 to 850, and overlap with the OIB range. In contrast, K/Ba and Rb/Ba abundance ratios range to lower values than oceanic basalts, from 40 to 10 and from 0.12 to 0.025 respectively (Figures 28b and 29). Also, in the back-arc basalts as the K/Ba ratios diminish, the arc signature (K/Nb, Ba/Nb) increases, (Figure 47); and as the Ti content increases, K/Ba increases and Zr/Nb diminishes (Figure 48). Hildreth and Moorbath (1988, 1991) observed that the SVZ lavas from the volcanic front have higher Nb, Ta, Zr and Hf than lavas from island arcs. Also, they noticed that $^{87}Sr/^{86}Sr$ correlates inversely with Ba/Nb and positively with K. Based on this evidence, they considered that these characteristics are related to the process of crustal contamination, whereby crustal melts in equilibrium with Ti-rich residual phases cause increases in Nb, Zr and $^{87}Sr/^{86}Sr$ and decreases in Ti content. If this hypothesis is correct, the process of crustal contamination should decrease the arc signature (Ba/Nb), Ti content and Zr/Nb ratios and increase K/Ba and Rb/Ba ratios, K content and Sr isotopic ratios. In order to produce the observed variation in the back-arc alkaline basalts by the lower crust we need a contaminant that would keep the K/Rb nearly in the range of oceanic basalts, increase the arc signature (Ba/Nb, K/Nb), increase the Zr/Nb ratios, decrease the Ti content, and decrease K/Ba and Rb/Ba ratios; trends that are in disagreement with those mentioned by Hildreth and Moorbath, (1988, 1991). Moreover, all the alkaline basalts plot on the "mantle array" in $^{87}Sr/^{86}Sr$-$^{143}Nd/^{144}Nd$ diagram, and they are indistinguishable from oceanic island basalts. Nevertheless, the alkaline lavas systematically show high $^{207}Pb/^{204}Pb$, $^{208}Pb/^{204}Pb$ at a given $^{206}Pb/^{204}Pb$ relative to the northern hemisphere reference line (Hart, 1984), and they are slightly higher than the field for Nazca plate metallic sediments (Hickey et al., 1986) (Figure 20, 21, 22). In contrast to the trends observed by Hildreth and Moorbath (1988) in the volcanic front lavas, no correlation was found in the alkaline basalts between $^{87}Sr/^{86}Sr$, $^{143}Nd/^{144}Nd$ and $^{206}Pb/^{204}Pb$, or between $^{87}Sr/^{86}Sr$ and SiO_2, K, K/Ce or Rb/Sr, which argues against crustal contamination (Figures 23 and 36). A good correlation, however, was found between Sr, Nd and Pb isotopic ratios and incompatible element ratios indicative of arc signature, like Ba/Nb and Ba/Ce (Figure 37). This kind of correlation is expected from slab derived contributions (Arculus and Johnson, 1981). Therefore, the chemical compositions of the alkaline lavas are not easily explained by either crustal melt or bulk crust contamination. All the evidence indicates that in the alkaline basalts either there was no important crustal contamination or the crustal contamination did not produce a distinctive signature in the incompatible elements and the isotopic ratios.

VI.4. WHAT IS THE CAUSE OF THE ACROSS ARC GEOCHEMICAL TREND?

In a general way, the compositional differences between the volcanic front and the back arc Andean lavas at 36° S are characterized by higher major and incompatible element abundance (except SiO_2 and Al_2O_3, which are lower) P/Ce and Nb/Y abundance ratios, and lower Zr/Nb and (LILE or LREE)/HFSE abundance ratios in the basalts erupted behind the volcanic front (Figures 24, 25, 26, 29, 46, 47, 48).

Similar compositional differences between the front and back arc lavas are observed in most volcanic arcs (Gill, 1981). Several mechanisms have been advocated to explain theses across arc variation: 1) Differences in the degree of crystal fractionation (O'Hara 1973) 2) Differences in the degree of crustal contamination (Best 1975, Hildreth and Moorbath, 1988, 1991) 3) Differences in the residual phases in the magma source region (Jaques and White 1970, Tatsumi et al. 1986) 4) Differences in the depth of magma production and resultant differences in the degree of partial melting (Miyashiro, 1974; Morrice & Gill, 1986, Hickey et al., 1986) 5) Differences in the mantle source composition (Hickey et al, 1986; McCulloch and Gamble, 1991; Woodhead et al., 1993; Stolper and Newman, 1984).

Derivation of the alkaline lavas from a calcalkaline parental magma by fractional crystallization or vice versa is very unlikely, because it would imply that the liquid line of descent cross over the thermal divide that separates SiO_2 unsaturated lavas from SiO_2 saturated lavas, which is inconsistent with experimental results (Schairer and Yoder, 1960).

The CaO content in the alkaline basalts is higher than those of hypersthene normative and volcanic front basalts at same MgO content (Figure 24). One possible explanation is that assuming the same source composition the extent of melting in the volcanic front is higher than ≈ 20%, because based on experimental work (Kinzler and Grove, 1992; Falloon and Green; 1988) from 0 to ≈ 20% of melting, CaO content increases as degree of melting increases, but for higher than ≈ 20%, CaO content decreases as extent of melting increase. Another possibility is that the source in the volcanic front is more depleted in basaltic components than in the back arc source. The similarity between some incompatible element abundance ratios (i.e., Ti/Zr and Ce/Y) in the volcanic front and the alkaline lavas indicates that the degree of melting or the depletion of the source in the volcanic front lavas was not very different from that of the alkaline lavas. Different fractionation paths also could explain the variation in CaO between the volcanic front basalts and the alkaline lavas. For example, water retards fractionation of plagioclase (Baker and Eggler, 1983; Presnall et al, 1978; Sisson and Grove 1993 a,b,) and results in early fractionation of clinopyroxene (Gaetani and Grove 1993), decreasing the CaO content in the melt . Moreover, experimental work on the univariant curve liquid-Fo+An+Diop in the system CMAS at 1 bar shows that melts on the cotectic Plag-Ol-Cpx have different CaO content at both side of the thermal

divide that separate SiO_2 unsaturated lavas from SiO_2 saturated lavas, with higher CaO content for melts that plot on the SiO_2 undersaturated side (Libourel et al. 1989).

Another possible mechanism to consider the across arc geochemical variations is crustal contamination. The alkaline basalts erupted through distinct terranes of different ages ranging from Precambrian to Late Paleozoic, and lavas from the volcanic front erupted through Late Paleozoic to Mesozoic terranes. Surprisingly, lavas from the volcanic front and behind the front have similar Sr and Nd isotopic ratios, while the $^{206}Pb/^{204}Pb$ and $^{208}Pb/^{204}Pb$ isotopic ratios range to lower ratios in the alkaline basalts than the volcanic front lavas (Figure 31, 32, 33). The lower $^{208}Pb/^{204}Pb$ isotopic ratios in the alkaline basalts and their positive correlation with incompatible element ratios indicative of arc signature (Ba/Nb and Ba/Ce) is more concordant with a decreasing slab derived contribution rather than differences in crustal contamination (Arculus and Johnson, 1981) (Figure 37). Also, the $^{87}Sr/^{86}Sr$ ratios in the volcanic front basalts between 35° to 41° S do not show systematic change along strike; in contrast, the $^{143}Nd/^{144}Nd$ ratios of these lavas are lower in the region between 35° to 37° S than between 37° to 41° S (Figure 30). Similarly, the alkaline basalts, erupted behind the arc, show the same along strike isotopic trend as the volcanic front. These similar along the volcanic front and back-arc trends are not expected in lavas contaminated with crust of variable age and composition across the arc. Although Davidson et al., 1988; Tormey et al., 1989, 1991, 1992; Ferguson et al., 1992 consider that contamination with melts from the lower crustal is an important process in volcanic front lavas (Tatara-San Pedro Vn. and Planchon Vn), the similar Sr and Nd isotopic ratios in volcanic front and back arc lavas do not support this hypothesis. Moreover, B-^{10}Be and $^{230}Th/^{232}Th$-$^{238}U/^{232}Th$ systematics in the SVZ volcanic front lavas (including those from the northern SVZ) provide an unequivocal evidence in favor of subducting sediments (Morris et al 1990, Sigmarsson et al 1990). The systematics indicates mixing between two highly homogeneous components, with one of these end member as the slab component responsible for the increase of U/Th ratios, B and ^{10}Be. The only possibility is that crustal contamination would be restricted to a younger lower crust composed of subduction zone derived material accreted during previous Andean magmatism (Tormey et al. 1991, 1993). In order to evaluate crustal contamination using the trace element compositions of the lavas, where the contaminat is a younger lower crust composed of subduction zone derived material accreted during previous Andean magmatism, we choose Nevado Group I and the volcanic front (San Pedro Tatara and Planchon) primitive lavas (>7% MgO) because they have the highest arc signature (Ba/Nb) and Sr isotopic ratios. We observed that in both groups of lavas Mg# correlates positively with Nb/Y, Ce/Y and negatively with Ti/Nb and Ti/Zr ratios (Figures 46 and 49). These trends cannot be explained by crustal contamination with low Mg# melts generated in a younger arc related lower crust leaving garnet (Tormey et al. 1991) and/or Ti rich residual phases (Hildreth and Moorbath, 1988), because melts from the lower crust would decrease Ti/Nb, and Ti/Zr but

increase the Nb/Y, and Ce/Y abundance ratios with decreasing Mg#. Again, these trends are opposite to the trends observed in the Group I and volcanic front primitive lavas (Figures 46 and 49)

Tatsumi et al., (1986), related the variation across the arc with different residual phases in the magma source region. They consider that the melting in the mantle source is related to the break down of hornblende leaving phlogopite as a residual phase in the volcanic front area. In contrast, melting in the back-arc is related to the break down of the phlogopite with K-richterite as the residual phase. This variation in the residual phase in the mantle would generate a trend of decreasing K/Rb abundance ratios from the volcanic front toward the back arc. In contrast to this model, the K/Rb variation across the arc in the SVZ (36° S) shows the opposite trend to that described by Tatsumi et al., (1986) (Figure 29).

The compositional differences between the alkaline lavas and those from the volcanic front give conflicting evidences for the role of differences in the degree and pressure of melting. Anhydrous experimental data show that at constant temperature as the pressure increases, liquids saturated with Ol+Opx+Cpx+Sp become increasingly nepheline normative and Ca-rich pyroxene saturated (Stolper, 1980; Takahashi and Kushiro, 1983; Fujy and Scarfe, 1985; Falloon and Green, 1988; Falloon et al., 1988; Kinzler and Grove, 1992). Based on these experiments, the lower content of FeO and higher content of SiO_2 in the volcanic front lavas and the Hy-normative lavas than Ne-normative basalts at the same MgO contents indicate lower pressure of melting for the volcanic front and Hy-normative lavas (Figure 24).

Also, the differences between the amount of water supplied from the slab into the volcanic front and back arc sources is a fundamental factor controlling extent of melting and producing significant changes in the melt composition during melting and fractionational crystallization. For example, higher amounts of water in the source of the volcanic front and the hypersthene normative basalts (silica saturated lavas) than in the source of the nepheline normative lavas could be responsible for a) the higher contents of incompatible elements in the nepheline normative basalts (Figure 26), because the varying water content causes a west to east decrease in the extent of melting, and b) water expands the stability volume of some minerals, for example olivine, promoting the formation of melt with higher SiO_2 and lower FeO and MgO contents than in anhydrous conditions (Kushiro,1968). The addition of water to the mantle source will produce a competition between the effect of expanding the stability volume of olivine, which will reduce the amount of normative olivine in the basalts, and increasing the degree of melting, which will increase the normative olivine, (Stolper and Newman 1994). These experimental results and the major and trace element compositional variation between the volcanic front and the back arc indicate that melts generated closer to the trench are produced at lower pressure and with higher water content than those generated far from the trench.

There is, however, no correlation between chemical and Sr-Nd isotopic composition and distance from the trench (Figures 27, 28, 29 and 37). Although, Nevado Group I and the hypersthene normative lavas have compositions closer to the volcanic front lavas than Los Volcanes and Llancanelo basalts (Figure 18), the distance from the volcanic front to Nevado area is almost the double than that to Los Volcanes and Llancanelo areas (Figure 3). The lack of correlation between the distance from the trench and the arc signature (Ba/Nb, Ce/Nb, Ba/Ce) is evident in Figures 27, 28, 29, with Nevado Group I basalts being compositionally closer to the volcanic front lavas. Moreover, Ti/Ce and Nb/Ce abundance ratios are lower but Zr/Ce ratios range from similar to slightly lower in the volcanic front and Nevado Group I basalts than in Los Volcanes lavas (Figure 28c). Finally, the range of Ti/Zr and Ce/Y ratios in the volcanic front lavas is similar to Nevado Group I basalts (Figures 29 and 46). All of these variations cannot be explained by decreasing slab input and decreasing degree of melting with increasing distance from the trench to Nevado area, because decreasing melting coupled with decreasing slab imput in a single mantle source would have to decrease the Ti/Ce, Zr/Ce, Ba/Nb, Ba/Ce, Ce/Nb and increase the Ce/Y abundance ratios progressively from the volcanic front toward the Nevado area.

The volcanic front, Nevado Group II, Los Volcanes, Llancanelo and Buta Ranquil areas (except Barrancas Volcanoe of Pliocene age and some lavas from Llancanelo area of Pliocene-Pleistocene age) represent a range in age from Pleistocene to Present. In this case, the arc signature decreases from the volcanic front to the back arc as expected from variation in the slab imput. In contrast, if we consider Nevado Group I lavas, with the highest arc signature but erupted at the highest distance from the volcanic front, the observed correlation disappears. This lack of correlation is because Group I lavas represent an older range in age from Pliocene to Pleistocene, which is characterized by a change from hypersthene normative to nepheline normative lavas. Therefore, the across arc variation in some major and incompatible element abundances and ratios may reflect temporal changes in source composition perhaps caused by changes in the subduction process such as convergence rate and dip of subducting Nazca plate or subduction of an aseismic ridge like Juan Fernandez ridge (Nur and Ben-Avraham, 1983; 1989)

In summary, the across arc geochemical variation in the SVZ (36° S.) cannot be explained by crystal fractionation from a common parental magma, or differences in the MASH process across the arc or by different residual phases across the mantle wedge. In contrast, variation in the degree of partial melting and depth of magma segregation coupled with different amounts of water supplied from the slab across the arc are a likely mechanisms for explaining the variation in major and trace element, and isotopic composition between the Quaternary volcanic front and back-arc lavas. Nevado Group I lavas, erupted during the period Pliocene-Pleistocene, are not consistent with the mentioned trend across the arc, indicating temporal changes in the mantle source composition and in the melting regime, perhaps, caused by change in the conditions of subduction

of the Nazca plate.

VI.5. TEMPORAL GEOCHEMICAL VARIATIONS IN THE ALKALINE BASALTS

The lack of correlation between the geochemical signature of the lavas and distance to the trench may result because we are not comparing lavas of similar ages. The scarcity of radiometric dates make temporal geochemical variation a difficult task to assess. As mentioned before, the composite cones with multiple flows can be used to evaluate the temporal variation (Figure 38). Also, morphology, degree of erosion of monogenetic cones, formation of soil covering the flows and the overlapping of flows from different cones are used in defining relative age. In general, in the Nevado area we observe a change from hypersthene normative basalts to Group I and to Group II with younger age (Figure 39). This change represents an increase in incompatible element abundance from hypersthene normative to nepheline normative lavas and a decrease of the arc signature (Ba/Nb) with decreasing age (Figure 39). Also, the temporal variation between Groups I and II with a decrease in the arc signature is coupled with a change in Sr, Pb and Nd isotopic ratios, decreasing Sr and Pb and increasing the Nd isotopic ratios (Figures 37, 38 and 40).

In the Los Volcanes area (Pleistocene to Prehistoric), the composition of the lavas display a correlation with time; for example, increasing incompatible element and Nd isotopic ratios, diminishing arc signature and diminishing Sr and Pb isotopic ratios with decreasing age (Figure 35, 37, 41). Few samples were collected from Llancanelo area, but they show the same tendency as those from Los Volcanes area, except for the incompatible element abundance, which range to lower concentration in the younger flows at same MgO content (Figure 42).

Although all the lavas from Los Volcanes and Llancanelo areas are nepheline normative, in these areas there are older (Miocene) hypersthene normative basalts (Palauco basalts, Bermudez, 1987). Although these Miocene basalts have not been analyzed for trace elements, the temporal trend from older hypersthene normative to younger nepheline normative lavas with high abundance of incompatible element occurs in both Nevado and Los Volcanes areas

Finally, the Buta Ranquil area basalts are interpreted as mixtures of alkaline basalts and basaltic andesites from Tromen volcano (Figure 45), which make the temporal variation difficult to evaluate. Nevertheless, these lavas display a change from older lavas with arc signatures and high Sr and Pb isotopic ratios to younger lavas with low arc signature and Sr and Pb isotopic ratios (Figures 37 and 43).

In general, in each area there is a common pattern in the temporal variation: A trend from hypersthene normative lavas, with low concentration of incompatible elements, high arc signature and high Sr, Pb and low Nd isotopic ratios to younger nepheline normative lavas with high concentration of incompatible elements, low arc signature, and low Sr, Pb and high Nd isotopic

ratios. A similar trend occurs, in the cratonic area (Patagonia extraandina). Skewes and Stern (1979) and Kay et al. (1993) mentioned a change from hypersthene normative to nepheline normative in the Pali Aike volcanic field and Somuncura plateau respectively. Also, in the Somuncura plateau, Kay et al. (1993) observed an inverse correlation between incompatible element abundance and Sr isotopic ratios.

Another important piece of evidence for assessing the temporal geochemical changes can be obtained from the three strato-volcanoes in our area of study: Tromen, Payun Matru and Sierra del Nevado (Nevado, Pelado and Plateado volcanoes). Tromen erupted closest to the volcanic front, and is mainly built of andesites of subalkaline composition similar to the volcanic front (Llambias et al., 1982), whereas Payun Matrú erupted farther east, and has trachyte and trachyandesites of alkaline composition (Llambias, 1966). If only Quaternary lavas are considered, the variation in lava compositions from the Tromen Vn to Payun Matru Vn. are consistent with the observed compositional trend from Buta Ranquil to Llancanelo, Los Volcanes and Nevado Group II lavas. These compositional trends in the strato-volcanoes and in the cinder cones indicate a decreasing arc signature with increasing distance from the volcanic front

Pelado, Plateado (both Miocene) and Nevado volcano (Pliocene), erupted eastward of Payun Matru. They display a temporal compositional change from andesites of calkalkaline composition at Pelado and Plateado Vn. similar to the volcanic front to high K_2O calcalkaline compositions at Nevado, which are intermediate between the volcanic front and the Payun Matru lavas (Figure 15) (Bermudez, 1991). Lavas from the two older strato-volcanoes have compositions similar to those from the volcanic front. In summary the temporal trend in Nevado area is a) Miocene strato-volcanoes with calcalkaline lavas similar to the current volcanic front lavas; b) a Pliocene strato-volcanoe with high K_2O calcalkaline lavas; c) the hypersthene normative basalts erupted closer to the strato-volcanoes; d) replacement of stratovolcanoes by monogenetic cinder cones with eruptions of Ne-normative alkaline lavas with arc signature; and e) Ne-normative alkaline lavas without the arc signature.

Llambias et al. (1982, and pers. com. 1993), based on comparing Tromen, Payun Matru and Nevado strato volcanoes, considered that this variation in composition with time is related to eruption under different tectonic conditions. This temporal tectonic change is also suggested in the observation of Bermudez and Delpino (1989), when they mention that the alkaline basalts from Nevado area erupted through northwestern striking fractures, in contrast to Los Volcanes and Llancanelo lavas erupted along east-west fractures. Moreover, the existence of Mio-Plio-Early Pleistocene calcalkaline strato-cones to the east of the present volcanic front, made Muñoz and Stern (1989), Muñoz et al (1989) consider the existence of a Plio-early Pleistocene "volcanic front" that migrated westward to its current location. All of this evidence suggests a change in the tectonic condition in this area during the period from Mio-Pliocene to early Pleistocene. Although,

Muñoz et al. 1989, Muñoz and Stern 1989, Bermudez and Delpino 1989 consider the existence of a intra arc extensional event between 35° and 39° S since the early Pleistocene, Ramos (per. com. 1993) maintains that extensional fractures are the result of subduction related east-west compression.

VI.6. MULTIPLE VERSUS SINGLE, AND DEPLETED VERSUS ENRICHED MANTLE SOURCES

Several papers have been written addressing the variation in incompatible element abundances and ratios in lavas along and across strike of the SVZ (Hickey et al. 1986; Hildreth and Moorbath, 1988; Stern 1991b, Tormey et al., 1991, among others). They agree on at least two simple points: 1) different degree of melting of a single mantle source (MORB or OIB source) cannot explain the chemical trends of the SVZ lavas, and 2) the existence of residual minerals in the mantle wedge during magma generation cannot explain the HFSE depletion in the SVZ basalts. Therefore, there is more than one source contributing to the generation of the SVZ magmatism. The arc signature has two alternative possibilities: source contamination by subducted pelagic or continental sediments versus mixing assimilation storage and homogenization process (MASH) in a molten zone in the lower crust (Hildreth and Moorbath, 1988, Stern, 1991b). Hickey et al., (1986), in an study of across arc geochemical variation, found an inverse correlation between arc signature (Ba/Nb, Ba/Ce etc.) and incompatible element abundance. They proposed two different alternatives to explain this chemical variation: 1) a west to east decrease in the amount of fluid derived from the subducted slab, which also caused a west to east decrease in the degree of melting, or 2) a systematic west to east increase in enriched component derived from the subcontinental mantle lithosphere (Figure 10 in Hickey et al., 1986). In contrast, Hildreth and Moorbath (1988) suggested that such across arc variation reflect changes in MASH processes. All the previous studies of across arc geochemical variation in the SVZ were based on relatively short (<100 km) traverses. In our study the section across the arc represents ≈ 250 km.

As shown earlier, several important geochemical trends in the alkaline lavas cannot be explained by crustal contamination. Specifically, the following observations are not easily explained by invoking interaction with melts from the lower crust: 1) the "contaminant" should have K/Rb ratios in the range of oceanic basalts, increase the arc signature (Ba/Nb, Ba/Ce, K/Nb), the Zr/Nb ratios, and diminish Ti content, K/Ba and Rb/Ba ratios in the alkaline lavas (Figures 27, 28, 29, 47, and 48), 2) the similar range of Sr and Nd isotopic ratios for lavas erupted through crust of different age, thickness and composition from west to east (Figure 31), 3) the correlation between arc signature and isotopic ratios in the alkaline lavas, and the lack of correlation between Sr isotopic ratios and abundances of SiO_2 and K, and abundance ratios of K/Ce and Rb/Sr

(Figures 36 and 37), 4) the same along strike Sr and Nd isotopic trend in the alkaline basalts as in the volcanic front lavas (Figure 31), and 5) the variation in some incompatible element abundances and ratios, for example Zr/Ce, Ti/Zr, Ti/Nb, Nb/Y, Ce/Y and their correlation with Mg# (Figures 28c, 29, 46 and 49).

Also, previously we gave several lines of evidence that show that melting of a single source cannot explain the chemical signature of the alkaline basalts. A "two source" model is required to explain:

a) the across arc variation in major and incompatible element content, incompatible element abundance ratios and Pb, Sr and Nd isotopic composition, during the time interval Pleistocene-Holocene (Volcanic Front-Buta Ranquil-Los Volcanes-Llancanelo-Nevado Group II), which shows a west to east decrease in the arc signature (Figures 24, 25, 26, 28 abc, 29, 31, 32, 33); and b) the observed temporal correlation between arc signature, isotopic ratios, and incompatible element abundance in Los Volcanes lavas, Llancanelo lavas, and the changes observed from Hypersthene to Group I and to Group II lavas in Nevado area (Figures 35, 36, 38, 39, 40, 41, 42, 46, 49).

More complex petrogenetic models have been proposed for the across arc geochemical variations: McCulloch and Gamble (1991) and Woodhead et al (1993) postulate a depletion of high field strength elements in the mantle wedge by previous melting events associated with the formation and evolution of a back arc spreading system. Following the same idea for the SVZ, we test this model using Ti/Zr versus Nb/Y abundance ratios in primitive lavas (MgO>7%) from the volcanic front and back arc areas (Figure 46), assuming that the slab component did not modify the HFSE concentration in the mantle wedge. Melts generated from mantle sources progresively depleted by previous melt extractions should have decreasing Nb/Y and increasing Ti/Zr abundance ratios toward the volcanic front area. Figure 46 shows that although the Nb/Y abundance ratios decrease toward the volcanic front lavas, Ti/Zr abundance ratios display the same range of variation as those from the back arc lavas. Moreover, the increase in Ba/Nb from east to west would be associated with the increase of the slab component in a mantle source progressively more depleted toward the volcanic front by previous melt extraction. If this hypothesis were true, we would observe an inverse correlation between Ba/Nb (indicative of the flux of fluids coming from the slab and HFSE abundance (indicative of the extent of melting). Figure 50 shows an inverse correlation of Ba/Nb with Ti in primitive lavas from the volcanic front and back arc. In contrast, there is no clear correlation between the degree of melting indicated by the decrease of Nb or Zr contents and the flux of slab component (Ba/Nb ratios). This is opposite to what we expect, where the mantle should be progressively more depleted in Nb and Zr than Ti, assuming again that the slab component would not modify the HFSE concentration.

The trends in figure 50 are also inconsistent with west to east decreases in the amount of fluid

derived from the subducted slab and extent of melting (the first model of Hickey et al., 1986), because this model cannot explain the HFSE variation; i.e., when comparing Zr content and Ba/Nb abundance ratios in Planchon primitive lavas with those from the Los Volcanes area, it is clear that the Ba/Nb ratios differ by a factor of 3.5 but both groups have similar Zr contents. Although, progressive depletion of the mantle source coupled with increasing fluid flux toward the volcanic front may have played an important role in the chemistry of lavas across the arc (e.g., the negative correlation between Ba/Nb ratios and Ti contents, the incresing Ba/Nb, Zr/Nb and decreasing Nb/Y toward the volcanic front lavas), this model cannot explain some geochemical variations (for example, the range in Ti/Zr in the volcanic front lavas, and the lack of correlation between flux of the slab component, Ba/Nb, and extent of melting indicated by Nb or Zr content across the arc). Therefore, progressive mantle depletion by successive melt extraction from back arc to volcanic front coupled with increasing flux of fluids coming from the slab is not enough to explain the across arc chemical variation, and additional processes are required to explain these geochemical variation.

Stolper and Newman (1994) consider the mantle wedge as a chromatographic column, where the H_2O-rich fluid/melt coming from the slab (slab component), migrates through the wedge interacting with it via ion exchange and/or producing precipitation or dissolution of mineral phases in the mantle. In this concept, the length of the mantle column necessary to equilibrate the slab component with the initial mantle composition will be inversely proportional to the global partition coefficient of the element. For example, moderately incompatible elements (Ti, Y) will require a shorter mantle column to reach equilibrium with the initial mantle composition than highly incompatible elements (Nb, Ce). Moreover, the H_2O-rich slab component may cause a decrease in the MgO and FeO content in the basalts with increasing degrees of melting; that is, increasing the flux of water will increase the extent of melting and will expand the stability volume for olivine, promoting the formation of melt with higher SiO_2, lower FeO and MgO and lower incompatible element abundance. There is a competition between the effect of water, expanding the stability volume of olivine, which will reduce the normative olivine in the basalts, and increasing the degree of melting, which will increase the normative olivine in the basalts (Stolper and Newman 1994). A similar process was invoked by Kelemen et al. (1990, 1994), who consider that mantle-melt reaction processes could be responsible for the depletion of HFSE in arc magmas and the formation of high MgO andesites. As McKenzie (1984), Navon and Stolper (1987), McKenzie and O'Nions (1991), and Stolper and Newman (1994) proposed, if only two end members are involved in a chromatographic process, the magmatic output from the system can appear to require many mixing components and an unnecessarily complex model. For example, interaction of mantle progressively depleted by previous melting coupled with increasing H_2O-rich fluid coming from the slab and increasing melting toward the volcanic front could give a possible explanation to

why the arc signature (Ba/Nb) inversely correlate with Ti content but does not correlate with Nb or Zr abundances (Figure 50). In a chromatographic process involving the slab component and melt passing through the mantle wedge, the moderately incompatible elements (Ti, Y) will reach the equilibrium with the initial mantle composition before the highly incompatible elements (Nb, Ce). Therefore, in this case, Ti may be a better indicator of the extent of depletion of the mantle source than Nb or Zr.

Hickey et al., (1986), (in their second model) consider the existence of a depleted mantle wedge (MORB), and an enriched mantle component (OIB) whose abundance incresed toward the back-arc. They suggested that the enriched mantle component could be the subcontinental mantle lithosphere, which is assumed to be thicker toward the back arc. For continental margins the subcontinental lithosphere is a potential contributing geochemical reservoir (Allegre et al 1982, Hawkesworth et al 1983, Pearce 1983). In Japan Ebihara et al 1984, Nohda and Wasserburg 1986, Nohda et al 1988 observed the occurrence of secular variation in magma source composition beneath the back arc side of NE Japan. Nohda et al. (1988), attributed this variation to the injection of geochemically depleted asthenosphere into the preexisting mantle wedge during opening of the Japan Sea. They proposed a substantial role for the subcontinental upper mantle in introducing the enriched geochemical characteristics of the trench side magma. Hawkesworth and Ellam (1989) and Hawkesworth et al (1991) indicate that the subcontinental mantle can have enough concentration of LILE such that the melt could become enriched in these elements as it ascends through and equilibrates with the mantle. The thickening of the lithospheric mantle and the smaller degree of melting in the back arc than in the volcanic front, could made the effect of the lithospheric mantle more important in the back arc area. We consider that the enriched mantle component is not necessarily in the lithospheric mantle, but could be part of the heterogeneous asthenospheric mantle that forms the mantle wedge as was suggested by Morris and Hart, (1983). This heterogeneity in the mantle wedge may be the responsible for the across arc variation and the lack of correlation between the arc signature (Ba/Nb) and the degree of melting (Zr, Nb or Ce). An heterogeneous mantle wedge could produce melts with variable composition depending on the proportion of the mantle reservoir sampled during different extent of melting. For example, it is possible that the lower extent of melting in the back arc produces melts only from the enriched component in the mantle wedge, but higher extents of melting would produce melts from both (enriched and depleted) mantle components.

In summary, in order to explain the spatial geochemical variation in the SVZ (36^{o} S), we consider two possible processes a) the existence of an heterogeneous mantle wedge or a contribution from an enriched component in the lithosphere as pointed out by Hickey et al, (1986), which influence the composition not only of the back arc basalts, but also those of the volcanic front lavas; or b) the existence of a variable flux across the arc of a H_2O-rich slab component and

melt, which migrated through a progressively depleted mantle wedge toward the volcanic front suffering different extents of chromatographic interaction.

VI.6.1 Nevado Group I lavas. Arc - Back Arc transition?. Evidences for temporal changes in the condition of melting and in the mantle source composition.

Nevado Group I is an important group of alkaline lavas which indicates a transitional change between the hypersthene normative lavas and Group II basalts from Nevado area. Hypersthene normative and Group I lavas are older lavas (Pliocene-early Pleistocene), which have strong arc signature. Although they are compositionally more similar to the volcanic front basalts, they erupted far from the volcanic front (≈ 250 km). Figures 46 and 49 shows that Mg# correlates positively with Nb/Y, Ce/Y, Ce/Nb and negatively with Ti/Nb, Ti/Zr and Zr/Nb in the primitive lavas (MgO > 7%) from Group I. This variation not only separates Nevado Group I from Group II but also shows that the variation within Group I could not be explained by fractionation or accumulation of olivine, clinopyroxene or plagioclase, or by melting from a homogeneous mantle source, or by crustal contamination, because the samples with high Mg# have similar to higher incompatible element (Nb, Ce, Zr and P) abundances than samples with low Mg# (Figure 51). One extreme of Group I has high Mg#, Ce, Nb, P and Zr and low Ti and Y, and the other extreme has low Mg#, Ce, Nb, P and Zr and high Ti and Y. Also, the variability in the abundance of an element increases with its incompatibility. For example, Ce and Nb display larger increases from low to high Mg# than Zr. In this way, we observe a small variation in Zr for strong variation in Ce/Y in Nevado Group I (Figure 29 and 52). A very important point is that almost the same type of variations are observed in Planchon and some Tatara-San Pedro primitive basalts (>7% MgO) (Figures 29, 46, 49, 52).

A possible explanation for the geochemical variation in Group I lavas is a progressive change in source composition and conditions of melting with time. This compositional variation represents a gradual change from lavas with low Mg# and low (Nb, Ce, Zr, P)/(Ti, Y) abundance ratios, indicative of either high extent of melting or a depleted mantle source and more representative of volcanic front magmatism, to lavas with high Mg# and high (Nb, Ce, Zr, P)/(Ti, Y), indicative of either low extent of melting or an enriched mantle source, and more characteristic of the back arc lavas. Assuming that the mantle wedge is heterogeneous, as previously stated, a change in the flux of fluids coming from the slab may produce a change in the composition of the melts depending on the proportion of the different mantle reservoirs sampled during different extent of melting. With decreasing age the Nevado lavas clearly reflect a decrease in the flux of fluid coming from the slab. This decrease is indicated by the temporal change from the formation

of stratovolcanoes (Pelado, Plateado and Nevado) during the Mio-Pliocene, similar in composition to those in the present volcanic front, followed by hypersthene normative basalts with strong arc signature erupted closer to the strato-volcanoes, and later by monogenetic cinder cones with eruptions of Ne-normative alkaline lavas with arc signature (Group I) during the late Pliocene-early Pleistocene, to Ne-normative alkaline lavas without the arc signature (Group II) during the Pleistocene. Also, we showed earlier that the geochemical variations between Nevado Group I and Group II lavas reflects a change in source composition. Therefore, the transitional change in composition of Group I lavas indicates a gradual variation in the mantle source that was sampled by decreasing extent of melting produced by a decreasing slab component flux with time

VI.7. CHANGING THE "SLAB COMPONENT FLUX" WITH TIME

The temporal change in isotopic ratios, and incompatible element abundance ratios in all the studied volcanic fields, but principally in Nevado area, indicates important variations in the mantle source composition and in the melting regime with time (Figures 35, 37, 38, 39, 40, 41, 42). These temporal geochemical trends may be associated with changes in subduction of the Nazca plate. Present-day along strike changes in the dip of the subducting Nazca plate provide an example of how magmatism is related to gradual variation in the angle of subduction (Barazangi and Isacks, 1976). For example, to the north of the area of study, the gradual change from volcanism in the Central Volcanic Zone (16-28^{o} S) to the lack of recent volcanismin in the "flat slab" segment (28-33^{o}) is associated to a gradual variation in the angle of subduction from about 30^{o} to almost horizontal in the CVZ-"flat slab" segment transition (Barazangi and Isacks, 1976). Moreover, in both of these areas important temporal changes in the condition of subduction of the Nazca plate from Miocene to present-day have been associated with temporal changes in the geochemical characteristics of the lavas (Kay et al., 1987; 1988; 1991; and Coira et al., 1993).

Several models have been proposed to explain the variable subduction angle along the Andes. Nur and Ben Avraham (1983, 1989) proposed that the subduction of aseismic ridges leads to a decreasing angle of subduction; for example, the spatial association of the Juan Fernandez ridge and the "flat slab" segment (Barazangi and Isacks, 1976). In contrast, Cahill and Isacks (1992) are skeptical of this interpretation because the La Perdida ridge, a more substantial bathymetric feature than the Juan Fernandez ridge, is been subducted at the most steeply dipping portion of the Central Andes Wadati-Benioff zone. Moreover, Cahill and Isacks (1992) consider that attributing decreases in subduction angle to subduction of younger oceanic lithosphere is also unsatisfactory, because beneath central Chile the opposite correlation is seen; to the south of the Nazca ridge a decrease in the age of the oceanic lithosphere from 50 to 40 Ma. is associated to the steepening of the subducting angle. Bevis and Isacks (1984), Cahill and Isaks (1992) postulated, based on

flexures rather than tears in the Nazca plate produced by geometric accommodation to the arcuate shape of the leading edge of the South American plate. For example, the change in the shape of the edge of South American plate from concave to convex seaward will produce flexures in the Nazca plate from convex to concave upward.

Isacks (1988) postulated that the change in the plate margin shape is related to variable shortening in the Andes foreland. This change in shortening implies different subduction rates along the plate margin. The total convergence rate between South America and Nazca plate is the sum of the subduction and shortening rate. In other words, increasing shortening rate in the upper plate is associated with decreasing the subduction rate. Therefore, because the rate of convergence is roughly constant along the plate boundary (the pole of rotation being 70° to 85° distant), along strike variations in shortening of the continental plate (whatever the cause of this variation), are compensated by variations in the subduction rate (Cahill and Isacks, 1992). Thus, subduction angle and rate are controlled in part by tectonic processes occurring in the continental plate.

Dewey and Lamb (1992) investigated the pattern of active (last 5 Ma.) tectonics in the Andes between 49° S to 5° N, which lie in the obliquely convergent plate boundary zone between oceanic and continental lithosphere. In agreement with Cahill and Isacks (1992), they consider that the plate slip vector is the sum of all displacement, strain and rotation. Dewey and Lamb (1992) found that the pattern of active tectonics shows remarkable geografical variations in the way in which the plate slip vector is partitioned into displacement and strain. The sector between 39° and 34° S, which includes the area of our study, is considered by Dewey and Lamb (1992), as a tectonically transitional area between different styles of partitioning of the slip vector to the south and north of this area. To the south (39° to 47° S) the slip vector is partitioned into roughly orthogonal Benioff zone slip and both dextral shear and dextral slip Liquine-Ofqui fault system. In contrast, to the north (34° to 20° S) the slip vector is partitioned into Benioff zone slip and Andean crustal shortening. The transitional area (39° to 34° S) is a cross strike dextral transfer which deflect the Chile trench and the volcanic arc, and absorbs the shortening contrast between the southern and northern sectors. It is important to notice that this transitional area has a gradual increase in crustal thickness from 35 km at 39° S to 55-60 km at 33° S (Hildreth and Moorbath, 1988), which is consistent with a transition in styles of deformation from south to north. Moreover, this tectonically transitional area overlaps with the geochemically transitional area described by Stern et al, (1991) where alkaline basalts with arc signature are interspersed with arc stratovolcanoes and occupy both intra-arc as well as back-arc tectonic environment, which contrasts to the more southerly Patagonian alkaline basalt province (south of 39° S), where the alkaline basalts are in the back arc well behind the volcanic front stratovolcanoes.

Can this geophysical, geological and geochemical evidence be combined to explain the geochemical temporal variations in the studied volcanic fields, principally the Nevado area? For

example, the Nevado area is characterized by a temporal change from: a) Miocene strato-volcanoes with calcalkaline lavas similar to the current volcanic front lavas; b) a Pliocene strato-volcano with high K_2O calcalkaline lavas; c) late Pliocene-early Pleistocene hypersthene normative basalts erupted closely associated with the strato-volcanoes; d) from the late Pliocene- early Pleistocene to Pleistocene monogenetic cinder cones with eruptions of Ne-normative alkaline lavas with an arc geochemical signature ; and e) Pleistocene Ne-normative alkaline lavas without the arc signature.

Muñoz et al. 1989, Muñoz and Stern 1989, Bermudez and Delpino 1989 consider the transitional area, between 35° and 39° S, as part of a Plio-early Pleistocene "volcanic front" that migrated westward to its current location, followed by intra arc extensional events since the early Pleistocene, perhaps, caused by subduction of younger oceanic lithosphere. In contrast, Ramos (per. com. 1993) maintains that there is no structural or geophysical evidence in favor of intra-arc extension, but that extensional fractures and transcompressional basins are a result of the subduction related east-west compression. Cahill and Isacks (1992) did not observe consistent variation between subduction angle and the age of the subducting plate, and Dewey and Lamb (1992) did not observe evidence of intra-arc extension, but found poorly developed young deformation on the foreland side of the plate boundary zone, with the slip vector partitioned into the forearc deformation and Benioff slip vector; therefore, the intra-arc extension appears unlikely.

Based on stratigraphic analysis of Neogene sedimentation, southwest of Malargüe, Kraemer and Zulliger, (per. com., 1994), consider at least three periods of crustal shortening (E-W), with the formation of a thrust and fold belt; the last compressive event assigned to the late Pliocene. There is no indication of compression or extension during the Quaternary, which indicates an important change in the tectonic conditions of the area. All the evidence indicates that a change in the subduction regime and in the tectonic conditions of the continental lithosphere happened during the period from late Tertiary to early Quaternary. This evidence indicates an important change in the shortening rate in the continental plate; i.e., formation of a thrust and fold belt in the Miocene to late Pliocene followed by absence of deformation during the Quaternary. Following the model of Cahill and Isacks (1992), the decrease in the rate of shortening must be compensated by an increase in the subduction rate at a constant rate of convergence. It is important to mention that the models for calculating the rate of convergence, always require a time period sufficient for a reasonable number of magnetic anomalies ($\approx$ 3 Ma for NUVEL-1, DeMets et al., 1990). For the interval of time we are working with (late Pliocene-Present) the number of anomalies are few and a constant rate of convergence is an approximation. Moreover, if the Nazca plate is flexed rather than torn between the transitional area and the "flat slab segment", the shallowing of the subducted plate since the Miocene in the "flat slab" segment (Kay et al., 1991, 1989, 1988) will produce a contemporaneous steepennig of the subduction angle in the adjacent areas to the north (northern Puna) and south (transitional area) of the "flat slab" segment. Coira et al, (1993) found in the

magmatism of the northern Puna evidence for a steepening subducting angle for the same period of time. Therefore, for the zone of our study (within the transitional area, 35°-37°), we consider that the temporal geochemical variation in the lavas may be related to changes in subduction angle caused by the decreasing angle of subduction in the "flat slab" segment to the north, and an increase in the rate of subduction caused by the decrease in the rate of shortening in the continental plate, fom the Miocene-late Pliocene to the Quaternary.

How can temporal variations in the angle or rate of subduction affect the composition of the lavas? Spiegelman and McKenzie (1987), developed a simple 2-D model for melt extraction at subduction zones. They derived an analytical solution for corner flow in a constant porosity melt-saturated porous media. They concluded that if the dimensionless percolation velocity (wo/Uo, where wo is percolation velocity and Uo is subduction velocity) of fluid passing through the mantle wedge is below a "critical value", slab-derived fluids will be carried down by the matrix and the interaction with the mantle wedge will be restricted to the volcanic front area. In this case, there will be no arc signature behind the front because of the absence of slab derived fluids in that area. In contrast, if the dimensionless percolation velocity is above the critical value, the slab-derived fluid will pass through the mantle wedge, and the arc signature will be detected in the basalts erupted behind the front. The critical value for the dimensionless percolation velocity (wo/Uo) is a function of the angle of subduction (ß), velocity of subduction (Uo), matrix porosity (ø), magmatic volume flux per length of trench, density and shear viscosity of solid and melt (rs, rm, h, μ respectively). The simple model predicts that the volcanic front should show slab and shallow melting signature, while the magmatism behind the arc should show signs of deeper melting with or without slab signature. The distance behind the arc where this compositional change in the lavas occurs (Lt) depends on the angle of subduction (ß) and length scale of extraction (L). Therefore, to test this model we need the following data: a) angle of subduction near the plate junction, b) geochemical data as a function of position behind the arc, c) the subduction rate, and d) the magmatic flux per unit of length of arc. If Lt can be determined through a sampled traverse across the arc and the flux per length of trench is known, then constraints can be placed on wo/Uo (Figure 53). In our case (between 36° and 37° S.) we assume that the distance behind the arc where this compositional change in the lavas occurs (Lt) is on the order of ≈ 50 Km. The estimated angle of subduction near the plates junction is ≈ 25-30° (Cahill and Isacks, 1992). The present subduction rate is estimated in ≈ 9-11 cm/year (mean 10 cm/year), (Minster and Jordan, 1978). Estimation of the maximum eruptive rates per km of arc length for the past 1 million year for the volcanic front (Planchon-Co Azul) is in the order of 6.5 km^3/km Ma (Hildreth and Moorbath 1991). Using these data we make inferences about the present dimensionless percolation velocity (wo/Uo) (Figure 53 point a). The figure shows that presently fluids coming from the slab will not reach the back arc and the area behind the arc will be "disconnected" from the slab (no arc signature). This inference

is concordant with Nevado Group II lavas (Pleistocene) that lack an arc signature. During the Miocene-late Pliocene to Quaternary there was a change in Nevado area from an arc geochemical signature to no arc signature consistent with an steepening subduction angle in the transitional area due to the decreasing angle of subduction in the "flat slab" segment and/or an increase in the rate of subduction because of a decrease in the rate of shortening in the continental plate. Therefore we assumed a rate of subduction 2 to 3 cm/year slower in the Miocene-late Pliocene than in the Quaternary. Application of the Spiegelman-McKenzie (1987) model has two objectives: a) to evaluate if the temporal variation in the lavas could be related to a change in the condition of subduction, and b) to determine how large a change in subduction conditions is required to produce the observed temporal variation in the alkaline basalts. In any case, the model is a first approximation to understanding the relation between arc signature and subduction regime. We keep all the variables constant except the velocity of subduction, which is assumed $\approx$ 3 cm/year slower ($\approx$ 7 cm/year) during the Miocene-late Pliocene than the present rate ($\approx$ 10 cm/year). The result of this variation in the rate of subduction is a change from no arc signature for the Quaternary alkaline lavas (disconnected in Figure 53 point a) to Plio-Pleistocene alkaline lavas with arc signature erupted behind the front (connected in Figure 53 point b). The terms connected or disconnected indicate whether lavas erupted behind the volcanic front had a contribution from fluids coming from the slab (arc signature). To visualize the shape of the fluid and matrix streamlines in our case, we apply the analytical solution from Spiegelman and McKenzie (1987). Figure 54 clearly shows the change in the fluid streamlines with time if a change in the rate of subduction of 3 cm/year happened during the late Pliocene-Quaternary transition. Also, we could consider small changes in the angle of subduction (from 2 to 3°) during this period, which would produce the same change in the fluid streamlines. What this model is pointing out is that the subduction conditions for the Andes between 36° and 37° S. is close to the limit between connected and disconnected regime (Figure 54). Therefore, small changes in these conditions could produce variation in the path of the fluid streamlines and therefore temporal changes in the composition of the lavas erupted on and behind the volcanic front.

VII. CONCLUSIONS

Several different models have been proposed to explain the geochemical characteristics of the volcanic front lavas and the compositional variations along and across the arc in the SVZ. For example, the MASH process of Hildreth and Moorbath, (1988) and source-region contamination of Stern, (1991b). Also, Hickey et al. (1986), in a short transect across the volcanic front, consider that the west to east variation in the composition of the basaltic lavas may have been

caused either by lower degree of mantle melting, due to the smaller contribution of fluids from the slab, or by a greater imput from a thicker subcontinental lithosphere to the east. The absence of primitive basalts in the volcanic front is the major obstacle in assessing the relative roles of these alternative mechanisms in the generation of Andean lavas.

In this work we focus on alkaline basalts erupted at varying distances (300-500 km from the trench), behind the volcanic front between 35°-37°S. The study of the primitive alkaline basalts, which have strong arc signatures and erupted behind the volcanic front through distinct terranes of different ages (Precambrian to late Paleozoic), provides the necessary elements to evaluate the relative role of crustal contamination and mantle source composition in the generation of the volcanic front lavas.

The composition of the volcanic front and back-arc lavas indicates that although crustal contamination cannot be ruled out, there are difficulties with it as an explanation for both, the compositional variation in the most primitive lavas from the volcanic front and the across arc geochemical variation. For example, in the alkaline lavas the correlation between arc signature (Ba/Nb, Ba/Ce) and Sr, Nd and Pb isotopic composition is indicative of a slab derived contribution. Also, the alkaline basalts not only have similar Sr and Nd isotopic ratios to those of the volcanic front lavas, but they also show the same along strike isotopic trend as the volcanic front lavas.

In the different alkaline basalt volcanic fields we were able to identify a temporal variation in the composition of the alkaline lavas. Considering the period Pliocene to Prehistoric, the oldest lavas are hypersthene normative. These basalts have a composition similar to the volcanic front lavas, consistent with higher degree of melting at lower pressure than the alkaline lavas, except for the case of Buta Ranquil basalts, where young hypersthene normative lavas are the result of mixing between the alkaline lavas and basaltic andesites from the strato-volcanoe Tromen. In general, the temporal trend is defined by a change from hypersthene to Group I nepheline normative lavas, characteized by an increase in the concentration of incompatible elements, both groups with strong arc signature and high Sr, Pb and low Nd isotopic ratios to younger nepheline normative lavas, Group II, with weaker arc signature, and lower Sr, Pb and higher Nd isotopic ratios. Although the change from older lavas with strong arc signature to younger lavas with weak arc signature is transitional in time, the period of time that best represents this temporal change is during late Pliocene-early Pleistocene. The temporal variation in the composition of the alkaline lavas is a clear evidence of temporal change in the composition of the mantle source and in the melting regime. Based on the application of the simple 2D model for the corner flow in the subduction zone (Spiegelman and McKenzie, 1987), we consider that the temporal variation in the back arc lavas ranging from high arc signature to low arc signature during the period late Pliocene-early Pleistocene could be related to small variation in the condition of subduction (rate and/or angle of

subduction) of the Nazca plate along the SVZ (35°-37° S) during that period of time.

Considering the period of time ranging from middle Pleistocene to Prehistoric, the across arc variation in major element composition could be explained if the alkaline lavas reflect a decrease in the degree of melting, and an increase in the depth of magma segregation. Also, for the same period of time the Pb isotopic ratios and the incompatible element ratios characteristic of an arc signature decrease toward the back-arc. This evidence is consistent with across arc chemical variations produced by decreasing the degree of mantle melting coupled with smaller contribution of fluids from the slab toward the back-arc.

Although, progressive depletion of the mantle source coupled with increasing fluid flux toward the volcanic front may have played an important role in the chemistry of lavas across the arc, this model cannot explain the variations in Nb, Zr, Ti, Y, P and Ce abundances and ratios. The systematics of incompatible element abundances and ratios involving high field strength elements (Nb, Zr, Ti), Y, P and Ce and the correlation between those ratios and Mg# clearly indicate that neither primitive lavas erupted behind the arc (Nevado volcanic field and Llancanelo volcanic field lavas) nor primitive lavas (MgO >7 %) from the volcanic front (Planchon) could be explained as originating from a homogeneous source by a combination of melting, fractional crystallization and crustal contamination. We suggest that these geochemical characteristics could be explained by one or both of two different processes: a) the existence of two different mantle sources, one an enriched source (OIBS), not necessarily the lithospheric mantle, which would influence the composition not only of the back-arc basalts but also the volcanic front lavas, and b) a change from back arc to volcanic front characterized by progressive mantle depletion by successive melt extraction coupled with increasing the flux of slab component (fluid and/or melt), where the mantle wedge works as a chromatographic column. In this case, the fluids coming from the slab would suffer ion exchange reaction and/or mineral phase precipitation or dissolution in the mantle wedge (Kelemen, 1994, Stolper and Newman 1994). These two possibilities agree almost completely with the two potential processes proposed by Hickey et al., 1986.

REFERENCES

Allégre C., Dupré B., Richard P., Rousseau D. and Brooks C., Subcontinental versus suboceanic mantle II. Nd-Sr-Pb isotopic comparison of continental tholeiites with mid-oceanic ridge tholeiites, and the structure of the continental lithosphere. Earth Planet. Sci Lett. 57:25-34, 1982.

Anderson A., Swihart G., Artioli G. and Geiger C., Segregation vesicles, gas filter-pressing, and igneous differentiation. J. of Geology 92:55-72, 1984.

Arculus R. and Johnson R., Island-arc magma sources: A geochemical assessment of the roles of slab-derived components and crustal contamination. Geochem. J., 15:109-133, 1981.

Arculus R. and Powell R.; Source component mixing in the regions of arc magma generation. J.Geophys. Res. 91:5913-5926, 1986.

Barazangi M. and Isacks B., Spatial distribution of earthquakes and subduction of the Nazca plate beneath South America. Geology 4:686-692, 1976.

Barker D. and Eggler D., Fractionation path of Atka (Aleutians) high alumina basalts. Constraints from phase relations. J. of Volc. and Geoth. Res. 18:387-409, 1983.

Bermudez A., Sierra del Nevado. El Limite oriental del arco volcanico Neogeno entre los 35°30'-36°00' S , Argentina. VI Congreso Geologico Chileno 318-322, 1991.

Bermudez A., Basaltos Alcalinos Terciarion en la Sierra de Palauco. Provincia de Mendoza. Argentina. Internat. Symp. Andean Volc. in the X Congreso Geologico Argentino, Tucuman, 238-242, 1987.

Bermudez A. and Delpino D., La provincia basaltica Andino Cuyana. Asoc. Geol. Argentina, Rev., XLIV: 318-322, 1989.

Bermudez A. and Delpino D., La provincia Andino Cuyana (35°-37° L.S.) Argentina. Internat. Symp. Andean Volc. in the X Congreso Geologico Argentino, Tucuman, 243-245, 1987.

Best M., Migration of hydrous fluids in the upper mantle and potassium variation in calc-alkaline rocks. Geology 3:429-432, 1975.

Bevis M. and Isacks B., Hypocentral trend surface analysis: Probing the geometry of Benioff zones. J. Geophys. Res. 89:6153-6170, 1984.

Cahill T. and Isacks B., Seismicity and Shape of the Subducted Nazca Plate. J. Geophys. Res. 97:17503-17529, 1992

Caminos R., Cordillera Frontal. In: Segundo Simposio de Geologia Regional Argentina. Córdoba, Academia Nacional de Ciencias 1:397-453, 1979.

Charrier R. and Vicent J., Liminary and geosynclinal Andes: major orogenic phases and synchronical evolution of the central and Magallean sector of the Argentine-Chilean Andes. Intern. Upper Mantle Proj. Conf. on Solid Earth Problem., Bs. As.,2:451-470, 1972.

Coira B., Kay M. S. and Viramonte J., Upper Cenozoic magmatic evolution of the Argentine Puna - A model for changing subduction geometry. Internat. Geol. Review 35 (8): 677-720, 1993

Criado-Roque P., Subcuenca de Alvear (Provincia de Mendoza). In: Segundo Simposio de Geologia Regional Argentina. Córdoba, Academia Nacional de Ciencias 1:811-836, 1979.

Criado-Roque P. and Ibañez G., Provincia Geologica SanRafaelino-Pampeana. In: Segundo Simposio de Geologia Regional Argentina. Córdoba, Academia Nacional de Ciencias 1:837-869, 1979

Davidson J., Ferguson K., Colucci M. and Dungan M., The origin and evolution of magmas from the San Pedro-Pellado volcanic complex, S. Chile: multicomponent sources and open system evolution. Contrib. Mineral. Petrol., 100:429-445, 1988.

Delpino D., Erupciones basalticas a traves de fracturas de retroarco Andino (35°-36° L.S.), Mendoza, Argentina. Internat. Symp. Andean Volc. in the X Congreso Geologico Argentino, Tucuman, 233-237, 1987.

DeMets C., Gordon R., Argus D and Stein S., Current plate motions. Geophys. J. Int. 101:425-478, 1990.

Dewey J. and Lamb S., Active tectonics of the Andes. Tectonophysics 205:79-95, 1992.

Dungan M. and others, The life history of an Andean volcano. Eos, Transactions, Am. Geophys. Union, vol. 73 38:406-407, 1992.

Drake R. , Chronology of Cenozoic igneous and tectonic events in the central Chilean Andes-latitudes 35°30' to 36°S. J. Volcanol Geothermal Res 1:265-284, 1976.

Drake R., Vergara M., Munizaga F. and Vicente J., Geochronology of Mesozoic-Cenozoic magmatism in central Chile, Lat. 31-36S. Earth Sci. Rev. 18:353-363, 1982.

Ebihara M., Nakamura Y., Wakita H., Kurasawa H. and Konda T., Trace element compositions of Teriary volcanic rocks of northeast Japan. Geochem. J. 18:287-295, 1984.

Falloon T. and Green D. Anhydrous partial melting of peridotite from 8 to 35 kb and the petrogenesis of MORB. J. of Petrology, special lithosphere issue 379-414, 1988.

FalloonT., Green D., Hatton C. and Harris K., Anhydrous partial melting of a fertile and depleted peridotite from 2 to 30 kb and application to basalt petrogenesis. J of Petrology 29-6:1257-1282, 1988.

Ferguson K., Dungan M., Davidson J. and Colucci M., The Tatara-San Pedro volcano, 36 S, Chile: A chemically variable, dominantly mafic magmatic system. J. Petrol. in press, 1992.

Frey F., Green D. and Roy S., Integrated models of basalt petrogenesis: a studyof quartz tholeiites to olivine melilitites from southeastern Australia utilizing geochemical and experimental petrological data. J. of Petrology 19:463-513, 1978.

Frey F., Gerlach D., Hickey R., Lopez-Escobar L. and Munizaga-Villaricencio F., Petrogenesis of the Laguna del Maule volcanic complex, Chile (36 S). Contrib. Mineral. Petrol. 88:133-149, 1984.

Fuji T. and Scarfe C., Composition of liquids coexisting with spinel lherzolite at 10 kbar and the genesis of MORBs. Contrib. Mineral. Petrol. 90:18-28, 1985.

Futa K. and Stern C., Sr and Nd isotopic and trace elemet compositions of Quaternary volcanic centers of the southern Andes. Earth Planet. Sci Lett. 88:253-262, 1988.

Gaetani G., Grove T. and Bryan W., The influence of water on the petrogenesis of subduction related igneous rocks. Nature 365:332-334, 1993.

Gerlach D., Frey F., Moreno Roa H. and Lopez Escobar L., Recent volcanism in the Puyehue-Cordon Caulle region, southern Andes, Chile (40 S); petrogenesis of evolved lavas. J. Petrol. 29:333-382, 1988.

Gill J., Shoshonitic and OIB alkali basalts in Fiji. Eos, Trans. AGU, 67:1277, 1986.

Gill J., Orogenic andesites and plate tectonics. Springer, Berlin-New York, 390 p., 1981.

Gladney E. and Roelandts I., Compilation of elemental concentration data for USGS BHVO-1, MAG-1, QLO-1, RMG-1, SCO-1, SDC-1, SGR-1 and STM-1. Geostands. Newsletter 12:253-362, 1988.

Gonzalez Ferran O. and Vergara M., Reconocimiento Geologico de la Cordillera de los Andes entre los paralelos 35^{o} y 38^{o} L.S. Univ. Chile, Inst. Geol. Publ. 24:1-119, 1962.

Green D., The origin of basaltic and nephelinitic magmas. Trans. Leicester Lit. Phil. Soc. 64:28-54, 1970.

Gust D. and Perfit M., Phase relations of a high-Mg basalt from the Aleutians island arc. Implications for primary island arc basalts and high-Al basalts. Contrib. Mineral. Petrol. 97:7-18, 1987.

Hanus V. and Vanek J., Morphology of the Andean Wadati-Benioff zone, andesitic volcanism, and tectonic features of the Nazca plate. Tectonophysics 44:65-77, 1978.

Hart S., A large scale isotopic anomaly in the southern hemisphere mantle. Nature 309:753-757, 1984.

Hart S. and Dunn T., Experimental cpx/melt partitioning of 24 trace elements. Contrib. Mineral. Petrol. 113:1-8, 1993.

Hauri E., Geochemical and fluid dynamic investigations into the nature of chemical heterogeneity in the Earth's Mantle. Ph.D. Thesis MIT-WHOI joint program, 1992.

Hawkesworth C. and Ellam R., Chemical fluxes and wedge replenishment rates along recent destructive plate margins. Geology 17:46-49, 1989

Hawkesworth C., Hergt J., Ellam R. and McDermontt F., Element fluxes associated with subduction related magmatism. Philos. Trans. R. Soc. London Ser. A 335:393-405, 1991.

Hawkesworth C., Erlank A., Marsh J., Menzies M. and Van Calsteren P., Evolution of continental lithosphere: evidence from volcanics and xenoliths in southern Africa. In Hawkesworth C and Norry M. (eds.) Continental basalts and mantle xenoliths. Shiva, Nantwich, pp 111-138, 1983.

Herron E., Cande S. and Hall B., An active spreading center collides with a subduction zone: A geophysical survey of the Chile Margin triple junction. Geol. Soc. Amer. Memoir 154:683-701, 1981.

Herron E., Chile margin near lat. 38 S: Evidence for a genetic relationship between continental and marine geologic features or a case of curious coincidences? In L. Kulm et al. (eds) Nazca plate: Crustal formation and Andean convergence. Geol. Soc. Amer. Memoir 154:755-760, 1981.

Hickey R., Frey F., Gerlach D. and Lopez Escobar L., Multiple source for basaltic arc rocks from central south Chile: Trace element and isotopic evidence for contributions from subducted oceanic crust, mantle, and continental crust. J. Geophys. Res. 91:5963-5983, 1986.

Hickey-Vargas R., Moreno Roa H., Lopez Escobar L. and Frey F., Geochemical variation in Andean basaltic and silicic lavas from the Villarrica-Lanin volcanic chain (39.5 S): An evaluation of source heterogeneity, fractional crystallization and crustal assimilation. Contrib. Mineral. Petrol. 103:361-386, 1989.

Hickey-Vargas R., Andean Magma: Peeled or MASHed?. Nature 350:381-382, 1991.

Hildreth W., Grunder A. and Drake R. , The Loma Seca tuff and the Calabozos Caldera: A major ash-flow and caldera complex in the southern Andes of central Chile. Geol. Soc. Am. Bull., 95:45-54, 1984.

Hildreth W. and Moorbath S., Crustal contributions to arc magmatism in the Andes of central Chile. Contrib. Mineral. Petrol. 98:455-489, 1988.

Hildreth W. and Moorbath S., Reply to comment on "Crustal contributions to arc magmatism in the Andes of central Chile". Contrib. Mineral. Petrol. 108:247-252, 1991.

Hildreth W. and Drake R., Volcan Quizapu, Chilean Andes. Bull. Volcanol. 54:93-125, 1992.

Hussong D., Edwardt P., Johnson S., Campbell J. and Sutton G., Crustal structure of the Peru-Chile trench: 8°-12°S. In Sutton G. et al. (eds) The Geophysics of the Pacific Ocean Basin and its Margin. Amer. Geophy. Union, Geophysical Monograph 19:71-85, 1976.

Hofmann A. and White W., Ba, Rb, Cs in the Earth's mantle. Z. Naturforsch., 38a, 256-266, 1983.

Isacks B., Uplift of the Central Andes plateau and bending of the Bolivian orocline. J. Geophys. Res. 93: 3211-3231, 1988

Jackes P. and White A., Composition of island arcs and continental growth. Earth Planet. Sci Lett. 12:224-230, 1970

Jordan T., Isacks B., Allmendinger R., Brewer J., Ramos V. and Ando C., Andean tectonics related to geometry of subducted nazca plate. Geol. Soc. Am. Bull. 94: 341-361, 1983.

Kay R. Geochemical constraints on the origin of Aleutian magmas. In Talwani M., Pitman III W. (eds) Island Arcs, Back-arc Basins, and Deep-sea Trenches. Amer. Geophy. Union, Maurice Ewing Series 1:229-242, 1977

Kay R., Volcanic arc magmas: Implications of a melting-mixing model for elemet recycling in the crust-upper mantle system. J. Gelolgy 88:497-522, 1980

Kay S. M., Maksaev V., Moscoso R., Mpodozis C. and Nasi C., Probing the Andean evolving lithosphere: Mid-Late tertiary magmatism in Chile (29-30.5 S) over the modern zone of subhorizontal subduction. J. Geophys. Res. 92:6173-6189, 1987.

Kay S. M., Maksaev V., Moscoso R., Mpodozis C., Nasi C. and Gordillo C., Tertiary Andean magmatism in Argentina and Chile between 28-33°S; Correlation of magmatic chemistry with a changing Benioff zone. J. South Amer. Earth Sc.1:21-38, 1988.

Kay S. M., Mpodozis C., Rasmos V. and Munizaga F., Magma source variations for mid-late Tertiary magmatic rocks associated with a shallowing subduction zone and thickening crust in the central Andes (28 to 33°S). In Harmon R and Rapela C.(eds): Andean Magmatism and its tectonic setting. Geol. Soc. Amer. spec. paper 265:113-137, 1991.

Kay S. M., Ardolino A., Franchi M. and Ramos V. Constraints on the origin of Somuncura plateau from the distribution and geochemistry of its mafic volcanic rocks. Draft for publication 1993.

Kelemen P., Johnson K. Kinzler R. and Irving A., High-field-strength element depletions in arc basalts due to mantle-magma interaction. Nature 345:521-524, 1990.

Kelemen P, Shimizu N. and Dunn T., Relative depletion of niobium in some arc magmas and the continental crust: Partitioning of K, Nb, La, and Ce during melt/rock reaction in the upper

mantle. Earth Plan. Sc. Lett. 1994.

Kinzler R. and Grove T., Primary magmas of mid-ocean ridge basalts 1.Experiments and Methods. J. Geophys. Res. 97:6907-6926, 1992

Kinzler R. and Grove T., Primary magmas of mid-ocean ridge basalts 2. Applications. J. Geophys. Res. 97:6907-6926, 1992.

Kinzler R. and Grove T., Corrections and further discussion of the primary magmas of mid-ocean ridge basalts, 1 amd 2. J. Geophys. Res. 98:22,339-22,3347, 1992

Kinzler R., Mantle melting processes at the spinel-garnet transition (17-21 kb). EOS transactions, AGU abstracts Vol 73 - 43, 1992.

Kulm L, Schweller W. and Masias A. A preliminar analysis of the subduction processes along the Andean continental margin, 6° to 45° S., In Talwani M. and Pitman III W. (eds), Island Arcs, Back-arc Basins, and Deep-sea Trenches. Amer. Geophy. Union, Maurice Ewing Series 1:229-242, 1977

Kushiro I and Yoder H., Silicate systems including a vapor phase. Annual 1967-1968 repot from the Carnegie Inst. Geophy. Lab. 1520:153-158, 1968.

Kushiro I., Liquidus relations in the system Forsterite-Diopside-Silica-H2O at 20 kbs. Annual 1967-1968 repot from the Carnegie Inst. Geophy. Lab. 1520:158-161, 1968.

Llambias E., Geología y petrografía del volcán Payún Matrú. Acta Geologíca Lilloana 8:265-310, 1966.

Llambias E., Dandefer J., Palacios M. and Brogioni N., Las rocas ígneas cenozóicas del volcán Domuyo y áreas adyacentes. VII Congreso Geológico Argentino, Neuquen, Actas 2:569-584, 1978.

Llambias E., Palacios M. and Dandefer J., Las Erupsiones Holocenas del volcán Tromen (Provincia del Neuquen), y su significado en un perfil transversal E-O a la Latitud 37°S. Quinto Congreso Latinoamericano de Geologia, Argentina, Actas 3:537-545, 1982.

Libourel G., Boivin P. and Biggar G., The univariant curve liquid=forsterite+anorthite+diopside in the system CMAS at 1 bar: solid solutions and melt structure. Contrib. Mineral. Petrol. 102:406-421, 1989.

Lopez Escobar L. and Frey F., Rocas volcanicas Cuaternarias de Chile central-sur (33-41 S): Modelos petrogeneticos sugeridos por las Tierras Raras. Congreso Geologico Chileno II: F223-F255, 1976.

Lopez Escobar L., Frey F. and Vergara M., Andesites and high -alumina basalts from the central-south Chile High Andes: Geochemical evidences bearing on their petrogenesis. Contrib. Mineral. Petrol. 63:199-228, 1977

Lopez Escobar L., Vergara M. and Frey F., Petrology and geochemistry of lavas from Antuco volcano, a basaltic volcano of the southern Andes (37.25 S). J. Volcanol. Geoth. Res. 11:329-352, 1981.

Luhr J., Allan J., Carmichael I., Nelson S. and Hasenaka T., Primitive calc-alkaline and alkaline rock types from the western Mexican volcanic belt. J. Geophys. Res. 94 b4:4515-4530, 1989.

MacDonald G. and Katsura T., Chemical composition of Hawaiian lavas. J. of Petrology 5:82-133, 1964.

McCulloch M. and Gamble J., Geochemical and geodynamical constraints on subduction zone magmatism. Earth Plan. Sc. Lett. 102:358-374, 1991.

McKenzie D.,The generation and compaction of partially molten rock. J. Petrol. 25:713-765, 1984.

McKenzie D. and O'Nions R., Partial melt distribution from inversion of rare earth element concentrations. J. Petrol 32:1021-1091, 1991.

McMillan N., Harmon R., Moorbath S., Lopez Escobar L. and Strong D.; Crustal sources involved in continental arc magmatism: A case study of volcan Mocho-Choshuenco, southern Chile. Geology 17:1152-1156, 1989.

Minster J. and Jordan T., Present-day plate motions. J. Geophys. Res. 83:5331-5354, 1978.

Miyashiro A., Volcanic rock series in island arcs and active continental margins. Am. J. Sci. 274:321-355, 1974.

Morrice M. and Gill J., Spatial patterns in the mineralogy of island arc magma series: Sangihe arc, Indonesia. J. Volcanol. Gotherm. Res. 19:135-165, 1986.

Morris J., Leeman W. and Tera F., The subducted component in island arc lavas: constraints from Be isotope and B-Be systematics. Nature 344:31-36, 1990.

Morris J. and Hart S., Isotopic and incompatible element constraints on the genesis of island arc volcanics from Cold Bay and Amak island, Aleutians, and inplications for Mantle structure. Geoch. Cosm. Acta 47:2015-2030, 1983.

Muñoz J., Stern C., Bermudez A., Delpino D., Dobbs M. and Frey F., El volcanismo Plio-Cuaternario a traves de los 34-39°S de los Andes. Revista de la Asociacion Geologica Argentina XLIV (1-4): 270-286, 1989.

Muñoz J. and Stern C., Alkali volcanism within the section of the Andean magmatic belt between 34-39oS where intraarc extension and volcanism are ocurring. Eos, Transact. Am. Geophys. Union 67-44:1281, 1986.

Muñoz J., Stern C., Bermudez A., Delpino D. and Dobbs M., El volcanism Plio-Cuaternario a traves de los 38-39S de los Andes. Actas X Congres. Geol. Argentino 4:199-201, (1987).

Muñoz J. and Stern C., Quaternary volcanic belt of the southern South America continental margin: Transverse structural and petrochemical variations across the segment 38-39 S. J. South Am. Earth Sci. 1:(2) 147-161, 1988.

Muñoz J. and Stern C., Alkaline magmatism within the segment 38-39 S. of the Plio-Quaternary volcanic belt on the southern South American continental margin. J. Geophys. Res. 94:4545-4560, 1989.

Naar D. and Hey R., Recent Pacific-Easter-Nazca plate motions. Copyright 1989 by Int. Union Geod. Geophys. AGU pp 9-30, 1989.

Nakamura Nakamura E., Campbell I. and Sun S., The influence of subduction processes on the geochemistry of Japanese alkaline basalts. Nature 316:55-58, 1985.

Nakamura E., Campbell I., McCulloch M. and Sun S., Chemical geodynamics in the back arc region around the Sea of Japan: Implications for the genesis of alkaline basalts in Japan, Korea and China. J. Geophys. Res. 94 B4: 4634-4654, 1989.

Navon O. and Stolper E., Geochemical consequences of melt percolation: The upper mantle as a chromatographic column. J. Geol. 95:285-307, 1987.

Niemeyer H. and Muñoz J., Geologia de la Hoja Laguna de las Lajas. SERNOGEOMIN, Serv., Carta Geol. Chile 57, 1-52, 1983.

Nohda S., Tatsumi Y., Otofuji Y., Matsuda T. and Ishizaka K., Asthenospheric injection and back-arc opening: isotopic evidence from northeast Japan. Chem. Geol. 68:317-327, 1988.

Nohda S. and Wassemburg G., Trends of Sr and Nd isotopes through time near the Japan Sea in northeastern Japan. Earth Plan. Sc. Lett. 78:157-167, 1986.

Nur A. and Ben-Avraham Z., Volcanic gaps due to oblique consumption of aseismic ridges. Tectonophysics 99:355-362, 1983.

Nur A. and Ben-Avraham Z.,. Oceanic plateau and the Pacific Ocean margins. In Ben-Avraham Z. (ed.) The evolution of the Pacific Ocean margins, Oxford Univ. Press, New York :3-19, 1989.

O'Donnell T. and Presnal D., Chemical variations of the glass and mineral phases in basalts dredged from 25o-30o N along the mid-Atlantic ridge. Am J. Sci. 280:845-868, 1980.

O'Hara M., Non-primary magmas and dubious mantle plume beneath Iceland. Nature 243:507-508, 1973.

Pearce J., Role of the subcontinental lithosphere in magma genesis at active continental margins. In: Continental basalts and mantle xenoliths, Hawkesworth C. and Norry M. (eds.), Shiva, Nantwich, pp 231-249, 1983.

Peccerillo A. and Taylor S., Geochemistry of Eocene calc-alkaline volcanics rocks from the Kastamonu area, nothern Turkey. Contrib. Mineral. Petrol. 58:63-81, 1976.

Perfit M., Gust D., Bence A., Arculus R. and Taylor S., Geochemical characteristics of island-arc basalts: Implications for mantle sources. Chem. Geol. 30:227-256, 1980.

Plafker G., Alaskan earthquake of 1964 and Chilean earthquake of 1960: Implications for arc tectonic. J. Geophys Res. 77:901-925, 1972

Polansky J., Rasgos geomorfologicos del territorio de la Provincia de Mendoza. Inst. Invest. Econ. Tecn. Mendoza 4:5-10, 1954.

Presnal D. Dixon J., O'Donnell T., Brenner N., Schrock R. and Dycus D.,

Liquidus phase relations on the join diopside-forsteritew-anorthite from 1 atm. to 20 kbar. Their bearing on the generation and crystallization of basaltic magmas. Contrib. Mineral. Petrol. 66:203-220, 1978.

Ramos V., Niemeyer H., Skarmeta J. and Muñoz J., Magmatic evolution of the austral Patagonian Andes. Earth Sci. Rev. 18:411-443, 1982.

Ramos V., Estructura. In: Relatorio Geologia y recursos naturales del Neuquen. Actas VII Congreso Geologico Argentino, Buenos Aires 1:99-118, 1978.

Ramos V., Jordan T., Almendinger R., Mpodozis C., Kay S., Cortes J. and Palma M, Paleozoic terranes of the central Argentine-Chilean Andes. Tectonics 5:855-880, 1986.

Ramos V., Late Proterozoic-Early Paleozoic of South America: a collisional history. Episodes 11:3:168-174, 1988.

Ramos V., Patagonia: un continente Paleozoico a la deriva. Actas IX Congreso Geologico Argentino II:311-325, 1984.

Rapela C., Spalletti L., Merodio J. and Aragon E., Temporal evolution and spatial variation of early Tertiary volcanism in the Patagonian Andes (40-42.30 S.). J. South Am. Earth Sci. 1:75-88, 1988.

Rapela C. and Kay S., Late Paleozoic to recent magmatic evolution of northern Patagonia. Episodes 11-3:175-182, 1988.

Rhodes J. M., Homogeneity of lava flows; chemical data for historic Mauna Loan eruptions. Proc. Lunar Planet. Sci. Conf. 13th, Part 2, 86:7111-7129, 1983.

Sato H., Nickel content of basaltic magmas: identification of primary magmas and a measure of the degree of olivine fractionation. Lithos 10:113-120, 1977.

Sack R., Walker D. and Carmichael I., Experimental petrology of alkaline lavas: constraints on cotectics of multiple saturation in natural basic liquids. Contrib. Mineral. Petrol. 96:1-23, 1987.

Scholl D., Marlow M. and Cooper A., Sediment subduction and offscraping at Pacific margins. In Talwani M. and Pitman III W. (eds), Island Arcs, Back-arc Basins, and Deep-sea Trenches. Amer. Geophy. Union, Maurice Ewing Series 1:199-210, 1977

Shaw D., Trace element fractionation during anatexis. Geoch Cosmoch. Acta 34: 237-243, 1970.

Sigmarsson O., Condomines M. Morris J. and Harmon R., Uranium and ^{10}Be enrichments by fluids in Andean arc magmas. Nature 346:163-165, 1990.

Sisson T. and Grove T., Experimental investigation of the role of water in calk-alkaline differentiation and subduction zone magmatism. Contrib. Mineral. Petrol. 113:143-166, 1993a.

Sisson T. and Grove T., Temperatures and water contents of low-MgO high-alumina basalts. Contrib. Mineral. Petrol. 113:167-184, 1993b.

Skewes M. and Stern C., Petrology and geochemistry of alkali basalts and ultramafic inclusions from Pali-Aike volcanic field in the southern Chile and the origin of the Patagonian plateau lavas. J. Volcanol. Geotherm. Res. 6: 3-25, 1979.

Snedecor G. and Cochram W., Statistical methods. VI edition, Iowa State University Press, 1979.

Spigelman M.and McKenzie D., Simple 2-D models for melt extraction at mid-ocean ridges and island arcs. Earth Planet. Sci. Letts. 83:137-152, 1987.

Stauder W., Mechanism and spatial distribution of Chilean earthquakes with relation to subduction of the oceanic plate. J. Geophys. Res. 78:5033-50611973

Stern C., Futa K., Saul S and Skewes M., Nature and evolution of the subcontinental mantle lithosphere below southern South America. Rev. Geol. Chilena 27:41-53, 1986 a

Stern C., Futa K., Muehlenbachs K., Dobbs F., Muñoz J., Godoy E. and Charrier R. Sr, Nd, Pb and O isotopie composition of late Cenozoic volcanics, northermost SVZ (33-34o S). In : Harmon R. and Barreiro B. (eds) Andean Magmatism, Chemical and Isotopic Constraints. Shiva Publ. Co, Cheshire (U.K.), pp 96-105, 1984 a.

Stern C., Futa K. and Muehlenbachs K., Isotope and trace element data for orogenic andesites from the austral Andes In : Harmon R. and Barreiro B. (eds) Andean Magmatism, Chemical and Isotopic Constraints. Shiva Publ. Co, Cheshire (U.K.), pp 31-46, 1984 b.

Stern C., Frey F., Zartman R., Peng Z. and Kyser T., Trace element and Sr, Nd, Pb and O isotopic composition of Pliocene and Quaternary alkalic basalts of the Patagonian Plateau lavas of southernmost South America. Contrib. Minerl. Petrol. 104:294-308, 1990.

Stern C., Comment on "Crustal contributions to arc magmatism in the Andes of central Chile" by Hildreth W. and Moorbath S. Contrib. Mineral. Petrol. 108:241-246, 1991 a.

Stern C., Role of subduction erosion in the generation of Andean magmas. Geology 19:78-81, 1991b.

Swift S . and Carr M., The segmented nature of the Chilean seismic zone. Phys. Earth. Planet. Interiors 9:183-191, 1974.

Stolper E., A phase diagram for mid-ocean ridge basalts: preliminary results and implications for petrogenesis. Contrib. Mineral. Petrol. 74:13-27, 1980.

Stolper E. and Newman S., The role of water in the petrogenesis of Mariana trough magmas. Earth Plan. Sc. Lett. 121:293-325, 1994

Sun S-S and McDonough W., Chemical and isotopic systematics of oceanic basalts: implications for mantle composition and processes. In: Magmatism in the ocean basins, Saunders A. and Norry M. (eds.). Geol. Soc. Spec. Publ. 42:313-345, 1989.

Takahashi E. and Kushiro I., Melting of dry peridotite at high pressures and basalt magma genesis. Am. Min. 68:859-879, 1983.

Tatsumi Y, Sakuyama M., Fukuyama H. and Kushiro I., Generation of arc basalt magmas and thermal structure of the mantle wedge in subduction zones. J. Geophys Res 88:5815-5825, 1983.

Tatsumi Y., Migration of fluid phases and genesis of basalt magmas in subduction zones. J. Geophys. Res. 94:4697-4707, 1989.

Tatsumi Y., Hamilton D. and Nesbitt R., Chemical characteristics of fluid phase released from a subducted lithosphere and origin of arc magmas. Evidence from high-pressure experiments and natural rocks. J. Volcanol. Geotherm. Res. 29:293-309, 1986.

Taylor S. and Lennan, S., The continental crust: its composition and evolution. Blackwell Sc. Pub. 312 pp

Tormey D., Frey F. and Lopez Escobar L., Geologic history of the active Azufre-Planchon-Peteroa volcanic center (35.15 S) with implications for the origin of compositional gaps. Asoc. Geol. Argentina Rev. XLIV: (1-4) 420-430, 1989.

Tormey D., Hickey-Vargas R., Frey F. and Lopez Escobar L., Recent lavas from the Andean volcanic front (35-42 S): Interpretation of along-strike compositional variations. GSA Special Paper 265, Andean Magmatism (eds., Harmon R. and Rapela C., pp 57-77, 1991)

Tormey D., Frey F. and Lopez Escobar L., Geochemistry of the active Azufre-Planchon-Peteroa volcanic center (35.15 S) in the Andean Southern Volcanic Zone: Evidence for multiple sources and processes in constructing a Cordillean Arc magmatic system. J. Petrol., in press, 1993.

Turner J. and Baldis B., La estructura transcontinental del sector septentrional de la Patagonia. VII Congreso Geologico Argentino II:225-238, 1979.

Valencio D., Linares E. and Creer K., Paleomagnetismo y edades geologicas de algunos basaltos terciarios y cuartarios de Mendoza y Neuquen. IV Jornadas Geologicas Argentinas II:255-278, 1986.

Van der Plas L. and Tobi A., A chart for judging the reliability of point counting results. Am. J. Sci. 263:87-90, 1967.

Verma S. and Nelson S., Isotopic and trace element constraints on the origin and evolution of alkaline and calc-alkaline magmas in the northwestern Mexican volcanic belt. J. Geophys. Res. 94 B4: 4531-4544, 1989.

White W. and Patchett J., Hf-Nd-Sr isotopes and incompatible elemet abundances in island arcs: Implications for magma origins and crust-mantle evolution. Earth Planet. Sci. Lett. 67:167-185, 1984

Woodhead J., Eggins S. and Gamble J., High field strength element systematics in island arc and back arc basin basalts: evidence for multi-phase melt extraction and a depleted mantle wedge. Earth Plan. Sc. Lett. 114:491-504, 1993.

Schairer J. and Yoder H., The nature of residual liquids from crystallization, with data on the system Nepheline-Diopside-Silica. Am. J. Sci. 258.A:273-283, 1960.

Yrigoyen M., Cordillera Principal. In: Segundo Simposio de Geologia Regional Argentina. Córdoba, Academia Nacional de Ciencias 1:651-694, 1979.

Zindler A. and Hart S., Chemical geodynamics. Ann. Rev. Earth Plan. Sci. 14: 493-571, 1986

ACCURACY AND PRECISION EVALUATION

Precision

Alkaline Basalts

	Range in %	Precision in %
SiO2	0-0.4	0.14
TiO2	0-0.7	0.24
Al2O3	0-0.5	0.19
Fe2O3*	0-0.5	0.18
MnO	0-1.4	0.43
MgO	0-0.7	0.24
CaO	0-0.5	0.15
Na2O	0-3.0	0.76
K2O	0-0.8	0.21
P2O5	0-0.8	0.28

Precision

Alkaline Basalts

	Range in %	Precision in %
Rb	0-4.5	0.910
Sr	0-0.6	0.230
Ba	0-2.5	0.690
V	0-3.5	0.860
Cr	0-20	1.310
Ni	0-20	3.680
Zn	0-1.3	0.375
Ga	0-6.0	1.890
Y	0-3.4	0.980
Zr	0-5.0	0.350
Nb	0.1-10	1.280
Ce	0-14	2.420

Accuracy

	BHVO-1a	BHVO-1b Mean
Rb	11+/-2	19.960
Sr	403+/-25	403.770
Ba	139+/-14	135.610
V	317+/-12	287.130
Cr	289+/-22	286.170
Ni	121+/-2	142.700
Zn	105+/-5	109.950
Ga	21+/-2	21.410
Y	27.6+/-1.7	24.860
Zr	179+/-21	179.750
Nb	19+/-2	19.960
Ce	39+/-4	37.180

Table 1: BHVO-1a: Consensus literature values with one standard deviation for USGS standard rock BHVO-1 from Gladney and Roelandts (1988)
BHVO-1b: Mean of 50 analyses of USGS standard rock BHVO-1 that were obtained in this study concurrently with 135 XRF analyses for trace elements of Alkaline Basalts samples at University of Massachusetts, Amherst.
The range in major and trace elements indicate the range of 1 sigma standard deviation (in %) of duplicated XRF analyses for 135 samples.
Precision is the mean (in %) of standard deviation for all (135) duplicate analyses

TABLE 2: MODAL ANALYSES OF ALKALINE BASALTS

East Nevado 1	Olivine (1-3.4 mm)	Plagioclase (1-5 mm)	Clinopyroxene (1-2.5 mm)	Olivine/Pheno	Plagioclase/Pheno	Clinopyroxene/Pheno
15-1	9.0	4.0		69.2	30.8	0.0
15-2	14.0			100.0	0.0	0.0
15-3	12.0		1.0	92.3	0.0	7.7
15-4	10.0			100.0	0.0	0.0
15-5	16.0		8.0	69.2	0.0	30.8
15-6	13.0			100.0	0.0	0.0
15-7	13.0		7.0	65.0	0.0	35.0
15-8	12.5		8.0	61.0	0.0	39.0
16-1	7.0			100.0	0.0	0.0
16-2	9.0			100.0	0.0	0.0
16-3	10.0			100.0	0.0	0.0
16-4	5.0	3.0		62.5	37.5	0.0
16-5	7.5			100.0	0.0	0.0
16-6	7.5			100.0	0.0	0.0
16-8	8.0			100.0	0.0	0.0
16-9	10.0			100.0	0.0	0.0
17-1	10.0			100.0	0.0	0.0
East Nevado 2						
16-7	3.0	2.0		60.0	40.0	
West Nevado 1						
18-1	15.0			100.0	0.0	0.0
18-2	15.0			100.0	0.0	0.0
18-3	15.0			100.0	0.0	0.0
18-4	15.0			100.0	0.0	0.0
18-5	12.5			100.0	0.0	0.0
18-6	15.0			100.0	0.0	0.0
18-7	10.0			100.0	0.0	0.0
18-8	12.5			100.0	0.0	0.0
18-9	12.5			100.0	0.0	0.0
18-10	8.0			100.0	0.0	0.0
18-11	7.0			100.0	0.0	0.0
18-12	5.0			100.0	0.0	0.0
18-13	8.0			100.0	0.0	0.0
20-1	15.0			100.0	0.0	0.0
20-2	12.0			100.0	0.0	0.0
LV-55	16.0			100.0	0.0	0.0
West Nevado 2						
17-2	9.0			100.0	0.0	0.0
19-1	1.0	2.0	5.0	12.5	25.0	62.5
19-2	2.0	1.0	5.0	25.0	12.5	62.5
19-3	2.0		5.0	28.6	0.0	71.4
19-4	2.0		5.0	28.6	0.0	71.4
19-5	12.0			100.0	0.0	0.0
19-6	14.0			100.0	0.0	0.0
19-7	12.0			100.0	0.0	0.0
19-8	12.0			100.0	0.0	0.0
19-9	12.5			100.0	0.0	0.0
19-10	12.5			100.0	0.0	0.0
19-11	10.0			100.0	0.0	0.0
27-150384	15.0			100.0	0.0	0.0
MJA (flow)	11.0			100.0	0.0	0.0
66-83	3.0	8.0	17.0	10.7	28.6	60.7
6-110384	10.0	8.0	12.0	33.3	26.7	40.0
24-140384	13.0			100.0	0.0	0.0
West Llancanello 1						
21-5	10.0			100.0	0.0	0.0
21-7	12.0			100.0	0.0	0.0
West Llancanello 3						
21-1	3.0			100.0	0.0	0.0
21-2	2.0			100.0	0.0	0.0
21-3	5.0			100.0	0.0	0.0
21-4	10.0			100.0	0.0	0.0

1= Late Pliocene-Early Pleistocene 2= Pleistocene 3= Late Pleistocene-Early Holocene
4= Holocene 5= Prehistoric

The Modal analyses were performed by point-counting standard thin sections with 500 to 1000 points per section. Only phenocryst proportions are reported. "Pheno" represent total phenocryst proportion.

TABLE 2: MODAL ANALYSES OF ALKALINE BASALTS

West Llancanelo 3	Olivine (1-3.4 mm)	Plagioclase (1-5 mm)	Clinopyroxene (1-2.5 mm)	Olivine/Pheno	Plagioclase/Pheno	Clinopyroxene/Pheno
21-6*	1.0			100.0	0.0	0.0
21-8	1.0			100.0	0.0	0.0
Los Volcanes 1						
24-2	7.5			100.0	0.0	0.0
26-2	4.0			100.0	0.0	0.0
26-3	10.0			100.0	0.0	0.0
Los Volcanes 2						
22-6	7.5			100.0	0.0	0.0
22-7	10.0			100.0	0.0	0.0
22-8	7.0			100.0	0.0	0.0
25-11	10.0	17.5		36.4	63.6	0.0
26-4	10.0	6.0		62.5	37.5	0.0
Los Volcanes 3						
22-5	10.0	10.0	3.0	43.5	43.5	13.0
23-7		1.0		0.0	100.0	0.0
23-13	5.0	25.0		16.7	83.3	0.0
23-14	9.0	5.0		64.3	35.7	0.0
24-6	3.0	17.5	1.0	14.0	81.4	4.7
25-6	4.0			100.0	0.0	0.0
25-7	5.0			100.0	0.0	0.0
22-9	7.0	10.0		41.2	58.8	0.0
25-4	3.0	12.5		19.4	80.6	0.0
25-5	6.5	5.0		56.5	43.5	0.0
25-10	8.0	15.0		34.8	65.2	0.0
Los Volcanes 4						
23-1	3.0	10.0	5.0	16.7	55.6	27.8
23-2	2.0	2.0	3.0	28.6	28.6	42.9
23-3	4.0	2.0	3.0	44.4	22.2	33.3
24-7	4.0	10.0	4.0	22.2	55.6	22.2
25-8	8.0	18.0	2.0	28.6	64.3	7.1
25-9	3.0	5.0		37.5	62.5	0.0
26-1	8.0	18.0	5.0	25.8	58.1	16.1
26-5	5.0	13.0		27.8	72.2	0.0
26-6	8.0	17.0	5.0	26.7	56.7	16.7
26-7	2.0	20.0		9.1	90.9	0.0
Los Volcanes 5						
23-4	3.0	7.0	1.0	27.3	63.6	9.1
23-9	1.0	10.0	4.0	6.7	66.7	26.7
23-12	7.0	22.0		24.1	75.9	
24-1(A)	7.5	10.0	3.0	36.6	48.8	14.6
24-1(B)	5.0	10.0	2.0	29.4	58.8	11.8
24-3*	8.0	10.0		44.4	55.6	0.0
24-4	7.0	10.0	1.0	38.9	55.6	5.6
24-5	5.0	10.0	1.0	31.3	62.5	6.3
25-1	8.0	17.0	1.0	30.8	65.4	3.8
25-2	10.0	17.0		37.0	63.0	0.0
Vn. Barrancas 1						
26-10	0.0	0.0	0.0			0.0
26-11	16.0	13.0		55.2	44.8	
26-12	15.0	8.0		65.2	34.8	0.0
Buta Ranquil 3						
27-1	2.0	18.0	1.0	9.5	85.7	4.8
27-2	7.0	15.0	7.0	24.1	51.7	24.1
27-3	4.0	17.0	7.0	14.3	60.7	25.0
27-4	8.0	16.0		33.3	66.7	0.0
27-6	5.0	10.0		33.3	66.7	0.0
Cochiquito 3						
26-8	10.0			100.0	0.0	0.0
28-9	11.0			100.0	0.0	0.0
El Manzano 3						
22-4	15.0			100.0	0.0	0.0

1= Late Pliocene-Early Pleistocene 2= Pleistocene 3= Late Pleistocene-Early Holocene
4= Holocene 5= Prehistoric

The Modal analyses were performed by point-counting standard thin sections with 500 to 1000 points per section. Only phenocryst proportions are reported. "Pheno" represent total phenocryst proportion.

TABLE 3 ALTERATION AND CRYSTAL SORTING

	SiO2	TiO2	Al2O3	Fe2O3*	MnO	MgO	CaO	Na2O	K2O	P2O5
EL ESCORIAL										
23-2 Flow	48.52	1.91	17.02	10.36	0.16	6.08	10.00	3.79	1.42	0.46
23-3 Flow Vesicular	49.41	1.94	17.25	10.18	0.16	5.61	9.72	3.96	1.54	0.49
23-1 Flow	48.84	1.99	17.23	10.52	0.16	5.88	9.73	3.88	1.50	0.48
24-7 Flow	49.39	2.00	17.34	10.36	0.16	5.44	9.44	3.92	1.59	0.50
23-2 and 23-3 at 5 km from the vent; 23-1 at 7 km ; and 24-7 at 12 km										
Analytical errors in %										
23-1 Flow	0.10	0.00	0.20	0.20	0.30	0.00	0.00	0.60	0.00	0.30
23-2 Flow	0.10	0.00	0.30	0.00	0.40	0.70	0.00	0.60	0.20	0.20
24-7 Flow	0.20	0.30	0.20	0.20	0.00	0.30	0.20	0.80	0.20	0.40
23-3 Flow Vesicular	0.00	0.10	0.10	0.10	0.90	0.30	0.10	0.20	0.30	0.10
23-1 Flow	48.84	1.99	17.23	10.52	0.16	5.88	9.73	3.88	1.50	0.48
23-2 Flow	48.52	1.91	17.02	10.36	0.16	6.08	10.00	3.79	1.42	0.46
24-7 Flow	49.39	2.00	17.34	10.36	0.16	5.44	9.44	3.92	1.59	0.50
Mean	48.92	1.97	17.20	10.41	0.16	5.80	9.72	3.86	1.51	0.48
Standard Deviation	0.44	0.05	0.17	0.09	0.00	0.33	0.28	0.07	0.08	0.02
Standard Error in %	0.90	2.68	0.96	0.90	0.61	5.66	2.87	1.71	5.63	4.71
23-2 Flow	48.52	1.91	17.02	10.36	0.16	6.08	10.00	3.79	1.42	0.46
23-3 Flow Vesicular	49.41	1.94	17.25	10.18	0.16	5.61	9.72	3.96	1.54	0.49
Mean	48.96	1.92	17.13	10.27	0.16	5.85	9.86	3.88	1.48	0.48
Standard Deviation	0.63	0.02	0.16	0.12	0.00	0.34	0.20	0.12	0.08	0.02
Standard Error in %	1.28	1.14	0.94	1.18	0.00	5.73	2.05	3.19	5.67	5.06
24-7 Flow	49.39	2.00	17.34	10.36	0.16	5.44	9.44	3.92	1.59	0.50
23-3 Flow Vesicular	49.41	1.94	17.25	10.18	0.16	5.61	9.72	3.96	1.54	0.49
Mean	49.40	1.97	17.29	10.27	0.16	5.52	9.58	3.94	1.57	0.50
Standard Deviation	0.01	0.05	0.07	0.13	0.00	0.12	0.19	0.03	0.04	0.01
Standard Error in %	0.03	2.37	0.40	1.23	0.44	2.16	2.02	0.83	2.25	1.56

TABLE 3 ALTERATION AND CRYSTAL SORTING

	Rb	Sr	Ba	V	Cr	Ni	Zn	Ga	Y	Zr	Nb	Ce
EL ESCORIAL												
23-2 Flow	28.05	649.57	396.80	224.05	110.04	50.35	86.11	20.77	23.54	198.02	21.31	43.13
23-3 Flow Vesicular	29.89	651.41	416.41	215.46	83.83	39.82	86.70	21.50	24.54	212.53	22.49	47.20
23-1 Flow	28.41	663.21	406.04	218.86	97.82	47.33	83.39	20.99	24.09	203.10	22.26	46.12
24-7 Flow	31.30	673.10	438.69	212.72	74.13	38.34	86.73	21.31	24.56	220.30	24.30	49.96
23-2 and 23-3 at 5 km from the vent; 23-1 at 7 km ; and 24-7 at 12 km												
Analytical errors in %												
23-1 Flow	0.44	0.05	0.14	0.35	0.83	1.09	0.20	0.28	0.52	0.08	1.49	0.91
23-2 Flow	0.28	0.38	0.21	1.75	0.04	0.94	0.72	2.45	1.43	0.49	0.52	3.12
24-7 Flow	0.28	0.07	1.51	0.82	0.55	5.10	0.22	2.39	0.89	0.04	1.29	4.21
23-3 Flow Vesicular	0.79	0.52	0.26	0.59	3.30	4.12	0.29	0.08	0.87	0.63	1.31	1.18
23-1 Flow	28.41	663.21	406.04	218.86	97.82	47.33	83.39	20.99	24.09	203.10	22.26	46.12
23-2 Flow	28.05	649.57	396.80	224.05	110.04	50.35	86.11	20.77	23.54	198.02	21.31	43.13
24-7 Flow	31.30	673.10	438.69	212.72	74.13	38.34	86.73	21.31	24.56	220.30	24.30	49.96
Mean	29.25	661.96	413.84	218.54	94.00	45.34	85.41	21.02	24.06	207.14	22.62	46.40
Standard Deviation	1.78	11.81	22.01	5.67	18.26	6.25	1.78	0.27	0.51	11.68	1.53	3.42
Standard Error in %	6.09	1.78	5.32	2.60	19.42	13.78	2.08	1.29	2.12	5.64	6.75	7.38
23-2 Flow	28.05	649.57	396.80	224.05	110.04	50.35	86.11	20.77	23.54	198.02	21.31	43.13
23-3 Flow Vesicular	29.89	651.41	416.41	215.46	83.83	39.82	86.70	21.50	24.54	212.53	22.49	47.20
Mean	28.97	650.49	406.61	219.76	96.94	45.09	86.41	21.14	24.04	205.28	21.90	45.17
Standard Deviation	1.30	1.30	13.87	6.07	18.53	7.45	0.42	0.52	0.71	10.26	0.83	2.88
Standard Error in %	4.49	0.20	3.41	2.76	19.12	16.52	0.48	2.44	2.94	5.00	3.81	6.37
24-7 Flow	31.30	673.10	438.69	212.72	74.13	38.34	86.73	21.31	24.56	220.30	24.30	49.96
23-3 Flow Vesicular	29.89	651.41	416.41	215.46	83.83	39.82	86.70	21.50	24.54	212.53	22.49	47.20
Mean	30.60	662.26	427.55	214.09	78.98	39.08	86.72	21.41	24.55	216.42	23.40	48.58
Standard Deviation	1.00	15.34	15.75	1.94	6.86	1.05	0.02	0.13	0.01	5.49	1.28	1.95
Standard Error in %	3.26	2.32	3.68	0.90	8.68	2.68	0.02	0.63	0.06	2.54	5.47	4.02

TABLE 3 ALTERATION AND CRYSTAL SORTING

	Ba/Nb	Zr/Nb	Ce/Nb	Ce/Y	Rb/Ba	Ba/Ce	Rb/Ce	K/Rb
EL ESCORIAL								
23-2 Flow	18.62	9.29	2.02	1.83	0.07	9.20	0.65	421.44
23-3 Flow Vesicular	18.52	9.45	2.10	1.92	0.07	8.82	0.63	428.54
23-1 Flow	18.24	9.12	2.07	1.91	0.07	8.80	0.62	437.72
24-7 Flow	18.05	9.07	2.06	2.03	0.07	8.78	0.63	422.50
23-2 and 23-3 at 5 km from the vent; 23-1 at 7 km ; and 24-7 at 12 km								
Analytical errors in %								
23-1 Flow	1.63	1.57	2.40	1.43	0.58	1.05	1.35	0.44
23-2 Flow	0.73	1.01	3.64	4.55	0.49	3.33	3.40	0.48
24-7 Flow	2.80	1.33	5.50	5.10	1.79	5.72	4.49	0.48
23-3 Flow Vesicular	1.57	1.94	2.49	2.05	1.05	1.44	1.97	1.09
23-1 Flow	18.24	9.12	2.07	1.91	0.07	8.80	0.62	437.72
23-2 Flow	18.62	9.29	2.02	1.83	0.07	9.20	0.65	421.44
24-7 Flow	18.05	9.07	2.06	2.03	0.07	8.78	0.63	422.50
Mean	18.30	9.16	2.05	1.92	0.07	8.93	0.63	427.22
Standard Deviation	0.29	0.12	0.03	0.10	0.00	0.24	0.02	9.11
Standard Error in %	1.59	1.26	1.29	5.23	0.00	2.65	2.41	2.13
23-2 Flow	18.62	9.29	2.02	1.83	0.07	9.20	0.65	421.44
23-3 Flow Vesicular	18.52	9.45	2.10	1.92	0.07	8.82	0.63	428.54
Mean	18.57	9.37	2.06	1.88	0.07	9.01	0.64	424.99
Standard Deviation	0.07	0.11	0.06	0.06	0.00	0.27	0.01	5.02
Standard Error in %	0.38	1.21	2.75	3.39	0.00	2.98	2.21	1.18
24-7 Flow	18.05	9.07	2.06	2.03	0.07	8.78	0.63	422.50
23-3 Flow Vesicular	18.52	9.45	2.10	1.92	0.07	8.82	0.63	428.54
Mean	18.29	9.26	2.08	1.98	0.07	8.80	0.63	425.52
Standard Deviation	0.33	0.27	0.03	0.08	0.00	0.03	0.00	4.27
Standard Error in %	1.82	2.90	1.36	3.94	0.00	0.32	0.00	1.00

TABLE 3 ALTERATION AND CRYSTAL SORTING

	SiO2	TiO2	Al2O3	Fe2O3*	MnO	MgO	CaO	Na2O	K2O	P2O5
SANTA MARIA										
24*-3 Glassy Sample	47.18	1.89	16.64	11.27	0.17	7.61	10.11	3.22	1.25	0.46
24-5 Flow	47.19	1.91	17.52	10.94	0.17	7.02	10.67	3.35	1.23	0.45
24-1(A) Flow Vesicular	46.98	1.93	17.31	10.95	0.16	7.06	10.54	3.45	1.23	0.45
24-1(B) Flow	46.95	1.90	17.28	10.98	0.17	7.30	10.52	3.30	1.21	0.45
24-4 Bomb	47.10	1.96	17.20	11.08	0.17	7.11	10.50	3.65	1.26	0.46
24-3* is a glassy salple taken directly from a small vent in the crater; 24-5 at 1 km; 24-1 (A & B) are from the same point 5 km frm the vent.										
Analytical errors in %										
24-1(A) Flow Vesicular	0.00	0.10	0.10	0.20	0.80	0.30	0.00	1.30	0.20	0.40
24-1(B) Flow	0.10	0.40	0.10	0.10	0.00	0.30	0.20	0.10	0.00	0.00
24-5 Flow	0.30	0.40	0.40	0.30	1.00	0.10	0.30	0.70	0.40	0.50
24-4 Bomb	0.10	0.10	0.20	0.30	0.80	0.20	0.10	1.50	0.00	0.40
24*-3 Glassy Sample	0.10	0.10	0.30	0.10	0.20	0.10	0.10	0.50	0.20	0.20
24-1(B) Flow	46.95	1.90	17.28	10.98	0.17	7.30	10.52	3.30	1.21	0.45
24-5 Flow	47.19	1.91	17.52	10.94	0.17	7.02	10.67	3.35	1.23	0.45
Mean	47.07	1.90	17.40	10.96	0.17	7.16	10.59	3.33	1.22	0.45
Standard Deviation	0.17	0.00	0.17	0.03	0.00	0.20	0.10	0.04	0.01	0.00
Standard Error in %	0.37	0.22	0.98	0.26	0.00	2.74	0.96	1.17	1.10	0.94
24-1(A) Flow Vesicular	46.98	1.93	17.31	10.95	0.16	7.06	10.54	3.45	1.23	0.45
24-1(B) Flow	46.95	1.90	17.28	10.98	0.17	7.30	10.52	3.30	1.21	0.45
Mean	46.96	1.91	17.29	10.96	0.16	7.18	10.53	3.37	1.22	0.45
Standard Deviation	0.02	0.02	0.02	0.02	0.00	0.17	0.01	0.10	0.01	0.00
Standard Error in %	0.05	0.96	0.13	0.17	0.43	2.33	0.10	3.10	1.10	1.10
24-1(A) Flow Vesicular	46.98	1.93	17.31	10.95	0.16	7.06	10.54	3.45	1.23	0.45
24-4 Bomb	47.10	1.96	17.20	11.08	0.17	7.11	10.50	3.65	1.26	0.46
Mean	47.04	1.94	17.25	11.01	0.17	7.08	10.52	3.55	1.25	0.46
Standard Deviation	0.09	0.02	0.08	0.09	0.00	0.03	0.03	0.14	0.02	0.01
Standard Error in %	0.19	1.24	0.47	0.80	1.70	0.46	0.28	4.05	1.70	1.54
24-1(A) Flow Vesicular	46.98	1.93	17.31	10.95	0.16	7.06	10.54	3.45	1.23	0.45
24-1(B) Flow	46.95	1.90	17.28	10.98	0.17	7.30	10.52	3.30	1.21	0.45
24-5 Flow	47.19	1.91	17.52	10.94	0.17	7.02	10.67	3.35	1.23	0.45
Mean 1 (A-B) & 24-5	47.04	1.91	17.37	10.96	0.16	7.13	10.57	3.37	1.23	0.45
24*-3 Glassy Sample	47.18	1.89	16.64	11.27	0.17	7.61	10.11	3.22	1.25	0.46
Mean 24-1 (A-B) & 5	47.04	1.91	17.37	10.96	0.16	7.13	10.57	3.37	1.23	0.45
Mean	47.11	1.90	17.01	11.12	0.17	7.37	10.34	3.29	1.24	0.45
Standard Deviation	0.10	0.02	0.51	0.22	0.01	0.34	0.32	0.11	0.02	0.00
Standard Error in %	0.21	0.89	3.02	1.98	4.29	4.63	3.12	3.31	1.31	0.78

TABLE 3 ALTERATION AND CRYSTAL SORTING

	Rb	Sr	Ba	V	Cr	Ni	Zn	Ga	Y	Zr	Nb	Ce
SANTA MARIA												
24*-3 Glassy Sample	24.61	705.85	336.64	241.90	202.67	94.63	100.09	20.41	22.36	176.77	20.15	43.04
24-5 Flow	21.85	765.57	329.16	227.59	139.74	66.76	85.48	18.98	21.21	170.43	19.58	40.21
24-1(A) Flow Vesicular	21.81	759.40	337.28	228.96	138.12	66.64	88.10	20.76	21.64	171.47	20.36	44.23
24-1(B) Flow	21.89	755.31	324.76	223.59	141.43	75.97	89.54	19.78	21.14	167.56	19.66	42.18
24-4 Bomb	22.27	730.00	341.72	232.45	145.84	66.29	82.50	20.11	22.49	172.96	20.16	42.91
24-3* is a glassy salple taken directly from a small vent in the crater; 24-5 at 1 km; 24-1 (A & B) are from the same point 5 km frm the vent.												
Analytical errors in %												
24-1(A) Flow Vesicular	0.07	0.00	0.16	0.68	2.13	1.42	0.33	2.05	1.30	0.35	2.19	3.01
24-1(B) Flow	1.29	0.17	0.64	0.64	1.32	4.48	0.48	1.61	2.69	0.37	0.32	13.27
24-5 Flow	1.02	0.48	1.05	0.59	0.25	1.20	0.06	0.90	1.32	0.52	1.08	1.83
24-4 Bomb	0.50	0.14	0.97	1.43	0.00	0.37	0.19	0.72	0.25	0.15	0.67	0.51
24*-3 Glassy Sample	0.55	0.11	0.13	0.04	0.81	0.03	0.46	0.58	1.02	0.09	0.42	1.69
24-1(B) Flow	21.89	755.31	324.76	223.59	141.43	75.97	89.54	19.78	21.14	167.56	19.66	42.18
24-5 Flow	21.85	765.57	329.16	227.59	139.74	66.76	85.48	18.98	21.21	170.43	19.58	40.21
Mean	21.87	760.44	326.96	225.59	140.59	71.37	87.51	19.38	21.18	169.00	19.62	41.20
Standard Deviation	0.03	7.25	3.11	2.83	1.20	6.51	2.87	0.57	0.05	2.03	0.06	1.39
Standard Error in %	0.13	0.95	0.95	1.25	0.85	9.13	3.28	2.92	0.23	1.20	0.29	3.38
24-1(A) Flow Vesicular	21.81	759.40	337.28	228.96	138.12	66.64	88.10	20.76	21.64	171.47	20.36	44.23
24-1(B) Flow	21.89	755.31	324.76	223.59	141.43	75.97	89.54	19.78	21.14	167.56	19.66	42.18
Mean	21.85	757.36	331.02	226.28	139.78	71.31	88.82	20.27	21.39	169.52	20.01	43.21
Standard Deviation	0.06	2.89	8.85	3.80	2.34	6.60	1.02	0.69	0.35	2.76	0.49	1.45
Standard Error in %	0.26	0.38	2.67	1.68	1.67	9.25	1.15	3.42	1.65	1.63	2.47	3.36
24-1(A) Flow Vesicular	21.81	759.40	337.28	228.96	138.12	66.64	88.10	20.76	21.64	171.47	20.36	44.23
24-4 Bomb	22.27	730.00	341.72	232.45	145.84	66.29	82.50	20.11	22.49	172.96	20.16	42.91
Mean	22.04	744.70	339.50	230.71	141.98	66.47	85.30	20.44	22.07	172.22	20.26	43.57
Standard Deviation	0.33	20.79	3.14	2.47	5.46	0.25	3.96	0.46	0.60	1.05	0.14	0.93
Standard Error in %	1.48	2.79	0.92	1.07	3.84	0.37	4.64	2.25	2.72	0.61	0.70	2.14
24-1(A) Flow Vesicular	21.81	759.40	337.28	228.96	138.12	66.64	88.10	20.76	21.64	171.47	20.36	44.23
24-1(B) Flow	21.89	755.31	324.76	223.59	141.43	75.97	89.54	19.78	21.14	167.56	19.66	42.18
24-5 Flow	21.85	765.57	329.16	227.59	139.74	66.76	85.48	18.98	21.21	170.43	19.58	40.21
Mean 1 (A-B) & 24-5	21.85	760.09	330.40	226.71	139.76	69.79	87.71	19.84	21.33	169.82	19.87	42.21
24*-3 Glassy Sample	24.61	705.85	336.64	241.90	202.67	94.63	100.09	20.41	22.36	176.77	20.15	43.04
Mean 24-1 (A-B) & 5	21.85	760.09	330.40	226.71	139.76	69.79	87.71	19.84	21.33	169.82	19.87	42.21
Mean	23.23	732.97	333.52	234.31	171.22	82.21	93.90	20.13	21.85	173.30	20.01	42.63
Standard Deviation	1.95	38.35	4.41	10.74	44.48	17.56	8.75	0.40	0.73	4.91	0.20	0.59
Standard Error in %	8.40	5.23	1.32	4.58	25.98	21.37	9.32	2.00	3.33	2.84	0.99	1.38

TABLE 3 ALTERATION AND CRYSTAL SORTING

	Ba/Nb	Zr/Nb	Ce/Nb	Ce/Y	Rb/Ba	Ba/Ce	Rb/Ce	K/Rb
SANTA MARIA								
24*-3 Glassy Sample	16.71	8.77	2.14	1.92	0.07	7.82	0.57	422.66
24-5 Flow	16.81	8.70	2.05	1.90	0.07	8.19	0.54	468.07
24-1(A) Flow Vesicular	16.57	8.42	2.17	2.04	0.06	7.63	0.49	468.93
24-1(B) Flow	16.52	8.52	2.15	2.00	0.07	7.70	0.52	460.01
24-4 Bomb	16.95	8.58	2.13	1.91	0.07	7.96	0.52	470.43
24-3* is a glassy salple taken directly from a small vent in the crater; 24-5 at 1 km; 24-1 (A & B) are from the same point 5 km frm the vent.								
Analytical errors in %								
24-1(A) Flow Vesicular	2.35	2.54	5.20	4.31	0.23	3.17	3.08	0.27
24-1(B) Flow	0.96	0.69	13.59	15.96	1.93	13.91	14.56	1.29
24-5 Flow	2.13	1.60	2.91	3.15	2.07	2.88	2.85	1.42
24-4 Bomb	1.64	0.82	1.18	0.76	1.47	1.48	1.01	0.50
24*-3 Glassy Sample	0.55	0.51	2.11	2.71	0.68	1.82	2.24	0.75
24-1(B) Flow	16.52	8.52	2.15	2.00	0.07	7.70	0.52	460.01
24-5 Flow	16.81	8.70	2.05	1.90	0.07	8.19	0.54	468.07
Mean	16.67	8.61	2.10	1.95	0.07	7.95	0.53	464.04
Standard Deviation	0.21	0.13	0.07	0.07	0.00	0.35	0.01	5.70
Standard Error in %	1.23	1.48	3.37	3.63	0.00	4.36	2.67	1.23
24-1(A) Flow Vesicular	16.57	8.42	2.17	2.04	0.06	7.63	0.49	468.93
24-1(B) Flow	16.52	8.52	2.15	2.00	0.07	7.70	0.52	460.01
Mean	16.55	8.47	2.16	2.02	0.07	7.67	0.51	464.47
Standard Deviation	0.04	0.07	0.01	0.03	0.01	0.05	0.02	6.31
Standard Error in %	0.21	0.83	0.65	1.40	10.88	0.65	4.20	1.36
24-1(A) Flow Vesicular	16.57	8.42	2.17	2.04	0.06	7.63	0.49	468.93
24-4 Bomb	16.95	8.58	2.13	1.91	0.07	7.96	0.52	470.43
Mean	16.76	8.50	2.15	1.98	0.07	7.80	0.51	469.68
Standard Deviation	0.27	0.11	0.03	0.09	0.01	0.23	0.02	1.06
Standard Error in %	1.60	1.33	1.32	4.65	10.88	2.99	4.20	0.23
24-1(A) Flow Vesicular	16.57	8.42	2.17	2.04	0.06	7.63	0.49	468.93
24-1(B) Flow	16.52	8.52	2.15	2.00	0.07	7.70	0.52	460.01
24-5 Flow	16.81	8.70	2.05	1.90	0.07	8.19	0.54	468.07
Mean 1 (A-B) & 24-5	16.63	8.55	2.12	1.98	0.07	7.84	0.52	465.67
24*-3 Glassy Sample	16.71	8.77	2.14	1.92	0.07	7.82	0.57	422.66
Mean 24-1 (A-B) & 5	16.63	8.55	2.12	1.98	0.07	7.84	0.52	465.67
Mean	16.67	8.66	2.13	1.95	0.07	7.83	0.55	444.17
Standard Deviation	0.06	0.16	0.01	0.04	0.00	0.01	0.04	30.41
Standard Error in %	0.34	1.80	0.66	2.18	0.00	0.18	6.49	6.85

TABLE 3 ALTERATION AND CRYSTAL SORTING

	SiO2	TiO2	Al2O3	Fe2O3*	MnO	MgO	CaO	Na2O	K2O	P2O5
LAS BOMBAS										
23-4 Flow	46.71	2.16	17.22	11.34	0.17	6.66	10.94	3.48	1.20	0.40
23-9 Bomb	47.75	2.16	17.49	11.06	0.17	5.76	10.21	3.83	1.44	0.42
23-10 Bomb	47.64	2.14	17.34	11.07	0.17	5.80	10.06	3.67	1.43	0.43
23*-11 Pyroclast	47.77	2.13	17.29	10.93	0.17	5.83	10.05	3.61	1.40	0.44
Analytical errors in %										
23-4 Flow	0.10	0.20	0.40	0.00	0.30	0.00	0.40	0.20	0.80	0.40
23-9 Bomb	0.10	0.20	0.10	0.00	0.50	0.10	0.00	0.30	0.00	0.40
23-10 Bomb	0.20	0.10	0.00	1.20	0.90	0.70	0.00	0.70	0.10	0.20
23*-11 Pyroclast	0.00	0.10	0.10	0.30	1.20	0.30	0.10	0.00	0.10	0.30
23-9 Bomb	47.75	2.16	17.49	11.06	0.17	5.76	10.21	3.83	1.44	0.42
23-10 Bomb	47.64	2.14	17.34	11.07	0.17	5.80	10.06	3.67	1.43	0.43
Mean	47.69	2.15	17.41	11.06	0.17	5.78	10.13	3.75	1.43	0.43
Standard Deviation	0.08	0.01	0.11	0.01	0.00	0.03	0.10	0.11	0.01	0.01
Standard Error in %	0.16	0.69	0.63	0.08	0.00	0.53	0.98	2.96	0.54	1.66
Mean 23-9 &10	47.69	2.15	17.41	11.07	0.17	5.78	10.14	3.75	1.43	0.43
23*-11 Pyroclast	47.77	2.13	17.29	10.93	0.17	5.83	10.05	3.61	1.40	0.44
Mean	47.73	2.14	17.35	11.00	0.17	5.80	10.09	3.68	1.42	0.43
Standard Deviation	0.05	0.01	0.09	0.10	0.00	0.03	0.06	0.10	0.02	0.01
Standard Error in %	0.11	0.69	0.50	0.89	0.00	0.57	0.57	2.79	1.55	1.31
23-4 Flow	46.71	2.16	17.22	11.34	0.17	6.66	10.94	3.48	1.20	0.40
Mean 23-9 &10	47.69	2.15	17.41	11.07	0.17	5.78	10.14	3.75	1.43	0.43
Mean	47.20	2.16	17.32	11.20	0.17	6.22	10.54	3.62	1.32	0.42
Standard Deviation	0.70	0.01	0.14	0.19	0.00	0.62	0.57	0.19	0.16	0.02
Standard Error in %	1.48	0.39	0.78	1.74	1.27	9.98	5.43	5.24	12.47	3.91
23-4 Flow	46.71	2.16	17.22	11.34	0.17	6.66	10.94	3.48	1.20	0.40
23*-11 Pyroclast	47.77	2.13	17.29	10.93	0.17	5.83	10.05	3.61	1.40	0.44
Mean	47.24	2.14	17.26	11.13	0.17	6.24	10.50	3.55	1.30	0.42
Standard Deviation	0.75	0.02	0.05	0.29	0.00	0.59	0.63	0.09	0.14	0.02
Standard Error in %	1.59	1.09	0.29	2.62	1.27	9.41	5.99	2.45	10.93	5.23

TABLE 3 ALTERATION AND CRYSTAL SORTING

	Rb	Sr	Ba	V	Cr	Ni	Zn	Ga	Y	Zr	Nb	Ce
LAS BOMBAS												
23-4 Flow	18.82	674.97	298.43	251.83	105.43	59.02	89.66	20.60	21.86	156.66	18.36	35.28
23-9 Bomb	24.80	680.33	344.82	243.90	77.05	44.27	91.86	21.68	23.38	185.95	22.11	40.55
23-10 Bomb	25.06	683.09	342.53	241.32	81.29	45.09	91.75	21.29	23.37	180.61	22.55	41.15
23*-11 Pyroclast	26.54	663.02	340.29	245.21	86.93	48.76	97.08	21.00	23.60	176.70	21.24	44.41
Analytical errors in %												
23-4 Flow	1.83	0.03	1.70	0.81	1.72	4.83	0.23	3.29	1.00	0.47	2.03	1.11
23-9 Bomb	1.10	0.29	0.68	0.91	0.01	4.77	0.11	1.79	0.73	0.19	1.28	1.72
23-10 Bomb	2.37	0.21	0.29	0.20	3.31	1.69	0.17	1.14	1.38	0.31	0.10	4.40
23*-11 Pyroclast	1.13	0.18	2.04	0.90	1.76	3.48	0.04	2.73	0.47	0.56	0.56	6.21
23-9 Bomb	24.80	680.33	344.82	243.90	77.05	44.27	91.86	21.68	23.38	185.95	22.11	40.55
23-10 Bomb	25.06	683.09	342.53	241.32	81.29	45.09	91.75	21.29	23.37	180.61	22.55	41.15
Mean	24.93	681.71	343.68	242.61	79.17	44.68	91.81	21.49	23.38	183.28	22.33	40.85
Standard Deviation	0.18	1.95	1.62	1.82	3.00	0.58	0.08	0.28	0.01	3.78	0.31	0.42
Standard Error in %	0.74	0.29	0.47	0.75	3.79	1.30	0.08	1.28	0.03	2.06	1.39	1.04
Mean 23-9 &10	24.93	681.71	343.68	242.61	79.17	44.68	91.81	21.49	23.38	183.28	22.33	40.85
23*-11 Pyroclast	26.54	663.02	340.29	245.21	86.93	48.76	97.08	21.00	23.60	176.70	21.24	44.41
Mean	25.74	672.37	341.98	243.91	83.05	46.72	94.44	21.24	23.49	179.99	21.79	42.63
Standard Deviation	1.14	13.22	2.39	1.84	5.49	2.88	3.73	0.34	0.16	4.65	0.77	2.52
Standard Error in %	4.42	1.97	0.70	0.75	6.61	6.18	3.95	1.61	0.68	2.59	3.54	5.90
23-4 Flow	18.82	674.97	298.43	251.83	105.43	59.02	89.66	20.60	21.86	156.66	18.36	35.28
Mean 23-9 &10	24.93	681.71	343.68	242.61	79.17	44.68	91.81	21.49	23.38	183.28	22.33	40.85
Mean	21.88	678.34	321.05	247.22	92.30	51.85	90.73	21.04	22.62	169.97	20.35	38.07
Standard Deviation	4.32	4.77	31.99	6.52	18.57	10.14	1.52	0.63	1.07	18.82	2.81	3.94
Standard Error in %	19.75	0.70	9.97	2.64	20.12	19.56	1.67	2.97	4.74	11.07	13.80	10.35
23-4 Flow	18.82	674.97	298.43	251.83	105.43	59.02	89.66	20.60	21.86	156.66	18.36	35.28
23*-11 Pyroclast	26.54	663.02	340.29	245.21	86.93	48.76	97.08	21.00	23.60	176.70	21.24	44.41
Mean	22.68	669.00	319.36	248.52	96.18	53.89	93.37	20.80	22.73	166.68	19.80	39.85
Standard Deviation	5.46	8.45	29.60	4.68	13.08	7.25	5.25	0.28	1.23	14.17	2.04	6.46
Standard Error in %	24.07	1.26	9.27	1.88	13.60	13.46	5.62	1.36	5.41	8.50	10.29	16.20

TABLE 3 ALTERATION AND CRYSTAL SORTING

	Ba/Nb	Zr/Nb	Ce/Nb	Ce/Y	Rb/Ba	Ba/Ce	Rb/Ce	K/Rb
LAS BOMBAS								
23-4 Flow	16.25	8.53	1.92	1.61	0.06	8.46	0.53	529.32
23-9 Bomb	15.60	8.41	1.83	1.73	0.07	8.50	0.61	481.02
23-10 Bomb	15.19	8.01	1.82	1.76	0.07	8.32	0.61	472.38
23*-11 Pyroclast	16.02	8.32	2.09	1.88	0.08	7.66	0.60	438.22
Analytical errors in %								
23-4 Flow	3.73	2.50	3.14	2.11	3.53	2.81	2.94	2.63
23-9 Bomb	1.96	1.47	3.00	2.45	1.78	2.40	2.82	1.10
23-10 Bomb	0.39	0.41	4.50	5.78	2.66	4.69	6.77	2.47
23*-11 Pyroclast	2.60	1.12	6.77	6.68	3.17	8.25	7.34	1.23
23-9 Bomb	15.60	8.41	1.83	1.73	0.07	8.50	0.61	481.02
23-10 Bomb	15.19	8.01	1.82	1.76	0.07	8.32	0.61	472.38
Mean	15.40	8.21	1.83	1.75	0.07	8.41	0.61	476.70
Standard Deviation	0.29	0.28	0.01	0.02	0.00	0.13	0.00	6.11
Standard Error in %	1.88	3.45	0.39	1.22	0.00	1.51	0.00	1.28
Mean 23-9 &10	15.40	8.21	1.83	1.75	0.07	8.41	0.61	476.70
23*-11 Pyroclast	16.02	8.32	2.09	1.88	0.08	7.66	0.60	438.22
Mean	15.71	8.27	1.96	1.82	0.08	8.04	0.61	457.46
Standard Deviation	0.44	0.08	0.18	0.09	0.01	0.53	0.01	27.21
Standard Error in %	2.79	0.94	9.38	5.06	9.43	6.60	1.17	5.95
23-4 Flow	16.25	8.53	1.92	1.61	0.06	8.46	0.53	529.32
Mean 23-9 &10	15.40	8.21	1.83	1.75	0.07	8.41	0.61	476.70
Mean	15.83	8.37	1.88	1.68	0.07	8.44	0.57	503.01
Standard Deviation	0.60	0.23	0.06	0.10	0.01	0.04	0.06	37.21
Standard Error in %	3.80	2.70	3.39	5.89	10.88	0.42	9.92	7.40
23-4 Flow	16.25	8.53	1.92	1.61	0.06	8.46	0.53	529.32
23*-11 Pyroclast	16.02	8.32	2.09	1.88	0.08	7.66	0.60	438.22
Mean	16.14	8.43	2.01	1.75	0.07	8.06	0.57	483.77
Standard Deviation	0.16	0.15	0.12	0.19	0.01	0.57	0.05	64.42
Standard Error in %	1.01	1.76	6.00	10.94	20.20	7.02	8.76	13.32

TABLE 3 ALTERATION AND CRYSTAL SORTING

	SiO2	TiO2	Al2O3	Fe2O3*	MnO	MgO	CaO	Na2O	K2O	P2O5
WEST OF LAS CHINCHES										
15-7 (more altered)	46.02	1.50	15.53	10.64	0.18	9.22	12.06	3.17	1.37	0.68
15-8 (less altered)	45.65	1.48	15.31	10.70	0.18	9.99	11.76	3.14	1.42	0.68
Analytical errors in %										
15-7	0.00	0.10	0.00	0.20	0.30	0.10	0.00	1.00	0.00	0.40
15-8	0.20	0.20	0.10	0.20	0.10	0.20	0.20	0.00	0.20	0.40
15-7	46.02	1.50	15.53	10.64	0.18	9.22	12.06	3.17	1.37	0.68
15-8	45.65	1.48	15.31	10.70	0.18	9.99	11.76	3.14	1.42	0.68
Mean	45.84	1.49	15.42	10.67	0.18	9.61	11.91	3.15	1.39	0.68
Standard Deviation	0.26	0.01	0.16	0.04	0.00	0.55	0.21	0.02	0.03	0.00
Standard Error in %	0.57	0.99	1.01	0.38	0.77	5.71	1.77	0.56	2.28	0.21

TABLE 3 ALTERATION AND CRYSTAL SORTING

	Rb	Sr	Ba	V	Cr	Ni	Zn	Ga	Y	Zr	Nb	Ce
WEST OF LAS CHINCHES												
15-7 (more altered)	28.13	1218.82	752.59	281.25	296.73	151.69	85.84	19.34	22.25	155.55	17.82	63.65
15-8 (less altered)	34.18	1022.88	730.39	261.36	317.49	151.95	86.50	19.42	22.36	150.56	17.75	64.73
Analytical errors in %												
15-7	1.36	0.38	0.47	0.81	0.03	0.69	0.11	2.48	1.65	0.47	1.71	2.77
15-8	0.20	0.04	0.07	1.66	1.65	0.91	0.29	0.17	0.24	0.04	0.37	1.33
15-7	28.13	1218.82	752.59	281.25	296.73	151.69	85.84	19.34	22.25	155.55	17.82	63.65
15-8	34.18	1022.88	730.39	261.36	317.49	151.95	86.50	19.42	22.36	150.56	17.75	64.73
Mean	31.16	1120.85	741.49	271.31	307.11	151.82	86.17	19.38	22.31	153.06	17.79	64.19
Standard Deviation	4.28	138.55	15.70	14.06	14.68	0.18	0.47	0.06	0.08	3.53	0.05	0.76
Standard Error in %	13.73	12.36	2.12	5.18	4.78	0.12	0.54	0.29	0.35	2.31	0.28	1.19

TABLE 3 ALTERATION AND CRYSTAL SORTING

	Ba/Nb	Zr/Nb	Ce/Nb	Ce/Y	Rb/Ba	Ba/Ce	Rb/Ce	K/Rb
WEST OF LAS CHINCHES								
15-7 (more altered)	42.23	8.73	3.57	2.86	0.04	11.82	0.44	404.89
15-8 (less altered)	41.15	8.48	3.65	2.89	0.05	11.28	0.53	344.15
Analytical errors in %								
15-7	2.18	2.18	4.48	4.42	1.83	3.24	4.13	1.36
15-8	0.44	0.41	1.70	1.57	0.27	1.40	1.53	0.40
15-7	42.23	8.73	3.57	2.86	0.04	11.82	0.44	404.89
15-8	41.15	8.48	3.65	2.89	0.05	11.28	0.53	344.15
Mean	41.69	8.61	3.61	2.88	0.05	11.55	0.49	374.52
Standard Deviation	0.76	0.18	0.06	0.02	0.01	0.38	0.06	42.95
Standard Error in %	1.83	2.05	1.57	0.74	15.71	3.31	13.12	11.47

TABLE 4: CHEMICAL COMPOSITION OF THE ALKALINE BASALTS, NEVADO VOLCANIC FIELD

	East Nevado 1																East Nevado 2	West Nevado 1
	15-3	15-8	16-9	15-4	15-7	15-2	16-3	15-5	15-6	16-8	16-6	16-4	16-5	16-1++	15-1	16-2++	16-7	18-1
	NW Ponon	A. Capataz	Chanchos	P. Trehue	A. Capataz	NW Ponon	Grande	Chilena	Toldos	Chato	Tordillos	Nevado	Nevado	P. Agua	Carreras	P. Agua	P. Trehue	Yeguas
SiO2	45.72	45.65	47.85	47.01	46.02	45.81	47.48	47.79	48.48	50 35	49.92	49.87	49 91	47 50	48.53	47 48	48.44	47.88
TiO2	1.62	1.48	1 47	1.45	1.50	1.65	1.66	1 38	1.55	1 15	1 47	1.45	1 52	2 14	1.61	2 09	1.65	1 56
Al2O3	15 10	15.31	15.60	15 89	15.53	15.78	15.14	15 92	15.50	16.07	15.74	16 00	15.74	14.10	16 57	14.22	17.66	15.20
Fe2O3	11.55	10 70	11.38	11.30	10 64	11.39	11.36	10 29	11.29	9.30	11.54	11.34	11 47	11.55	11.20	11 44	10.76	11.26
MnO	0.19	0.18	0.18	0.18	0.18	0.19	0.18	0 18	0 17	0.17	0.17	0.16	0 17	0 15	0.17	0 15	0 17	0.17
MgO	11 05	9.99	9.83	9.29	9.22	8.95	8.88	8.80	8.53	8.27	8.25	8 18	7 87	7 09	6.74	6.04	5 67	9 90
CaO	10 51	11.76	9.78	10.25	12.06	10 83	9.95	10.90	9.51	9.42	8.64	8 71	8 76	11.64	10.56	12.19	10.92	9.26
Na2O	2.88	3.14	3.04	3 50	3.17	3.33	3.74	3.34	3.73	3.74	3.60	3 63	3 68	3 99	3.56	3 83	3 77	3.45
K2O	1.09	1.42	0.85	0.98	1.37	1.30	1.19	1 35	0.95	1 45	0 85	0 83	0 88	1.72	0.94	1 73	1.01	1.15
P2O5	0 63	0 68	0.38	0.40	0.68	0.65	0.56	0.48	0.40	0.44	0.27	0 27	0 29	0 58	0.51	0.57	0.38	0 38
Total	100.32	100 32	100.36	100 25	100.38	99.89	100.12	100.42	100 10	100 36	100 44	100 42	100.29	100.47	100.40	99.74	100.42	100.20
Mg#	0 68	0.67	0.66	0 64	0.66	0 63	0.63	0.65	0 62	0 66	0.61	0.61	0.60	0 58	0.57	0.54	0 54	0.66
FeO*/MgO	0.94	0.96	1 04	1.10	1.04	1.15	1.15	1 05	1 19	1 01	1 26	1 25	1.31	1.47	1.50	1.71	1.71	1.02
Qz																		
Or	6 4	8.4	5.1	5.8	8 1	7 7	7 0	8.0	5.6	8.6	5 0	4 9	5.2	10.2	5 6	10 2	6.0	6.8
Ab	13.8	8.2	22.8	17.7	9 4	13 0	19 4	16.6	24.6	26.4	30.4	30 7	31 2	12 7	24 4	12.7	22.6	21.5
An	25.1	23.5	26.4	24.8	24 1	24 3	21 0	24.5	22 7	22.8	24.3	24 9	23 8	15.5	26 4	16 5	28 3	22 6
Ne	5.8	10.0	1.6	6.5	9.4	8.2	6.6	6.3	3.8	2 8				11.4	3 1	10 7	5 1	4 2
Diop	18.6	24.7	16.0	19 1	25.4	20.5	20 1	21.5	17 8	17 1	13.7	13 5	14.5	31 5	18 6	33 2	19 3	16.9
Hy											1 7	0 9	0.4					
Ol	23.5	18.8	22.3	20 1	17 0	18 9	18.8	17 4	19.1	17.3	19.2	19 5	18 8	11.1	15.4	8.5	12 7	21.8
Mnt	1.7	1.6	1.7	1 6	1 5	1.7	1.7	1.5	1.6	1.4	1.7	1.6	1.7	1 7	1.6	1.7	1 6	1.6
Ilm	3.1	2.8	2 8	2.8	2.9	3.1	3.2	2 6	2.9	2.2	2.8	2.8	2.9	4.1	3.1	4.0	3.1	3 0
Ap	1 5	1.6	0 9	0 9	1 6	1.5	1.3	1.1	0.9	1.0	0 6	0 6	0.7	1 4	1.2	1.3	0 9	0.9

++ Alkaline basalts with quartz xenocryst 1 Late Pliocene-Early Pleistocene 2 Pleistocene

TABLE 4: CHEMICAL COMPOSITION OF THE ALKALINE BASALTS, NEVADO VOLCANIC FIELD

	East Nevado 1																East Nevado 2	West Nevado 1
	15-3	15-8	16-9	15-4	15-7	15-2	16-3	15-5	15-6	16-8	16-6	16-4	16-5	16-1++	15-1	16-2++	16-7	18-1
	NW Ponon	A. Capataz	Chanchos	P. Trehue	A. Capataz	NW Ponon	Grande	Chilena	Toldos	Chato	Tordillos	Nevado	Nevado	P. Agua	Carreras	P Agua	P. Trehue	Yeguas
Rb	21 22	34 18	17 50	22.22	28.13	30.03	27 01	30 93	21 66	40.46	16 84	16 16	18 05	21.08	18.25	21.28	21.70	28 32
Sr	829.74	1022.88	634 81	677.83	1218.82	817.89	746.21	1036 36	665 89	994.57	583.07	587 37	579 52	783.39	595.24	768.23	647 74	614.48
Ba	532.57	730.39	399.33	505 95	752.59	603.45	418 78	936.36	521.32	791.94	406.30	408 25	454.43	537.42	392 71	685.10	486 70	422.47
V	233.89	261.36	181 95	201 03	281 25	231.21	181.67	239.63	192.39	168.49	195.69	174.62	159 35	133 58	210.32	135.30	225 90	200.53
Cr	429.98	317.49	372 14	302 04	296.73	268.96	305 40	284.47	305.49	296.14	265.34	264.93	235 31	259.43	164.95	257.43	82 84	396.50
Ni	214.03	151.95	161.95	151 91	151 69	138.29	149 00	136 79	110.89	174.39	139.55	139 37	119 03	179.35	58.22	184 29	26 86	203.44
Zn	93.59	86 50	88.80	88.83	85.84	86.84	88 76	86.78	82.22	84.93	102.88	103 42	87 87	97.96	88.64	106 71	78 87	91 43
Ga	19.09	19.42	20.39	20.19	19.34	19.42	20.68	18.82	21.60	19.10	21 22	21 17	22.48	21.13	20 33	21.71	20 56	19.27
Y	23 32	22.36	20.40	20.97	22.25	25.13	21.93	21.99	21.11	20.20	19.33	19 15	20 62	17.68	22 00	17.38	21.64	21.77
Zr	154 78	150.56	119.56	122.45	155 55	153.93	139 21	150.41	111.73	167 03	119 65	118 27	117 60	186 11	121.99	184.41	121.72	140.07
Nb	16.70	17 75	10.39	12.06	17.82	17.21	16 49	13.02	9 79	15 01	8 90	8 42	8.67	37.80	11 35	36.80	12.27	14 15
Ce	47.66	64.73	36.94	39 29	63.65	51.78	47 32	56.16	32.74	51.85	30.43	31 42	37 75	51.90	37.57	50.09	35 18	38.85
Ba/Nb	31 89	41 15	38.43	41 95	42.23	35 06	25 40	71.92	53.25	52.76	45.65	48 49	52 41	14 22	34.60	18 62	39 67	29 86
Ce/Nb	2 85	3 65	3.56	3 26	3.57	3 01	2.87	4 31	3.34	3.45	3.42	3 73	4.35	1 37	3 31	1.36	2 87	2.75
Zr/Nb	9 27	8.48	11.51	10 15	8.73	8 94	8.44	11.55	11 41	11.13	13.44	14 05	13 56	4 92	10.75	5 01	9 92	9.90
Nb/Y	0 72	0.79	0 51	0 58	0.80	0 69	0.75	0.59	0.46	0.74	0.46	0 44	0 42	2 14	0 52	2 12	0 57	0.65
Ce/Y	2.04	2 90	1.81	1 87	2.86	2 06	2.16	2.55	1.55	2.57	1 57	1 64	1 83	2 94	1 71	2 88	1 63	1.79
K/Rb	425.25	344.15	405.11	365 76	404 89	359.10	364 52	360.99	364.10	297.30	420.50	424 32	406.57	678.14	428 95	674 11	386.00	335.93
Ba/Rb	25.10	21 37	22 82	22.77	26.75	20.10	15 51	30 27	24.07	19 57	24 13	25 26	25.18	25.49	21 52	32 20	22.43	14.92
P/Ce	57.32	45.85	45.25	44.65	46.49	55.12	51.37	37.38	52 65	37.12	39 01	36 81	33.18	49.11	59 24	49.23	46 52	43.02
Ba/Ce	11.17	11 28	10.81	12.88	11.82	11 65	8.85	16 67	15.92	15.27	13.35	12.99	12.04	10.36	10.45	13.68	13.84	10 87
Sr/Ce	17.41	15.80	17 18	17 25	19.15	15 80	15.77	18.45	20 34	19 18	19 16	18 69	15 35	15 09	15 84	15.34	18.41	15.82
Ti/Zr	62.63	59 01	73.51	70.80	57.93	64.30	71.36	55 12	83 11	41.42	73.40	73 30	77.44	69.03	79.27	68 07	81 12	66.55
K/Ba	16.94	16.11	17.75	16 06	15 13	17 87	23 51	11.92	15.13	15.19	17.43	16 80	16 15	26 60	19.93	20 94	17.21	22 52

++ Alkaline basalts with quartz xenocryst 1 Late Pliocene- Early Pleistocene 2 Pleistocene

TABLE 4: CHEMICAL COMPOSITION OF THE ALKALINE BASALTS, NEVADO VOLCANIC FIELD

	West Nevado 1																
	20-2	20-1	LV-55	55-83	18-4	18-9	18-6	18-3	50-83	18-5	18-8	18-7++	18-2	18-10	18-13	18-12	54-83	18-11
	Negro	Negro	Vacas	Vacas	Yeguas	Vacas	Yeguas	Yeguas	Yeguas	Yeguas	Vacas	Yeguas	Yeguas	Vacas	Vacas	Vacas	Vacas	Vacas
SiO2	46.73	46.51	47.26	47.43	48 20	47 59	47.45	48 05	48.46	48.34	47.36	48 38	48 77	48 69	48.66	48.37	47.71	48.99
TiO2	1 26	1 28	1 40	1 47	1 67	1 44	1 54	1.53	1 70	1 55	1 49	1 59	1 56	1 54	1.53	1.53	1 48	1 60
Al2O3	15.04	15.02	14.57	14 99	14.54	15.25	15.34	15.28	14.68	15.37	15.44	15.56	15 97	16 60	16.63	16 56	15.66	17.16
Fe2O3	10.79	10 86	11.37	11.03	11 08	10.96	10.81	10 74	10.91	10.62	11.19	10.41	11.37	10 63	10.54	10.50	9 95	10 43
MnO	0.18	0.18	0 20	0.18	0.17	0 18	0.18	0.18	0.17	0.18	0.18	0 17	0.18	0 17	0.17	0 17	0.15	0 17
MgO	11 76	11 46	10.92	10.43	10 20	9.90	9.69	9.50	9.44	9.37	9.31	8.28	7.45	6 98	6.86	6.74	6 16	5.91
CaO	9.51	10 00	9.12	9.40	8.86	9.97	10.04	9.68	9.01	9.66	9.72	10 27	9.55	10 42	10.47	10.86	11 23	10.54
Na2O	3.09	3.10	3.04	2.98	3 57	3.38	3.19	3.46	3.76	3 44	3.33	3.69	3.29	3 59	3.71	3 67	3 06	3 78
K2O	1.27	1.21	1.28	1 23	1 19	1.32	1.34	1.35	1.27	1.39	1.22	1.24	1.01	1.22	1.24	1 21	1 19	1 29
P2O5	0.51	0.49	0.47	0.47	0.45	0.46	0.51	0.55	0.45	0.55	0.46	0.50	0.45	0 48	0.49	0.49	0.45	0.51
Total	100 12	100.10	99.63	99 61	99.92	100.45	100.09	100 30	99.84	100.46	99.70	100.08	99 59	100.30	100.29	100.09	97 04	100.38
Mg#	0.71	0.70	0.68	0.68	0.67	0.67	0.66	0 66	0 66	0.66	0.65	0.64	0.59	0.59	0.59	0.59	0 58	0.56
FeO*/MgO	0.83	0.85	0.94	0.95	0.98	1.00	1.00	1 02	1.04	1 02	1.08	1.13	1.37	1.37	1.38	1.40	1.45	1.59
Qz																		
Or	7.5	7.2	7 6	8 0	7.0	7.8	7.9	8.0	7.5	8.2	7.2	7 3	6.0	7.2	7.3	7 1	7 0	7.6
Ab	16 1	14 6	19 8	19.9	23.3	17.7	18.3	20.5	21 5	21.2	19.7	21.1	27.6	22.9	22.5	21.1	22 0	23.6
An	23.5	23.5	22.3	24.4	20.2	22.5	23.6	22.2	20.1	22.4	23.6	22.2	25.9	25 6	25.1	25.2	25 5	26.1
Ne	5.5	6.3	3.2	2.2	3 7	6.0	4.8	4 8	3.7	4.3	4.6	5.5	0.1	4.0	4.8	5.4	2.1	4.5
Diop	16.5	18.5	16.1	14.0	16.9	19.4	18.6	18 1	22 2	17 8	17.6	20.7	15 2	18 8	19.4	20 9	22 4	18.9
Hy																		
Ol	25.1	23.9	24.2	24.9	22 0	20.7	20.4	20 2	17.9	19.9	20.5	16.6	18.1	15.3	14.7	14.0	11.8	13.0
Mnt	1.6	1.6	1.7	1.7	1.6	1 6	1.6	1 6	1 6	1 5	1.6	1 5	1.7	1 5	1.5	1.5	1 4	1 5
Ilm	2 4	2.4	2.7	2.7	3.2	2.7	2.9	2 9	3.2	2.9	2.8	3.0	3.0	2 9	2.9	2.9	2 8	3.1
Ap	1 2	1 1	1.1	1.0	1.0	1 1	1.2	1 3	1.0	1 3	1.1	1 2	1.0	1.1	1.1	1.1	1.0	1 2

++ Alkaline basalts with quartz xenocryst 1 Late Pliocene-Early Pleistocene 2 Pleistocene

TABLE 4: CHEMICAL COMPOSITION OF THE ALKALINE BASALTS, NEVADO VOLCANIC FIELD

	West Nevado 1																	
	20-2	20-1	LV-55	55-83	18-4	18-9	18-6	18-3	0-83(Ly-5(	18-5	18-8	18-7++	18-2	18-10	18-13	18-12	54-83	18-11
	Negro	Negro	Vacas	Vacas	Yeguas	Vacas	Yeguas	Yeguas	Yeguas	Yeguas	Vacas	Yeguas	Yeguas	Vacas	Vacas	Vacas	Vacas	Vacas
Rb	32.41	29.28	32.20	25.30	24.46	31.01	25.17	29.41	25 00	31 62	27 80	28 18	21.97	25.53	27 23	24 05	20 00	26.85
Sr	842 12	799.95	768.00	780.00	684 26	795.90	908.71	943.05	666 00	947 33	690 93	862.97	739.66	797.42	807 90	803.47	735.00	849.34
Ba	628.09	583 39	850.00	622 00	482.30	600.69	679.19	682.98	469.00	683 70	412.90	633 64	476.80	582.20	594.34	578.55	555.00	613 71
V	226.20	205.38	195.00	213.00	186.08	207.42	217 38	196 05	198.00	191 39	256.58	195.31	246 64	209.73	211.91	209.75	206 00	226 60
Cr	503.46	504.04	423.00	387.00	378.92	347.56	281.31	283.93	367.00	270.66	182 44	242.12	302 47	152.09	142.58	145 40	205.00	94 39
Ni	284.32	262 16	255.00	238.00	201.16	211.37	178 46	181.36	189.00	174.21	70.66	131 74	119.37	65.22	56.18	61.19	54 00	36.04
Zn	83.26	84.05	417.00	87.00	94.62	88.22	92.94	93.77	104.00	87 79	76.40	86 11	93.31	86.42	78.87	82.55		80.29
Ga	18.55	17.72	26 20	19.90	19 29	18 71	19 67	19.38	21.00	19 83	19.81	19 59	20.30	19.82	20.76	20.62		22.13
Y	20.75	20.39	28.00	21 60	20 23	21 48	20 95	22.64	20.80	21.98	22 01	22 49	22.79	23.01	23.23	22.92	29.00	24.55
Zr	140.44	126.30	157 00	155 00	145.68	141.58	149.98	156.76	159.00	161.19	149 20	155.58	122 19	158.22	153 92	151 24	161 00	160.54
Nb	15.34	14 04	13.70	14 70	21 57	13.54	16.08	18.28	22.90	18.29	17.72	16 41	11.01	14.34	14.95	14.53	16.00	16.10
Ce	50 59	47.44	53.60	52 30	43.36	45.46	53.13	58 88	48.60	57 75	43.58	55.86	43.65	48 51	50 67	46.36		54.58
Ba/Nb	40.95	41.55	62.04	42 31	22.36	44 36	42.24	37 36	20 48	37.38	23 30	38.61	43 31	40 60	39.76	39.82	34.69	38 12
Ce/Nb	3.30	3.38	3.91	3 56	2.01	3 36	3.30	3 22	2.12	3.16	2 46	3.40	3 97	3 38	3.39	3.19		3.39
Zr/Nb	9.16	9 00	11 46	10 54	6.75	10 46	9.33	8 58	6.94	8.81	8 42	9.48	11 10	11.03	10.30	10.41	10.06	9 97
Nb/Y	0.74	0 69	0.49	0 68	1.07	0.63	0.77	0.81	1.10	0.83	0 81	0 73	0.48	0.62	0.64	0.63	0.55	0.66
Ce/Y	2.44	2 33	1.91	2 42	2.14	2 12	2.54	2.60	2.34	2 63	1 98	2 48	1 92	2.11	2.18	2.02		2.22
K/Rb	324 02	343.91	330 00	401.95	404.21	352.57	441.29	379.93	421.05	363 88	363.12	365.88	382.01	395.08	376 51	415.94	493.94	398.53
Ba/Rb	19.38	19.93	26.40	24 59	19.72	19.37	26.98	23.22	18.76	21.62	14.85	22.49	21 70	22.81	21 83	24 06	27 75	22.86
P/Ce	43.82	45.26	38.27	39 55	45 19	44.26	42.14	40.77	40.68	41 87	46.37	39.38	44.59	43.45	42.55	46.22		40.46
Ba/Ce	12.42	12.30	15 86	11 89	11.12	13.21	12.78	11 60	9.65	11.84	9 48	11 34	10.92	12.00	11.73	12.48		11.24
Sr/Ce	16 65	16.86	14 33	14 91	15.78	17.51	17.10	16.02	13.70	16.40	15.85	15 45	16.95	16.44	15 94	17 33		15.56
Ti/Zr	53 96	60.66	53.46	56.93	68.72	61.14	61.60	58 40	64.25	57.61	59.91	61 19	76.54	58 35	59.71	60.69	55.11	59 90
K/Ba	16 72	17.26	12.50	16 35	20.50	18.20	16.35	16.36	22.44	16.83	24 45	16 27	17.60	17.32	17.25	17.29	17.80	17.44

++ Alkaline basalts with quartz xenocryst 1 Late Pliocene- Early Pleistocene 2 Pleistocene

TABLE 4: CHEMICAL COMPOSITION OF THE ALKALINE BASALTS, NEVADO VOLCANIC FIELD

	West Nevado 2																
	27-150384++	19-6	19-5	24-140384	19-11	24	10-120384	21-140384	19-8++	MJA (flow)	84-1	19-10	83-62	19-9	2-170484	83-66++	19-7	46
	Mondaca	Leon	M. Jarilla	Borbaran	Masuco	Coloradas	E La Suiza	Bayo	L. Corral	M. Jarilla	Molongo	Solitario	Masuco	Solitario	Suiza	Montura	Borbaran	Pelado
SiO2	45.82	46 68	46.89	46.69	47.57	48.94	47 69	48 03	48 03	47 24	47 23	46.92	46.83	47.25	47 20	45 84	47 00	52 19
TiO2	1 41	1 46	1.36	1 47	1 47	1 25	1 41	1 60	1 68	1 45	1 60	1 37	1 43	1.39	1.45	1 73	1 83	1 06
Al2O3	14.22	14.38	15 21	14.90	15.01	15.07	15.38	14 36	15.17	16.13	14 95	16.15	14 32	16.43	14 93	15 60	14.74	15.81
Fe2O3	11 10	10.47	10.43	10 37	10.78	9.84	10 00	9 96	10 81	10.58	10.62	10.42	10 46	10.42	10 06	10.64	10.92	8.62
MnO	0 18	0 17	0.18	0.18	0.17	0 17	0.17	0 15	0.17	0 18	0.18	0.19	0.16	0.18	0 18	0 17	0 17	0.18
MgO	12.57	11.79	11 04	10 48	10 17	9.87	9.82	9.73	9 72	9.63	9.61	9.49	9.37	9 02	8 92	8 70	8 67	7.96
CaO	9.67	9.46	9.96	10.12	9.89	9.33	10.47	10 76	9.22	10.35	10.23	10 16	11 62	10.23	12.17	12 74	11 35	7.99
Na2O	2.84	3.39	3 03	3 44	3.57	3.35	3.43	3.31	3 73	2.96	3.29	3.22	3.33	3.34	3 57	2 81	3.52	3.75
K2O	1.18	1.28	1 19	1 36	1.24	1.42	1.16	1.35	1 32	1.00	1.29	1 47	1.25	1.51	0 88	1.09	1.75	1.66
P2O5	0.53	0.64	0 41	0.67	0.47	0.45	0.52	0.48	0 56	0.40	0.58	0 54	0.55	0 53	0 67	0 39	0.50	0.37
Total	99.53	99 74	99 71	99.68	100.34	99.68	100.05	99 73	100.41	99.93	99.58	99.92	99.32	100 30	100.03	99.70	100 44	99 58
Mg#	0.71	0.71	0.70	0.69	0 68	0 69	0.68	0.68	0.66	0.67	0 67	0 67	0.66	0.66	0.66	0.64	0 64	0 67
FeO*/MgO	0.79	0.80	0.85	0.89	0 95	0 90	0.92	0.92	1 00	0 99	0.99	0.99	1.01	1 04	1.02	1 10	1.13	0 98
Qz																		
Or	7.0	7 6	7.0	8 3	7.3	8.2	6.9	8.0	7 8	5.9	7.6	8.7	7 4	8 9	5.2	6 4	10.4	9.6
Ab	14 1	16 4	15.6	13 2	17.8	22.8	18 1	17.6	21 2	19.2	12.2	15.6	13.1	16.0	15.2	9 5	10.6	29.5
An	22 6	20 2	24.4	21.2	21.3	22.1	23.2	20.3	20 8	27 8	20.1	25.3	20.4	25 4	22.1	26.7	19 2	22.4
Ne	5.4	6.7	5 4	7.4	6 7	2.9	5.9	5 6	5 6	3.2	8 9	6.3	8.2	6.7	8.1	7.7	10.4	
Diop	17.7	18 2	18.1	25.4	20.0	17 2	20.6	24.2	17.3	17.0	28.1	17.6	27.3	17 8	27 5	27 7	27 5	12.0
Hy																		9.4
Ol	26.3	24.0	22.8	17.7	20 8	20 8	19.2	17 5	20.7	20.7	15.7	20.2	16.5	19 2	15.2	15.1	15.2	11.5
Mnt	1.6	1.5	1.5	1.5	1.6	1 4	1.5	1 4	1 6	1.5	1.5	1 5	1.5	1 5	1.5	1 6	1.6	1.3
Ilm	2.7	2.8	2.6	2.8	2.8	2.4	2.7	3.0	3.2	2 8	2.9	2.6	2.7	2 6	2 8	3.3	3.5	2 0
Ap	1 2	1.5	1.0	1.5	1.1	1 1	1 2	1.1	1.3	0.9	1.1	1.2	1.3	1 2	1.6	0 9	1 2	0.9

++ Alkaline basalts with quartz xenocryst 1 Late Pliocene-Early Pleistocene 2 Pleistocene

TABLE 4: CHEMICAL COMPOSITION OF THE ALKALINE BASALTS, NEVADO VOLCANIC FIELD

	West Nevado 2																	
	27-150384++	19-6	19-5	24-14038[1]	19-11	24	10-12038[1]	1-14038	19-8++	MJA (flow)	84-1	19-10	83-62	19-9	2-170484	83-66++	19-7	46
	Mondaca	Leon	M Jarilla	Borbaran	Masuco	Coloradas	E La Suiza	Bayo	L. Corral	M. Jarilla	Molongo	Solitario	Masuco	Solitario	Suiza	Montura	Borbaran	Pelado
Rb	29.30	34.62	27 18	36.10	30 24	39.30	27.80	27 00	32.37	18 60	31.80	38 28	26 00	39 80	16.90	19.90	45.91	56.80
Sr	847 00	892.26	764 57	936.00	810 93	795.00	858.00	784 00	821 98	800.00	878.00	1149.18	814 00	1166 28	1008.00	684.00	897.63	888.00
Ba	607 00	652.08	498.89	645.00	666 03	655 00	615.00	563.00	529.93	533.00	623.00	950 10	710.00	1003 94	678 00	510.00	572 57	816.00
V	216 00	198.23	229.86	220.00	210.25	182.00	246.00	216.00	195.45	238.00	197.00	224.94	232.00	236.49	206 00	288 00	220 90	162.00
Cr	537 00	437.36	488.84	444.00	347.56	424 00	418 00	481 00	306.61	292.00	318 00	289.72	427.00	266.33	352.00	306 00	354 42	433.00
Ni	318 00	276.04	210.11	221 00	191.57	199 00	226.00	153.00	187.52	145.00	188.00	146 08	141.00	123.43	222.00	95.00	139.39	186.00
Zn	98.00	83.10	84.42	90 00	88.19	84 00	90.00	95.00	98 85	94 00	97 00	92 45		91.43	89.00	77.00	95.34	92.00
Ga	18.60	17.40	20.01	18 40	18.55	18.40	19.10	22.00	19 54	19.70	18.70	19.94		20.40	18.00	18.40	21 04	19.50
Y	20.90	21.32	20.51	21 30	21 42	18.30	20.20	25.00	21 98	21.00	21.50	22.07	25.00	22.64	21.30	22.50	20.62	18.40
Zr	146 00	139.01	123.20	164 00	132.23	150.00	154.00	151.00	147 14	151.00	158.00	150.74	146.00	161.70	167.00	121 00	152.70	175.00
Nb	17 10	19.02	12.30	18 50	13.58	15.70	15.80	21 00	19 29	14 40	19.20	16.20	13.00	15.90	19.50	13 60	24.79	16.30
Ce	57.00	58.33	47 98	67 60	51.36	57.90	56 60		53 62	50.70	58 20	65.97		63.65	67.30	41 70	52.29	59 00
Ba/Nb	35.50	34.28	40 56	34.87	49.05	41.72	38 92	26.81	27.47	37.01	32 45	58.65	54.62	63.14	34.77	37.50	23 10	50.06
Ce/Nb	3.33	3.07	3 90	3.65	3.78	3.69	3.58		2.78	3.52	3.03	4 07		4.00	3.45	3 07	2 11	3.62
Zr/Nb	8.54	7.31	10.02	8.87	9.74	9.55	9.75	7.19	7.63	10.49	8.23	9.31	11 23	10.17	8.56	8.90	6 16	10.74
Nb/Y	0.82	0 89	0.60	0 87	0.63	0.86	0.78	0.84	0 88	0.69	0.89	0.73	0.52	0 70	0 92	0.60	1 20	0.89
Ce/Y	2.73	2.74	2.34	3 17	2.40	3 16	2.80		2 44	2.41	2.71	2.99		2.81	3.16	1.85	2 54	3.21
K/Rb	334.61	307.17	362.54	312.51	340.95	298 90	346.39	415.07	339.04	447.21	336.24	319.66	399.11	315.16	432 27	453.45	316.98	242.61
Ba/Rb	20.72	18.84	18.36	17 87	22.03	16.67	22.12	20.85	16.37	28.66	19.59	24 82	27.31	25.23	40.12	25 63	12.47	14.37
P/Ce	40.58	47 96	37.20	43.32	40.11	34.22	40.10		45.90	34.35	43.42	35.39		36.41	43.45	40.71	41.73	27.37
Ba/Ce	10.65	11.18	10.40	9.54	12.97	11.31	10.87		9.88	10.51	10.70	14.40		15.77	10 07	12.23	10.95	13.83
Sr/Ce	14 86	15.30	15.94	13 85	15.79	13.73	15.16		15 33	15.78	15.09	17.42		18.32	14.98	16.40	17 17	15.05
Ti/Zr	57.86	63.14	66 03	53.74	66.69	50.04	54.89	63.52	68.61	57.61	60.82	54.61	58.72	51.39	52.05	85.76	71.65	36.38
K/Ba	16.15	16.31	19 75	17.49	15.48	17 93	15.66	19.91	20 71	15.61	17.16	12.88	14.62	12.49	10.77	17.69	25 42	16.89

++ Alkaline basalts with quartz xenocryst 1 Late Pliocene- Early Pleistocene 2 Pleistocene

TABLE 4: CHEMICAL COMPOSITION OF THE ALKALINE BASALTS, NEVADO VOLCANIC FIELD

	West Nevado 2										
	11-40484	83-8	MJC (block)	6-110384++	MJB	84-7	83-71	48-La	19-4	19-1	19-2
	Negro NE	Nevado	M. Jarilla	Negro SW	M. Jarilla	Balas	Corral	L. Atravesada	Mondaca	Mondaca	Mondaca
SiO2	48 37	48.41	48 05	47.27	48.27	47 72	48 95	48 19	46 68	46.42	46.86
TiO2	1 55	1 36	1 60	1 27	1.59	1 52	1 72	1 55	1 74	1 68	1 70
Al2O3	15 49	16 28	16.47	16.42	16.62	16.41	15.43	16.94	17.39	17 29	17 79
Fe2O3	9.50	9.75	10.76	10.02	10 81	10 38	10.20	10.38	10.76	10.73	10 73
MnO	0.15	0.18	0 18	0.19	0 18	0.17	0.16	0 18	0 17	0 18	0.17
MgO	7.86	7.81	7 78	7.64	7 52	7.13	7 00	6.83	6.67	6 55	6.28
CaO	6.79	10.03	10.23	11.98	10 20	11 15	11.39	10.63	11.04	11 76	10 83
Na2O	3.37	3.56	3.35	3.15	3 64	3 42	3.46	3.36	3.40	3.27	3.44
K2O	1.53	1.69	1.00	1.23	1 05	1.26	1.58	1.35	1 30	1.36	1 38
P2O5	0.50	0.49	0 39	0.43	0 40	0.49	0.55	0.50	0.56	0.59	0 61
Total	95 11	99 55	99 81	99.60	100 28	99.65	100 44	99 90	99 70	99 84	99.78
Mg#	0 65	0 64	0 61	0.63	0.61	0.60	0.60	0 59	0 58	0.57	0 56
FeO*/MgO	1 09	1 12	1 24	1 18	1.29	1.31	1.31	1 37	1 45	1 47	1 54
Qz											
Or	9.0	10.0	5 9	7.3	6.2	7 5	9.3	8.0	7.7	8.0	8 2
Ab	28.5	18.7	22 9	10.6	22.5	15.6	19.2	14.4	16.7	13.9	17 7
An	22.6	23.5	27.0	26.1	25 9	25 6	21.9	25.1	28.3	28.5	29 0
Ne		6 2	3.0	8.0	4.5	6 7	5.5	7.2	6 4	7 4	6 2
Diop	6.3	18.9	17 4	30.8	17.1	27 3	25 3	24 8	18.7	21.3	17 0
Hy	8.2										
Ol	14 1	17.2	17.3	10.8	16.6	12.0	12.3	14.0	14 6	13.5	14.5
Mnt	1 4	1.4	1.6	1.4	1 6	1.5	1.5	1.7	1 6	1 6	1 6
Ilm	2.9	2.6	3.1	2.3	3.0	2 8	3.3	2.9	3 3	3.2	3 2
Ap	1.2	1.1	0 9	1.0	0.9	1.1	1.3	1 2	1 3	1 4	1 4

++ Alkaline basalts with quartz xenocryst 1 Late Pliocene-Early Pleistocene 2 Pleistocene

TABLE 4: CHEMICAL COMPOSITION OF THE ALKALINE BASALTS, NEVADO VOLCANIC FIELD

	West Nevado 2										
	11-40484	83-8	MJC (block)	6-110384++	MJB	84-7	83-71	48-La	19-4	19-1	19-2
	Negro NE	Nevado	M Jarilla	Negro SW	M. Jarilla	Balas	Corral	L. Atravesada	Mondaca	Mondaca	Mondaca
Rb	33.00	44.40	19 00	29.00	22.30	26.50	43.00	27.00	31.05	33 26	33 97
Sr	907.00	1004 00	669 00	972.00	677.00	809 00	868.00	886.00	1003.64	1026.12	1054.73
Ba	728.00	827.00	438 00	743.00	457.00	641 00	610 00	680.00	670.99	749 73	681.11
V	220.00	213.00	224.00	239.00	222.00	228 00	224.00	245.00	253.08	283 33	248 37
Cr	294.00	301.00	225.00	284.00	297.00	185 00	271.00	160.00	97.98	93 49	74 17
Ni	86.00	128.00	71.00	114.00	75.00	63 00	64 00	48.00	52.52	54 89	43.99
Zn	89.00	115.00	98.00	81.00	98 00	88 00	94 00	94.00	82.41	82 01	83.44
Ga		19.40	18.70	18.80	21.60	20 90	21.00	20 20	21.59	20 94	21.41
Y	29.00	21.90	22.60	22.50	22.30	22.80	28.00	24.00	23.13	25 12	23.53
Zr	176.00	184.00	139.00	139 00	133.00	149.00	153 00	165.00	145.30	146.53	157.53
Nb	18.00	16.90	11 30	9.20	12 40	12.50	17.00	15.70	15.65	16.06	16.37
Ce		68.30	42 70	52.40	46.20	52.30		58.90	51.62	65 05	52 87
Ba/Nb	40.44	48.94	38.76	80.76	36.86	51.28	35 88	43 31	42.88	46 68	41.61
Ce/Nb		4.04	3.78	5.70	3.73	4.18		3.75	3.30	4.05	3.23
Zr/Nb	9.78	10.89	12.30	15.11	10.73	11.92	9.00	10 51	9.28	9.12	9.62
Nb/Y	0 62	0 77	0 50	0.41	0 56	0 55	0 61	0 65	0 68	0.64	0.70
Ce/Y		3.12	1 89	2.33	2 07	2.29		2 45	2.23	2.59	2.25
K/Rb	384 89	315.42	437.79	352.38	390.88	393.15	305 03	413.54	347.30	339.70	337.00
Ba/Rb	22.06	18.63	23 05	25.62	20.49	24.19	14.19	25.19	21.61	22 54	20.05
P/Ce		31.12	39.55	35.81	37.79	41.06		36.83	47.09	39 58	49.94
Ba/Ce		12.11	10.26	14.18	9.89	12.26		11.55	13.00	11.53	12.88
Sr/Ce		14.70	15.67	18.55	14.65	15.47		15.04	19.44	15 77	19.95
Ti/Zr	52.80	44.21	69.18	54.56	71.67	61.32	67.40	56.32	71.71	68.69	64.66
K/Ba	17.45	16.93	18.99	13.75	19.07	16 25	21 50	16.42	16.07	15 07	16.81

++ Alkaline basalts with quartz xenocryst 1 Late Pliocene- Early Pleistocene 2 Pleistocene

TABLE 4: CHEMICAL COMPOSITION OF THE ALKALINE BASALTS, LLANCANELO VOLCANIC FIELD

	West Llancanello 1		West Llancanello 3					
	21-7	21-5	21-3	21-2	21-4	21-1	21-6	21-8
	El Morado	El Sauno	El Chachao	Chihuido	El Chachao	Chihuido	Piedras Blancas	Piedras Blancas
SiO2	47.46	47 24	46 77	46.91	47.00	48 08	48 73	48.51
TiO2	1.46	1 58	1.61	1.71	1.77	1 89	1.66	1.74
Al2O3	15.69	15.64	16 47	16.43	16.59	16.98	17.84	17.70
Fe2O3	10.59	10.88	11 68	11.92	11 08	11.48	10.85	11.05
MnO	0.17	0.17	0.18	0.18	0.17	0.17	0.16	0 16
MgO	9.88	9.64	8 79	8.45	7.96	6.52	6.07	5 71
CaO	10.38	10.13	10.44	10 17	10 47	10.26	10.35	10.27
Na2O	3.24	3.22	3.19	3 39	3.59	3 65	3.84	3.95
K2O	0.96	1.01	0.89	0 95	1.13	0.96	0.74	0 81
P2O5	0.42	0.48	0.38	0.41	0.52	0.39	0.33	0.37
Total	100.24	99 98	100.40	100 50	100.28	100 39	100.54	100.27
Mg#	0.67	0.66	0.62	0.61	0.61	0 56	0.55	0 53
FeO*/MgO	0.97	1 02	1.20	1.27	1.25	1 59	1.61	1.74
Qz								
Or	5 67	5.96	5.26	5 59	6 69	5.68	4 36	4.79
Ab	18.99	19.63	18.36	19 19	18 10	23.65	26.00	25.66
An	25.44	25.22	28.00	26.82	25.80	27 11	29.27	28.16
Ne	4.56	4 14	4.68	5.14	6.66	3.93	3.50	4.22
Diop	18.88	17 78	17.39	17 14	18.58	17 46	16.40	16.82
Hy								
Ol	20.46	20.58	20.03	19 62	17.29	15 37	14.60	13.86
Mnt	1.54	1 58	1.69	1.73	1.61	1.66	1.57	1.60
Ilm	2.77	3.00	3 05	3.26	3.36	3 58	3.06	3.30
Ap	0.97	1 11	0.88	0.94	1.19	0 91	0.75	0 85

1 Late Pliocene-Early Pleistocene 3 Late Pleistocene-Early Holocene

TABLE 4: CHEMICAL COMPOSITION OF THE ALKALINE BASALTS, LLANCANELO VOLCANIC FIELD

	West Llancanello 1		West Llancanello 3					
	21-7	21-5	21-3	21-2	21-4	21-1	21-6	21-8
	El Morado	El Saino	El Chachao	Chihuido	El Chachao	Chihuido	Piedras Blancas	Piedras Blancas
Rb	18 98	19 16	18.55	16 84	23.00	16.66	13 89	15 34
Sr	670.74	721.95	586.56	565 40	860 68	589.63	617.07	673 01
Ba	426 43	441.22	343.89	351.82	423.90	332.17	306.66	347 39
V	219.86	223.34	217.37	205.52	227 41	213.43	184.50	202.74
Cr	483 40	451.09	250 89	228.78	193.77	127.30	95.60	79.30
Ni	160 45	166.86	116.50	109.41	89.41	50.34	39.45	31.17
Zn	79 92	90.27	86 76	78.96	85.51	87.29	93.79	90.82
Ga	18 38	19.48	19 04	18.06	19 65	20.51	20.84	22.17
Y	20 29	20.51	21.64	18.44	22.62	22.66	20.69	22 57
Zr	142.65	151.06	126.42	127 77	162 68	144.55	134 77	147 24
Nb	13.51	16 03	12.62	13.39	18.99	15.21	10 79	12.40
Ce	45 36	47.82	29.77	38.34	45.34	33 70	29.53	34.84
Ba/Nb	31.56	27.53	27.25	26.28	22.32	21 84	28.42	28 02
Ce/Nb	3 36	2.98	2.36	2 86	2 39	2.22	2.74	2 81
Zr/Nb	10 56	9.42	10.02	9 54	8 57	9.50	12.49	11.87
Nb/Y	0 67	0.78	0 58	0.73	0 84	0.67	0.52	0.55
Ce/Y	2 24	2.33	1 38	2.08	2 00	1.49	1.43	1.54
K/Rb	419.89	436.74	398.29	466.34	408 58	478.86	440.47	438.89
Ba/Rb	22.47	23.03	18.54	20.89	18.43	19.94	22 08	22 65
P/Ce	40.41	43.72	55.71	46.33	49.57	51.02	48.03	45 85
Ba/Ce	9 40	9.23	11.55	9.18	9 35	9.86	10.39	9.97
Sr/Ce	14 79	15 10	19.70	14.75	18.98	17.50	20.90	19.32
Ti/Zr	61 40	62.78	76 21	80.42	65.26	78.18	73.89	70 85
K/Ba	18 69	18.97	21 48	22 32	22.17	24.02	19.95	19 38

1 Late Pliocene-Early Pleistocene

3 Late Pleistocene-Early Holocene

TABLE 4: CHEMICAL COMPOSITION OF THE ALKALINE BASALTS, LOS VOLCANES VOLCANIC FIELD

	Los Volcanes 1			Los Volcanes 2					Los Volcanes 3										
	26-3	26-2	24-2	22-7	22-6	25-11	22-8	26-4	25-10	22-9	22-5++	25-7	25-5	25-4	23-14	23-13	23-7	24-6	25-6
	Hermita	Hermita	P Lajas	Rauquilco	Rauquilco	Fortunoso	Rauquilco	Hermita	Vazquez	Vazquez	Bridge	Pipeline	L Colorada	Janiloso	Cortadera	Aguita	Payun Matru	Paso	Pipeline
SiO2	47.05	47 00	47.78	47 74	47.90	49 18	47.30	51.16	47.58	47 17	48 41	47.91	47 86	46.98	46 94	47 34	47.48	47 33	47 19
TiO2	1 77	2.13	1 99	1.73	1.70	1.91	1.71	1 76	1 76	1 74	1 73	1 90	1.87	1 85	2.22	1.93	1 90	2 18	2.18
Al2O3	16 03	16 99	17.45	16 45	16 63	16.14	16.39	16.73	15 94	15 78	16 13	16.60	16 86	17 53	17.36	17.92	17 60	18 26	18 15
Fe2O3	11.30	11 82	11.18	10.74	11.02	11 85	10.69	9.85	12.21	12 04	11 01	11.12	11.13	10.90	11.17	10.76	11 17	11 14	11 17
MnO	0.17	0 17	0.18	0 18	0 18	0 16	0.17	0.17	0 17	0 17	0 17	0 17	0 17	0.16	0 17	0.16	0 17	0 17	0 17
MgO	8 33	6.65	6.17	7.53	7.35	7.24	7 18	5.55	8 26	7 98	7 66	7 49	7 10	6.91	6.60	6.31	5.92	5 86	5.79
CaO	10.42	10 34	9.28	9.88	10.37	8 82	11 01	7.15	10 10	10 48	10.25	10 00	10 47	10.90	9.73	10.38	10 58	9.72	9 71
Na2O	3.23	3.59	3.74	3 60	3 45	4 02	3 45	4 65	3.56	3 45	3 25	3 71	3.32	3.28	3.79	3.57	3.55	3 77	3 74
K2O	1.07	1.01	1.50	1 46	1 16	0 89	1.29	2.12	0 56	0.55	0.82	1.06	0.86	0.86	1.33	0.95	1.12	1 24	1.24
P2O5	0.37	0.42	0.54	0.51	0.44	0 27	0.48	0 65	0.31	0.31	0.32	0.38	0.36	0 35	0 58	0.40	0.45	0.51	0 51
Total	99.73	100 13	99.81	99.81	100.19	100.47	99.67	99.80	100 43	99.65	99.74	100.35	100.00	99 72	99.88	99 71	99.93	100.16	99 83
Mg#	0.62	0 55	0 55	0.61	0.60	0 57	0.60	0.55	0 60	0 59	0.61	0.60	0 58	0.58	0.57	0.56	0 54	0.54	0 53
FeO*/MgO	1 22	1 60	1.63	1.28	1.35	1 47	1.34	1.60	1 33	1 36	1.29	1.34	1.41	1.42	1.52	1 54	1.70	1 71	1 74
Qz																			
Or	6.3	6 0	8 9	8.6	6.8	5.3	7 6	12 5	3.3	3 2	4 9	6 2	5 1	5 1	7 8	5.6	6 6	7.3	7 3
Ab	19 0	20.7	23.3	20.2	21.3	29.1	17 5	33 3	23.4	22 2	25 3	22 2	23.5	20.1	20.8	22 3	21 4	21.8	22.7
An	26.1	27 3	26.4	24.5	26.5	23.4	25 4	18.5	25.9	26 0	27.0	25 5	28.6	30.5	26.4	30.1	28.8	29 3	29.1
Ne	4.5	5.2	4.5	5 5	4.3	2.7	6 3	3.3	3.7	3.8	1 2	5 0	2.5	4 2	6 1	4.3	4 7	5 5	4.8
Diop	18.9	17 5	13.3	17.4	18 1	15.3	21 4	10 4	18 2	19 6	17.8	17 7	17.2	17.4	14.8	15.4	17.1	12 9	12.9
Hy																			
Ol	18.1	15.6	15 8	16.6	16.4	17.8	14.6	14 6	19 2	18 0	17 0	16.6	16 1	15 5	15.7	14.9	14 1	16 5	15.0
Mnt	1 6	1 7	1.6	1 6	1.6	1 7	1 6	1 4	1 8	1 8	1 6	1.6	1.6	1.6	1.6	1 6	1.6	1.6	1 6
Il	3.4	4 1	3.8	3.3	3.2	3.6	3.2	3.4	3.3	3 3	3.3	3 6	3.6	3 6	4.2	3.7	3 6	4 1	4.1
Ap	0 9	1 0	1.2	1 2	1 0	0.6	1.1	1.5	0 7	0 7	0.7	0 9	0.8	0.8	1.3	0.9	1.0	1.2	1.2

++ Alkaline Basalts with quartz xennocryst 1 Late Pliocene-Early Pleistocene 2 Pleistocene 3 Late Pleistocene-Early Holocene 4 Holocene 5 Prehistoric

TABLE 4: CHEMICAL COMPOSITION OF THE ALKALINE BASALTS, LOS VOLCANES VOLCANIC FIELD

	Los Volcanes 1			Los Volcanes 2					Los Volcanes 3									
	26-3	26-2	24-2	22-7	22-6	25-11	22-8	26-4	25-10	22-9	22-5++	25-7	25-5	25-4	23-14	23-13	23-7	24-6	25-6
	Hermita	Hermita	P. Lajas	Rauquilco	Rauquilco	Fortunoso	Rauquilco	Hermita	Vazquez	Vazquez	Bridge	Pipeline	L. Colorada	Jarilloso	Cortadera	Aguita	Payun Matru	Paso	Pipeline
Rb	21 5	16 2	29.7	32.1	22.8	16.5	25.2	33 8	9 3	9 2	13 8	15.5	12.9	14 4	21.5	11.6	19.6	16 1	12 1
Sr	600.3	699.9	839.6	705.4	665 2	527.9	690.9	702 2	514 4	510 6	539.2	583.0	619.6	659.7	812.6	696 3	736 5	811 5	626.6
Ba	300 0	303 7	480.6	428.1	385.4	296 9	412.9	576 5	191 6	182 1	245.9	329.2	258.8	257 1	405.8	276 3	361.9	321.5	255.2
V	222.9	231.5	189 8	213 7	212.6	170.6	256.6	112.5	204 0	193 9	206.8	199 0	213.8	220 5	213 5	203 0	232.1	210.5	212.8
Cr	254 9	100.2	30.4	221 2	193 3	210.0	182 4	159.5	278 4	259 9	248 5	184 6	181.9	152 1	76.8	111 8	73.1	46 1	193.5
Ni	109 8	49.7	44.1	94.2	71 3	89.3	70.7	60.7	105 1	102 3	88.5	74 9	74.2	69.9	51.3	51 8	46 1	33 8	78.6
Zn	89.8	88.4	76.5	85.1	84.2	88.0	76.4	75.7	102 4	97 3	91.9	81.4	92.8	82.0	92.4	81.6	95.6	85 8	91.5
Ga	19 8	21.6	21 3	20.1	20.5	20.4	19.3	20.5	21.5	20 5	21.4	21.3	21 1	20 5	21.4	20.8	21.1	21 7	20.8
Y	20 8	22.6	24.0	22.7	22.2	19.3	22.2	24.0	20 0	19 3	21.3	22.9	21 8	21 0	24.8	22.5	23.4	22.5	20 7
Zr	153.5	149.4	170.2	180.1	141 2	121.9	149.2	232 7	109.0	100 5	130.6	180.1	141.3	131 0	205.3	175 7	172.7	174.2	134 9
Nb	18 5	18.6	23.8	21.4	15 8	12.3	17.7	30 3	9 4	8.8	12 2	16.8	15.6	14 2	27.2	16.2	18 8	21.8	14.8
Ce	36.0	37 3	50.9	48.9	40.8	25.8	43 6	61 9	24.4	24 5	29.8	37 2	33.8	28.2	46.3	34 0	39.2	41 8	31.6
Ba/Nb	16 3	16 4	20.2	20.0	24 4	24 2	23.3	19 0	20 5	20 8	20.2	19 6	16.6	18 1	14 9	17 1	19.2	14.8	17.3
Ce/Nb	2 0	2 0	2.1	2.3	2.6	2 1	2 5	2 0	2.6	2 8	2 4	2.2	2 2	2 0	1.7	2 1	2 1	1 9	2.1
Zr/Nb	8 3	8.0	7.2	8.4	9 0	9 9	8.4	7 7	11.7	11 5	10.7	10 7	9.1	9 2	7.5	10 8	9.2	8.0	9.1
Nb/Y	0 9	0.8	1.0	0.9	0.7	0 6	0.8	1 3	0 5	0 5	0.6	0.7	0.7	0.7	1.1	0.7	0 8	1 0	0 7
Ce/Y	1 7	1 7	2.1	2.2	1 8	1 3	2.0	2.6	1.2	1 3	1 4	1.6	1.5	1 3	1.9	1 5	1.7	1.9	1.5
K/Rb	412.4	518.7	420.2	376.6	420 9	450.7	425.0	519.0	495 9	494 7	496.3	564.8	551 5	499.5	511.4	684.5	476.3	636.8	847.3
Ba/Rb	13 9	18.8	16.2	13.3	16 9	18.1	16.4	17 0	20.6	19 8	17 9	21 2	20.0	17.9	18.9	23 9	18.5	19.9	21 1
P/Ce	44.6	48 5	45.9	45 3	47.2	46.0	47.6	46.1	54.7	54 3	46.2	44.6	46 9	53 8	54.5	50.7	49.9	53.1	70.3
Ba/Ce	8 3	8.1	9.4	8.7	9 5	11.5	9.5	9 3	7.8	7 4	8.3	8.8	7.7	9.1	8.8	8.1	9.2	7.7	8 1
Sr/Ce	16 7	18.8	16.5	14.4	16 3	20.5	15 9	11 3	21.1	20 8	18 1	15.7	18.4	23.4	17.6	20 5	18.8	19 4	19.8
Ti/Zr	68 92	85.58	70.15	57.61	72.29	93.81	68 63	45 44	96.86	103 55	79 33	63 35	79.28	84.68	64 80	65 98	66 01	75 05	96.64
K/Ba	29.58	27.63	25.96	28 28	24 88	24 97	25 94	30 45	24 04	24 94	27.75	26.63	27.56	27.89	27.11	28.67	25.78	31.97	40.17

++ Alkaline basalts with quartz xenocryst 1 Late Pliocene-Early Pleistocene 2 Pleistocene 3 Late Pleistocene-Early Holocene 4 Holocene 5 Prehistoric

TABLE 4: CHEMICAL COMPOSITION OF THE ALKALINE BASALTS, LOS VOLCANES VOLCANIC FIELD

	Los Volcanes 4										Los Volcanes 5						
	25-8	26-1	23-2	26-5	23-1	25-9	26-6	23-3	24-7	26-7	24-3	24-1B	24-4	24-1A	24-5	23-4	25-2
	Pipeline	P Huincan	Escorial	Huemul	Escorial	Pipeline	Bayo	Escorial	Escorial	Zampal	Santa Maria	Santa Maria	Santa Maria	Santa Maria	Santa Maria	Bombas	Media Luna
SiO2	46 92	46.98	48.52	47.24	48.84	47.64	48.74	49.41	49 39	47.69	47 18	46 95	47 10	46.98	47 19	46 71	48 21
TiO2	2.02	1.94	1.91	2 22	1 99	2 37	1.81	1.94	2 00	2.11	1.89	1 90	1.96	1.93	1 91	2 16	1 85
Al2O3	17.30	17.77	17.02	17.72	17 23	17.15	17.36	17 25	17 34	19.13	16.64	17 28	17 20	17.31	17 52	17 22	17.23
Fe2O3	11.20	10 77	10.36	11.08	10 52	11.53	10.55	10 18	10 36	10.57	11.27	10.98	11 08	10.95	10 94	11 34	10.67
MnO	0 16	0 16	0.16	0 16	0.16	0 17	0.18	0 16	0.16	0.16	0.17	0 17	0 17	0.16	0 17	0.17	0 17
MgO	7.29	7.05	6.08	5.90	5.88	5.67	5.62	5 61	5.44	4.65	7.61	7.30	7.11	7.06	7.02	6.66	6 42
CaO	10.27	10 20	10.00	10.03	9 73	9 66	9.57	9.72	9.44	9.77	10.11	10.52	10 50	10.54	10.67	10.94	9 19
Na2O	3.52	3 36	3.79	3.80	3.88	3.81	3.77	3 96	3.92	4.03	3.22	3.30	3.65	3.45	3.35	3 48	3.96
K2O	1 06	1.05	1.42	1.21	1 50	1.41	1.46	1.54	1.59	1 27	1.25	1.21	1 26	1.23	1.23	1 20	1.44
P2O5	0 43	0.42	0.46	0 49	0.48	0 55	0.51	0.49	0 50	0 59	0.46	0.45	0.46	0.45	0 45	0 40	0.51
Total	100 18	99 70	99.72	99.85	100 20	99.94	99.57	100 26	100.16	99 98	99 80	100.04	100.48	100.06	100 44	100 28	99.63
Mg#	0 59	0 59	0.56	0.54	0 55	0 52	0.54	0.55	0.54	0.49	0.60	0 59	0 59	0 59	0 59	0 56	0.57
FeO*/MgO	1.38	1 38	1.53	1.69	1 61	1 83	1.69	1.63	1 71	2.05	1.33	1.35	1 40	1 40	1 40	1 53	1 50
Qz																	
Or	6.3	6 2	8.4	7.1	8 9	8.3	8 7	9.1	9.4	7.5	7.4	7 2	7.5	7.3	7 3	7 1	8.5
Ab	19.8	21 0	23.4	21.9	24.4	23.3	25 7	25 7	26.6	24.3	20.2	18.6	18 0	18.5	18 7	17 0	24.1
An	28.3	30.3	25.2	27.7	25.2	25.5	26.1	24 7	25 0	30.3	27.3	28.8	26 8	28.1	29.1	27 8	25.0
Ne	5 4	4 0	4.7	5.6	4.6	4.9	3.4	4.2	3.5	5.3	3.8	5.0	7 0	5.8	5.3	6 8	5.1
Diop	16 2	14.3	17.6	15 5	16.4	15.5	14 8	16.7	15 3	11.8	16.3	16.8	18 2	17.3	17 1	19 6	14 2
Hy																	
Ol	16 7	16.6	13.3	14 1	13.5	14.0	13.8	12 6	12 9	12.8	17 5	16.5	15 7	15.8	15.8	14.4	15 6
Mnt	1 6	1.6	1.5	1.6	1 5	1.7	1.5	1 5	1.5	1.5	1.6	1 6	1 6	1.6	1.6	1 6	1.6
Il	3 8	3.7	3.6	4.2	3.8	4 5	3.4	3.7	3 8	4.0	3.6	3.6	3.7	3.7	3 6	4 1	3.5
Ap	1.0	1 0	1.1	1 1	1 1	1.3	1.2	1.1	1.2	1.4	1.1	1 0	1 1	1.1	1.1	0.9	1.2

++ Alkaline Basalts with quartz xennocryst 1 Late Pliocene-Early Pleistocene 2 Pleistocene 3 Late Pleistocene-Early Holocene 4 Holocene 5 Prehistoric

TABLE 4: CHEMICAL COMPOSITION OF THE ALKALINE BASALTS, LOS VOLCANES VOLCANIC FIELD

	Los Volcanes 4										Los Volcanes 5						
	25-8	26-1	23-2	26-5	23-1	25-9	26-6	23-3	24-7	26-7	24-3	24-1B	24-4	24-1A	24-5	23-4	25-2
	Pipeline	P. Huincan	Escorial	Huemul	Escorial	Pipeline	Bayo	Escorial	Escorial	Zampal	Santa Maria	Santa Maria	Santa Maria	Santa Maria	Santa Maria	Bombas	Media Luna
Rb	14.9	14 8	28 1	16.5	28.4	19 8	32 5	29 9	31 3	19.9	24.6	21.9	22.3	21 8	21 9	18 8	31.7
Sr	732 2	771 1	649 6	776.5	663.2	734.2	701.5	651 4	673 1	896.9	705.9	755.3	730 0	759 4	765.6	675.0	727.9
Ba	284.9	263 3	396 8	309 9	406 0	342.2	412.6	416.4	438 7	396.5	336.6	324.8	341 7	337.3	329.2	298.4	378.4
V	219 4	203 0	224 1	225 5	218 9	232 6	205 6	215.5	212 7	200.6	241.9	223.6	232 5	229 0	227.6	251.8	208 5
Cr	181.6	157 2	110 0	98.5	97 8	85.5	59 5	83.8	74 1	19.0	202.7	141.4	145 8	138.1	139.7	105.4	154 1
Ni	73 3	73.0	50.4	48.0	47.3	35.6	37.5	39.8	38 3	22.7	94 6	76.0	66.3	66.6	66 8	59.0	76.1
Zn	81.8	85.2	86.1	80.6	83.4	87.3	90.0	86 7	86 7	83 4	100 1	89.5	82 5	88 1	85 5	89.7	90.2
Ga	19.7	19.9	20.8	20 9	21.0	21.2	22 1	21.5	21 3	21 1	20 4	19 8	20.1	20.8	19.0	20.6	21.1
Y	20.3	19 6	23.5	22.1	24.1	24.1	25 4	24 5	24 6	23 7	22 4	21.1	22 5	21.6	21.2	21.9	23.5
Zr	155.3	153.3	198 0	169.5	203.1	201.8	200 7	212 5	220 3	188 8	176 8	167.6	173.0	171.5	170.4	156.7	204.5
Nb	19 8	19 8	21 3	22.3	22.3	25.6	22 2	22.5	24 3	21 5	20.2	19.7	20.2	20.4	19 6	18.4	23.8
Ce	36 6	36 1	43 1	41 0	46 1	43.3	51.0	47.2	50 0	47 2	43 0	42 2	42 9	44 2	40 2	35.3	47.4
Ba/Nb	14 4	13 3	18.6	13 9	18.2	13.3	18.6	18.5	18 1	18 5	16 7	16 5	17 0	16 6	16 8	16 3	15 9
Ce/Nb	1 8	1 8	2.0	1 8	2.1	1.7	2.3	2.1	2.1	2.2	2 1	2 1	2 1	2 2	2.1	1.9	2.0
Zr/Nb	7 8	7 8	9.3	7.6	9 1	7.9	9.0	9 5	9.1	8.8	8 8	8.5	8 6	8.4	8 7	8.5	8.6
Nb/Y	1.0	1 0	0.9	1 0	0 9	1.1	0.9	0.9	1.0	0 9	0 9	0.9	0.9	0.9	0.9	0.8	1 0
Ce/Y	1 8	1.8	1.8	1 9	1 9	1.8	2.0	1.9	2.0	2 0	1 9	2.0	1 9	2.0	1 9	1.6	2.0
K/Rb	587 7	589.4	421.4	609 1	437 7	589.4	374.3	428.5	422 5	530 9	422.7	460 0	470.4	468.9	468.1	529.3	378.5
Ba/Rb	19.1	17 8	14.1	18.8	14.3	17.3	12 7	13 9	14 0	19.9	13.7	14.8	15 3	15.5	15.1	15.9	12.0
P/Ce	51 6	51 2	46 3	52.5	45 1	55.1	43 9	45.5	43 9	54.7	46.1	46.2	47 2	44.8	49.2	50.0	46.6
Ba/Ce	7.8	7 3	9 2	7.6	8 8	7.9	8.1	8.8	8.8	8 4	7.8	7.7	8 0	7.6	8 2	8.5	8.0
Sr/Ce	20 0	21.4	15.1	18.9	14.4	17.0	13 8	13 8	13 5	19 0	16.4	17.9	17 0	17.2	19 0	19 1	15.3
Ti/Zr	78.00	75 97	57.70	78.60	58.74	70.54	54.11	54.64	54.51	66.86	63 96	67.98	67 94	67.34	67 05	82.70	54.27
K/Ba	30.79	33 20	29.79	32.33	30.63	34.09	29.43	30.76	30 14	26.63	30.90	31.01	30.66	30.32	31 07	33.38	31 66

++ Alkaline basalts with quartz xenocryst 1 Late Pliocene-Early Pleistocene 2 Pleistocene 3 Late Pleistocene-Early Holocene 4 Holocene 5 Prehistoric

TABLE 4: CHEMICAL COMPOSITION OF THE ALKALINE BASALTS, LOS VOLCANES VOLCANIC FIELD

	Los Volcanes 5					
	25-3	25-1	23-11*	23-10	23-9	23-12
	Media Luna	Media Luna	Bombas	Bombas	Bombas	Bombas
SiO2	48.78	49.07	47 77	47.64	47 75	47 95
TiO2	1.85	1 80	2 13	2.14	2 16	2 32
Al2O3	17.55	17 14	17 29	17.34	17.49	18 36
Fe2O3	10.61	10 68	10.93	11 07	11.06	11.08
MnO	0.17	0.17	0.17	0.17	0.17	0 17
MgO	6 35	6 33	5.83	5 80	5.76	4.73
CaO	9.14	9.17	10.05	10.06	10.21	8.13
Na2O	3 94	3 70	3.61	3.67	3 83	4.65
K2O	1 50	1.46	1.40	1.43	1.44	1.73
P2O5	0.51	0.46	0 44	0.43	0 42	0.72
Total	100.39	99 97	99.61	99.75	100 28	99 85
Mg#	0 57	0.57	0 54	0 54	0 53	0.49
FeO*/MgO	1 50	1 52	1 69	1 72	1 73	2 11
Qz						
Or	8.9	8.6	8.3	8.4	8 5	10.2
Ab	25.1	26.7	22.2	21.4	20 5	25.9
An	25.8	25 9	26 9	26 6	26 3	24.1
Ne	4.5	2 5	4 5	5 3	6 5	7.3
Diop	13.3	13 6	16 6	16.9	17 8	9.6
Hy						
Ol	15.7	15 7	13.6	13.6	13 1	14 1
Mnt	1.5	1 6	1.6	1 6	1 6	1.6
Il	3.5	3.4	4 0	4 1	4.1	4 4
Ap	1.2	1 1	1.0	1 0	1 0	1.7

++ Alkaline Basalts with quartz xennocryst 1 Late Pliocene-Early Pleistocene 2 Pleistocene 3 Late Pleistocene-Early Holocene 4 Holocene 5 Prehistoric

TABLE 4: CHEMICAL COMPOSITION OF THE ALKALINE BASALTS, LOS VOLCANES VOLCANIC FIELD

	Los Volcanes 5					
	25-3	25-1	23-11*	23-10	23-9	23-12
	Media Luna	Media Luna	Bombas	Bombas	Bombas	Bombas
Rb	33.6	32.8	26 5	25.1	24.8	27 9
Sr	720.7	660.0	663 0	683 1	680 3	958.3
Ba	389.5	383.4	340 3	342 5	344.8	435 6
V	216.0	197.3	245.2	241.3	243.9	184.8
Cr	144.5	158.0	86 9	81.3	77 1	0.8
Ni	74.2	65.9	48.8	45.1	44.3	21.5
Zn	96.2	90 6	97.1	91.8	91 9	85.9
Ga	20 9	21 1	21 0	21 3	21 7	20.7
Y	23 5	24.3	23 6	23.4	23 4	25.3
Zr	213.6	211.0	176 7	180.6	186.0	233.5
Nb	24.1	24.4	21 2	22.6	22.1	30.1
Ce	47.9	47.4	44 4	41.2	40.6	55.9
Ba/Nb	16.2	15.7	16.0	15.2	15.6	14 5
Ce/Nb	2.0	1.9	2.1	1 8	1.8	1 9
Zr/Nb	8.9	8.7	8.3	8.0	8.4	7.8
Nb/Y	1.0	1.0	0.9	1 0	0.9	1 2
Ce/Y	2 0	2.0	1.9	1 8	1.7	2 2
K/Rb	372.1	368.9	438 2	472 4	481 0	515.0
Ba/Rb	11.6	11.7	12 8	13 7	13.9	15 6
P/Ce	46 2	42 3	42 7	45.8	45.4	56.2
Ba/Ce	8.1	8 1	7.7	8 3	8.5	7 8
Sr/Ce	15 0	13 9	14 9	16.6	16 8	17.1
Ti/Zr	51.90	51.15	72.20	70 97	69.61	59 51
K/Ba	32.06	31.57	34 18	34 56	34.60	33 01

++ Alkaline basalts with quartz xenocryst 1 Late Pliocene-Early Pleistocene 2 Pleistocene 3 Late Pleistocene-Early Holocene 4 Holocene 5 Prehistoric

TABLE 4: CHEMICAL COMPOSITION OF THE ALKALINE BASALTS, BUTA RANQUIL VOLCANIC FIELD

	Barranca Vn.			Buta Ranquil Vn 3						Cochiquito Vn 3			El Manzano 3
	26-12	26-10	26-11	27-6	27-4	BR16-81	27-2	27-1	27-3	26-9	26-8	C7-81	22-4
SiO2	47 06	53.93	46.91	46.99	48.32	48 66	50.32	50.46	52 45	48 53	48.87	48.09	49.95
TiO2	1 38	1 52	1.39	1 14	1 56	1.58	1 43	1.42	1 32	1 42	1.43	1 36	1.23
Al2O3	16 18	18.07	16.08	17.25	17.03	16.22	16.69	16.60	16 81	16.78	16.97	16.72	17.03
Fe2O3	11.29	9.34	11 29	10.46	11 15	11 79	10 35	10.27	9.46	9.81	9.76	11 44	9.44
MnO	0 17	0.17	0 17	0.17	0.17	0.16	0.16	0.16	0.15	0.16	0.16	0.17	0.15
MgO	10.21	3.38	10.11	7.87	7.03	6 99	6.92	6.83	6 10	8.43	8 18	7 68	7.50
CaO	10 02	6.46	10.03	12 35	10 47	9 95	9.50	9.44	8.58	9.30	9 42	9.03	9.42
Na2O	2.80	4.69	2 73	2.54	3.30	3.53	3.53	3 59	3 72	3.68	3.48	3 58	3.44
K2O	0 76	1.57	0.78	1.13	0 57	0 64	0.99	1.05	1 37	1 49	1.45	1 40	1 00
P2O5	0 25	0.54	0.25	0.31	0.22	0 22	0.25	0.25	0 26	0.53	0.53	0.54	0.39
Total	100.11	99.66	99 74	100 20	99.81	99 74	100.13	100.06	100 23	100 12	100.25	100 01	99.54
Mg#	0.67	0.44	0 66	0.62	0.58	0 57	0.60	0.59	0.59	0.65	0 65	0 60	0 64
FeO*/MgO	0.99	2 49	1 00	1 20	1 43	1 52	1 35	1 35	1 40	1.05	1 07	1 34	1.13
Qz													
Or	4.5	9 3	4.6	6.7	3.3	3 8	5 9	6 2	8.1	8.8	8 6	8 3	5 9
Ab	20.1	39.6	20 0	13.6	25.9	27.3	29.9	30.4	31 4	22.4	23.8	23 4	29 1
An	29.3	23 7	29.3	32.4	30.0	26 5	26.8	26.1	25 1	24 9	26.4	25 4	28 1
Ne	2.0		1 7	4 3	1 1	1 4				4.8	3 0	3 7	
Diop	15 2	4 0	15 3	21.9	16.8	17 6	15.3	15.6	12 9	14 4	13 8	13 0	13 1
Hy		15.0					1.3	0.7	9.3				2 2
Ol	23.2	1 7	23.0	16.1	16 6	16 9	15.2	15.4	8 0	18.7	18 4	19.7	15.7
Mnt	1 6	1.4	1.6	1.5	1.6	1 7	1 5	1.5	1.4	1.4	1 4	1 7	1 4
Ilm	2.6	2.9	2.6	2.2	3.0	3.0	2 7	2.7	2 5	2 7	2.7	2.6	2 3
Ap	0 6	1.3	0.6	0 7	0.5	0 5	0 6	0.6	0.6	1.2	1.2	1 3	0 9
Rb	13.5	26.0	14 0	30.8	7.8	8.6	21.6	26 1	37.4	43.4	40 2	38 1	19 5
Sr	877.8	866.3	622.2	594.5	449 9	450 0	475 9	356.1	493.3	759 7	761.8	728 0	725.1
Ba	327 9	450 5	269 3	298.4	137.6	138 0	235 2	227.2	319.6	409.7	423.6	443 0	441.0
V	199 4	99.0	208.4	253.3	219 2	214.0	196.5	191.9	173.9	181.8	179.0	190 0	175 0
Cr	423 9	0.7	442.1	113.4	154.8	220 0	186.9	192.4	144.2	257 9	247.2	270 0	254 0
Ni	180 2	4.1	194.9	70.2	61.3	73.0	72 8	69.2	57 4	110.9	107.0	120 0	100.0
Zn	81.0	56.6	87 3	78.4	85.3	103 0	76 8	78.2	75.5	72.2	73 6	131 0	74 0
Ga	17.9	15.8	18 0	17.3	19.3	19.4	19 5	19.0	18 7	18.5	19 8	18 2	18.8
Y	17.8	21.8	17.9	21 5	21.2	20.4	20 5	20.1	20.4	22.8	23 1	22 7	17.9
Zr	104 5	178.1	102 0	101 8	120.8	123 0	151.3	161.8	178.8	167.2	169.9	175 0	131 6
Nb	6.8	17.2	7.7	3.5	6.9	7.1	9.9	10.0	12 4	16.7	16.9	16 3	11 5
Ce	25.2	51 3	26.5	20.6	21.7	22 9	31.1	27.2	33.2	52.6	49.8	49.6	32.7
Ba/Nb	48.2	26.2	34.8	85.3	19.9	19.4	23.8	22.8	25.7	24.5	25 1	27 2	38.4
Ce/Nb	3.7	3.0	3.4	5.9	3.2	3.2	3.1	2.7	2.7	3 2	3.0	3 0	2 8
Zr/Nb	15.3	10.4	13 2	29.1	17.5	17 3	15.3	16.2	14.4	10.0	10.1	10.7	11.5
Nb/Y	0.4	0.8	0.4	0.2	0.3	0.3	0 5	0.5	0.6	0 7	0.7	0.7	0 6
Ce/Y	1 4	2.4	1 5	1 0	1 0	1 1	1 5	1.4	1 6	2 3	2.2	2.2	1 8
K/Rb	469.1	501 9	464.8	304.0	598.3	617.8	382.6	334.5	304.6	284.6	300.4	305 0	426 2
Ba/Rb	24 3	17.4	19 3	9.7	17.6	16.0	10 9	8.7	8 6	9 4	10.5	11.6	22.7
P/Ce	42.9	46.0	41.7	66.0	44.6	41.9	34.9	40.4	34 6	44.0	46.1	47.5	52.7
Ba/Ce	6.0	10.2	13.0	8.9	14.5		9.6	7.6	6.3	13.5	7.8		13 5
Sr/Ce	34.8	16.9	23.5	28.9	20.7	19.7	15 3	13.1	14 9	14.4	15.3	14.7	22.2
Ti/Zr	79 18	51.17	81.61	67.04	77.61	77.01	56.59	52.63	44.29	50.97	50.30	46.59	55.81
K/Ba	19.34	28.91	24 08	31.40	34.09	38.50	35.09	38.40	35.61	30.13	28 48	26.23	18 80

3 Late Pleistocene-Early Holocene Baranca Vn. is Pliocene

TABLE 4: CHEMICAL COMPOSITION OF THE ALKALINE BASALTS, ADDITIONAL DATA

	Vn. Barrancas		Buta Ranquil	Cochiquito			Tromen		Malal Negro 1			Diamante Area		Los Volcanes	Llancanelo	Nevado
	VM11	VM13	BR15	C7	C6	C8	27-5	27-7	22-2	22-3	22-1	TR2	83W	TC10	TC5	83E
SiO2	51 61	51.67	50.75	47.97	48.83	48 11	55.39	59 07	60 07	60.16	60.16	45 87	49.81	47.44	47 56	50 20
TiO2	1 84	1.80	1 36	1.40	1.37	1 52	1.15	1.00	1 39	1.38	1.38	1.58	1 62	1.64	1 88	1 78
Al2O3	18.44	17.96	17.69	16 96	16 59	16.62	17 02	17.16	15 51	15.46	15.47	15 00	15.06	15 42	16.21	16.79
Fe2O3	10 83	10.69	11.48	11.79	11.79	12.87	7 64	6.47	8.12	8 08	8 04	10.70	8 90	10.95	11.88	8 44
MnO	0 16	0.16	0.16	0.17	0.17	0.17	0.13	0.11	0.16	0 16	0 16	0.18	0.15	0 17	0 17	0 13
MgO	4 02	3.56	6 41	7 84	7 81	6 84	5 07	3.00	1.95	1.92	1 80	10.63	6 14	9 68	7 78	5.71
CaO	6.84	6 79	8.42	8.72	8.91	9.15	7.15	5.55	4 50	4.46	4 47	10.37	11.20	9.96	9 63	10.28
Na2O	4.61	4.54	3.68	3.59	3 56	3 84	3 99	4.37	4.40	4 36	4.36	3 63	3.04	3 71	3.90	4.06
K2O	1 36	1.41	1.26	1 45	1 28	0.86	2 32	2.75	3 58	3 59	3 62	1 21	1 53	1 02	0 99	1.14
P2O5	0.37	0.38	0 24	0.37	0 37	0 37	0.40	0.31	0.61	0.60	0 60	0 54	0.32	0.48	0 43	0.28
Total	100.08	98.96	101.45	100.26	100.68	100.35	100 24	99.78	100.29	100 16	100 04	99.71	97.77	100.47	100 43	98.81
Mg#	0 45	0.42	0.55	0 59	0 59	0.54	0 59	0 51	0 35	0 34	0.33	0.69	0 60	0.66	0.59	0.60
FeO*/MgO	2 42	2.70	1 61	1.35	1.36	1 69	1 36	1.94	3 74	3 80	4.02	0.91	1 30	1 02	1 37	1.33
Qz							0 1	5.6	7 1	7.4	7.5					
Or	8.0	8.3	7.5	8 6	7 6	5.1	13.7	16.2	21 1	21.2	21.4	7 2	9 0	6 0	5.9	6.7
Ab	39.0	38 4	31 1	22.4	25.3	26.1	33.8	36 9	37 2	36 9	36.9	12 2	24 8	19 1	22 1	28.5
An	25 6	24 5	28.0	25.9	25.5	25.6	21.7	19.1	12 0	12 0	12.0	21.1	22.9	22.4	23 8	24 2
Ne				4.3	2.6	3.5						10.1	0.5	6.7	5 9	3 2
Diop	4 9	5.6	10.0	12 3	13.3	14 4	9 2	5 3	5 4	5.2	5.3	21 7	24 9	19.4	17.3	20 4
Hy	3 0	6.4	1 8				16 7	12.5	11 5	11.5	11.1					
Ol	12.6	8 9	17.2	20.5	20.1	19.0						20.8	9.6	20.1	18 1	9 8
Mnt	1 6	1.6	1 7	1.7	1.7	1.9	1.1	0 9	1.2	1.2	1.2	1.6	1 3	1.6	1 7	1 2
Ilm	3 5	3.4	2.6	2.7	2 6	2.9	2.8	1 9	2.7	2.6	2.6	3.0	3.1	3.1	3.6	3.4
Ap	0 9	0 9	0.6	0.9	0.9	0.9	0 9	0 7	1 4	1.4	1 4	1.3	0 7	1.1	1.0	0.7
Rb		22.0		35.0			78.2	99.0	135.0	135.7	138.9	26.0	34 0	24.0	22.0	18.0
Sr		348.0		726 0			636.2	541 6	279.5	277.7	282 4	760.0	920 0	680.0	580 0	555 0
Ba		591.0		467.0			533.7	607.6	678 9	696.6	765 8	580.0	549.0	370.0	390 0	294 0
V		125.0		199.0			133.3	91 5	72 6	86.5	82.0	260.0		210.0	230 0	
Cr		73.0		262.0			124.4	23 5	0.0	0.0	0.0	500.0	198 0	420.0	201 0	155.0
Ni		27.0		86.0			56.7	19 1	8.2	7.2	6 1	200.0	112 0	184.0	115 0	129.0
Zn							68.3	56.5	104.1	93.6	108.2		0 0			
Ga							17.4	18 9	19.4	20.2	19.9		0 0			
Y		48.0		27 0			21.7	21 1	50 7	50.5	51 6	18.0	19.0	17.0	21.0	12 0
Zr		321.0		174 0			266.1	327 3	392.9	388 5	397 4	147 0	150.0	163.0	128 0	124.0
Nb		15.0		17.0			20.1	20.3	15.8	15.6	15.8	14.0	15 0	24 0	16 0	13.0
Ce							53.4	59.9	91 8	86.1	93.2	54.1	42.3	41 4	31 7	22.3
Ba/Nb		39.4		27.5			26.5	29.9	43.1	44.5	48.3	41.4	36 6	15 4	24 4	22 6
Ce/Nb							2 7	2.9	5 8	5.5	5.9	3.9	2 8	1.7	2.0	1.7
Zr/Nb		21.4		10.2			13.2	16.1	24.9	24.8	25 1	10 5	10.0	6.8	8 0	9.5
Nb/Y		0.3		0.6			0.9	1.0	0.3	0.3	0.3	0.8	0 8	1 4	0 8	1.1
Ce/Y							2.5	2.8	1.8	1.7	1.8	3.0	2 2	2 4	1 5	1.9
K/Rb		532.0		343.9			246.1	230.2	220.0	219.4	216.3	22.3	16.1	15.4	17 7	525.8
Ba/Rb		26.9		13.3			6.8	6.1	5.0	5.1	5.5	22.3	16.1	15.4	17 7	16.3
P/Ce							32.3	22.6	29.0	30.5	28.2	43.6	33.0	50.6	59.2	54.8
Ba/Ce							10.0	10 1	7.4	8.1	8.2	10.7	13.0	8 9	12.3	13.2
Sr/Ce							11.9	9.0	3.0	3.2	3.0	14.0	21.7	16.4	18 3	24.9
Ti/Zr		33.62		48 24			25 80	18.28	21.27	21.30	20.76	64.44	64.75	60 32	88.05	86 06
K/Ba	19 10		22.40			13.38	31 67	33.58	42.63	38.86	51.77	18.30	34.33	21.71	27.95	

The data for Barrancas and Cochiquito is from Bermudez Delpino,(1989); for Volcanes Llancanelo, Nevado and Diamante is from Stern et al.(1991) and for Tromen and Malal Negro this study.

Table 5: Isotopic Composition of the Alkaline Basalts

	87Sr/86Sr	143Nd/144Nd	206Pb/204Pb	207Pb/204Pb	208Pb/204Pb
Nevado Area					
Eastern Nevado					
15-5 (I)	0.704208	0.512779	18.594	15.585	38.418
15-4 (II)	0.703997		18.410	15.607	38.350
16-1 (II?)	0.703981	0.512829	18.389	15.582	38.222
Western Nevado					
18-7 (I)	0.703903	0.512823	18.551	15.587	38.384
Llancanelo Area					
21-1(III)	0.704024	0.512777	18.400	15.567	38.269
21-7 (I)	0.704116	0.512766	18.503	15.580	38.387
Los Volcanes Area					
23-1 (IV)	0.703903	0.512789	18.351	15.554	38.184
25-1 (V)	0.703902	0.512806	18.403	15.573	38.260
25-7 (III)	0.704069	0.512758	18.310	15.595	38.248
25-11 (II)	0.704131	0.512743	18.383	15.594	38.339
Buta Ranquil					
27-4 (III)	0.703769	0.512847	18.470	15.582	38.321
27-6 (III)	0.704130		18.541	15.593	38.371
I Late Pliocene-Early Pleistocene			II Pleistocene		
III Late Pleistocene-Early Holocene			IV Holocene		V Prehistoric

TABLE 6: MASS BALANCE CALCULATION FOR THE HYPERSTHENE NORMATIVE LAVAS FROM BUTA RANQUIL

	Tromen	Buta Ranquil Nepheline Lava	Buta Ranquil Hypersthene Lava			
	27-7	27-4	27-1 Calc	27-1 Obser	Residual	Allowed Resi
SiO2	59.20	48.41	50.31	50.42	0.11	2.82
TiO2	1.00	1.57	1.45	1.42	-0.03	0.07
Al2O3	17.19	17.07	17.05	16.59	-0.46	0.91
Fe2O3*	6.49	11.17	10.28	10.26	-0.02	0.49
MnO	0.11	0.17	0.16	0.16	0.00	0.02
MgO	3.00	7.04	6.28	6.83	0.55	0.28
CaO	5.57	10.49	9.56	9.43	-0.13	0.43
Na2O	4.38	3.30	3.50	3.59	0.09	0.36
K2O	2.75	0.57	0.97	1.05	0.08	0.10
P2O5	0.31	0.22	0.24	0.25	0.01	0.03
Proportions	0.18	0.81	S(R)^2 =		0.55	

	Tromen	Buta Ranquil Nepheline Lava	Buta Ranquil Hypersthene Lava			
	27-7	BR16-81	27-1 Calc	27-1 Obser	Residual	Allowed Resi
SiO2	59.20	48.79	50.46	50.42	-0.04	3.31
TiO2	1.00	1.58	1.48	1.42	-0.06	0.08
Al2O3	17.19	16.26	16.38	16.59	0.21	1.04
Fe2O3*	6.49	11.82	10.87	10.26	-0.61	0.59
MnO	0.11	0.16	0.15	0.16	0.01	0.02
MgO	3.00	7.01	6.30	6.83	0.53	0.33
CaO	5.57	9.98	9.19	9.43	0.24	0.49
Na2O	4.38	3.54	3.68	3.59	-0.09	0.40
K2O	2.75	0.64	1.00	1.05	0.05	0.12
P2O5	0.31	0.22	0.24	0.25	0.02	0.03
Proportions	0.17	0.83	S(R)^2 =		0.75	

	Tromen	Buta Ranquil Nepheline Lava	Buta Ranquil Hypersthene Lava			
	27-7	27-4	27-2 Calc	27-2 Obser	Residual	Allowed Resi
SiO2	59.20	48.41	50.15	50.25	0.10	2.72
TiO2	1.00	1.57	1.47	1.43	-0.04	0.07
Al2O3	17.19	17.07	17.06	16.67	-0.39	0.88
Fe2O3*	6.49	11.17	10.37	10.33	-0.04	0.47
MnO	0.11	0.17	0.16	0.16	0.00	0.02
MgO	3.00	7.04	6.36	6.91	0.55	0.27
CaO	5.57	10.49	9.65	9.49	-0.16	0.41
Na2O	4.38	3.30	3.48	3.52	0.04	0.35
K2O	2.75	0.57	0.94	0.99	0.05	0.10
P2O5	0.31	0.22	0.24	0.25	0.02	0.03
Proportions	0.17	0.83	S(R)^2 =		0.50	

	Tromen	Buta Ranquil Nepheline Lava	Buta Ranquil Hypersthene Lava			
	27-7	BR16-81	27-2 Calc	27-2 Obser	Residual	Allowed Resi
SiO2	59.20	48.79	50.30	50.25	-0.05	3.50
TiO2	1.00	1.58	1.49	1.43	-0.06	0.09
Al2O3	17.19	16.26	16.37	16.67	0.30	1.10
Fe2O3*	6.49	11.82	10.97	10.33	-0.64	0.62
MnO	0.11	0.16	0.15	0.16	0.01	0.02
MgO	3.00	7.01	6.38	6.91	0.53	0.35
CaO	5.57	9.98	9.27	9.49	0.22	0.52
Na2O	4.38	3.54	3.66	3.52	-0.14	0.41
K2O	2.75	0.64	0.97	0.99	0.02	0.12
P2O5	0.31	0.22	0.23	0.25	0.02	0.03
Proportions	0.16	0.84	S(R)^2 =		0.86	

	Tromen	Buta Ranquil Nepheline Lava	Buta Ranquil Hypersthene Lava			
	27-7	27-4	27-3 Calc	27-3 Obser	Residual	Allowed Resi
SiO2	59.20	48.41	52.24	52.33	0.09	2.44
TiO2	1.00	1.57	1.36	1.32	-0.04	0.06
Al2O3	17.19	17.07	17.10	16.77	-0.33	0.79
Fe2O3*	6.49	11.17	9.49	9.44	-0.05	0.43
MnO	0.11	0.17	0.15	0.15	0.00	0.02
MgO	3.00	7.04	5.59	6.09	0.50	0.25
CaO	5.57	10.49	8.72	8.56	-0.16	0.37
Na2O	4.38	3.30	3.69	3.71	0.02	0.33
K2O	2.75	0.57	1.35	1.37	0.02	0.09
P2O5	0.31	0.22	0.25	0.26	0.01	0.02
Proportions	0.36	0.64	S(R)^2 =		0.39	

	Tromen	Buta Ranquil Nepheline Lava	Buta Ranquil Hypersthene Lava			
	27-7	BR16-81	27-3 Calc	27-3 Obser	Residual	Allowed Resi
SiO2	59.20	48.79	52.36	52.33	-0.03	2.91
TiO2	1.00	1.58	1.38	1.32	-0.06	0.07
Al2O3	17.19	16.26	16.57	16.77	0.20	0.92
Fe2O3*	6.49	11.82	9.95	9.44	-0.51	0.52
MnO	0.11	0.16	0.14	0.15	0.01	0.02
MgO	3.00	7.01	5.61	6.09	0.48	0.29
CaO	5.57	9.98	8.43	8.56	0.13	0.43
Na2O	4.38	3.54	3.83	3.71	-0.12	0.37
K2O	2.75	0.64	1.38	1.37	-0.01	0.11
P2O5	0.31	0.22	0.25	0.26	0.01	0.03
Proportions	0.35	0.65	S(R)^2 =		0.56	

TABLE 6: MASS BALANCE CALCULATION FOR THE HYPERSTHENE NORMATIVE LAVAS FROM BUTA RANQUIL

	Tromen	Buta Ranquil Nepheline Lava	Buta Ranquil Hypersthene Lava			
	27-7	27-4	27-1 Calc	27-1 Obser	Residual	Allowed Resi
Rb	99.04	7.84	24.67	26.08	-1.41	8.40
Sr	541.59	449.94	466.01	356.11	109.90	35.81
Ba	607.59	137.60	224.15	227.20	-3.05	53.74
V	91.51	219.17	195.17	191.94	3.23	16.36
Cr	23.52	154.79	130.25	192.35	-62.10	17.84
Ni	19.11	61.34	53.42	69.23	-15.81	6.41
Zn	56.46	85.29	79.80	78.18	1.62	7.54
Ga	18.88	19.34	19.22	18.99	0.23	2.48
Y	21.06	21.17	21.11	20.09	1.02	1.42
Zr	327.28	120.82	158.72	161.75	-3.03	16.72
Nb	20.33	6.90	9.37	9.98	-0.61	1.44
Ce	59.93	21.74	28.75	27.21	1.54	7.95

	Tromen	Buta Ranquil Nepheline Lava	Buta Ranquil Hypersthene Lava			
	27-7	BR16-81	27-1 Calc	27-1 Obser	Residual	Allowed Resi
Rb	99.04	8.60	24.17	26.08	-1.91	8.90
Sr	541.59	450.00	464.67	356.11	108.56	40.30
Ba	607.59	138.00	218.61	227.20	-8.59	57.12
V	91.51	214.00	192.35	191.94	0.41	17.68
Cr	23.52	220.00	185.58	192.35	-6.77	20.66
Ni	19.11	73.00	63.53	69.23	-5.70	7.15
Zn	56.46	103.00	94.72	78.18	16.54	8.73
Ga	18.88	19.40	19.26	18.99	0.27	2.66
Y	21.06	20.40	20.46	20.09	0.37	1.59
Zr	327.28	123.00	157.91	161.75	-3.84	18.77
Nb	20.33	7.10	9.36	9.98	-0.62	1.57
Ce	59.93	22.90	29.23	27.21	2.02	8.37

	Tromen	Buta Ranquil Nepheline Lava	Buta Ranquil Hypersthene Lava			
	27-7	27-4	27-2 Calc	27-2 Obser	Residual	Allowed Resi
Rb	99.04	7.84	23.06	21.57	1.49	8.30
Sr	541.59	449.94	464.71	475.92	-11.21	34.86
Ba	607.59	137.60	215.92	235.19	-19.27	53.03
V	91.51	219.17	197.59	196.52	1.07	16.06
Cr	23.52	154.79	132.68	186.90	-54.22	17.65
Ni	19.11	61.34	54.21	72.84	-18.63	6.33
Zn	56.46	85.29	80.37	76.83	3.54	7.40
Ga	18.88	19.34	19.24	19.46	-0.22	2.44
Y	21.06	21.17	21.13	20.53	0.60	1.38
Zr	327.28	120.82	155.15	151.29	3.86	16.30
Nb	20.33	6.90	9.13	9.88	-0.75	1.41
Ce	59.93	21.74	28.09	31.10	-3.01	7.87

	Tromen	Buta Ranquil Nepheline Lava	Buta Ranquil Hypersthene Lava			
	27-7	BR16-81	27-2 Calc	27-2 Obser	Residual	Allowed Resi
Rb	99.04	8.60	40.10	21.57	18.53	9.10
Sr	541.59	450.00	481.41	475.92	5.49	42.10
Ba	607.59	138.00	301.45	235.19	66.26	58.49
V	91.51	214.00	171.09	196.52	-25.43	18.26
Cr	23.52	220.00	151.30	186.90	-35.60	21.15
Ni	19.11	73.00	54.14	72.84	-18.70	7.33
Zn	56.46	103.00	86.67	76.83	9.84	9.03
Ga	18.88	19.40	19.20	19.46	-0.26	2.73
Y	21.06	20.40	20.61	20.53	0.08	1.67
Zr	327.28	123.00	194.04	151.29	42.75	19.57
Nb	20.33	7.10	11.70	9.88	1.82	1.62
Ce	59.93	22.90	35.78	31.10	4.68	8.53

	Tromen	Buta Ranquil Nepheline Lava	Buta Ranquil Hypersthene Lava			
	27-7	27-4	27-3 Calc	27-3 Obser	Residual	Allowed Resi
Rb	99.04	7.84	40.47	37.37	3.10	8.02
Sr	541.59	449.94	482.46	493.31	-10.85	32.28
Ba	607.59	137.60	305.68	319.61	-13.93	51.11
V	91.51	219.17	173.36	173.94	-0.58	15.20
Cr	23.52	154.79	107.73	144.16	-36.43	17.13
Ni	19.11	61.34	46.19	57.42	-11.23	6.10
Zn	56.46	85.29	74.92	75.48	-0.56	7.02
Ga	18.88	19.34	19.16	18.69	0.47	2.34
Y	21.06	21.17	21.12	20.44	0.68	1.27
Zr	327.28	120.82	194.62	178.83	15.79	15.17
Nb	20.33	6.90	11.70	12.43	-0.73	1.34
Ce	59.93	21.74	35.39	33.18	2.21	7.66

	Tromen	Buta Ranquil Nepheline Lava	Buta Ranquil Hypersthene Lava			
	27-7	BR16-81	27-3 Calc	27-3 Obser	Residual	Allowed Resi
Rb	99.04	8.60	22.61	37.37	-14.76	8.50
Sr	541.59	450.00	463.31	493.31	-30.00	36.56
Ba	607.59	138.00	210.56	319.61	-109.05	54.33
V	91.51	214.00	194.57	173.94	20.63	16.48
Cr	23.52	220.00	189.09	144.16	44.93	19.66
Ni	19.11	73.00	64.50	57.42	7.08	6.77
Zn	56.46	103.00	95.58	75.48	20.10	8.11
Ga	18.88	19.40	19.28	18.69	0.59	2.51
Y	21.06	20.40	20.46	20.44	0.02	1.43
Zr	327.28	123.00	154.44	178.83	-24.39	17.11
Nb	20.33	7.10	9.14	12.43	-3.29	1.47
Ce	59.93	22.90	28.60	33.18	-4.58	8.05

TABLE 6: MASS BALANCE CALCULATION FOR THE HYPERSTHENE NORMATIVE LAVAS FROM BUTA RANQUIL

	Tromen	Buta Ranquil Nepheline Lava	Buta Ranquil Hypersthene Lava			
	27-5	27-4	27-1 Calc	27-1 Obser	Residual	Allowed Resi
SiO2	55.25	48.41	50.33	50.42	0.09	3.15
TiO2	1.14	1.57	1.44	1.42	-0.02	0.08
Al2O3	16.98	17.07	17.03	16.59	-0.44	1.05
Fe2O3*	7.62	11.17	10.15	10.26	0.11	0.59
MnO	0.13	0.17	0.16	0.16	0.00	0.02
MgO	5.06	7.04	6.47	6.83	0.36	0.37
CaO	7.13	10.49	9.53	9.43	-0.10	0.53
Na2O	3.98	3.30	3.50	3.59	0.09	0.38
K2O	2.31	0.57	1.06	1.05	-0.01	0.11
P2O5	0.39	0.22	0.27	0.25	-0.02	0.03
Proportions	0.28	0.72	S(R)^2 =		0.35	

	Tromen	Buta Ranquil Nepheline Lava	Buta Ranquil Hypersthene Lava			
	27-5	BR16-81	27-1 Calc	27-1 Obser	Residual	Allowed Resi
SiO2	55.25	48.79	50.47	50.42	-0.05	3.32
TiO2	1.14	1.58	1.46	1.42	-0.04	0.09
Al2O3	16.98	16.26	16.43	16.59	0.16	1.07
Fe2O3*	7.62	11.82	10.66	10.26	-0.40	0.64
MnO	0.13	0.16	0.15	0.16	0.01	0.02
MgO	5.06	7.01	6.47	6.83	0.36	0.39
CaO	7.13	9.98	9.19	9.43	0.24	0.54
Na2O	3.98	3.54	3.65	3.59	-0.06	0.40
K2O	2.31	0.64	1.09	1.05	-0.04	0.11
P2O5	0.39	0.22	0.27	0.25	-0.02	0.03
Proportions	0.27	0.73	S(R)^2 =		0.38	

	Tromen	Buta Ranquil Nepheline Lava	Buta Ranquil Hypersthene Lava			
	27-5	27-4	27-2 Calc	27-2 Obser	Residual	Allowed Resi
SiO2	55.25	48.41	50.17	50.25	0.08	3.00
TiO2	1.14	1.57	1.45	1.43	-0.02	0.08
Al2O3	16.98	17.07	17.04	16.67	-0.37	1.00
Fe2O3*	7.62	11.17	10.25	10.33	0.08	0.56
MnO	0.13	0.17	0.16	0.16	0.00	0.02
MgO	5.06	7.04	6.53	6.91	0.38	0.36
CaO	7.13	10.49	9.62	9.49	-0.13	0.51
Na2O	3.98	3.30	3.48	3.52	0.04	0.37
K2O	2.31	0.57	1.02	0.99	-0.03	0.10
P2O5	0.39	0.22	0.27	0.25	-0.02	0.03
Proportions	0.26	0.74	S(R)^2 =		0.31	

	Tromen	Buta Ranquil Nepheline Lava	Buta Ranquil Hypersthene Lava			
	27-5	BR16-81	27-2 Calc	27-2 Obser	Residual	Allowed Resi
SiO2	55.25	48.79	50.32	50.25	-0.07	3.72
TiO2	1.14	1.58	1.47	1.43	-0.04	0.10
Al2O3	16.98	16.26	16.42	16.67	0.25	1.20
Fe2O3*	7.62	11.82	10.77	10.33	-0.44	0.71
MnO	0.13	0.16	0.15	0.16	0.01	0.02
MgO	5.06	7.01	6.52	6.91	0.39	0.44
CaO	7.13	9.98	9.26	9.49	0.23	0.61
Na2O	3.98	3.54	3.64	3.52	-0.12	0.43
K2O	2.31	0.64	1.05	0.99	-0.06	0.12
P2O5	0.39	0.22	0.26	0.25	-0.01	0.03
Proportions	0.25	0.75	S(R)^2 =		0.49	

	Tromen	Buta Ranquil Nepheline Lava	Buta Ranquil Hypersthene Lava			
	27-5	27-4	27-3 Calc	27-3 Obser	Residual	Allowed Resi
SiO2	55.25	48.41	52.25	52.33	0.08	2.33
TiO2	1.14	1.57	1.34	1.32	-0.02	0.06
Al2O3	16.98	17.07	17.06	16.77	-0.29	0.77
Fe2O3*	7.62	11.17	9.28	9.44	0.16	0.44
MnO	0.13	0.17	0.15	0.15	0.00	0.02
MgO	5.06	7.04	5.99	6.09	0.11	0.28
CaO	7.13	10.49	8.70	8.56	-0.14	0.39
Na2O	3.98	3.30	3.68	3.71	0.03	0.32
K2O	2.31	0.57	1.52	1.37	-0.15	0.08
P2O5	0.39	0.22	0.32	0.26	-0.06	0.03
Proportions	0.54	0.46	S(R)^2 =		0.17	

	Tromen	Buta Ranquil Nepheline Lava	Buta Ranquil Hypersthene Lava			
	27-5	BR16-81	27-3 Calc	27-3 Obser	Residual	Allowed Resi
SiO2	55.25	48.79	52.34	52.33	-0.01	1.79
TiO2	1.14	1.58	1.36	1.32	-0.03	0.05
Al2O3	16.98	16.26	16.68	16.77	0.09	0.58
Fe2O3*	7.62	11.82	9.61	9.44	-0.17	0.35
MnO	0.13	0.16	0.14	0.15	0.01	0.01
MgO	5.06	7.01	5.99	6.09	0.10	0.21
CaO	7.13	9.98	8.49	8.56	0.08	0.29
Na2O	3.98	3.54	3.78	3.71	-0.07	0.29
K2O	2.31	0.64	1.53	1.37	-0.16	0.07
P2O5	0.39	0.22	0.32	0.26	-0.06	0.02
Proportions	0.53	0.47	S(R)^2 =		0.09	

TABLE 6: MASS BALANCE CALCULATION FOR THE HYPERSTHENE NORMATIVE LAVAS FROM BUTA RANQUIL

	Tromen	Buta Ranquil Nepheline Lava	Buta Ranquil Hypersthene Lava			
	27-5	27-4	27-1 Calc	27-1 Obser	Residual	Allowed Resi
Rb	78.19	7.84	20.82	26.08	-5.26	8.35
Sr	636.20	449.94	483.49	356.11	127.38	42.28
Ba	533.65	137.60	210.49	227.20	-16.71	55.15
V	133.34	219.17	202.90	191.94	10.96	18.66
Cr	124.36	154.79	148.88	192.35	-43.47	21.16
Ni	56.67	61.34	60.36	69.23	-8.87	7.70
Zn	68.26	85.29	81.98	78.18	3.80	8.41
Ga	17.39	19.34	18.94	18.99	-0.05	2.60
Y	21.72	21.17	21.23	20.09	1.14	1.61
Zr	266.08	120.82	147.42	161.75	-14.33	17.03
Nb	20.11	6.90	9.33	9.98	-0.65	1.55
Ce	53.40	21.74	27.55	27.21	0.34	8.15

	Tromen	Buta Ranquil Nepheline Lava	Buta Ranquil Hypersthene Lava			
	27-5	BR16-81	27-1 Calc	27-1 Obser	Residual	Allowed Resi
Rb	78.19	8.60	20.58	26.08	-5.50	8.51
Sr	636.20	450.00	480.98	356.11	124.87	43.92
Ba	533.65	138.00	205.87	227.20	-21.33	56.20
V	133.34	214.00	199.56	191.94	7.62	19.04
Cr	124.36	220.00	202.96	192.35	10.61	23.53
Ni	56.67	73.00	70.00	69.23	0.77	8.23
Zn	68.26	103.00	96.75	78.18	18.57	9.17
Ga	17.39	19.40	19.00	18.99	0.01	2.65
Y	21.72	20.40	20.58	20.09	0.49	1.65
Zr	266.08	123.00	147.36	161.75	-14.39	17.68
Nb	20.11	7.10	9.33	9.98	-0.65	1.60
Ce	53.40	22.90	28.10	27.21	0.89	8.31

	Tromen	Buta Ranquil Nepheline Lava	Buta Ranquil Hypersthene Lava			
	27-5	27-4	27-2 Calc	27-2 Obser	Residual	Allowed Resi
Rb	78.19	7.84	19.58	21.57	-1.99	8.22
Sr	636.20	449.94	480.51	475.92	4.59	40.70
Ba	533.65	137.60	203.58	235.19	-31.61	54.15
V	133.34	219.17	204.57	196.52	8.05	18.13
Cr	124.36	154.79	149.52	186.90	-37.38	20.73
Ni	56.67	61.34	60.49	72.84	-12.35	7.52
Zn	68.26	85.29	82.34	76.83	5.51	8.18
Ga	17.39	19.34	18.99	19.46	-0.47	2.54
Y	21.72	21.17	21.24	20.53	0.71	1.55
Zr	266.08	120.82	144.93	151.29	-6.36	16.47
Nb	20.11	6.90	9.10	9.88	-0.78	1.51
Ce	53.40	21.74	27.00	31.10	-4.10	8.04

	Tromen	Buta Ranquil Nepheline Lava	Buta Ranquil Hypersthene Lava			
	27-5	BR16-81	27-2 Calc	27-2Obser	Residual	Allowed Resi
Rb	78.19	8.60	32.84	21.57	11.27	8.85
Sr	636.20	450.00	514.38	475.92	38.46	48.12
Ba	533.65	138.00	275.69	235.19	40.50	58.88
V	133.34	214.00	185.66	196.52	-10.86	20.43
Cr	124.36	220.00	186.44	186.90	-0.46	24.92
Ni	56.67	73.00	67.23	72.84	-5.61	8.75
Zn	68.26	103.00	90.78	76.83	13.95	9.86
Ga	17.39	19.40	18.68	19.46	-0.78	2.80
Y	21.72	20.40	20.84	20.53	0.31	1.81
Zr	266.08	123.00	172.71	151.29	21.42	19.19
Nb	20.11	7.10	11.62	9.88	1.74	1.70
Ce	53.40	22.90	33.50	31.10	2.40	8.62

	Tromen	Buta Ranquil Nepheline Lava	Buta Ranquil Hypersthene Lava			
	27-5	27-4	27-3 Calc	27-3 Obser	Residual	Allowed Resi
Rb	78.19	7.84	33.01	37.37	-4.36	7.65
Sr	636.20	449.94	516.31	493.31	23.00	33.63
Ba	533.65	137.60	279.22	319.61	-40.39	49.72
V	133.34	219.17	188.33	173.94	14.39	15.77
Cr	124.36	154.79	143.81	144.16	-0.35	18.84
Ni	56.67	61.34	59.63	57.42	2.21	6.73
Zn	68.26	85.29	79.15	75.48	3.67	7.16
Ga	17.39	19.34	18.63	18.69	-0.06	2.29
Y	21.72	21.17	21.35	20.44	0.91	1.26
Zr	266.08	120.82	172.72	178.83	-6.11	13.97
Nb	20.11	6.90	11.62	12.43	-0.81	1.34
Ce	53.40	21.74	33.05	33.18	-0.13	7.53

	Tromen	Buta Ranquil Nepheline Lava	Buta Ranquil Hypersthene Lava			
	27-5	BR16-81	27-3 Calc	27-3 Obser	Residual	Allowed Resi
Rb	78.19	8.60	19.38	37.37	-17.99	7.20
Sr	636.20	450.00	477.98	493.31	-15.33	27.90
Ba	533.65	138.00	199.09	319.61	-120.52	46.10
V	133.34	214.00	201.06	173.94	27.12	13.78
Cr	124.36	220.00	204.73	144.16	60.57	18.24
Ni	56.67	73.00	70.32	57.42	12.90	6.26
Zn	68.26	103.00	97.41	75.48	21.93	6.58
Ga	17.39	19.40	19.05	18.69	0.36	2.09
Y	21.72	20.40	20.56	20.44	0.12	1.03
Zr	266.08	123.00	144.95	178.83	-33.88	11.97
Nb	20.11	7.10	9.10	12.43	-3.33	1.20
Ce	53.40	22.90	27.58	33.18	-5.60	7.13

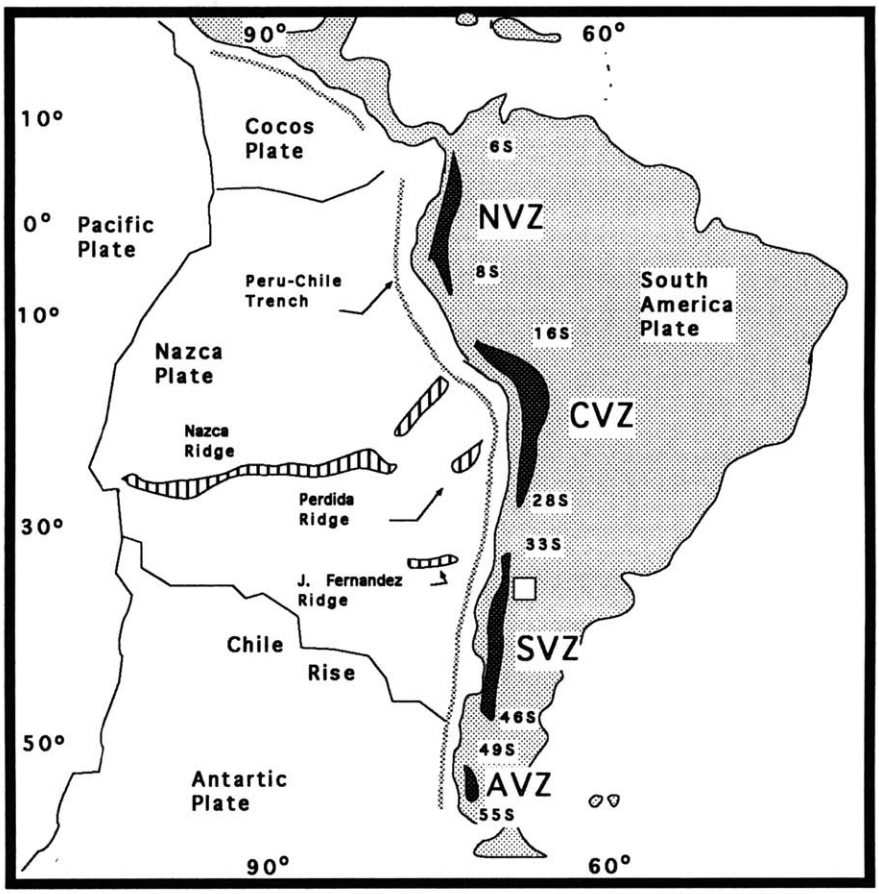

Figure 1 : Tectonic setting of western South America. Regions. The darkly shaded areas indicate Quaternary volcanism: NVZ, CVZ, SVZ and AVZ are Nothern, Central, Southern and Austral volcanic zones, respectively. White square at ≈ 35° S shows the studied area.

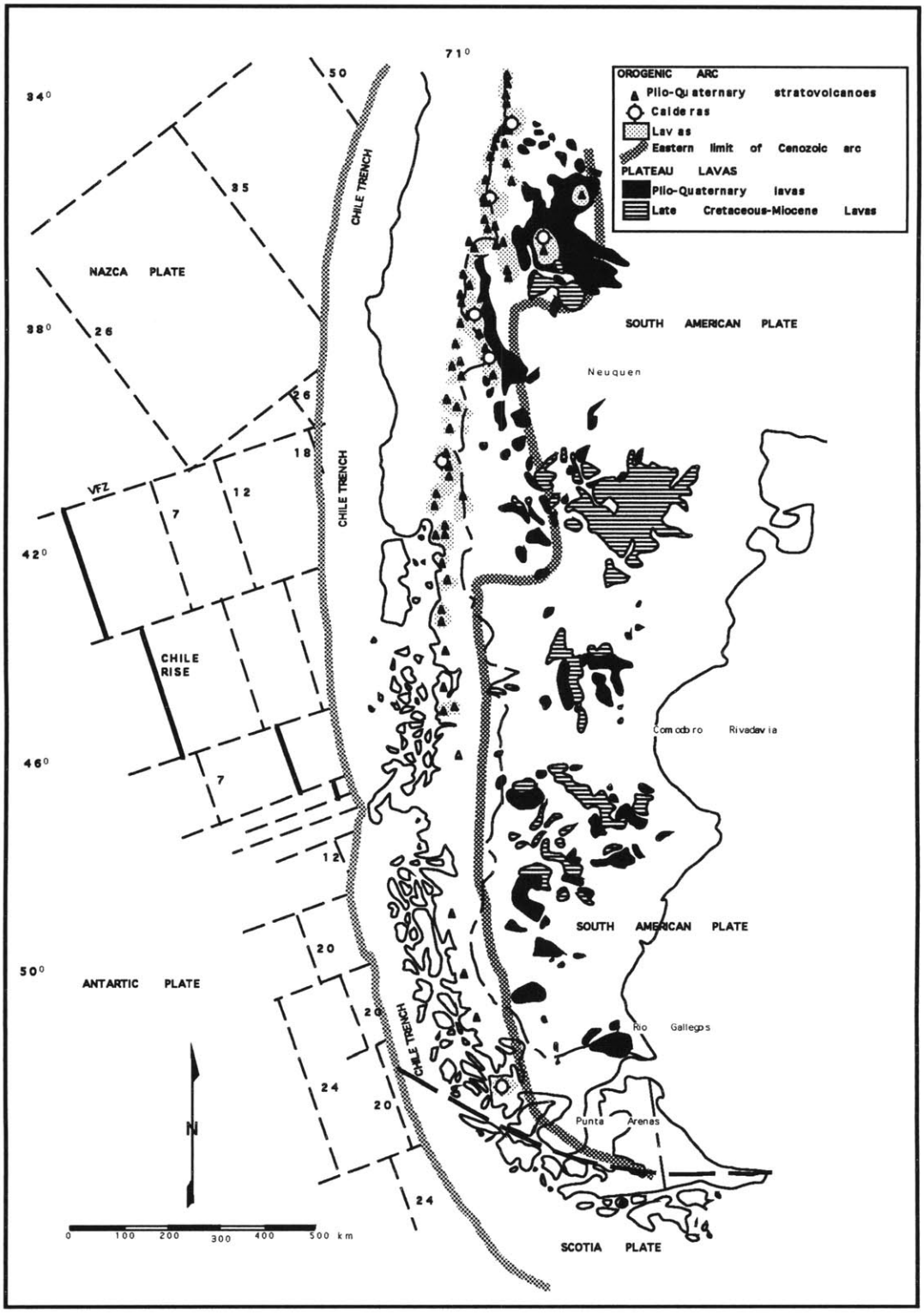

Figure 2: Map showing the outcrop of Pliocene and Quaternary (black) and older (lined) units of the Patagonian plateau lavas in southernmost South America (taken from Stern et al., 1990). South of 39° the volcanic front (calc-alkaline series) and back-arc (alkaline series) form two spatially and compositionally different volcanic associations. In contrast, between 35° - 39° no simple spatial or compositional division separates orogenic arc and back-arc lavas.

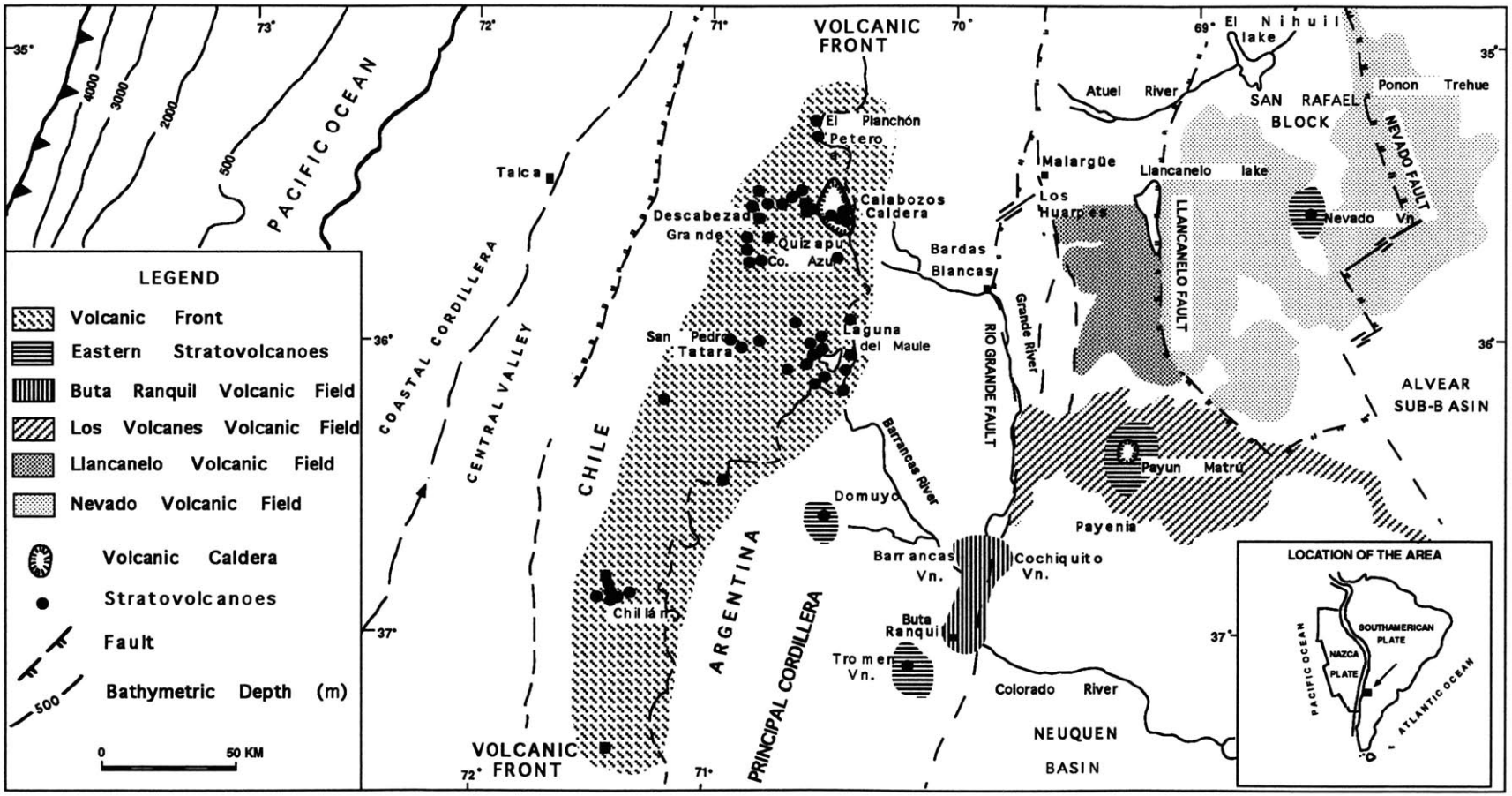

Figure 3: Map of Andean Region from 35°-37° S showing the different volcanic fields of Pliocene-Quaternary alkaline basalts erupted in the four physiographic provinces behind the volcanic front: Principal Cordillera, San Rafael block, Los Huarpes and Payenia depression and Alvear Sub-basin. Map modified from Bermudez and Delpino, (1989)

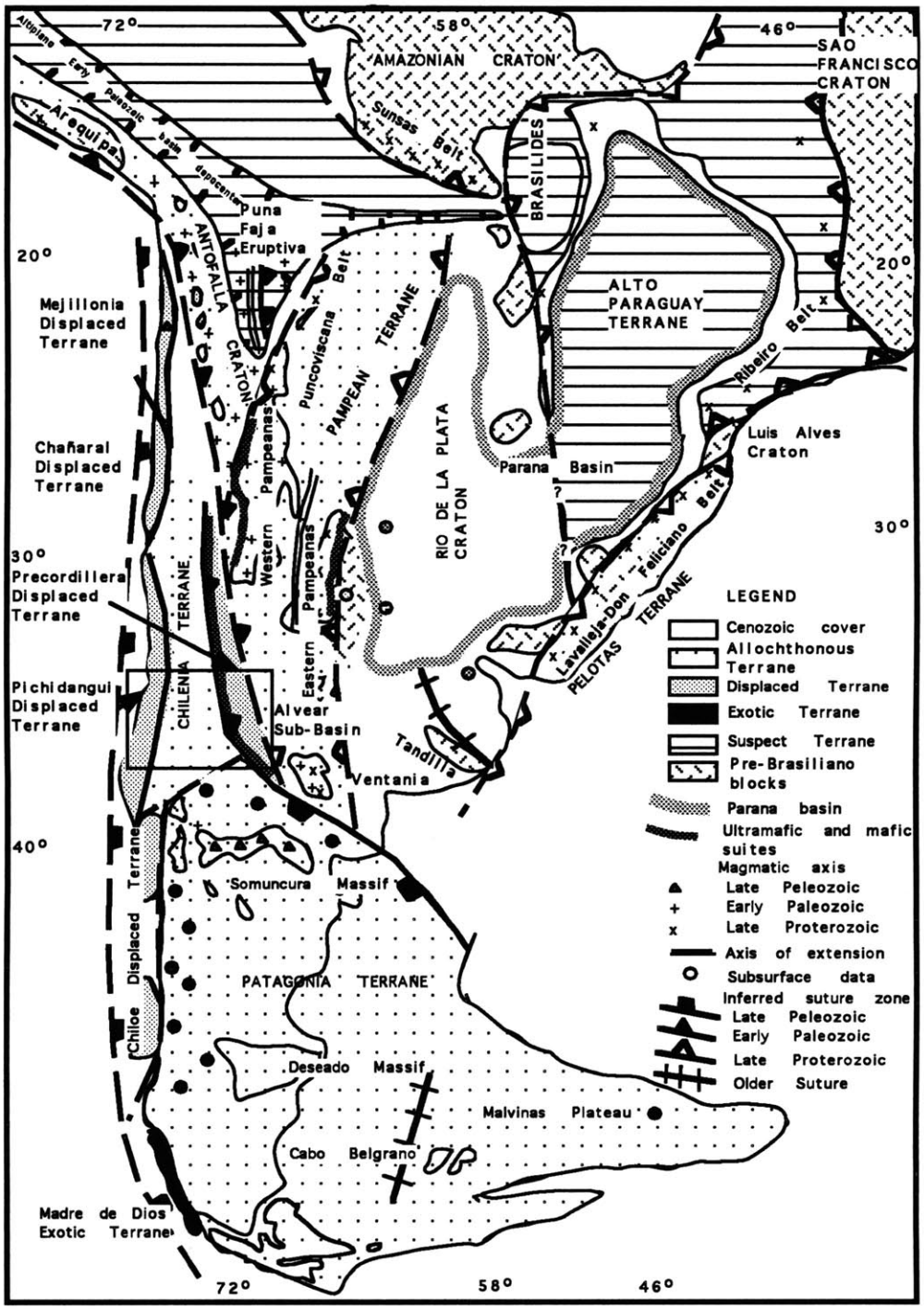

Figure 4: Main cratonic blocks and allochthonous terranes of southern South America. Taken from Ramos, (1988). This figure shows that the basement from the trench to the Alvear Sub-Basin is formed by distinct terranes accreted during different geologic times, Therefore, they have different crustal compositions. Rectangle at 36° approximates the studied area

GEOLOGY OF THE SAN RAFAEL BLOCK

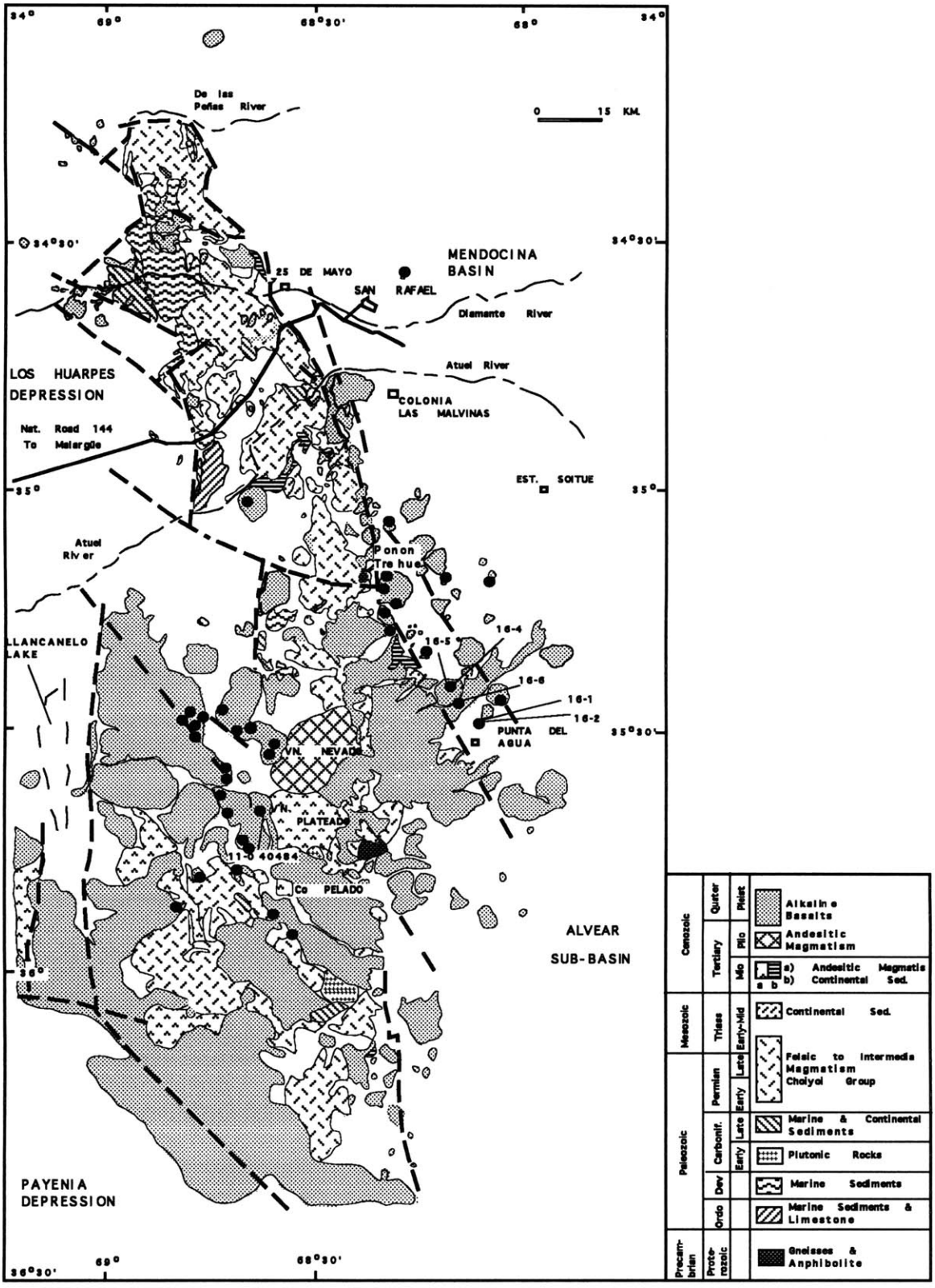

Figure 5: Geology of the San Rafael Block. The map shows the outcrops of Precambriam metamorphic basement, the importance of the Permo-Triassic felsic magmatism (Choiyoi Group), the Mio-Pliocene andesitic magmatism (Nevado Vn, Plateado Vn and Co Pelado) and the Nevado volcanic field of alkaline basalts with the sampling location (filled cicle). Map modified from Delpino (1989)

Nevado Volcanic Field, western sector

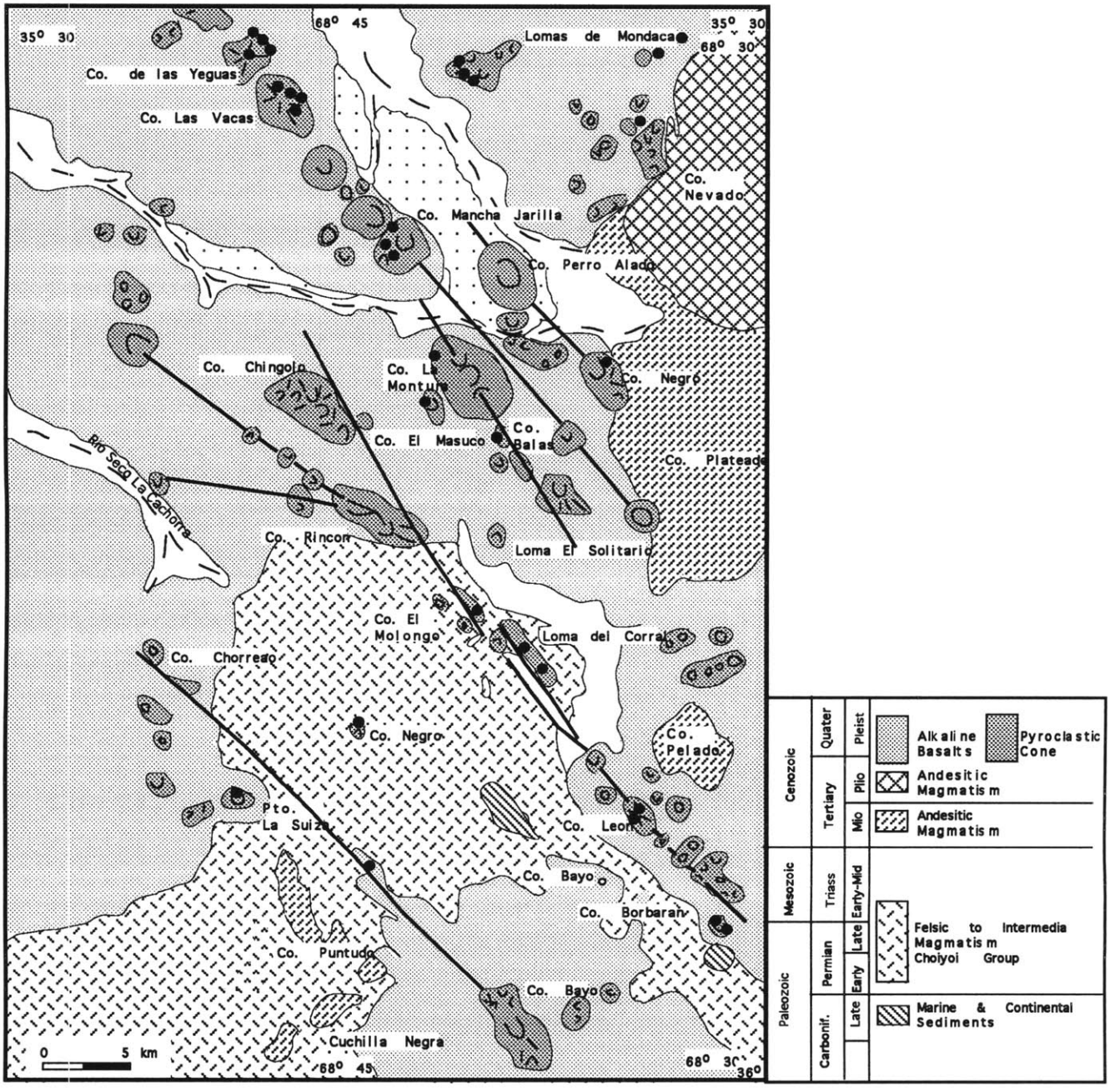

Figure 6: Detailed map of the Nevado volcanic field (western sector). The figure shows the composite cones (Las Vacas and Las Yeguas) and monogenetic cones aligned along fractures. Sampling locations indicated by filled circle. The map is from Bermudez and Delpino (1989).

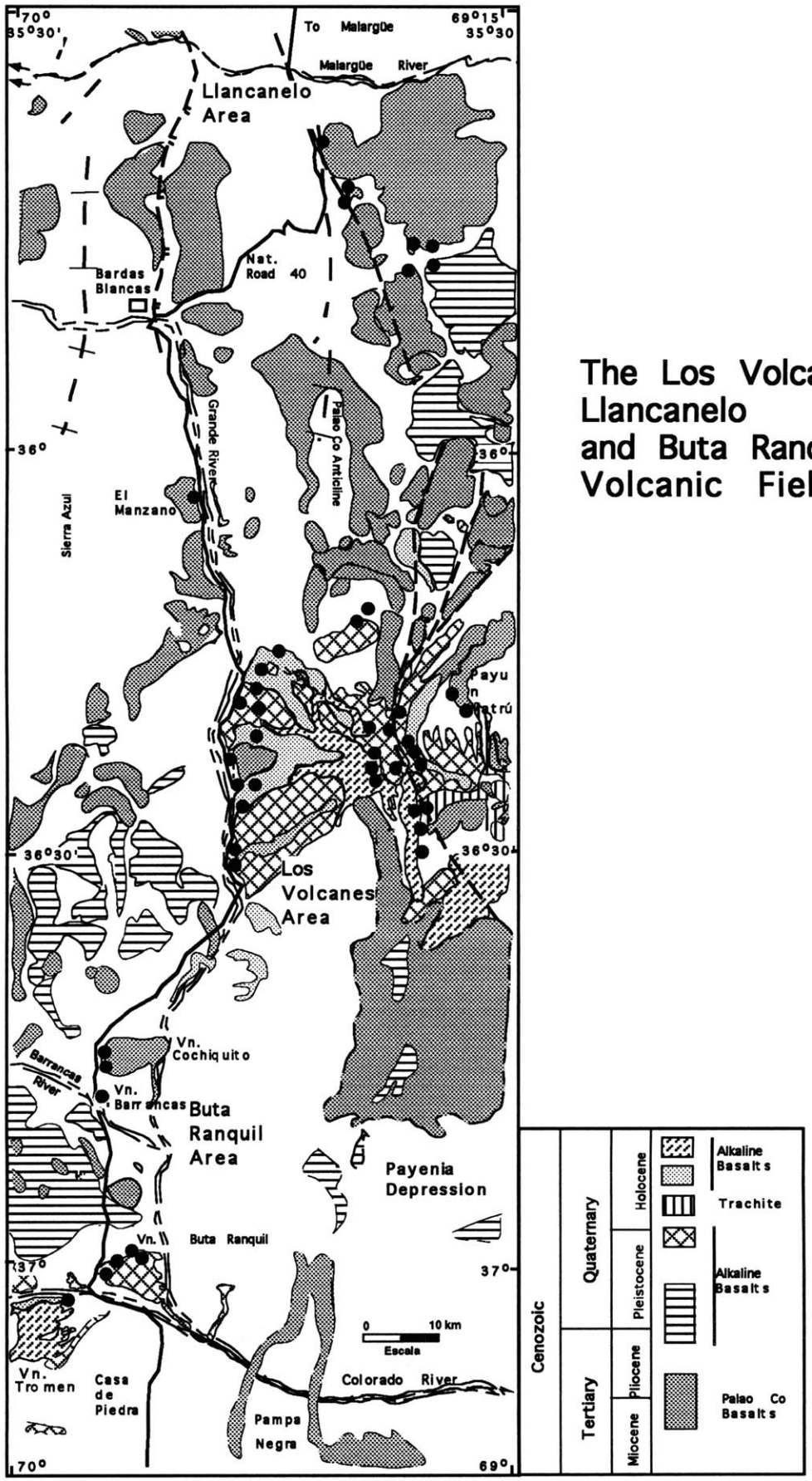

The Los Volcanes, Llancanelo and Buta Ranquil Volcanic Fields

Figure 7: Detailed map of the Los Volcanes, Llancanelo and Buta Ranquil volcanic fields. The figure shows the stratigraphic relation between the flows ranging in age from Miocene to Prehistoric. Also the figure shows part of the Payun Matru and Tromen stratovolcanoes and the sampling locations (filled circle). The Map is from Delpino (pers. com.,1993).

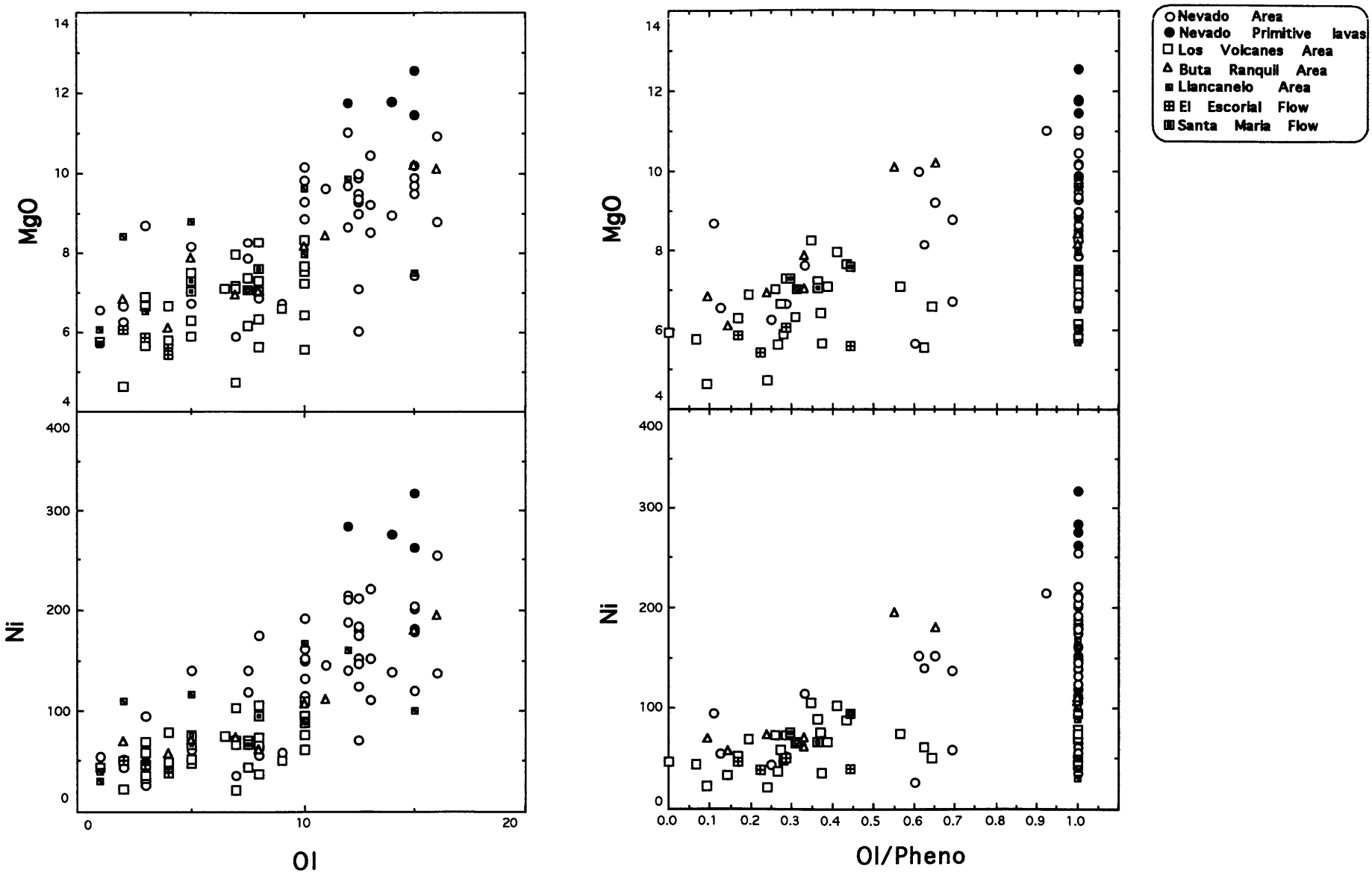

Figure 8: Olivine modal proportion versus Ni and MgO. MgO and Ni contents are positively correlated with the abundance of olivine, but samples with olivine proportion close to 15% range in Ni from 100 to 320 ppm.

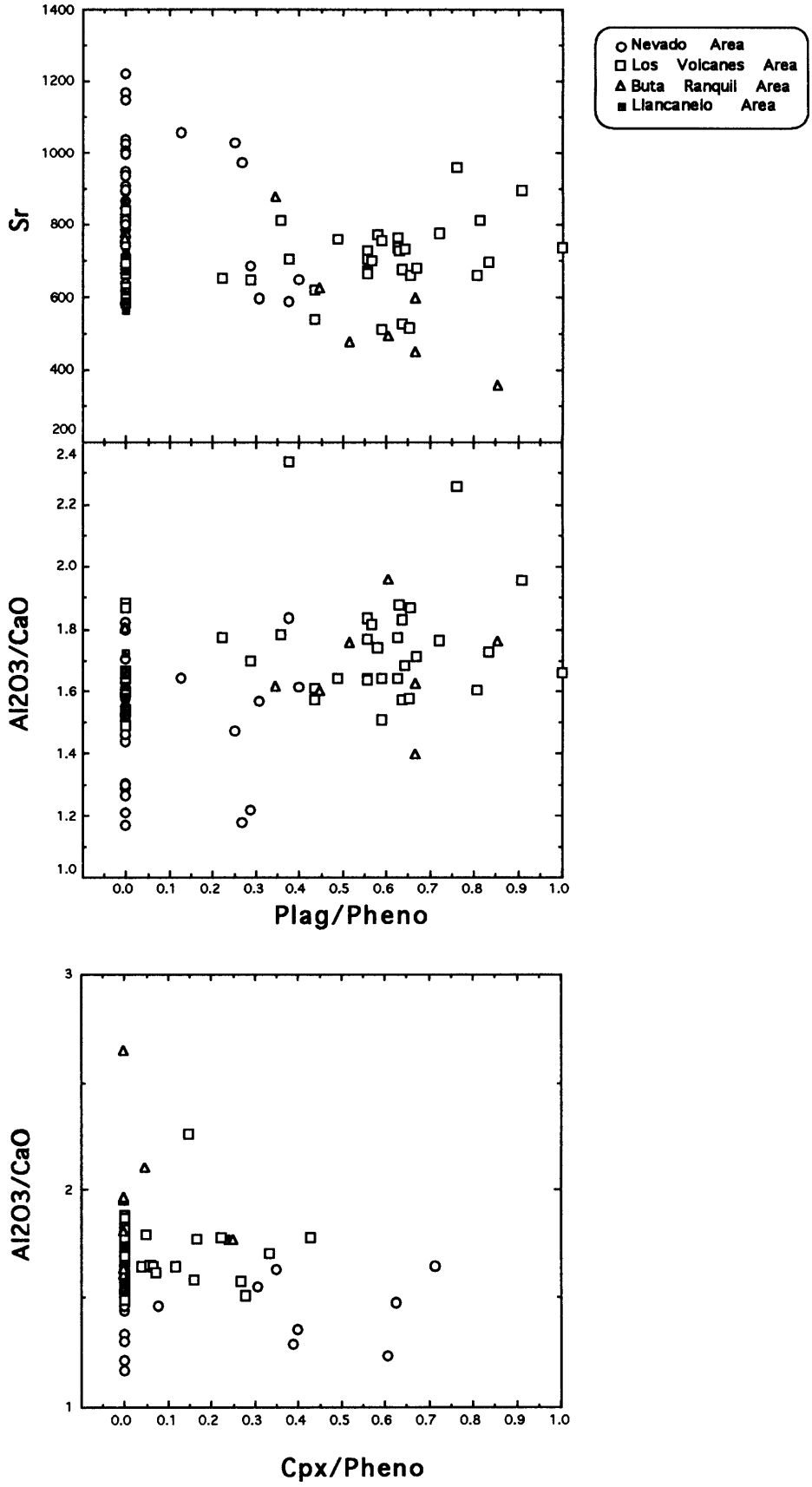

Figure 9: Al_2O_3/CaO, Sr versus plagioclase modal proportion and Al_2O_3/CaO versus clinopyroxene modal proportion. Sr and Al_2O_3/CaO ratios do not correlate with the modal proportion of plagioclase and clinopyroxene.

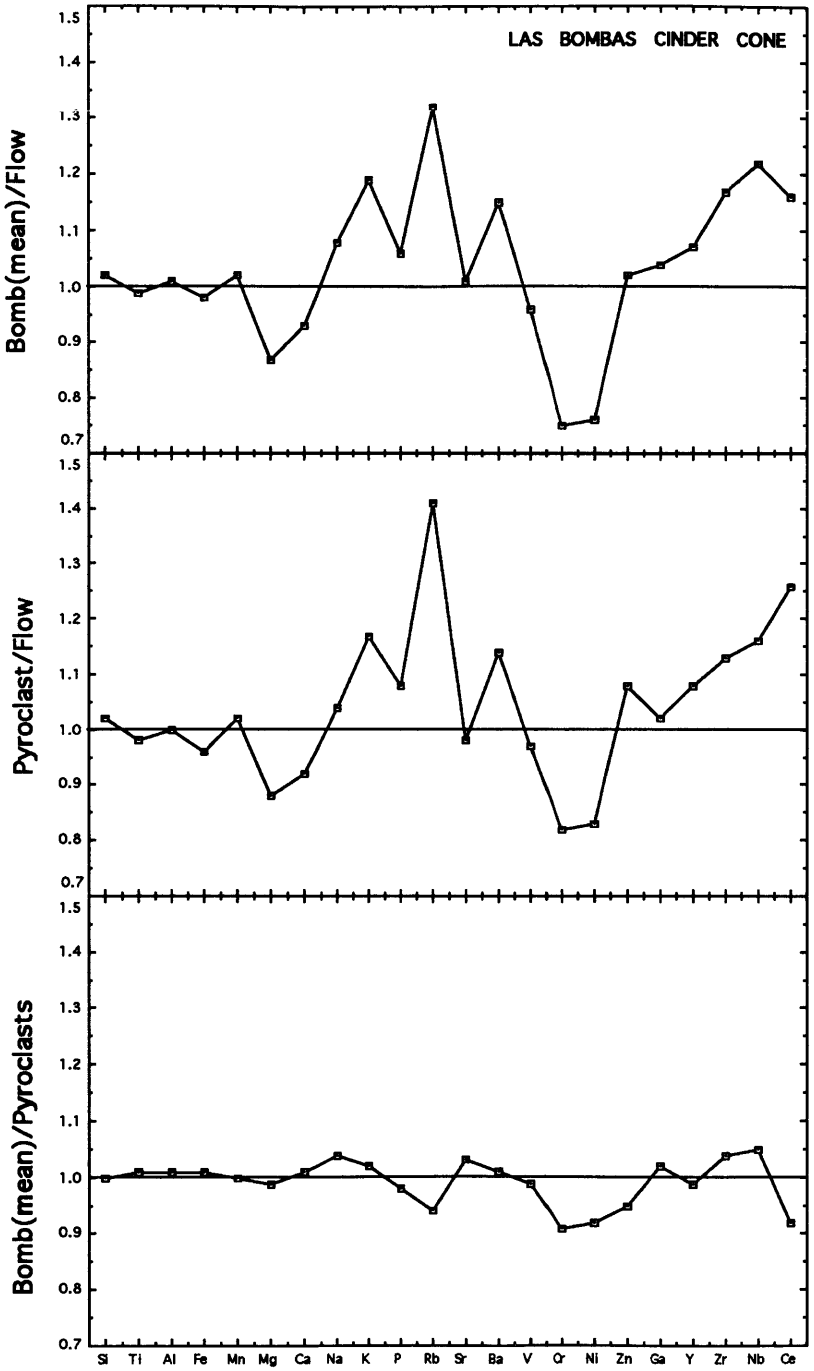

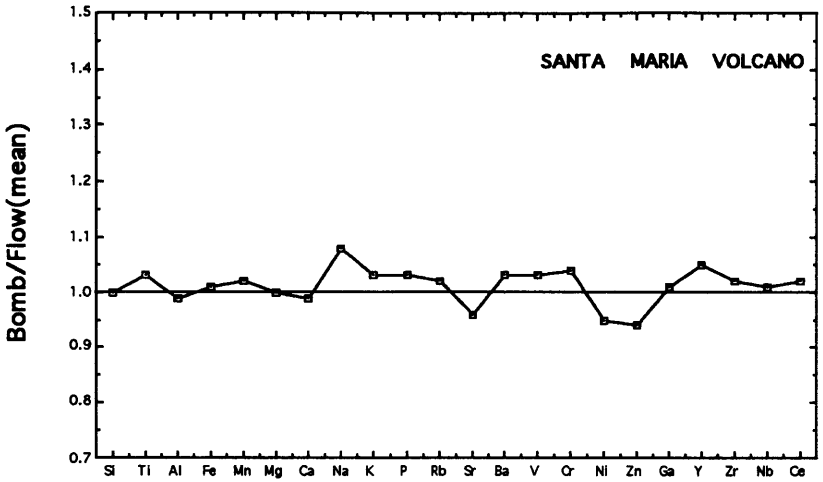

Figure 10: Compositional variation between flow, bomb and pyroclastic material. This figure shows that in C° Santa Maria there is no important difference in composition between flow and bomb. On the contrary, in C° Las Bombas the difference in composition between flow and bomb or pyroclastic material is significant. Flow composition in C° Santa Maria is the mean of three samples and bomb composition in C° Las Bombas is mean of two samples.

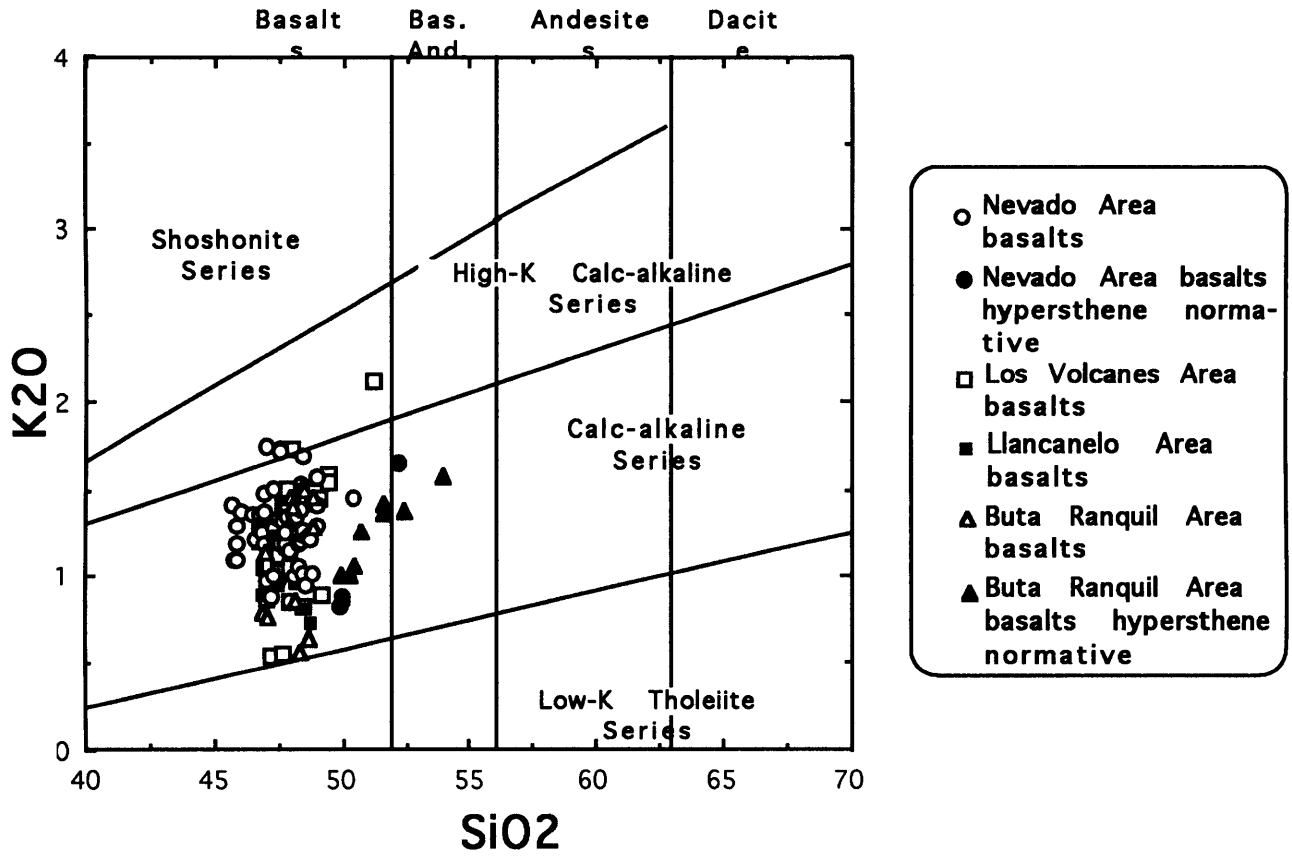

Figure 11: SiO_2-K_2O variation diagram for classifying volcanic rock types (Peccerillo and Taylor, 1976). The figure shows that almost all the lavas behind the volcanic front are basalts medium in K. The hypersthene normative basalts have higher SiO_2 content than the nepheline normative lavas.

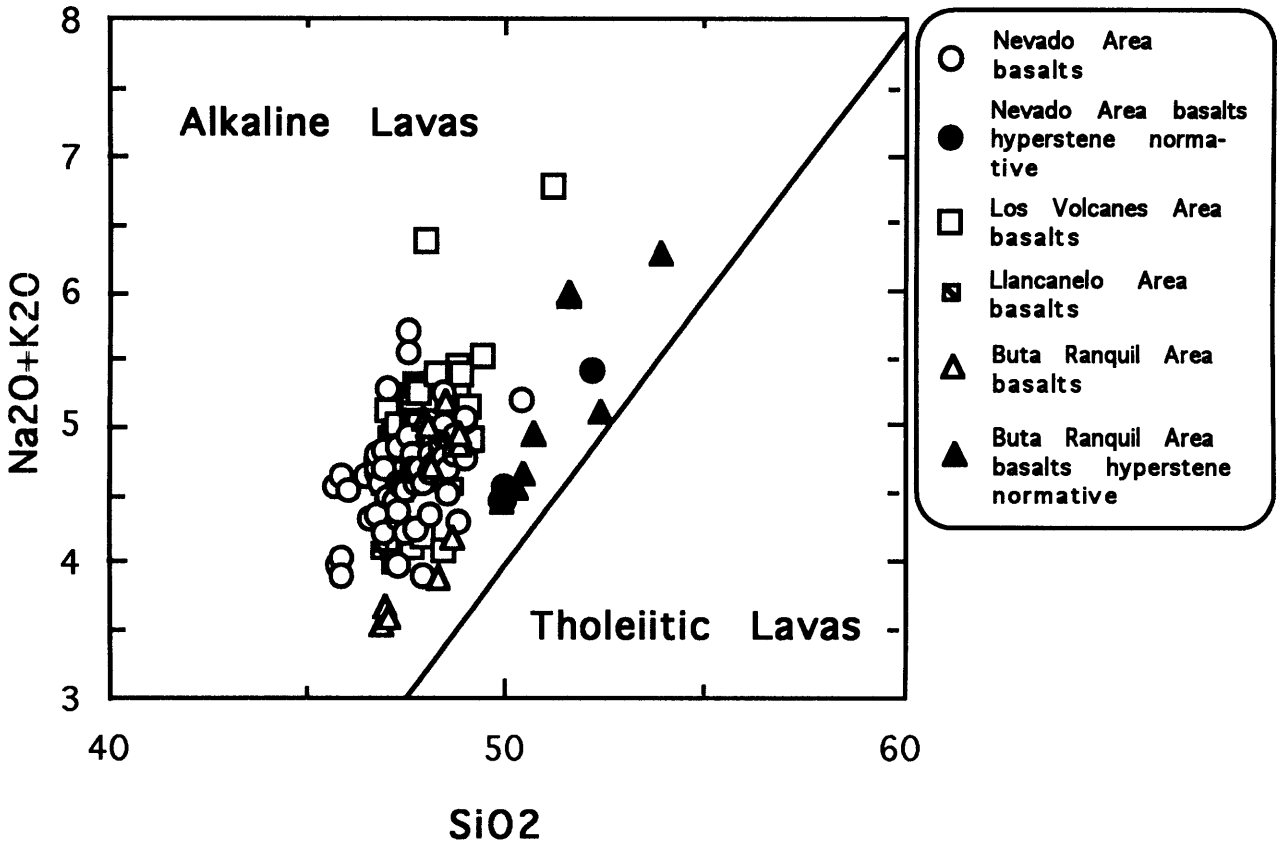

Figure 12: Total alkalis-SiO_2 variation diagram for classifying volcanic rock types (McDonald and Katsura, 1964). All the basalts are alkaline in composition. Hypersthene normative basalts have higher SiO_2 content than nepheline normative lavas.

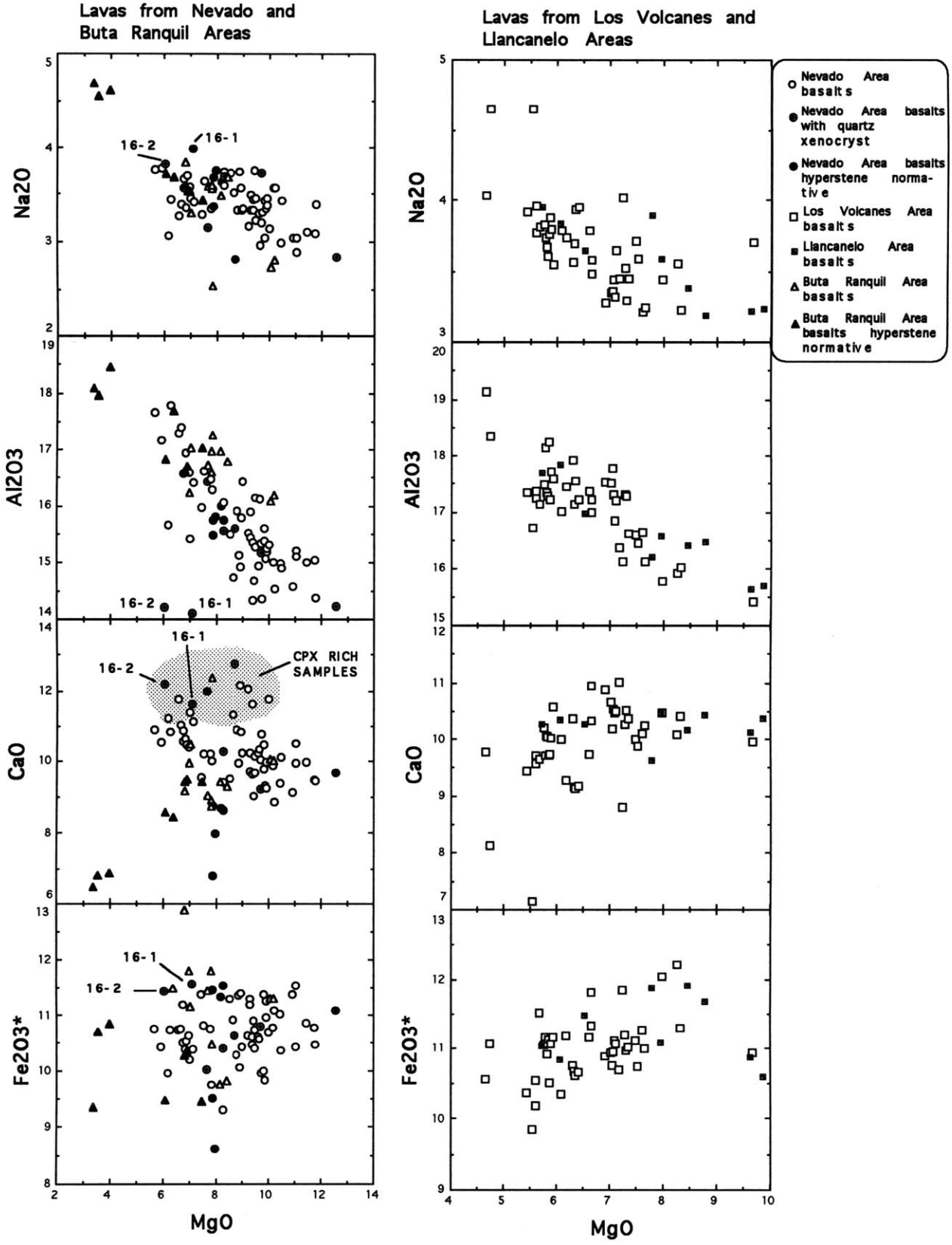

Figure 13: Major element-MgO variation diagram. The figure shows the different range in major element composition between the volcanic fields behind the volcanic front. Also, hypersthene normative basalts and basalts with quartz xenocrysts are shown. Shaded area represent samples with intergranular textures and clinopyronene as dominant phenocryst and samples with subophitic texture. Notice that the most primitive sample has quartz xenocryst

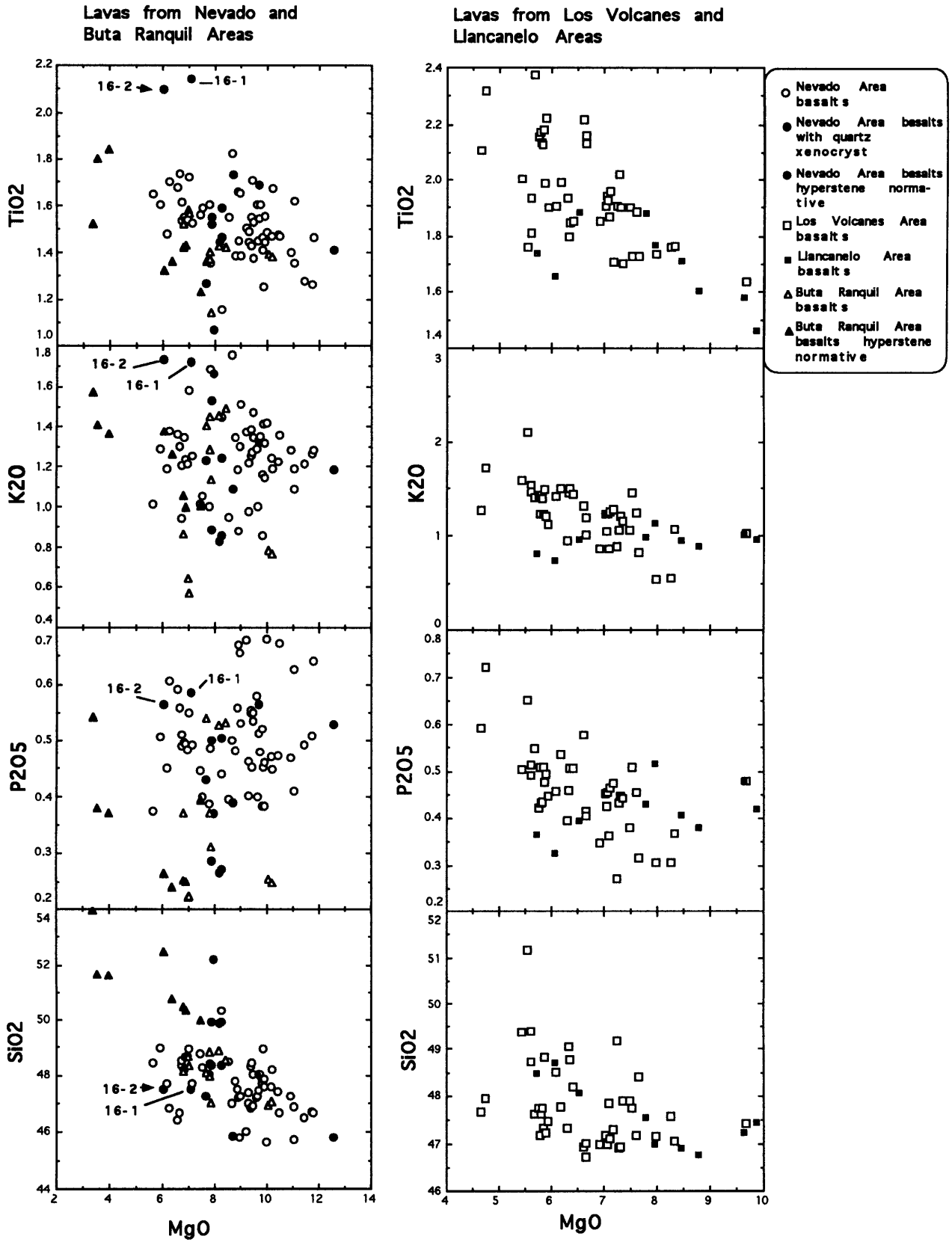

Figure 13: Major element-MgO variation diagram. The figure shows the different range in major element composition between the volcanic fields behind the volcanic front. Also, hypersthene normative basalts and basalts with quartz xenocrysts are shown.

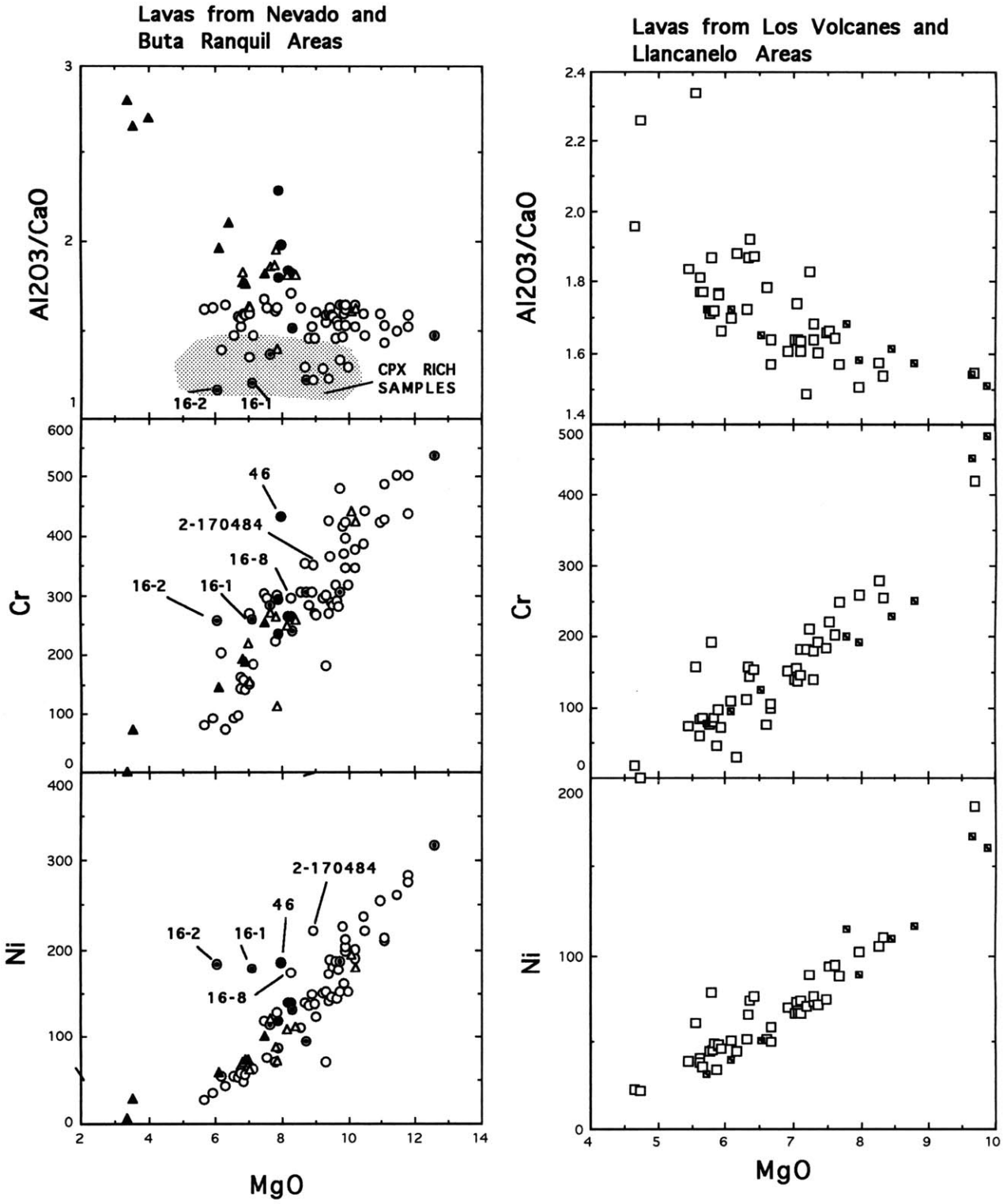

Figure 14 : Al_2O_3/CaO, Ni and Cr versus MgO variation diagram. The figure shows MgO positively correlate with Ni and Cr and negatively with Al_2O_3/CaO. It is important to notice that lavas with quartz xenocrysts have low Al_2O_3/CaO. Symbols as in figure 13. Shaded area represents samples with intergranular texture and clinopyroxene as the dominant phenocryst and samples with subophitic texture.

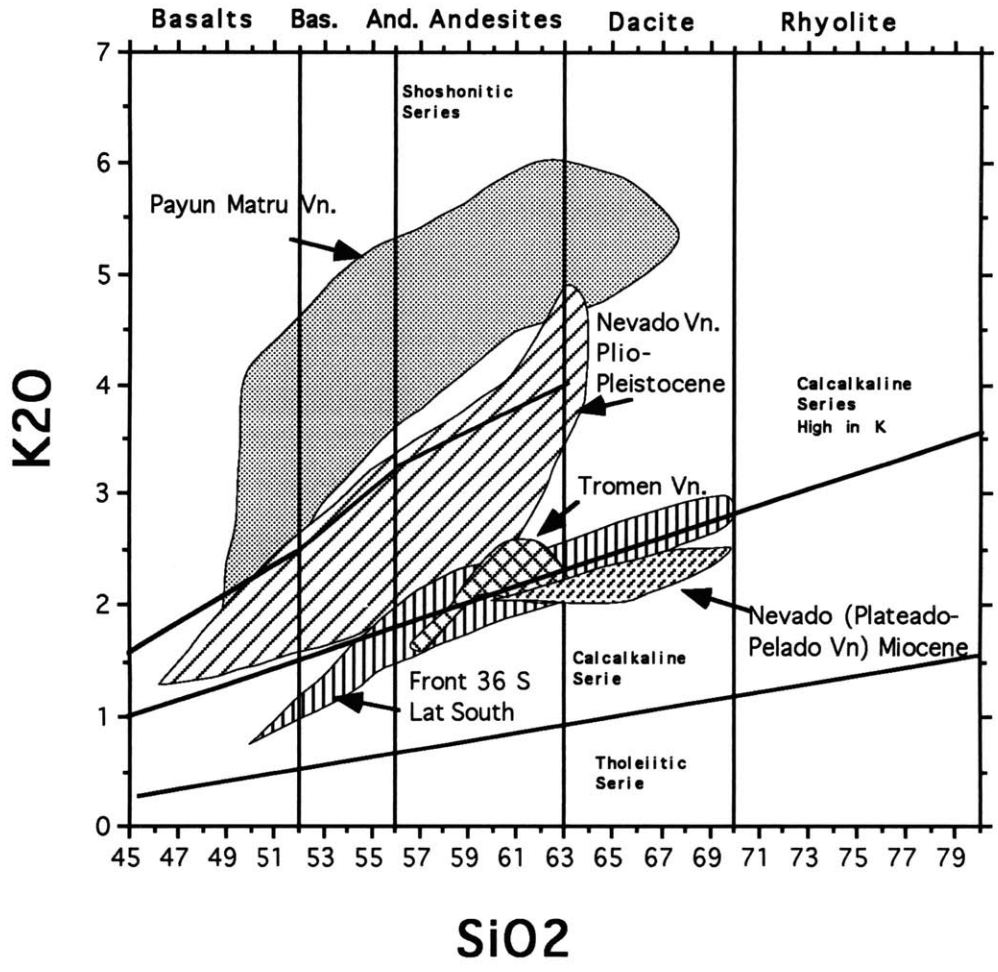

Figure 15: SiO_2-K_2O variation diagram (Peccerillo and Taylor, 1976). The figure shows the different K_2O content in the eastern stratovolcanoes. The data was taken from Llambias (1966) for Payun Matru, Llambias et al.,(1987) for Tromen, and from Bermudez (1991), for Nevado, Plateado and Pelado and the volcanic front at 36^0 (Maule, Maipo, Longavi and Chillan volcanoes).

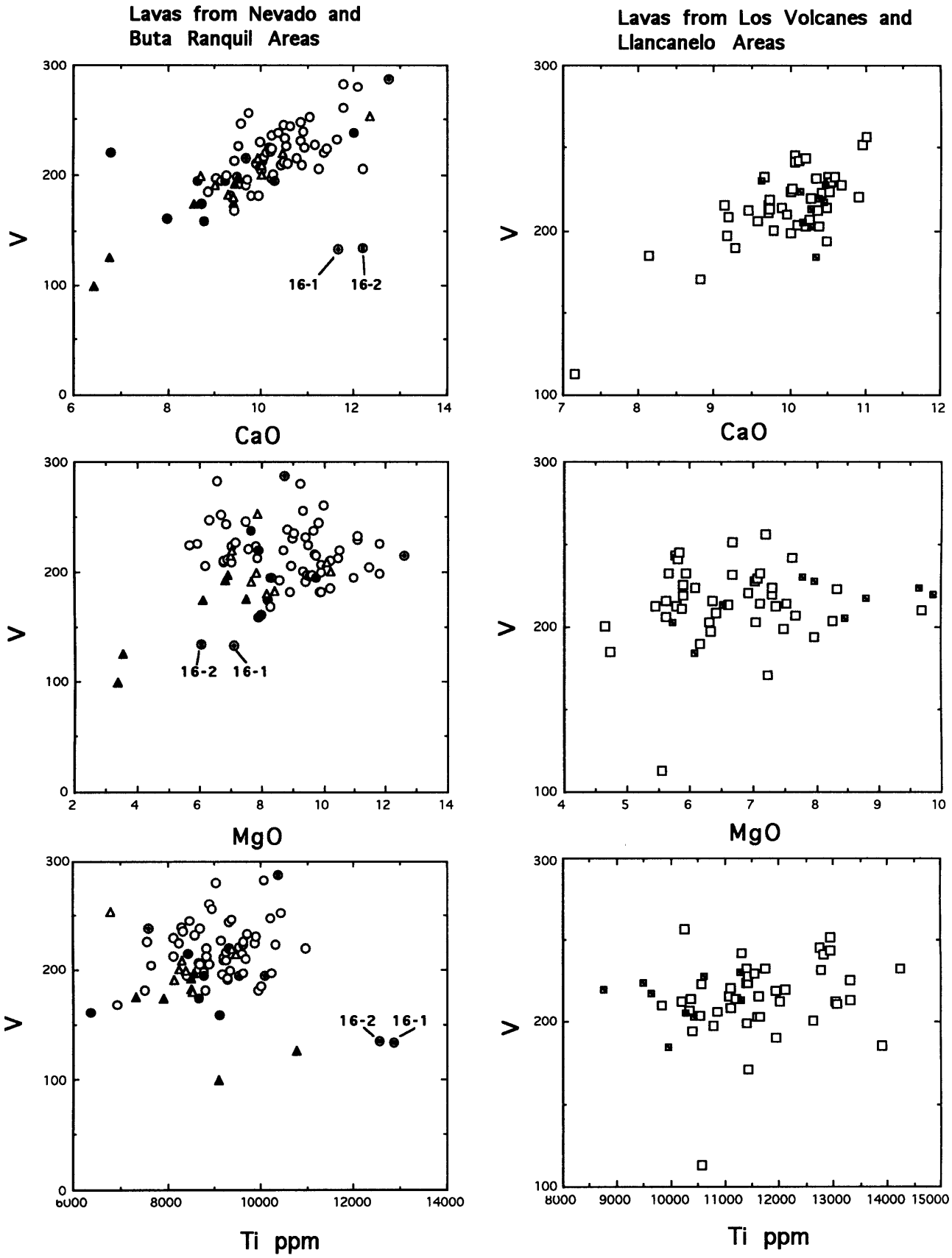

Figure 16: V versus MgO, Ti and CaO. The figure shows that V does not correlate with MgO or Ti, but it positively correlates with CaO. Symbols as in figure 13.

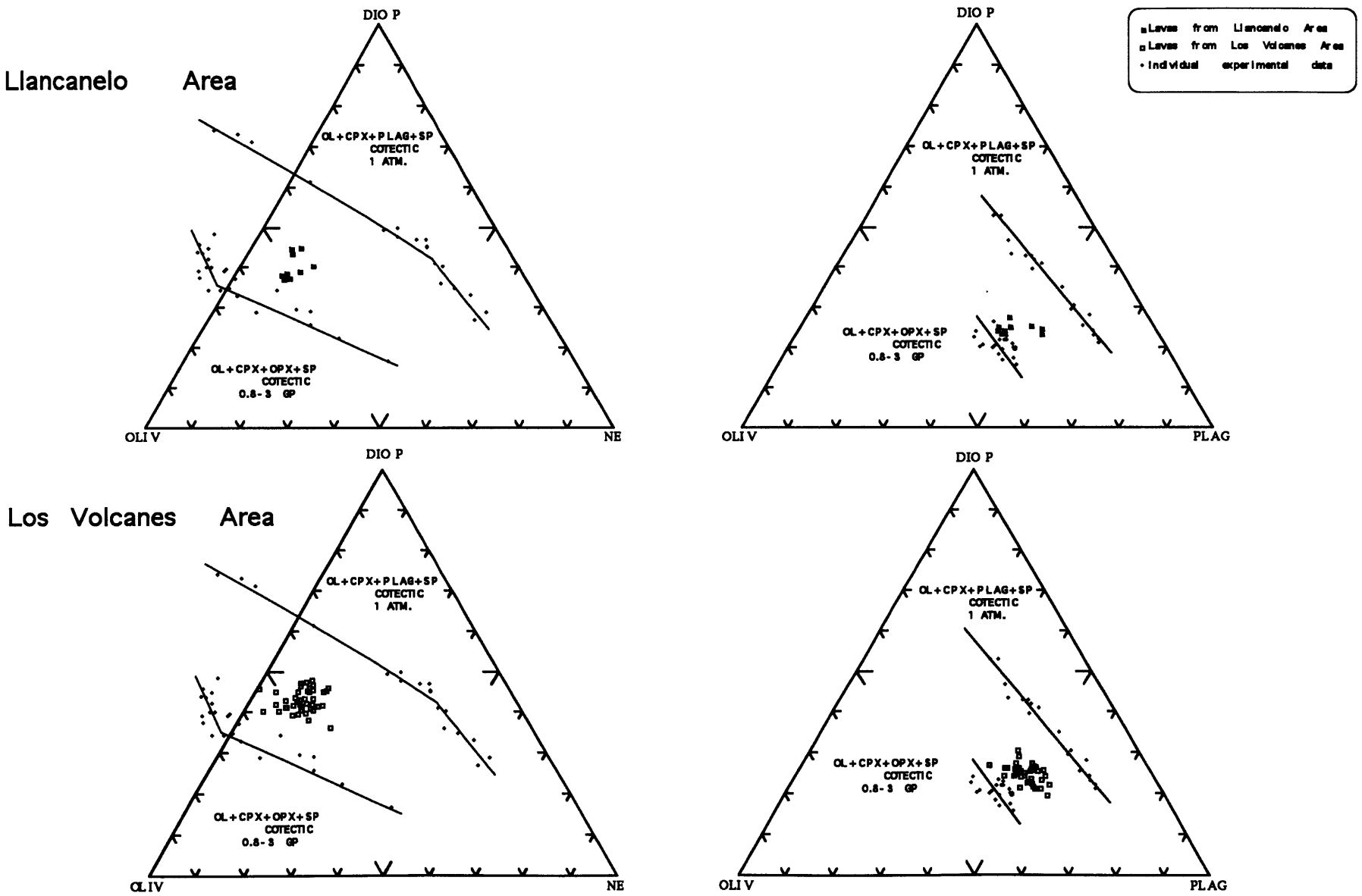

Figure 17: Projection of Intra-Back arc basalts onto the planes Diopside-Nepheline-Olivine and Diopside-Olivine-Plagioclase, following the algorithms of Sack et al. (1987). Shown for comparison is the 1 Atm cotectic of Sack et al. (1987) and the Oliv-Cpx-Opx-Sp cotectic from Stolper (1980), Takahashi & Kushiro (1983) and Fuii & Scarfe (1985).

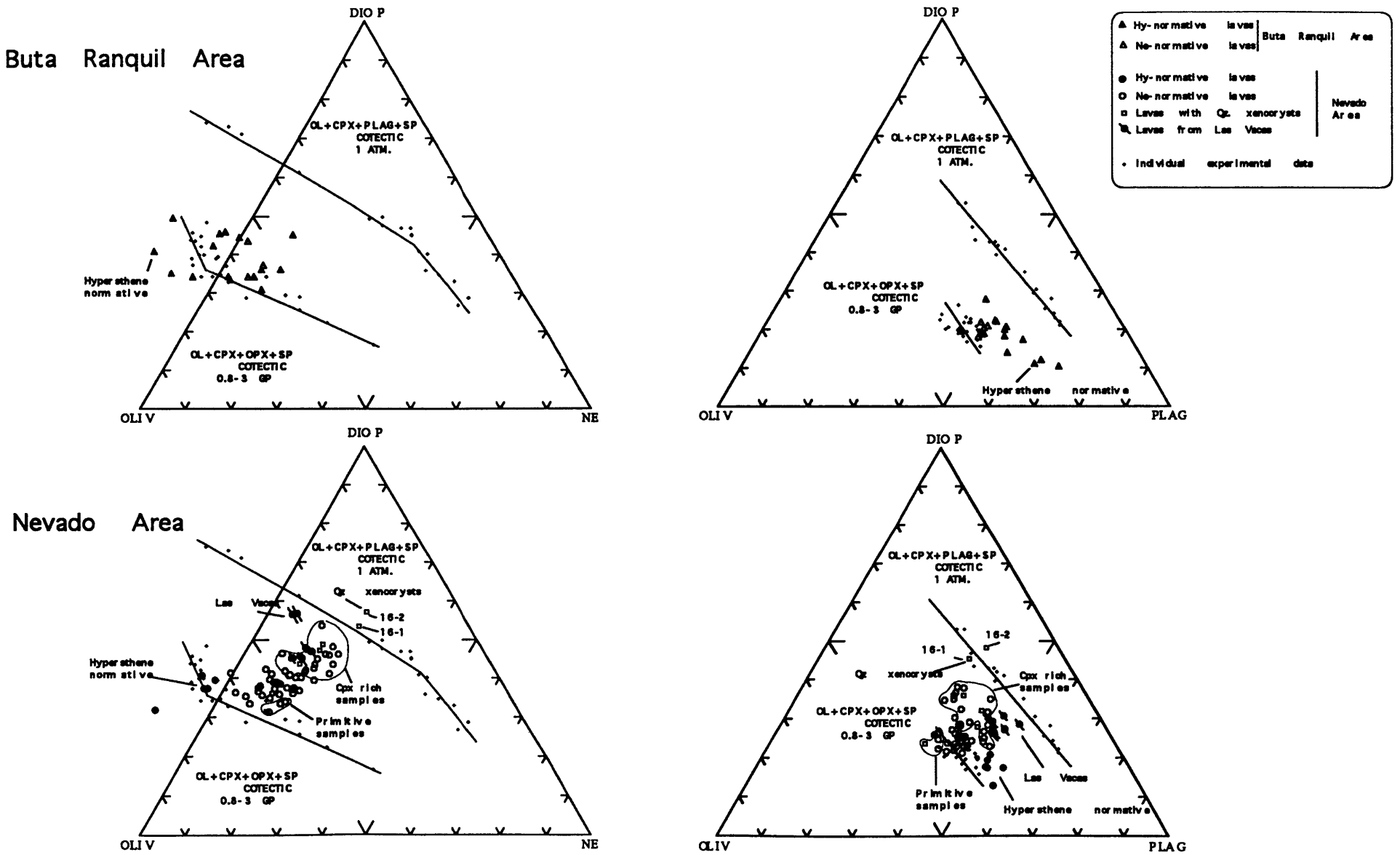

Figure 17: Projection of Intra-Back arc basalts onto the planes Diopside-Nepheline-Olivine and Diopside-Olivine-Plagioclase, following the algorithms of Sack et al. (1987). Shown for comparison is the 1 Atmcotectic of Sack et al. (1987) and the Oliv-Cpx-Opx-Sp cotectic from Stolper (1980), Takahashi & Kushiro (1983) and Fuji & Scarfe (1985). Area labeled "CPX rich samples" represents samples with intergranular texture with clinopyroxene as the dominant phenocryst and samples with subophitic textures. The four primitive lavas are 20-1, 2; 19-6 and 27-150384.

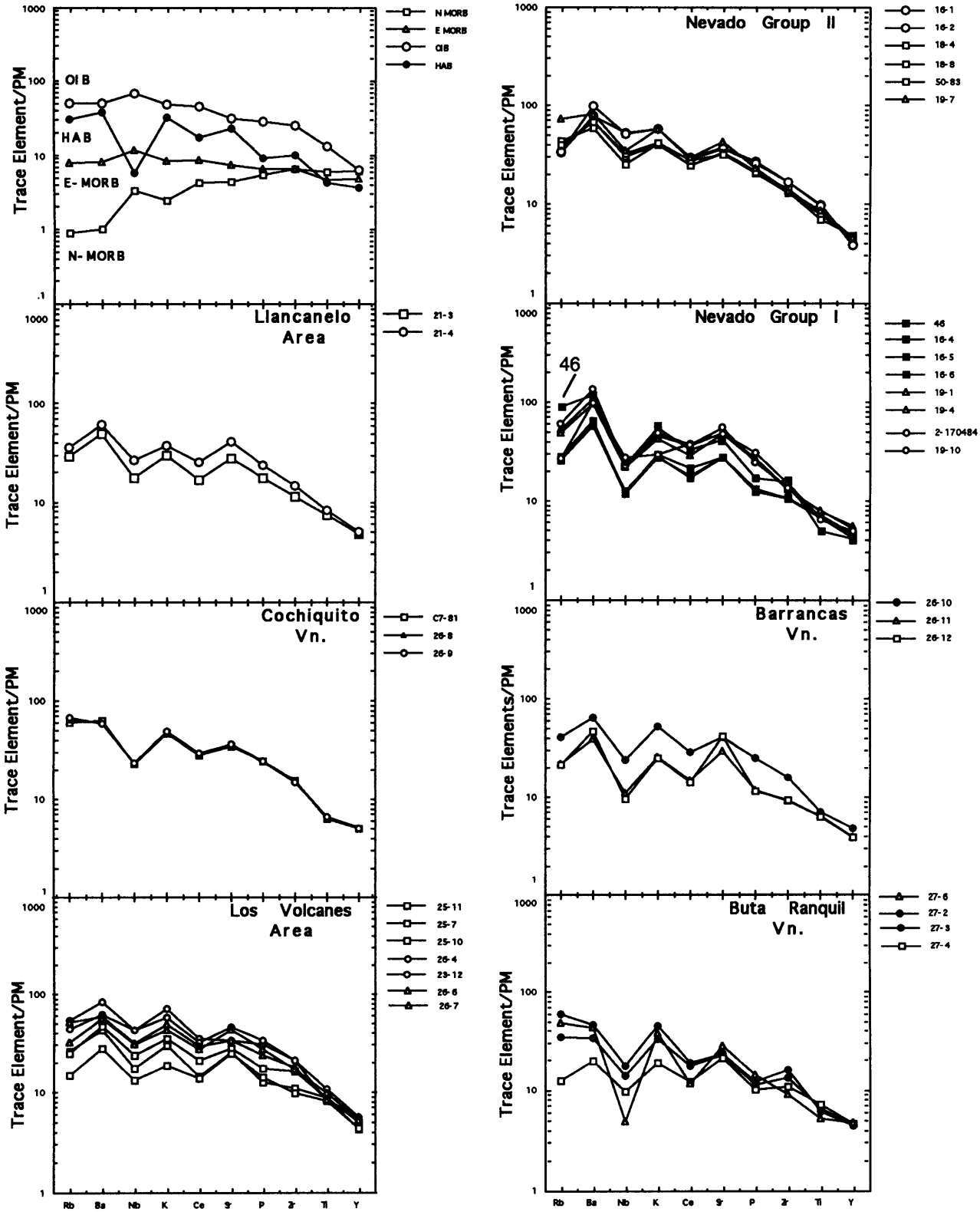

Figure 18: Primitive mantle normalized abundance patterns for intra-back arc basalts. Selected analyses are shown to cover all the compositional spectrum. E-N-MORB and OIB from Sun and McDonough (1989), and HAB from Planchon Vn. (Tormey et al.,1994). Hypersthene normative basalts are showed with filled symbols.

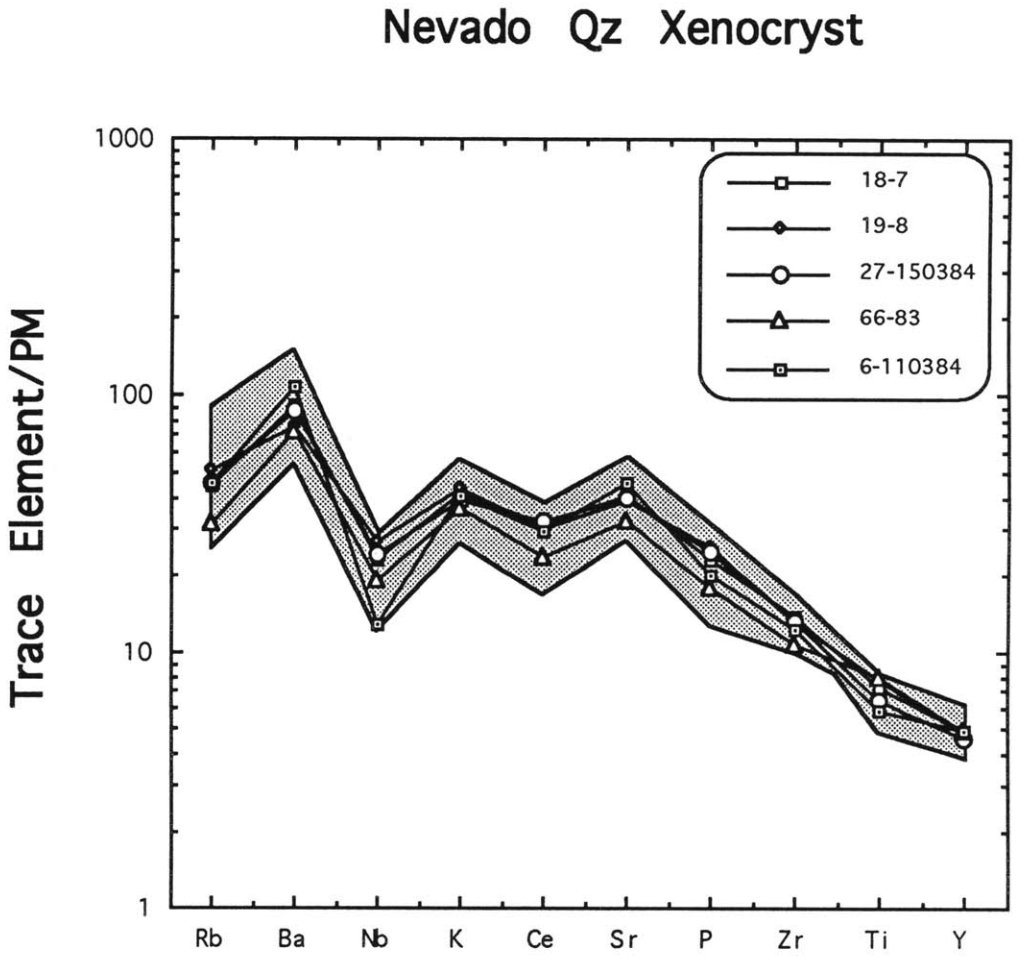

Figure 19: Primitive mantle normalized abundance pattern for Nevado Group I basalts that have quartz xenocryst. The figure shows that the composition of these lavas are in the range of composition of basalts from the same group without xenocryst (54 samples).

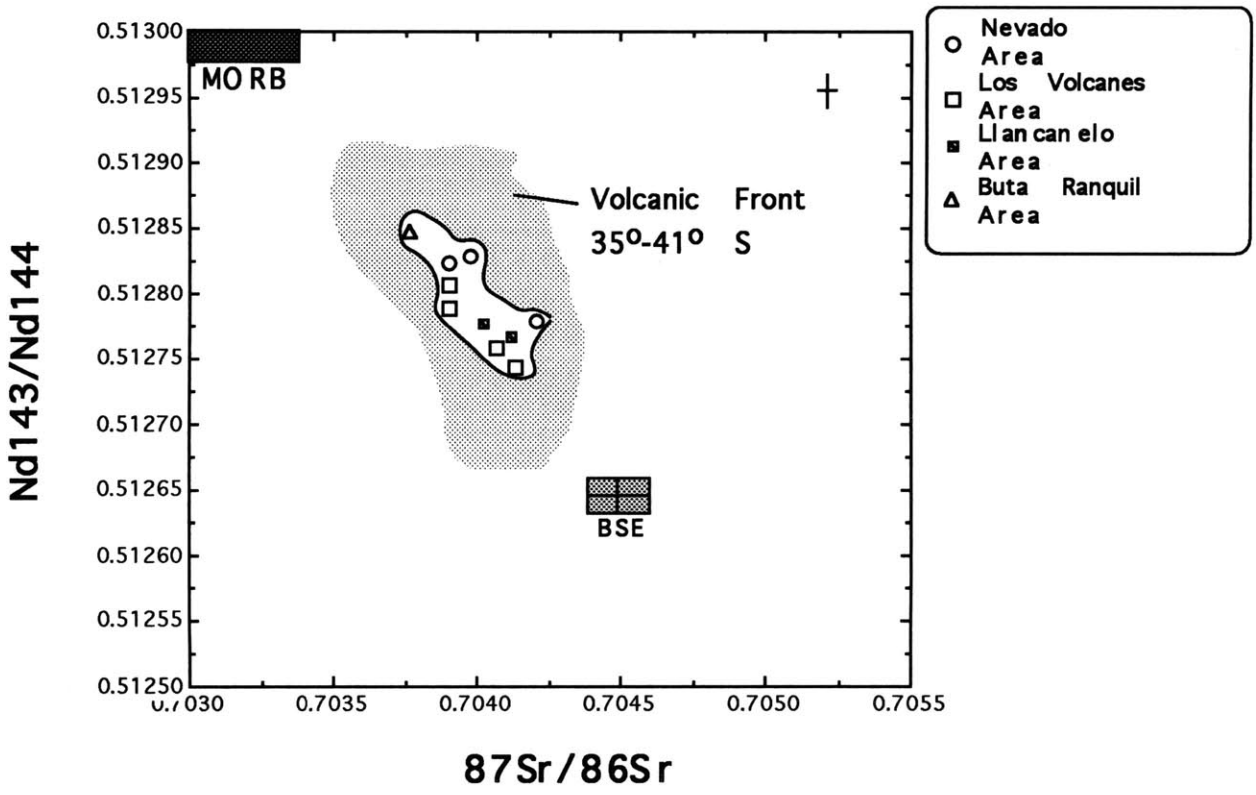

Figure 20: 87Sr/86Sr versus Nd143/Nd144. The alkaline basalts display negative correlation between Sr and Nd isotopic composition with all the points plotting inside the mantle array. Isotopic data for the volcanic front are from Frey et al. (1984); Hickey et al. (1986); Davidson et al. (1987, (1988); Hildreth and Moorbath (1988); Gerlach et al. (1988); Hickey-Vargas et al. (1989); Tormey et al (1991, 1993) and Ferguson et al.(1992).
BSE = Bulk Silicate Earth

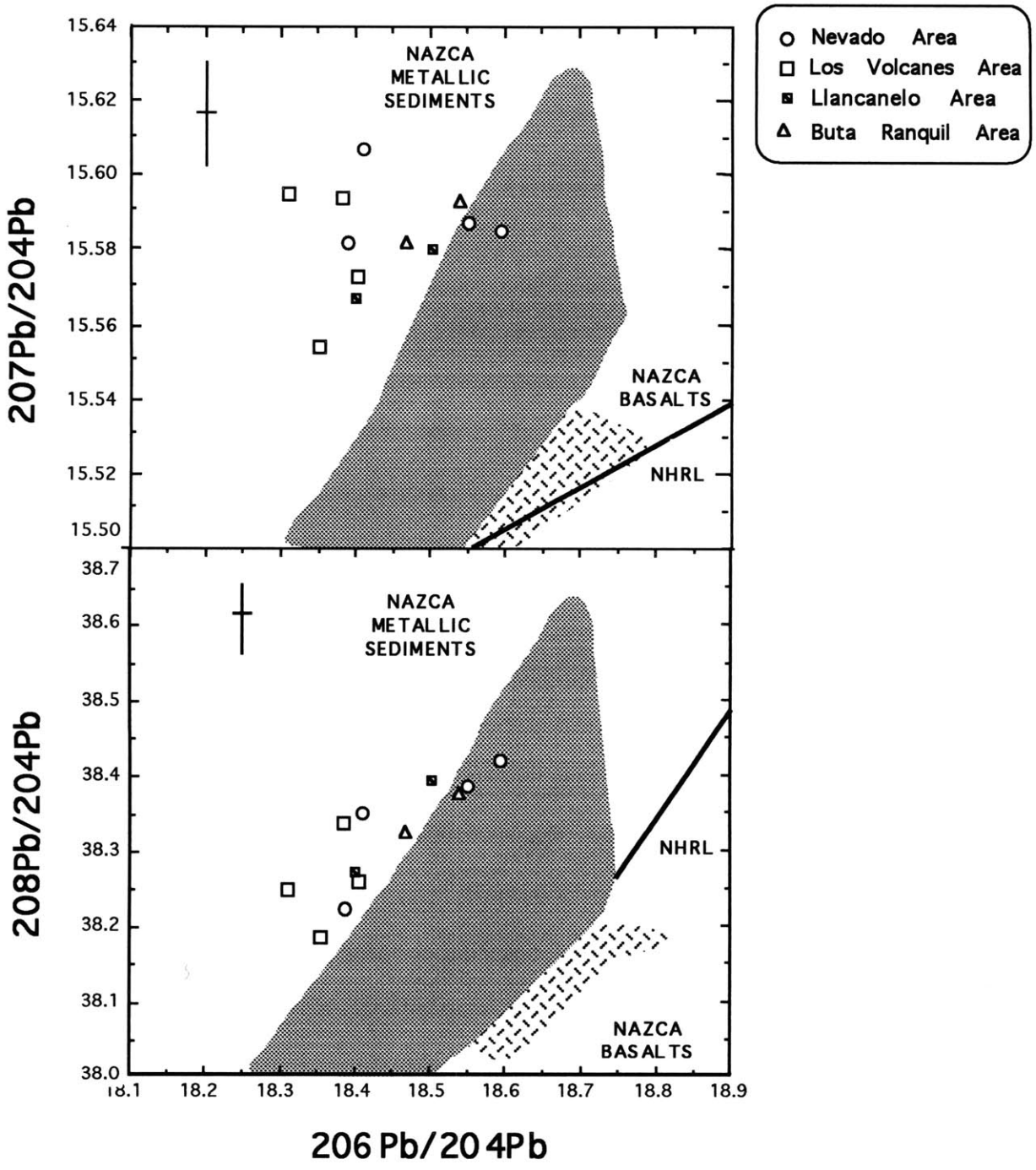

Figure 21: $^{207}Pb/^{204}Pb$ and $^{208}Pb/^{204}Pb$ versus $^{206}Pb/^{204}Pb$. Alkaline basalts display higher $^{207}Pb/^{204}Pb$ and $^{208}Pb/^{204}Pb$ at a given $^{206}Pb/^{204}Pb$ than Nazca plate basalts (MORB) and Nazca plate metallic sediments. Nazca plate basalts and sediments are from Barreiro (1984), Unruh & Tatsumoto (1976), Dasch (1981) and Tilton (1983) NHRL is from Hart (1984)

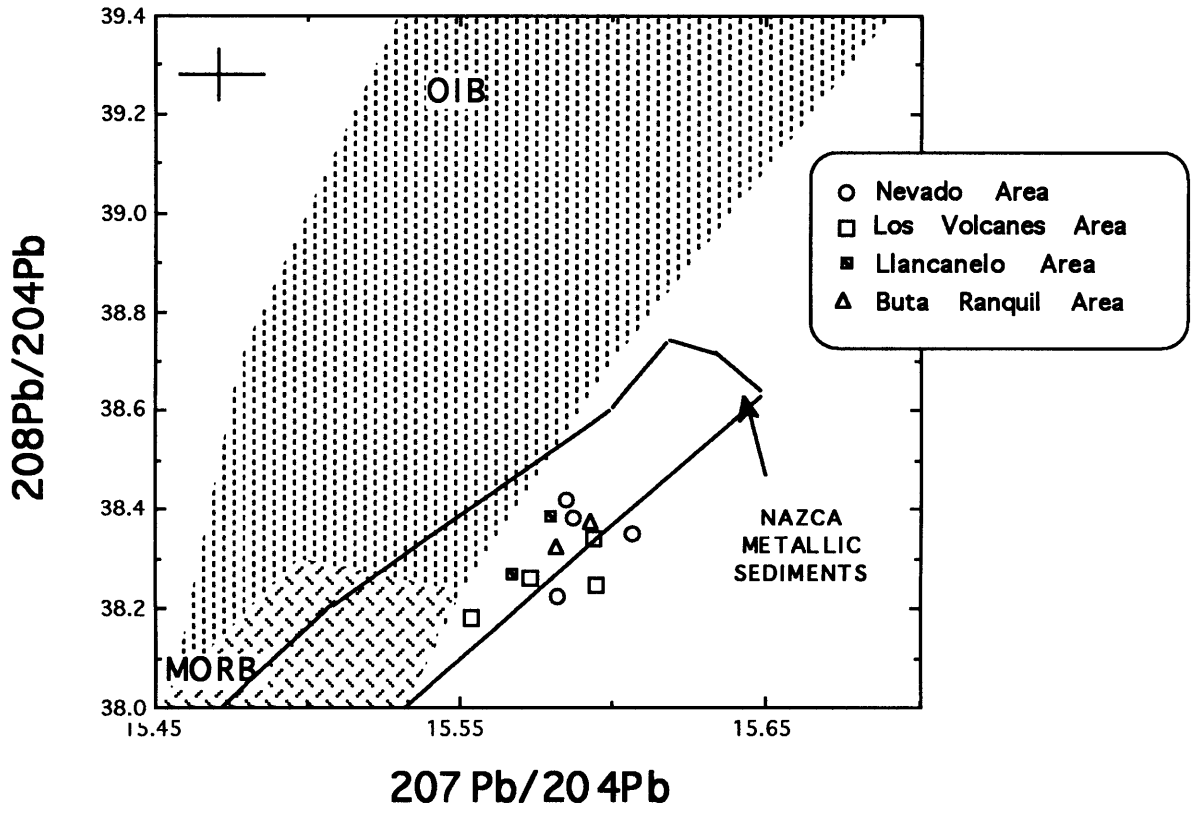

Figure 22: $^{208}Pb/^{204}Pb$ versus $^{207}Pb/^{204}Pb$. Alkaline basalts have higher $^{207}Pb/^{204}Pb$ at a given $^{208}Pb/^{204}Pb$ than MORB and OIB fields, overlapping with Nazca metallic sediments. Data for OIB, MORB, and Nazcametallic sediment are from Hickey et al. (1986)

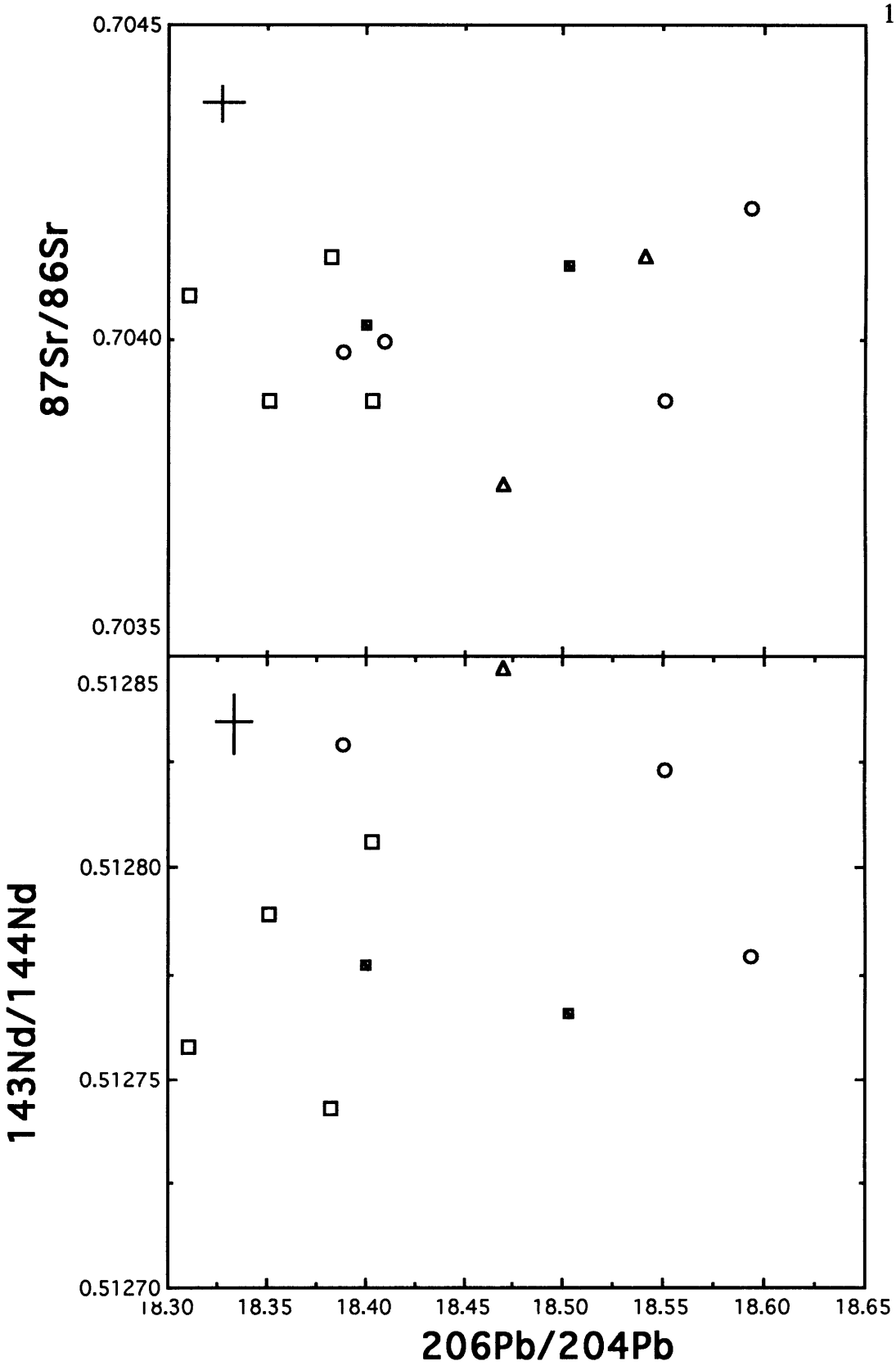

Figure 23 :143Nd/144Nd and 87Sr/86Sr versus 206Pb/204Pb. The Nd and Sr isotopic composition of the alkaline basalts do not display correlation with 206Pb/204Pb ratios. References as figure 20.

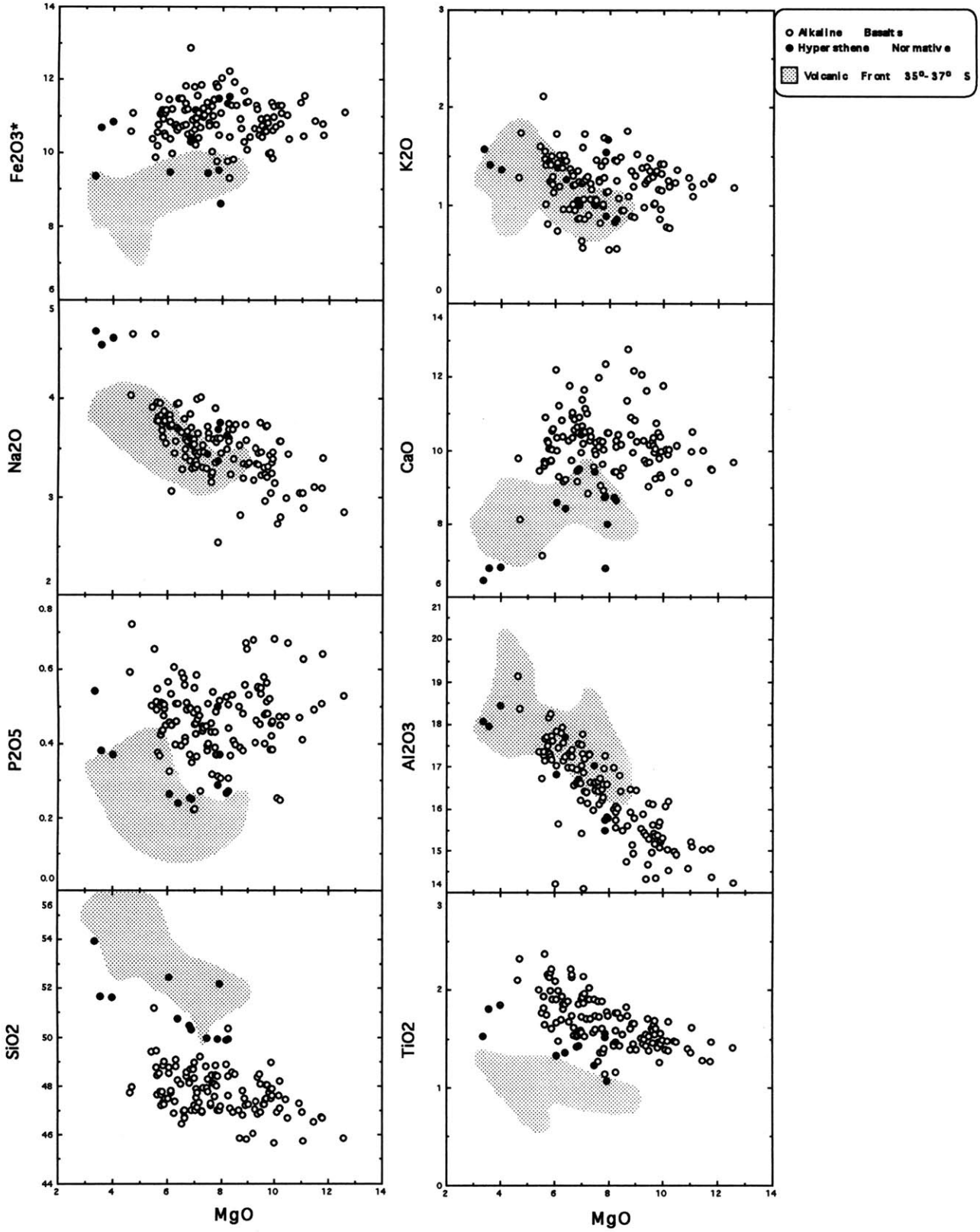

Figure 24: Major element-MgO variation diagram. Volcanic front lavas display different composition than the back-arc lavas. Hypersthene normative basalts have composition similar to those of the volcanic front. Data for the volcanic front are from Vn Planchon (Tormey et al., 1991;1993), and Vn Tatara-San Pedro (Davidson et al.,1988; 1989; and Ferguson et al., 1992). The range in SiO2 and MgO for the volcanic front is 50 - 55 and 4 - 9 wt% respectively

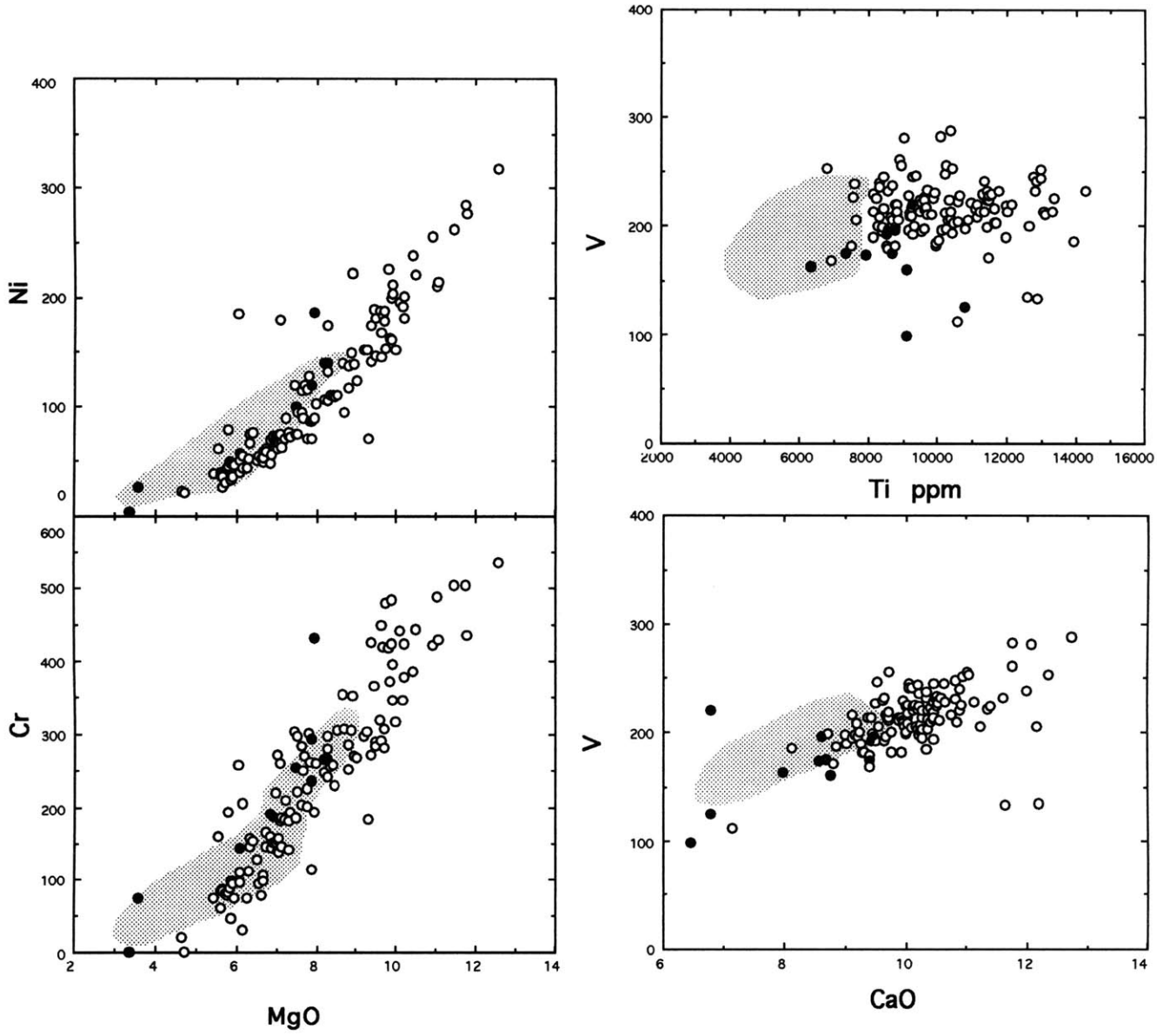

Figure 25: Cr and Ni versus MgO and Ti and CaO versus V. The volcanic front lavas display lower concentration in compatible elements than the back-arc basalts. The V content in the volcanic front lavas, like the back arc basalts, correlate with CaO but it does not correlate with Ti. Data form the volcanic front and references as in figure 24.

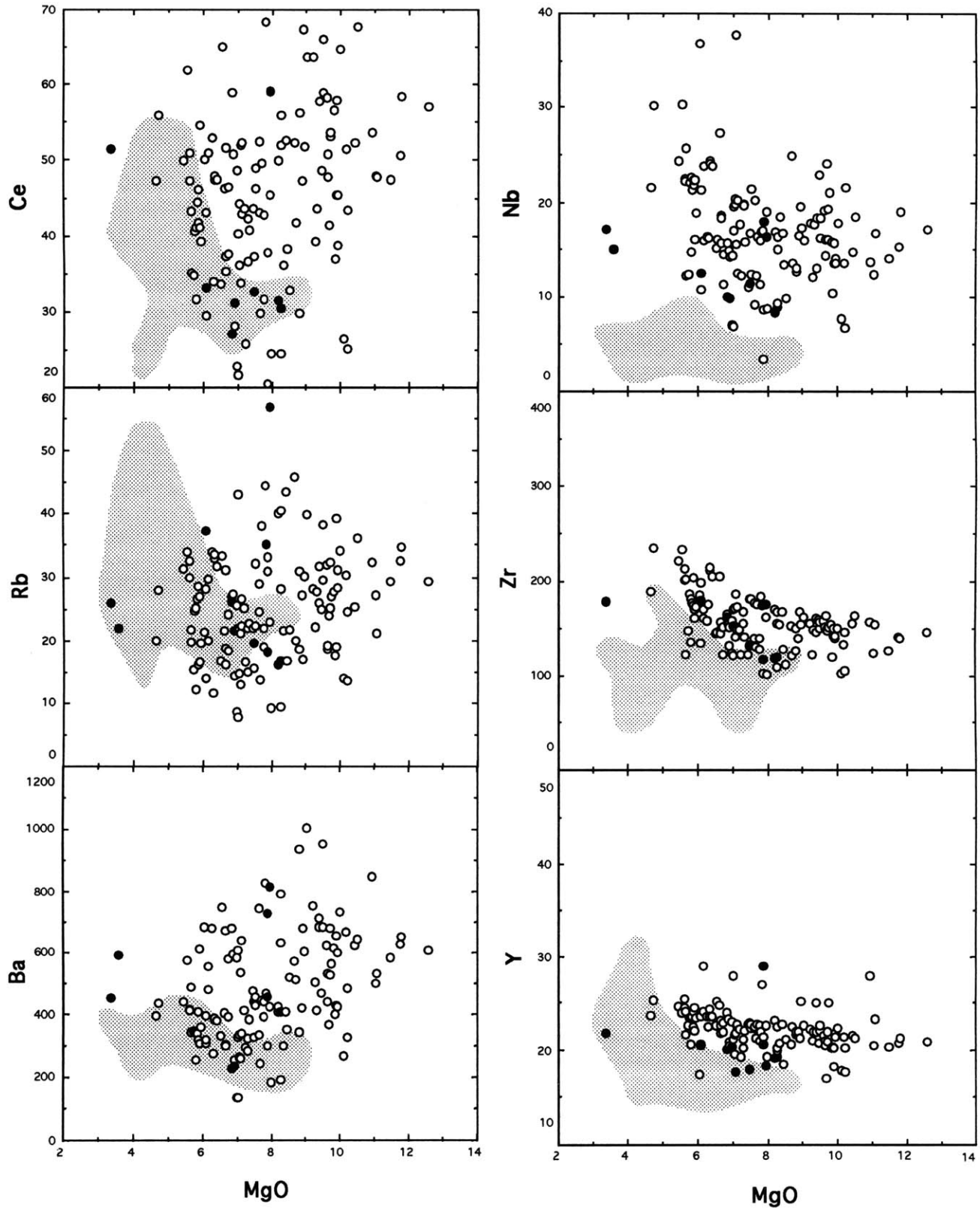

Figure 26: Incompatible trace element abundance versus MgO variation diagram. The back arc basalts display higher abundance of incompatible elements than lavas from the volcanic front. Data for the volcanic front and references as in figure 24.

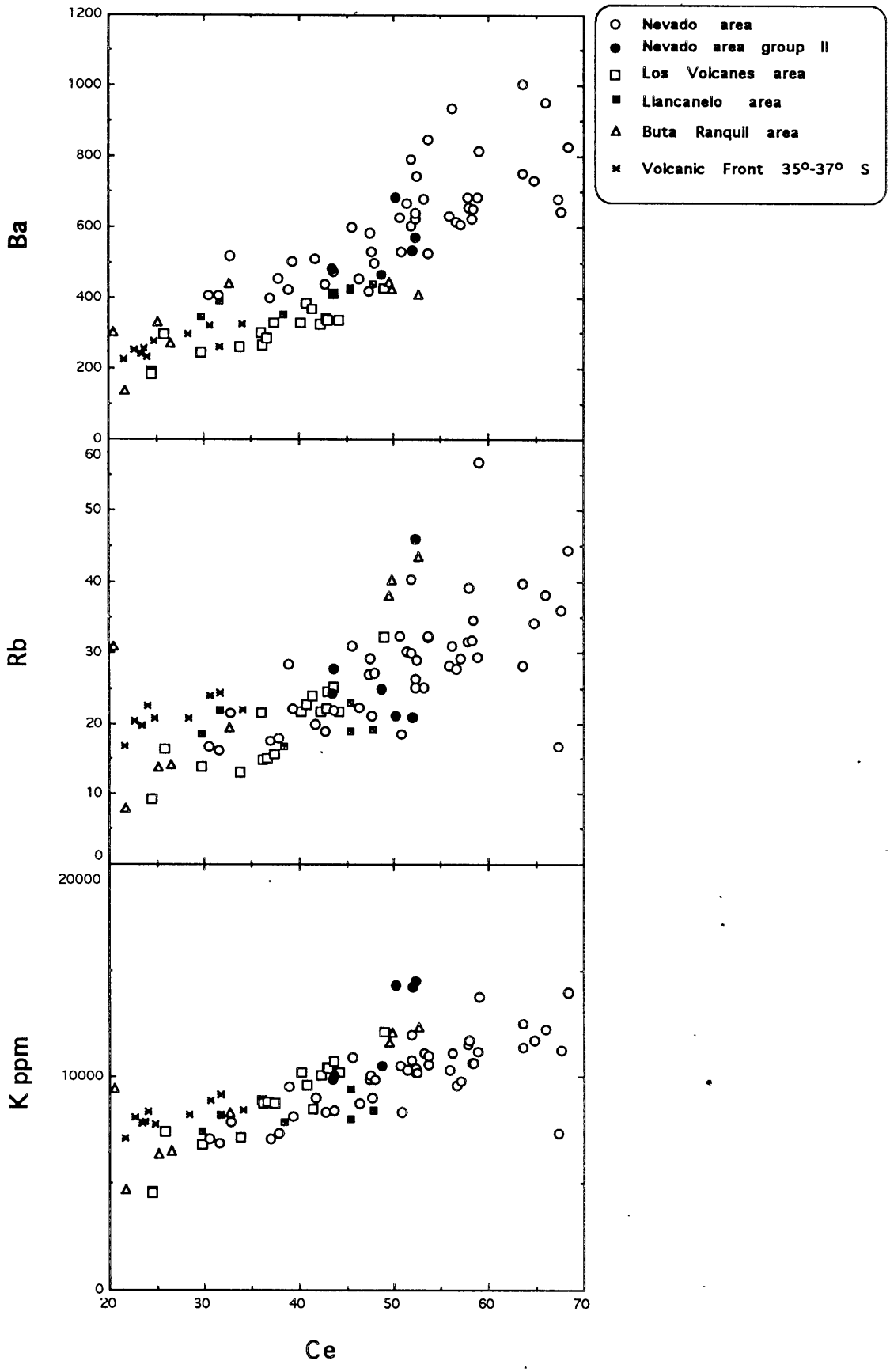

Figure 27a: Ba, K and Rb versus Ce for primitive basalts (MgO >7%)

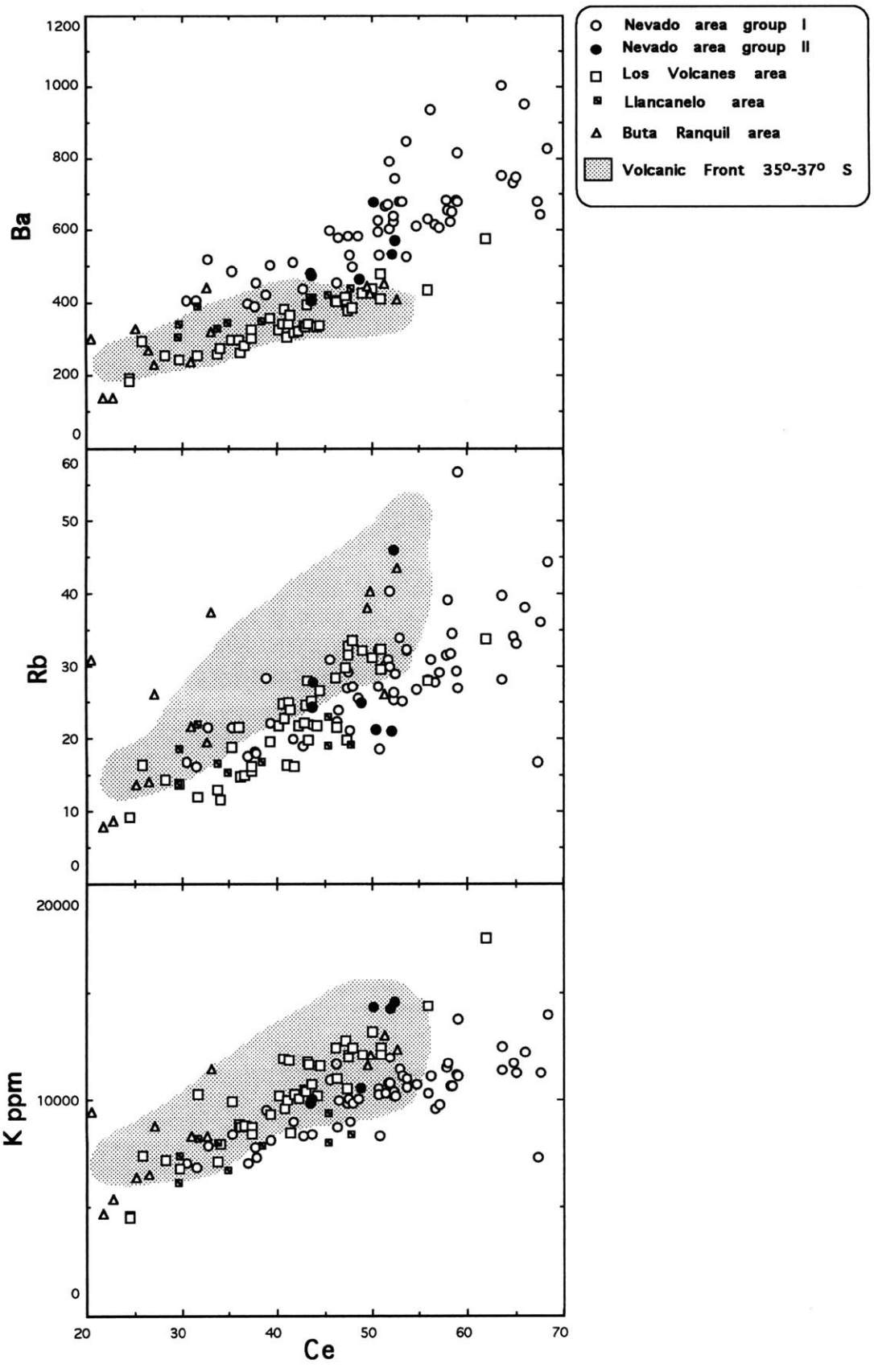

Figure 27a: Ba, K and Rb versus Ce . Volcanic Front lavas display enrichment that is similar in K and Ba, and higher in Rb than the back-arc basalts (with the exception of Nevado area basalts having the highest enrichment in Ba). Also the diagrams show that Los Volcanes and Buta Ranquil area basalts range to higher concentration of K than Nevado and Llancanelo area basalts (with the exception of Nevado group II). Data for the volcanic front as in figure 24.

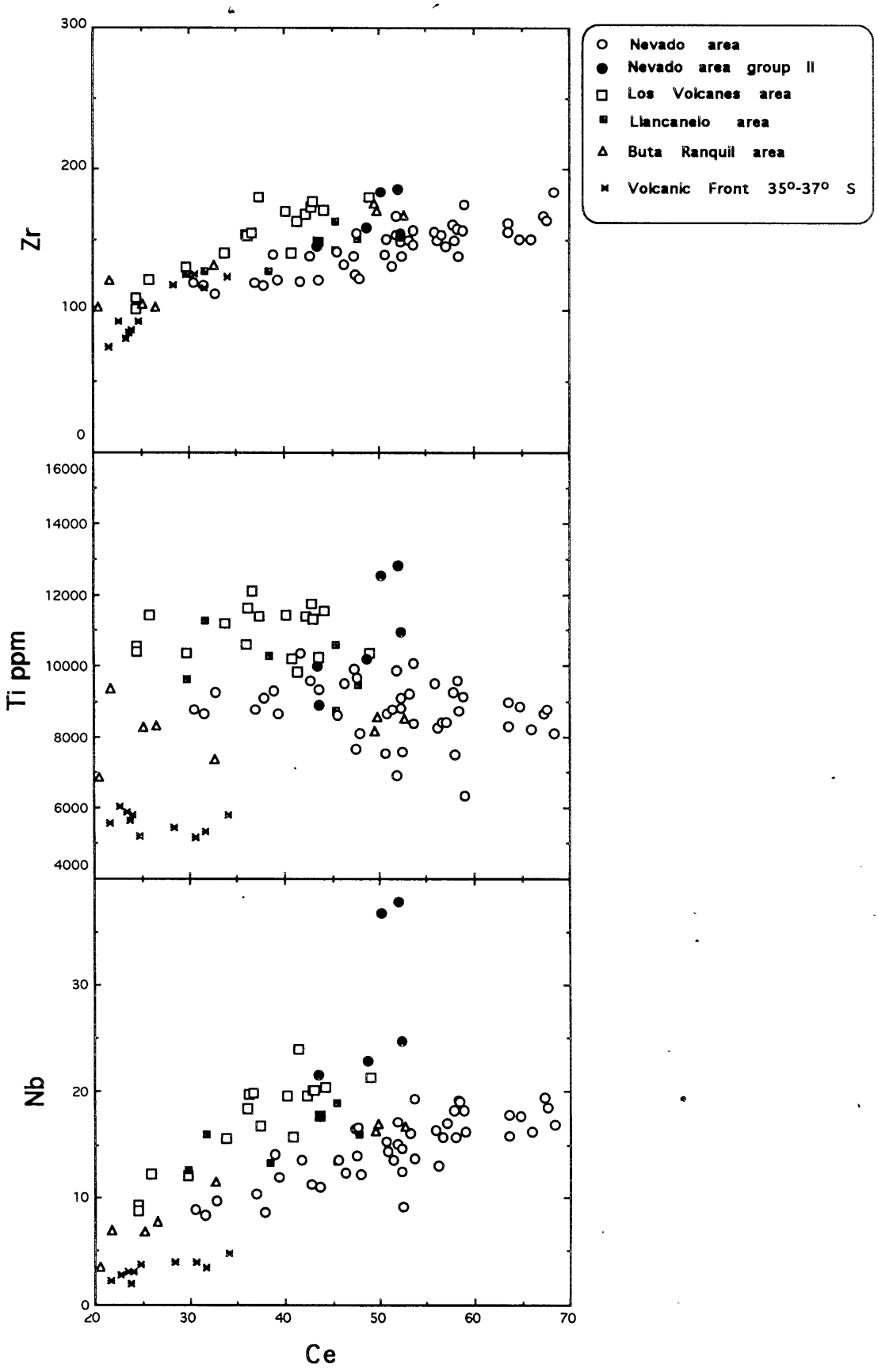

Figure 27b: Zr, Ti and Nb versus Ce for primitive basalts (MgO >7%)

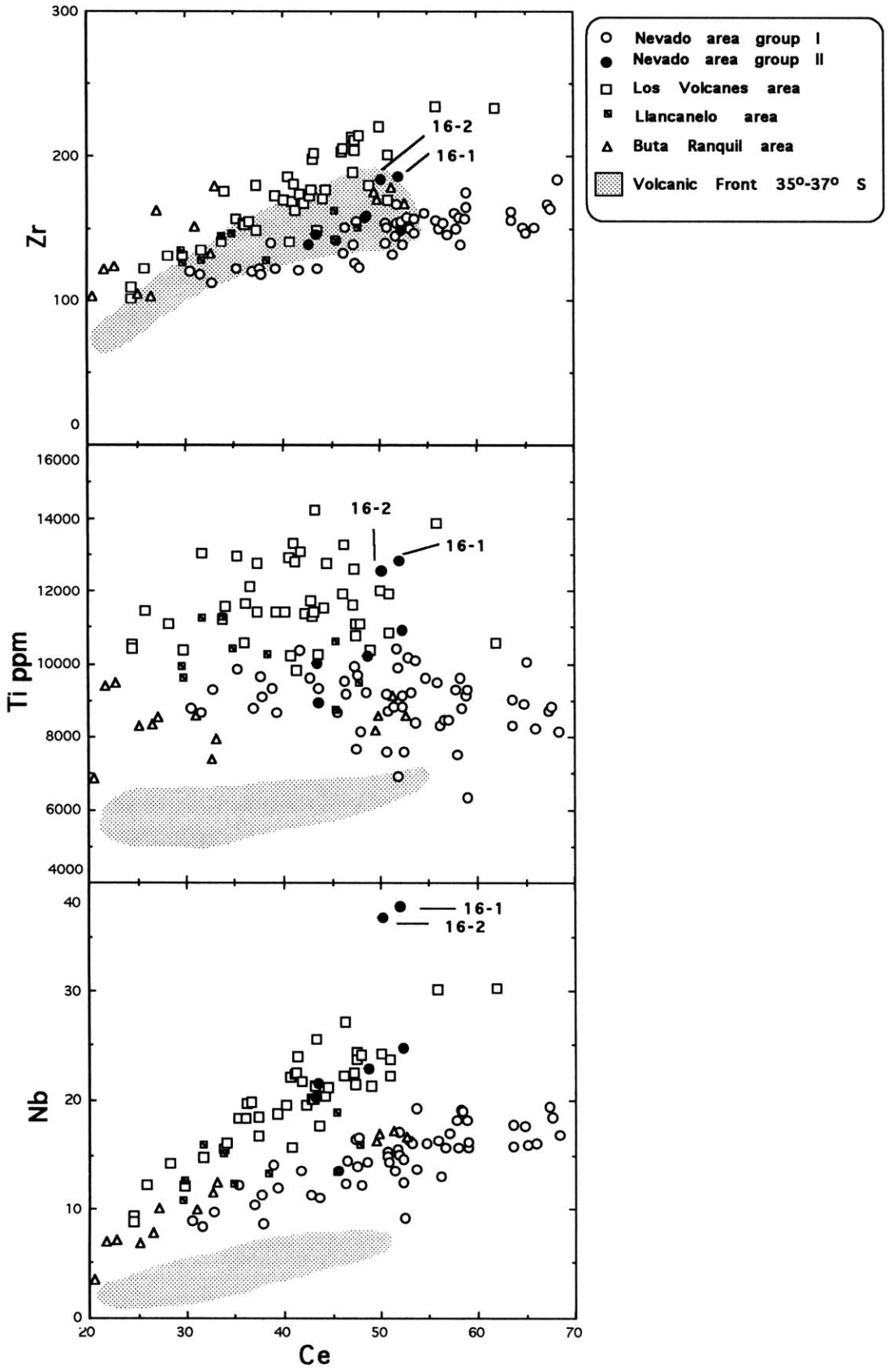

Figure 27b: Zr, Ti and Nb versus Ce. Volcanic Front lavas display lower enrichment in HFSE than the back-arc basalts (with the exception of Nevado area basalts having the lowest enrichment in Zr). Also the diagrams show that Los Volcanes area basalts range to higher concentration of HFSE than Nevado and Buta Ranquil area basalts (with the exception of Nevado group II). Data for the volcanic front as in figure 24.

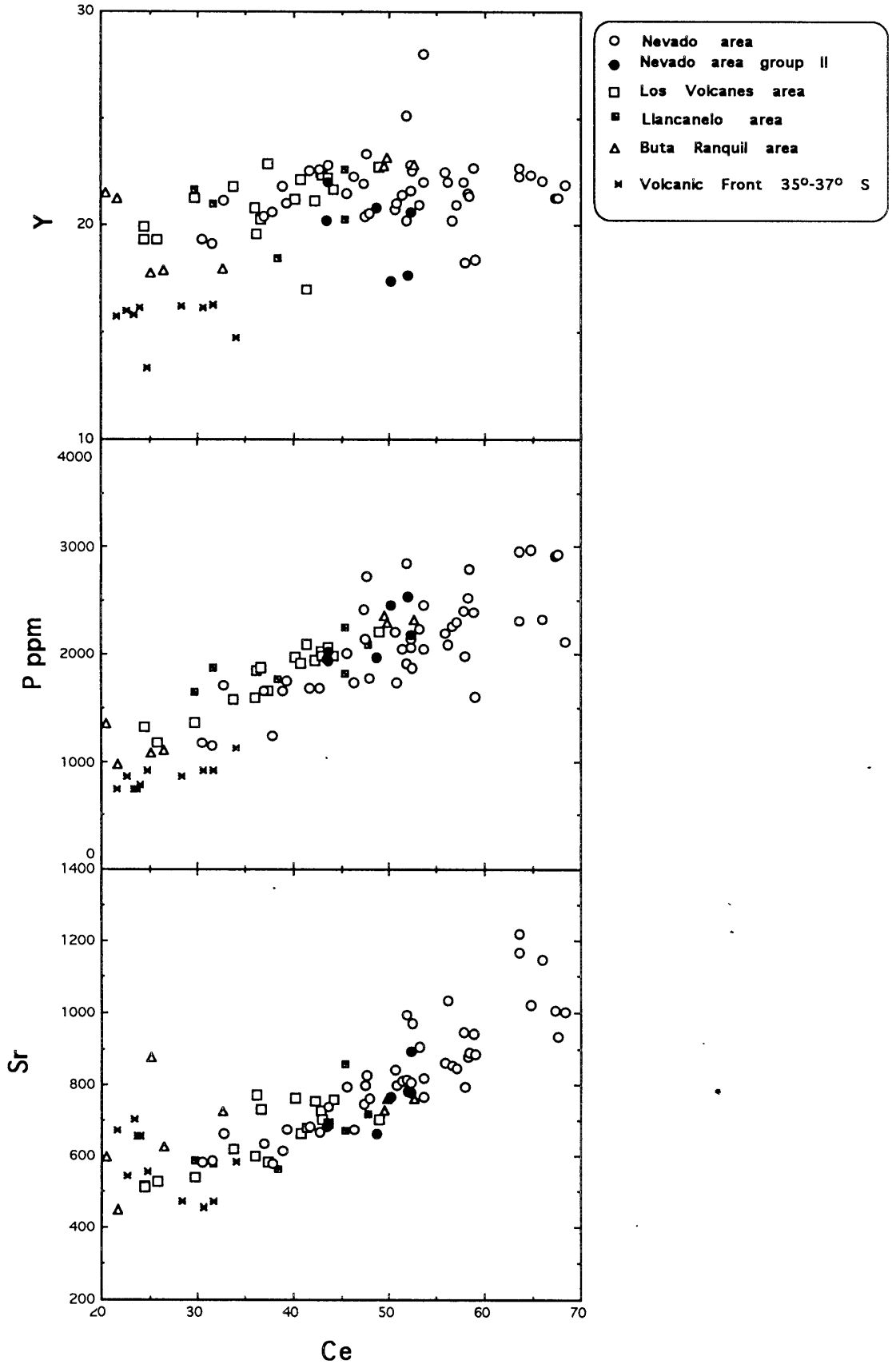

Figure 27c: Y, P and Sr versus Ce for primitive basalts (MgO >7%)

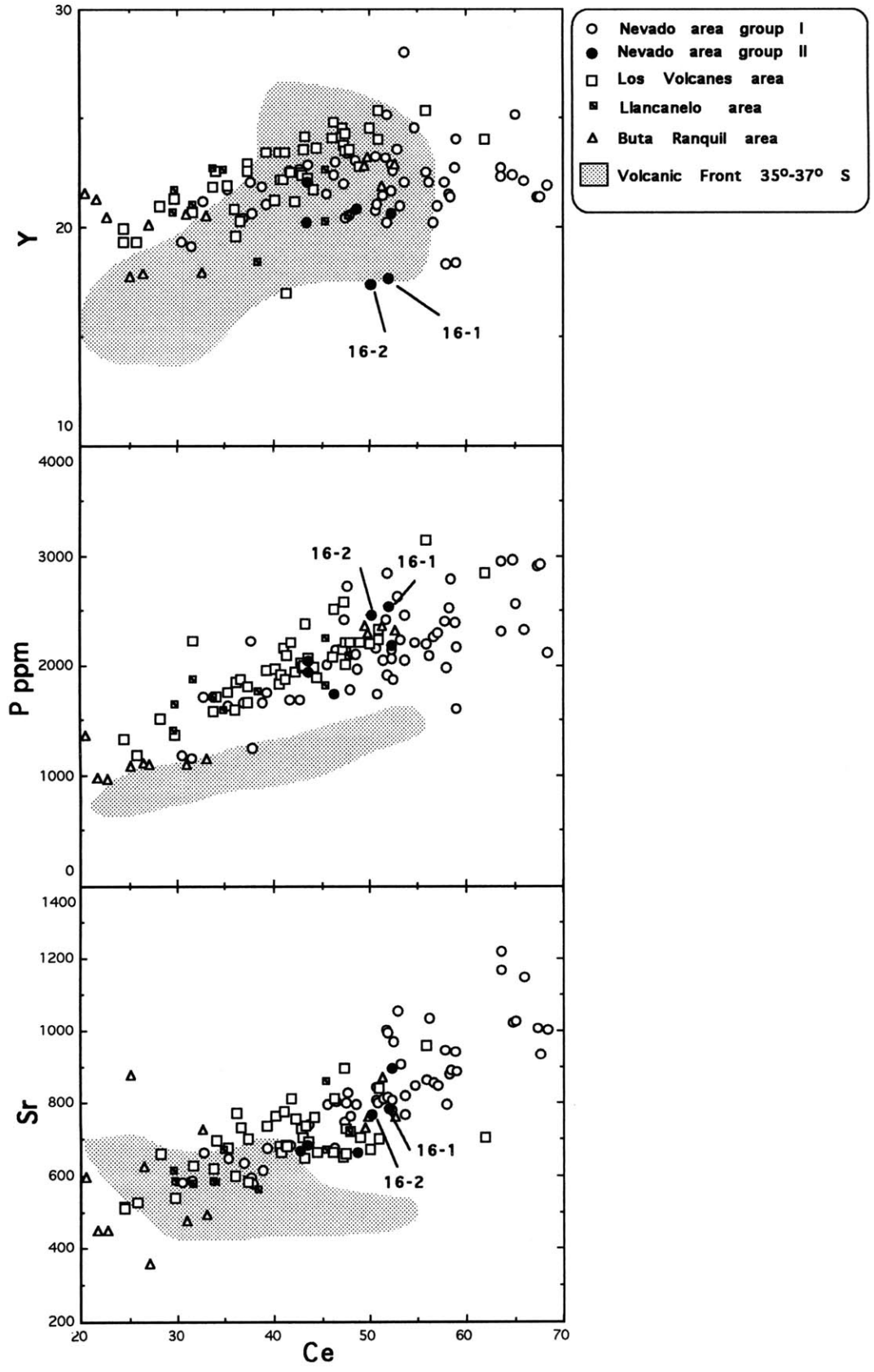

Figure 27c: Y, P and Sr versus Ce. Volcanic Front lavas display lower enrichment than the back-arc basalts. Also Sr trend in the volcanic front lavas is different (more compatible) than that in the back-arc basalts. The diagrams show that the volcanic fields behind the front overlap in Sr, P and Y with the Nevado area basalts ranging to lower concentration. Data for the volcanic front as in figure 24.

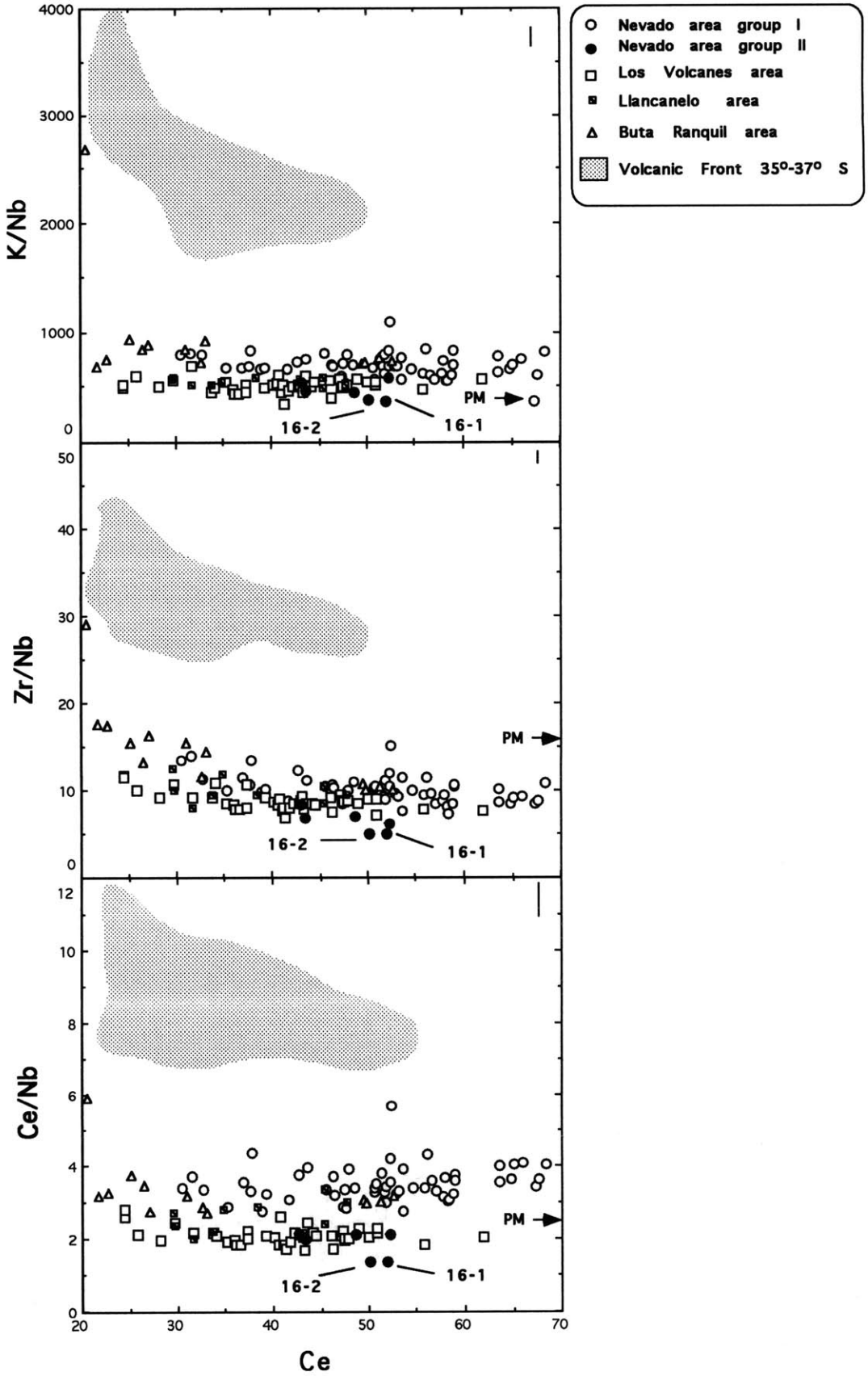

Figure 28a: K/Nb, Zr/Nb and Ce/Nb versus Ce diagram. These ratios are systematically higher in the volcanic front rocks than the back-arc lavas. The ratios are higher in Nevado area and Buta Ranquil area basalts than Los Volcanes and Llancanelo area basalts, with exception of Nevado group II basalts that display similar ratios as los Volcanes basalts. Data for the volcanic front as in figure 24. PM represents abundance ratios for Primitive Mantle.

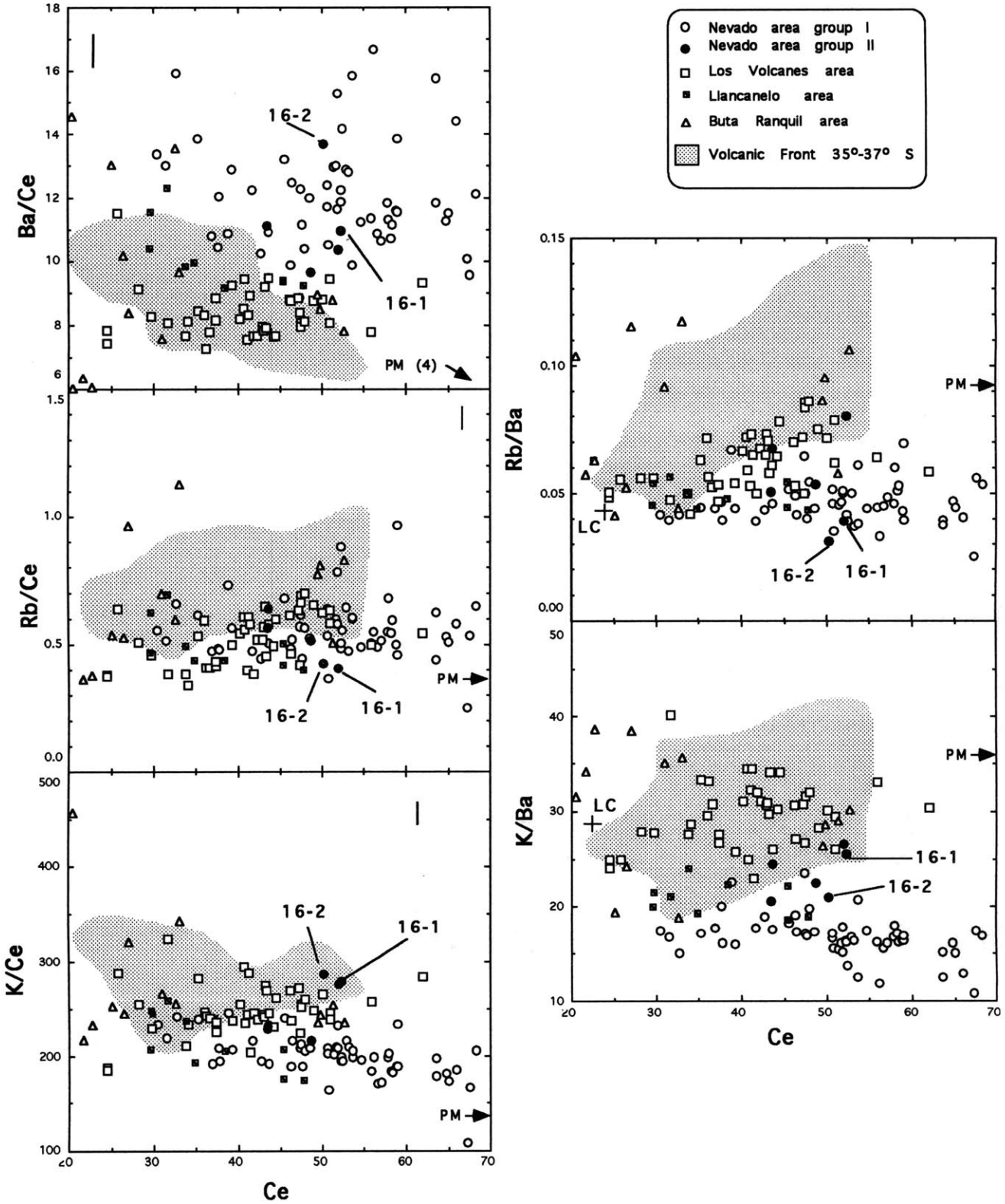

Figure 28b: Ba/Ce, Rb/Ce, K/Ce, Rb/Ba and K/Ba versus Ce. In the volcanic front lavas these ratios range from similar to higher than in the back-arc basalts, with the exception of Ba/Ce that is higher in Nevado area basalts. Los Volcanes and Buta Ranquil area rocks have higher ratios than Nevado and Llancanelo area basalts with the exception of Ba/Ce, higher in Nevado area lavas. Data for the volcanic front as in figure 24. PM and LC represent the abundance ratios for Primitive Mantle and Lower Crust (Taylor and McLennan, 1985) respectively.

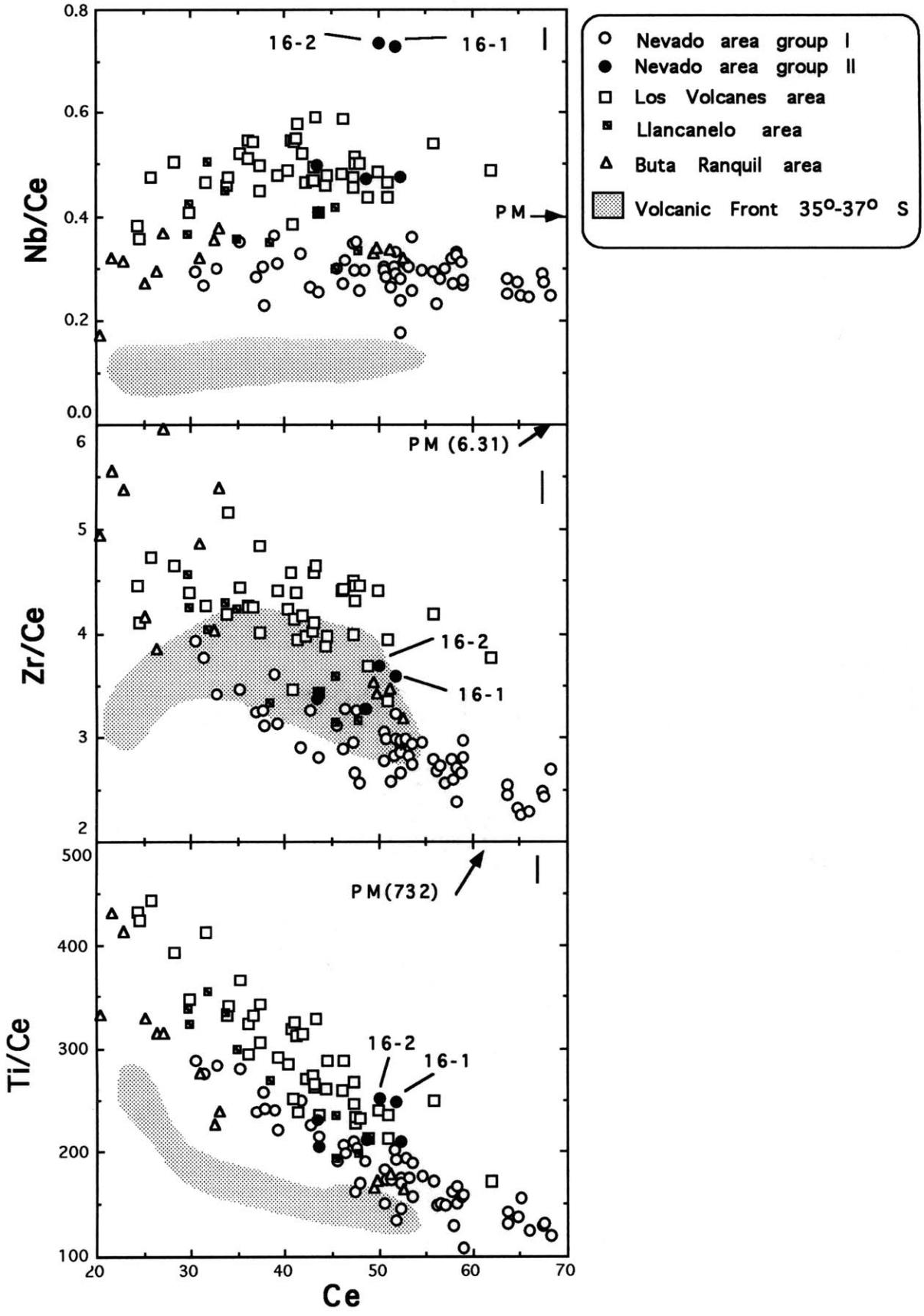

Figure 28c: Nb/Ce, Zr/Ce, Ti/Ce versus Ce. These ratios are systematically lower in the volcanic front lavas (except Zr/Ce) than the back-arc basalts. The ratios are higher in Los Volcanes and Llancanelo area basalts than Nevado and Buta Ranquil area lavas, with the exception of Zr/Ce ratios in Buta Ranquil area lavas. Data for the volcanic front as in figure 24. PM represent the abundance ratio for the Primitive Mantle (Sun and McDonough, 1989)

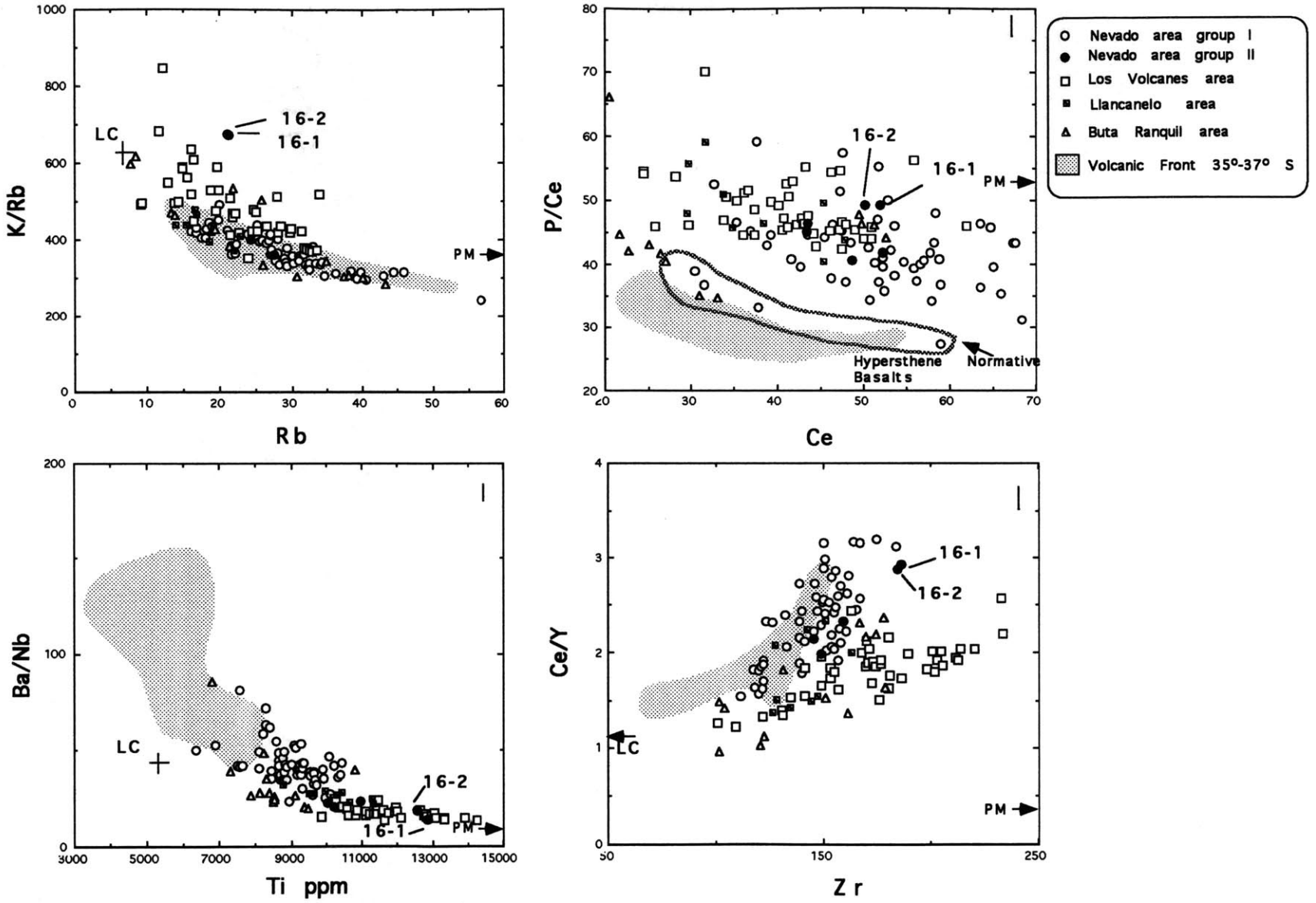

Figure 29: Ba/Nb versus Ti; K/Rb versus Rb; Ce/Y versus Zr and P/Ce versus Ce diagrams. These diagrams show that the volcanic front lavas range to composition similar to Nevado area basalts displaying higher Ba/Nb and Ce/Y ratios and lower K/Rb ratios than Los Volcanes area. On the other side, P/Ce ratios is lower in the volcanic front than the back-arc basalts, with the exception of the hypersthene normative basalts that have P/Ce ratios similar to the volcanic front. Data for the volcanic front as in figure 9. PM and LC represent the abundance ratios for Primitive Mantle and Lower Crust, respectively.

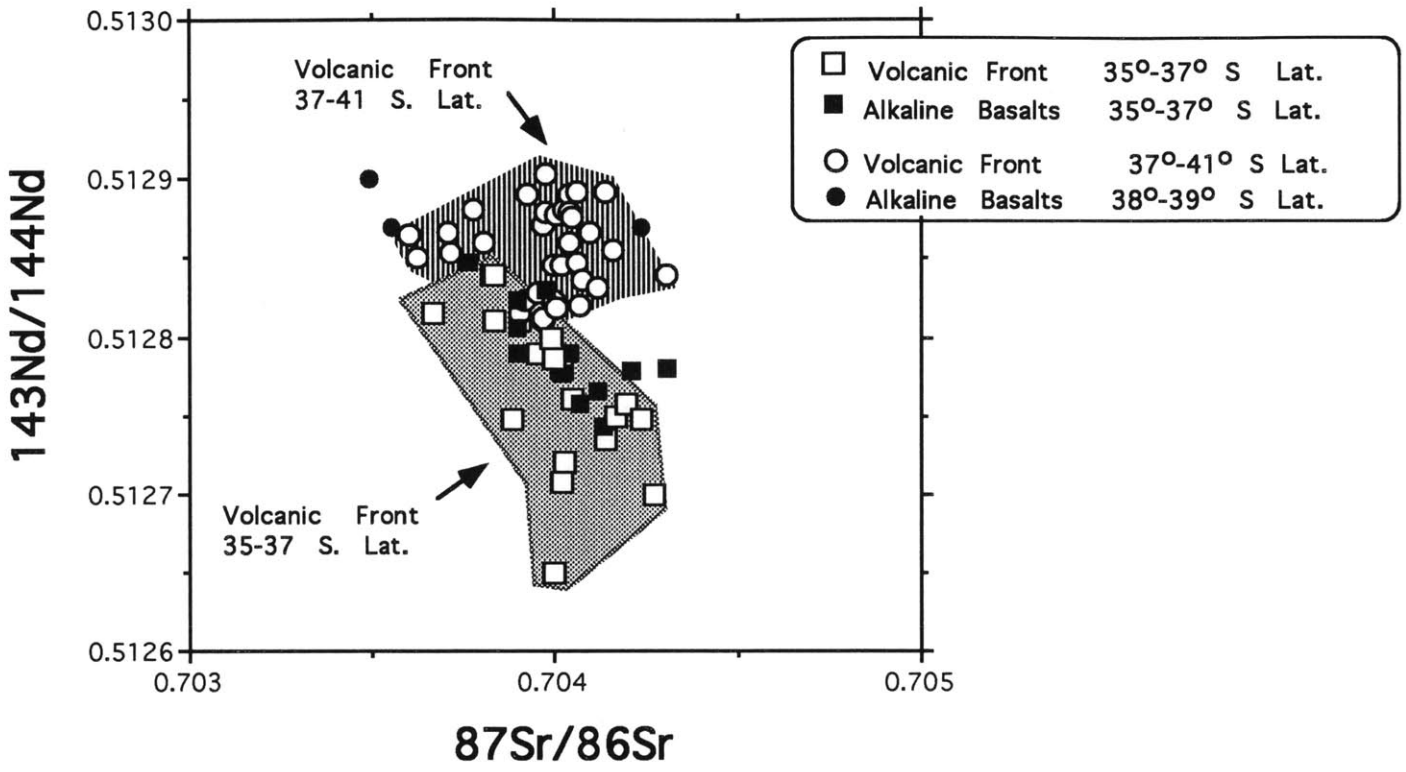

Figure 30: $^{143}Nd/^{144}Nd$ versus $^{87}Sr/^{86}Sr$. Along the volcanic front from 35° to 38° the lavas range in $^{87}Sr/^{86}Sr$ from 0.703670 to 0.704270 and there is no systematic along srtike change in $^{87}Sr/^{86}Sr$. In contrast, along the volcanic front $^{143}Nd/^{144}Nd$ ratios are lower in the 35°-37° region than in the 37°-41° region. An important result is that the along strike trend on the volcanic front is also seen in the alkaline basalts erupted behind the volcanic front. Isotopic data for the volcanic front are from Frey et al. (1984); Hickey et al. (1986); Davidson et al. (1987, 1988); Hildreth and Moorbath (1988); Gerlach et al. (1988); Hickey-Vargas et al. (1989); Tormey et al (1991, 1993). Data for the alkaline basalts between 38°-39° are from Stern et al. (1991), and between 35°-37° are from this research.

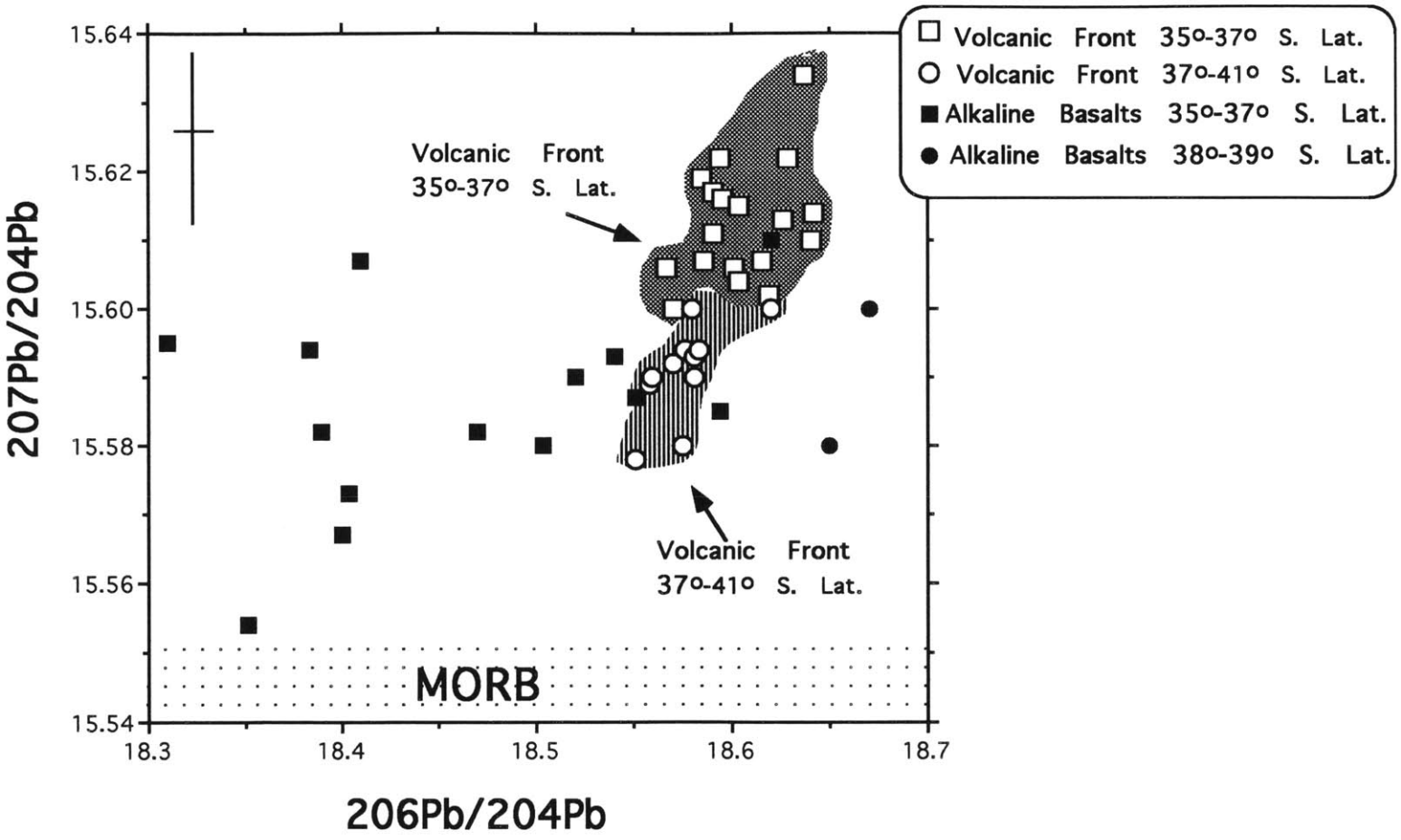

Figure 31: $^{207}Pb/^{204}Pb$ versus $^{206}Pb/^{204}Pb$ showing that Pb isotope ratios in the alkaline basalts range to lower ratios than volcanic front lavas. References for lavas from the volcanic front arethe same as in Figure 30.

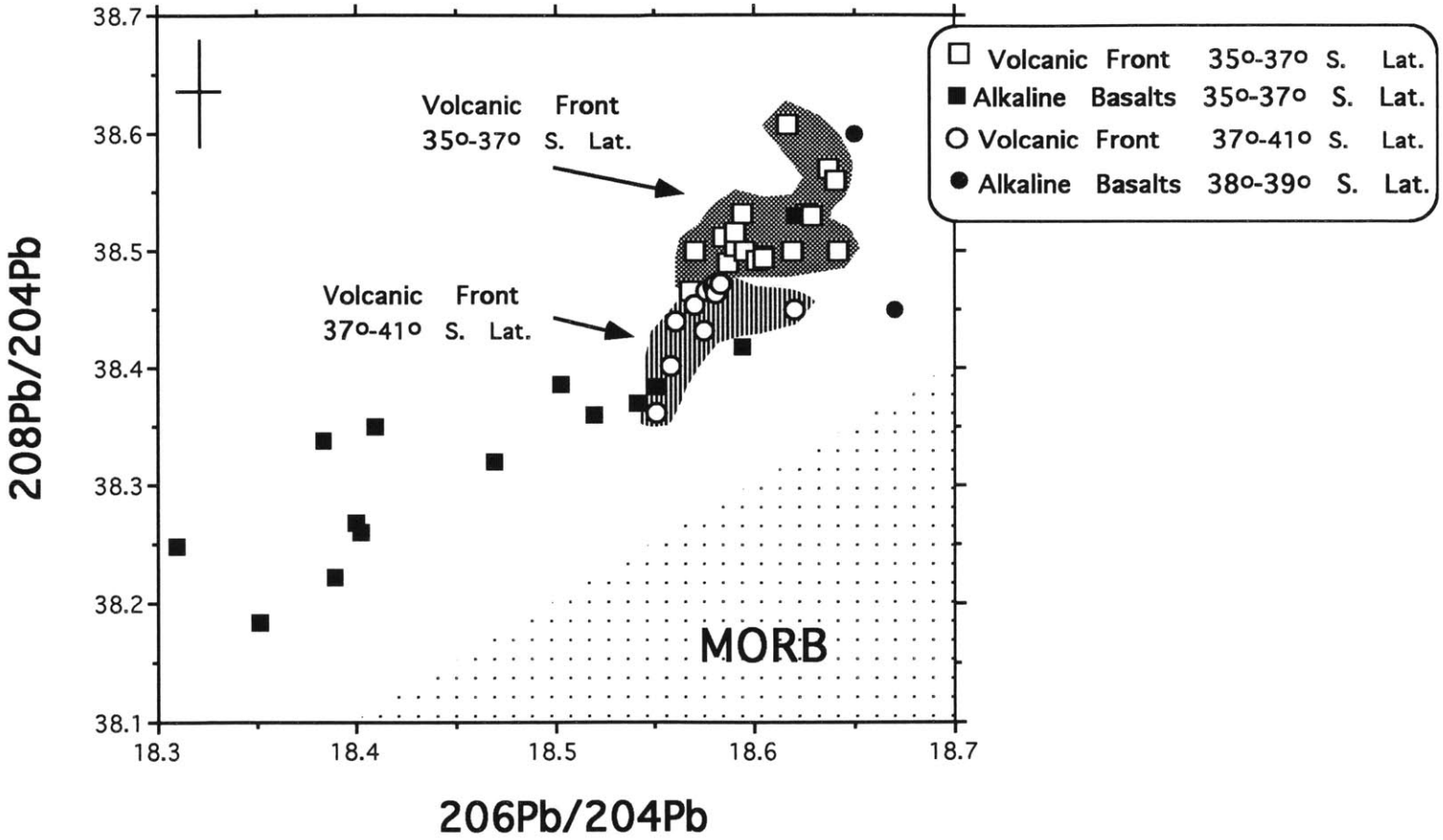

Figure 32: $^{208}Pb/^{204}Pb$ versus $^{206}Pb/^{204}Pb$ showing that Pb isotope ratios in the alkaline basalts range to lower ratios than volcanic front lavas. References for lavas from the volcanic front are the same as in Figure 30

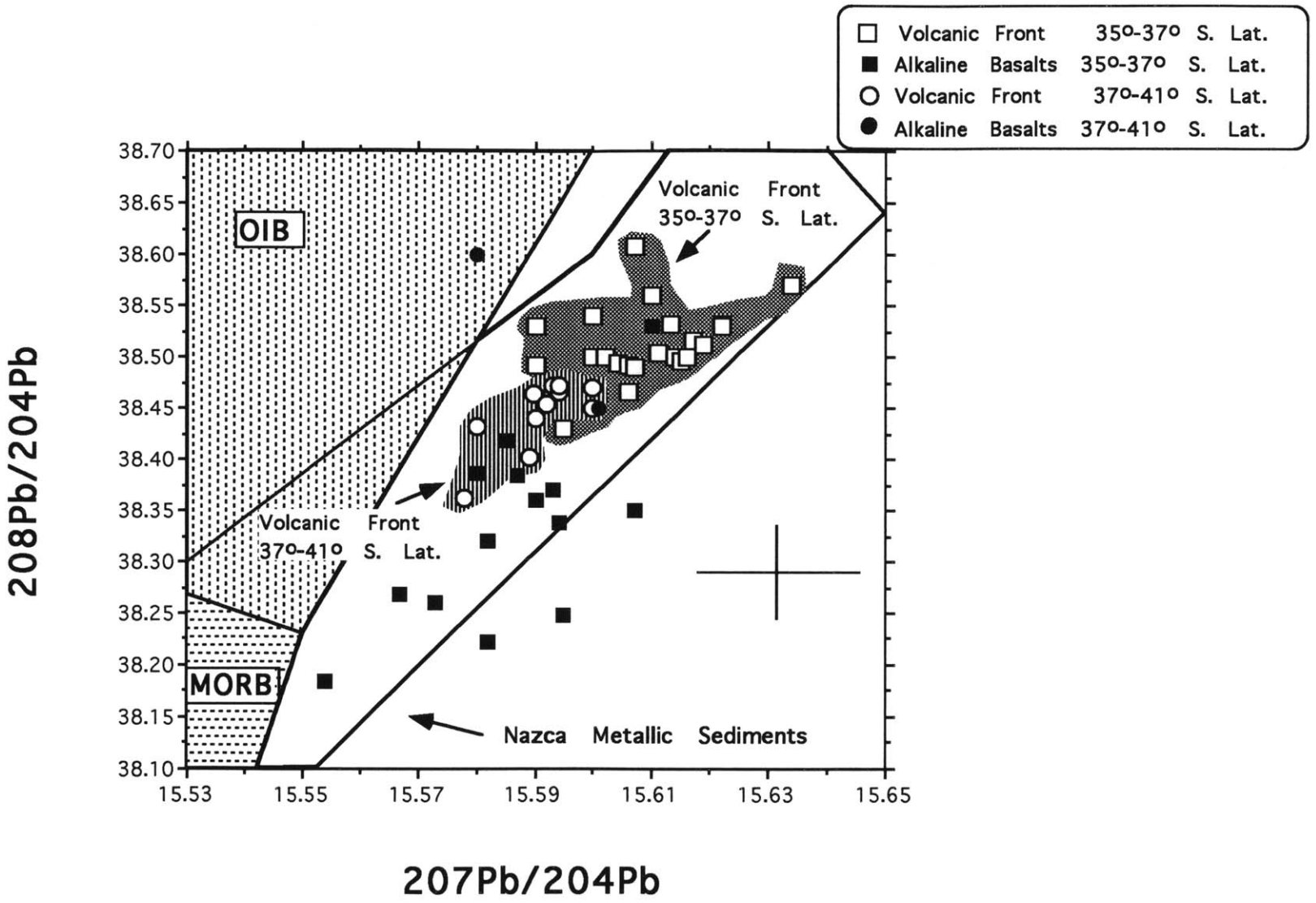

Figure 33: $^{208}Pb/^{204}Pb$ versus $^{207}Pb/^{204}Pb$ showing that like lavas on the volcanic front, Pb isotope ratios in the alkaline basalts do not overlap the fields for MORB and OIB. References for the volcanic front are the same as in Figure 30. References for MORB OIB and Nazca metalic sediments are taken from Hickey et al., (1986).

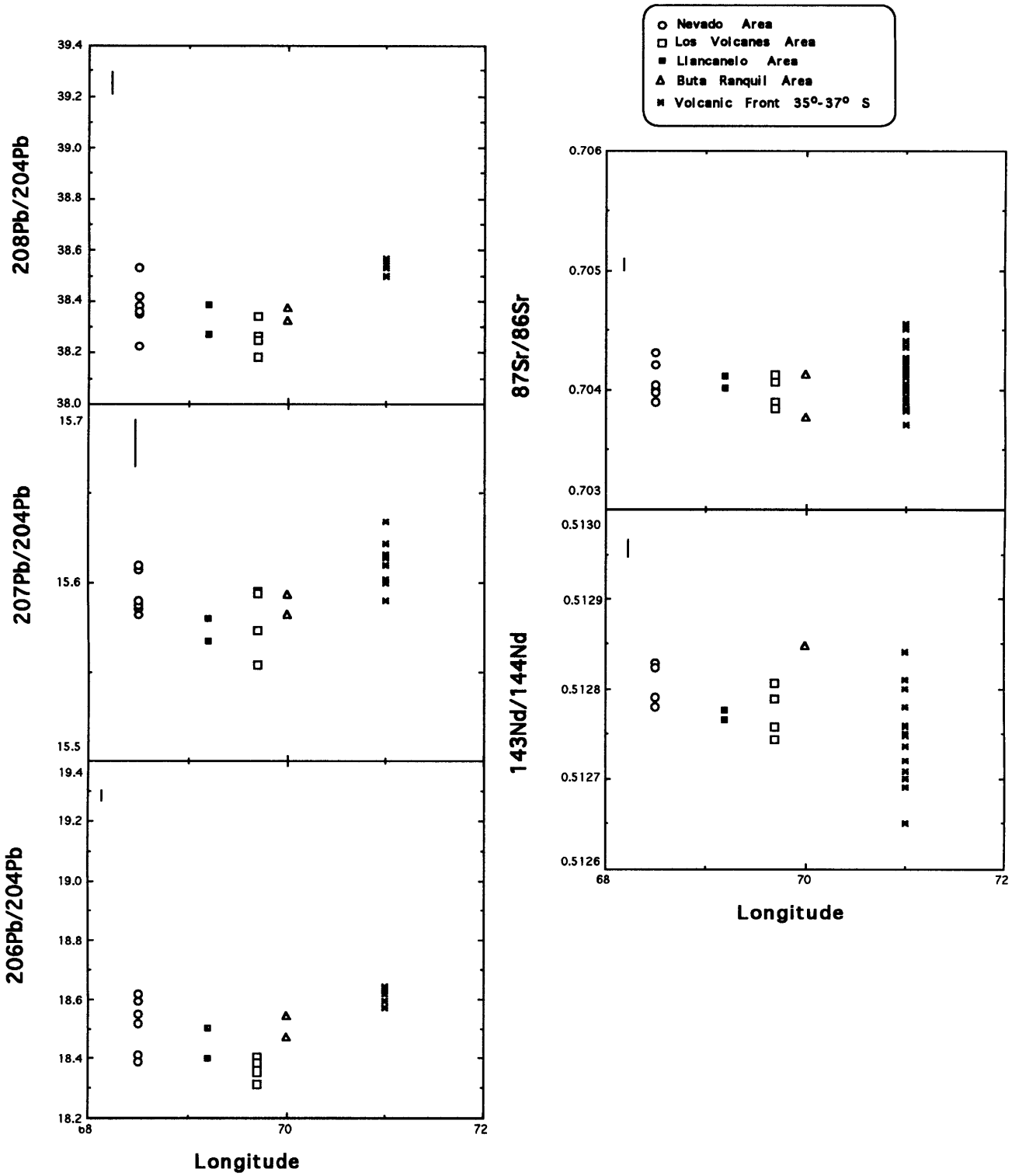

Figure 34: Sr, Nd and Pd isotopic composition versus longitude. The figure shows the isotopic composition for the volcanic front (35° to 37° S) and the differents volcanic fields behind it. Los Volcanes volcanic field basalts display the lowest base level in Pb isotopic ratios, and also lower base level for Nd and Sr isotopic ratios than Nevado volcanic field. Data for the volcanic front are from Frey et al. (1984); Hickey et al. (1986); Davidson et al. (1987, 1988); Hildreth and Moorbath (1988); Tormey et al. (1991,1993); Ferguson et al. (1992).

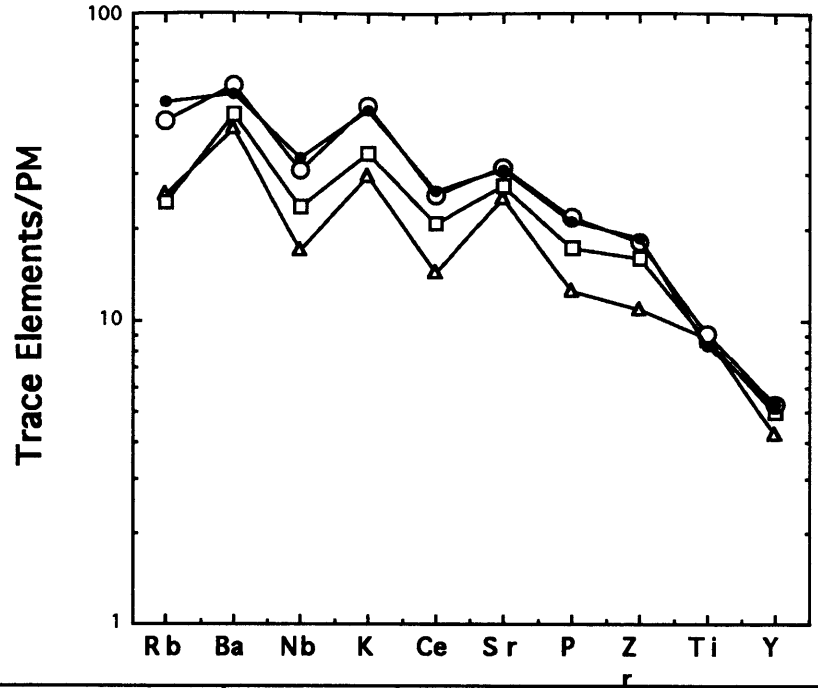

Sample	Stratigraphic age	87Sr/86Sr	143Nd/144Nd	208Pb/204Pb	Ba/Nb	MgO wt%
25-11	Pleistocene	0.704131	0.512743	38.339	24.20	7.24
25-7	Late Pleistocene - Early Holocene	0.704069	0.512758	38.248	19.61	7.49
25-1	Holocene	0.703902	0.512806	38.260	18.74	6.33
23-1	Prehistoric	0.703903	0.512789	38.184	15.74	5.88

Figure 35: Primitive mantle normalized diagram for Los Volcanes area basalts. With decreasing eruption age, $^{87}Sr/^{86}Sr$, $^{208}Pb/^{204}Pb$ and Ba/Nb decrease whereas $^{143}Nd/^{144}Nd$ and abundances of highly incompateble element increase.

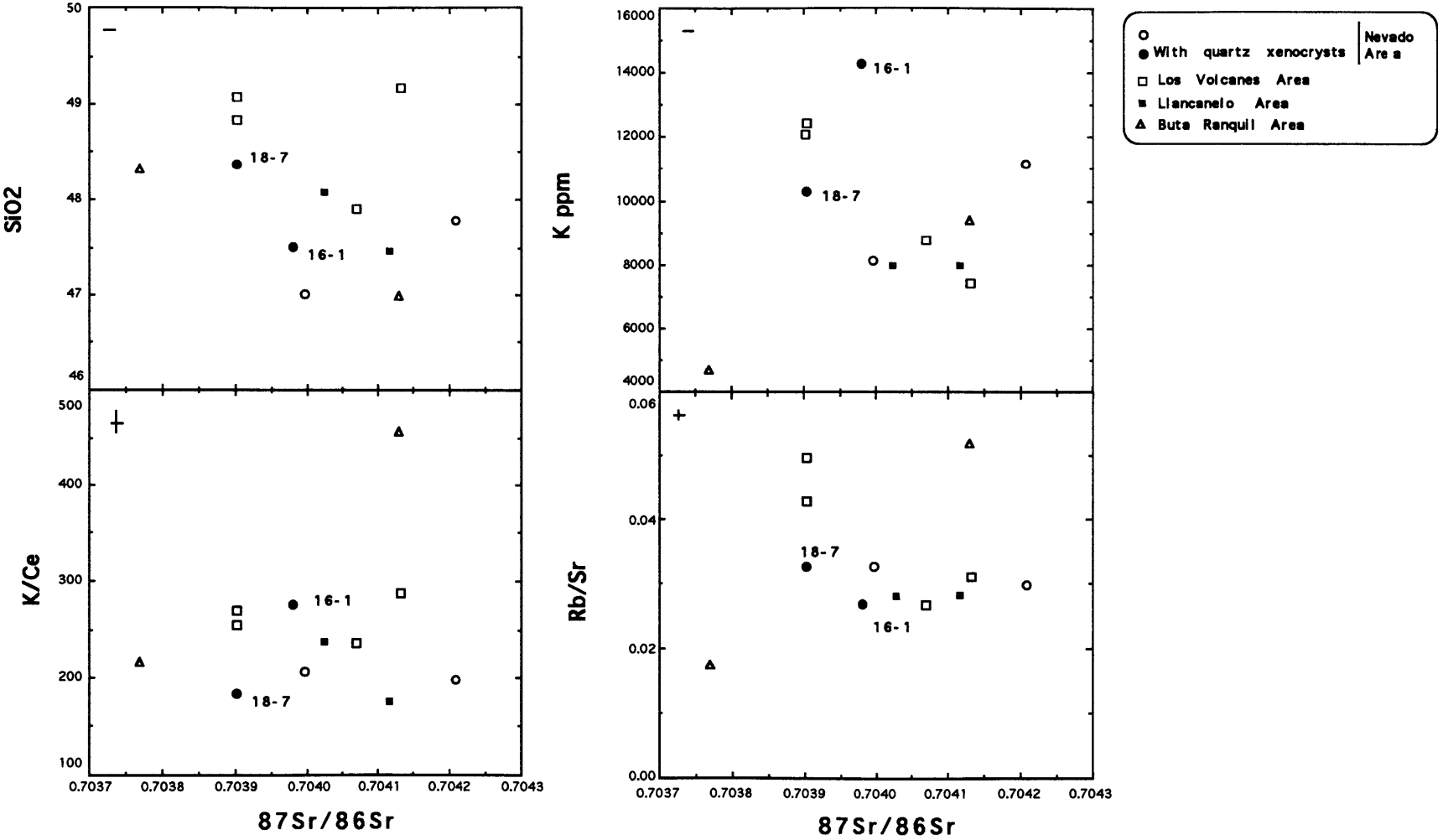

Figure 36: SiO2, K, K/Ce and Rb/Sr versus 87Sr/86Sr. Figure shows that there is no correlation between SiO2, K, K/Ce or Rb/Sr and Sr isotopic composition. The two samples from Nevado area with quartz xenocrysts (16-1 and 18-7) display lower 87Sr/86Sr than the others samples from the same area.

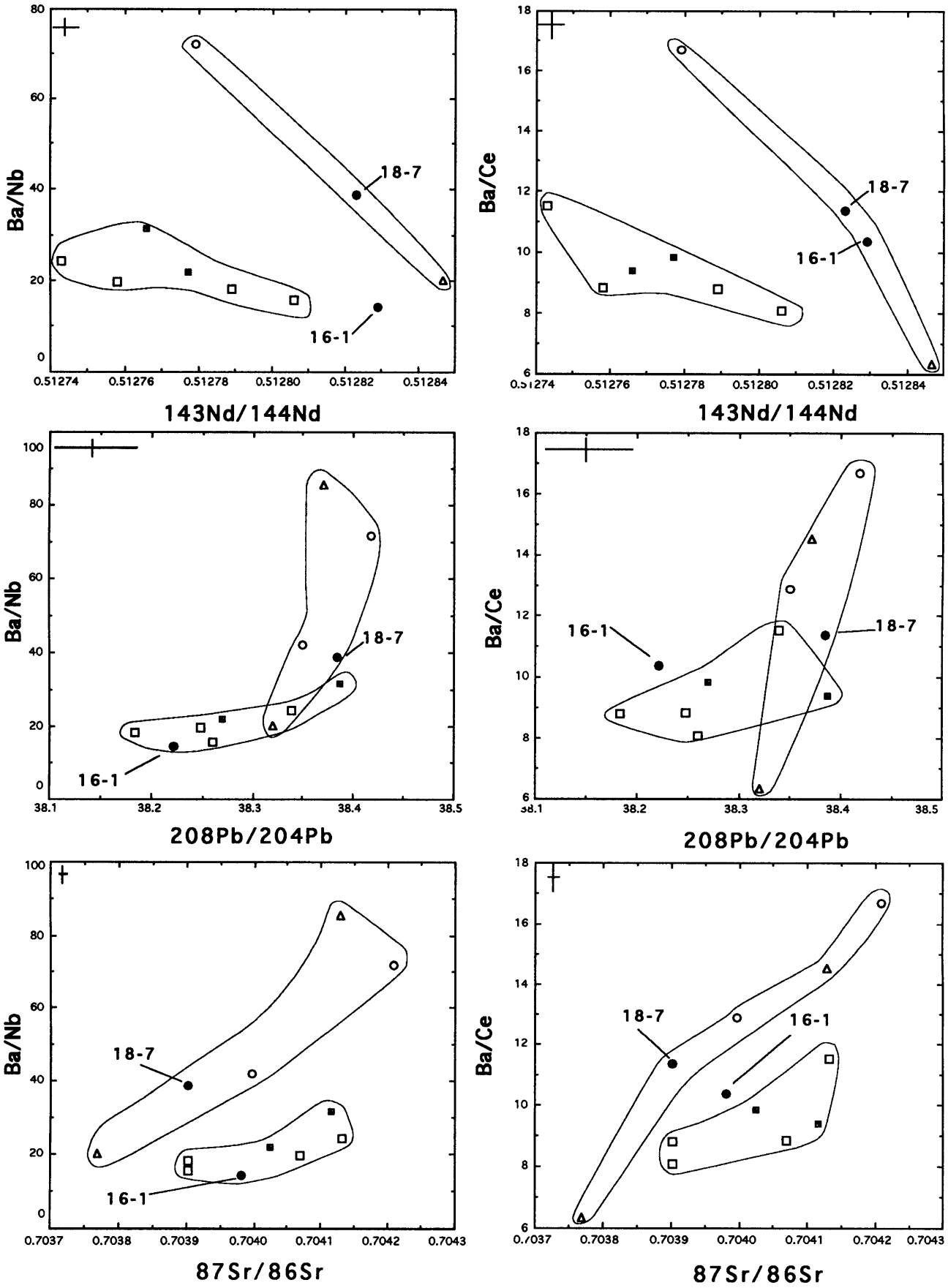

Figure 37: Ba/Nb, Ba/Ce versus Sr, Pb and Nd isotopic composition. Nevado and Buta Ranquil lavas as a group with high arc signature (Ba/Nb, Ba/Ce ratios), and Los Volcanes and Llancanelo basalts as another group with low arc signature. There is a clear correlation between the isotopic composition and the arc signature. Symbols as in Figure 36

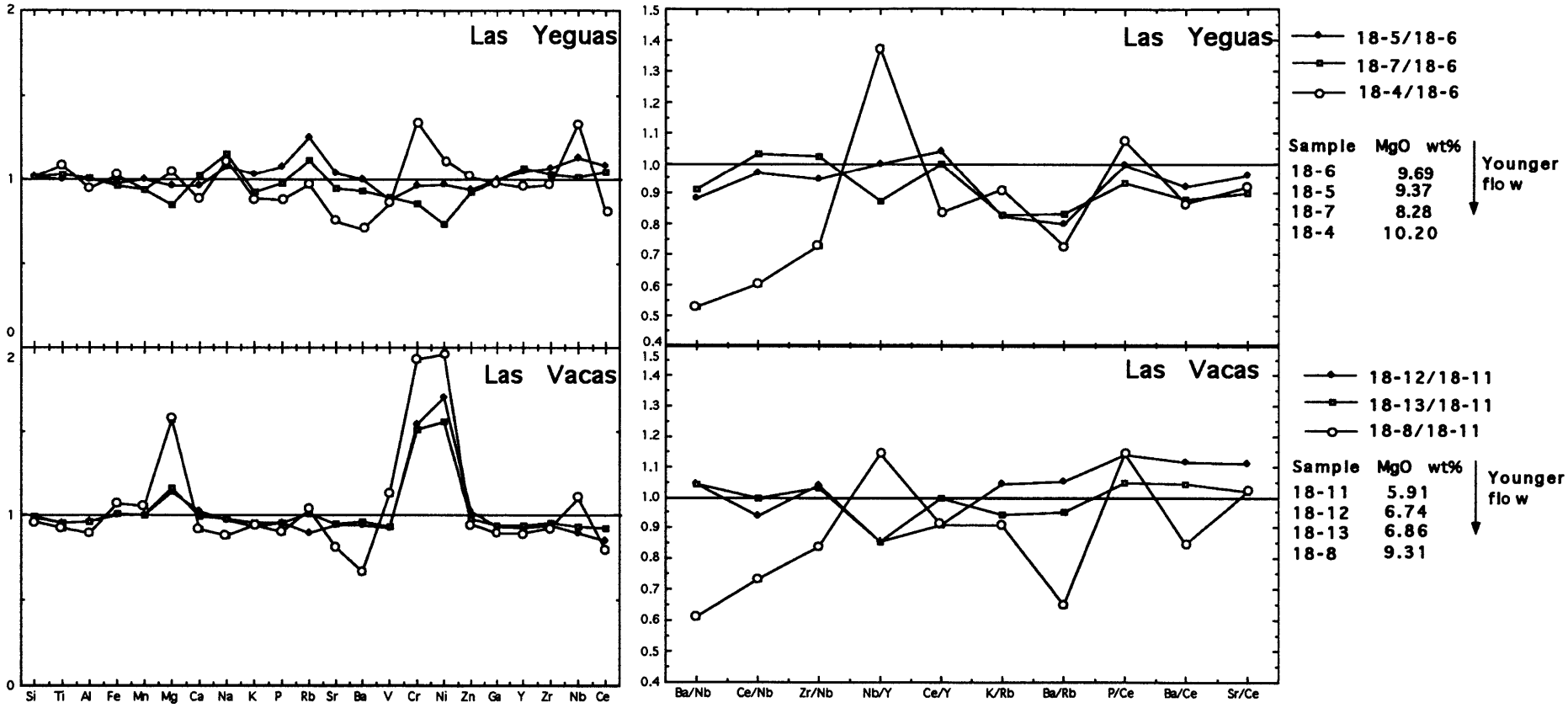

Figure 38: Compositional variation between four flows from the same composite cones Las Vacas and Las Yeguas (Nevado volcanic field). The three younger flows are compared with the oldest one. The last flow, a member of Group II shows the most important differences in composition, with respect to the older lavas. To avoid the effect of crystal fractionation we show the ratios between the incompatibles elements; again the younger flow displays the biggest differences

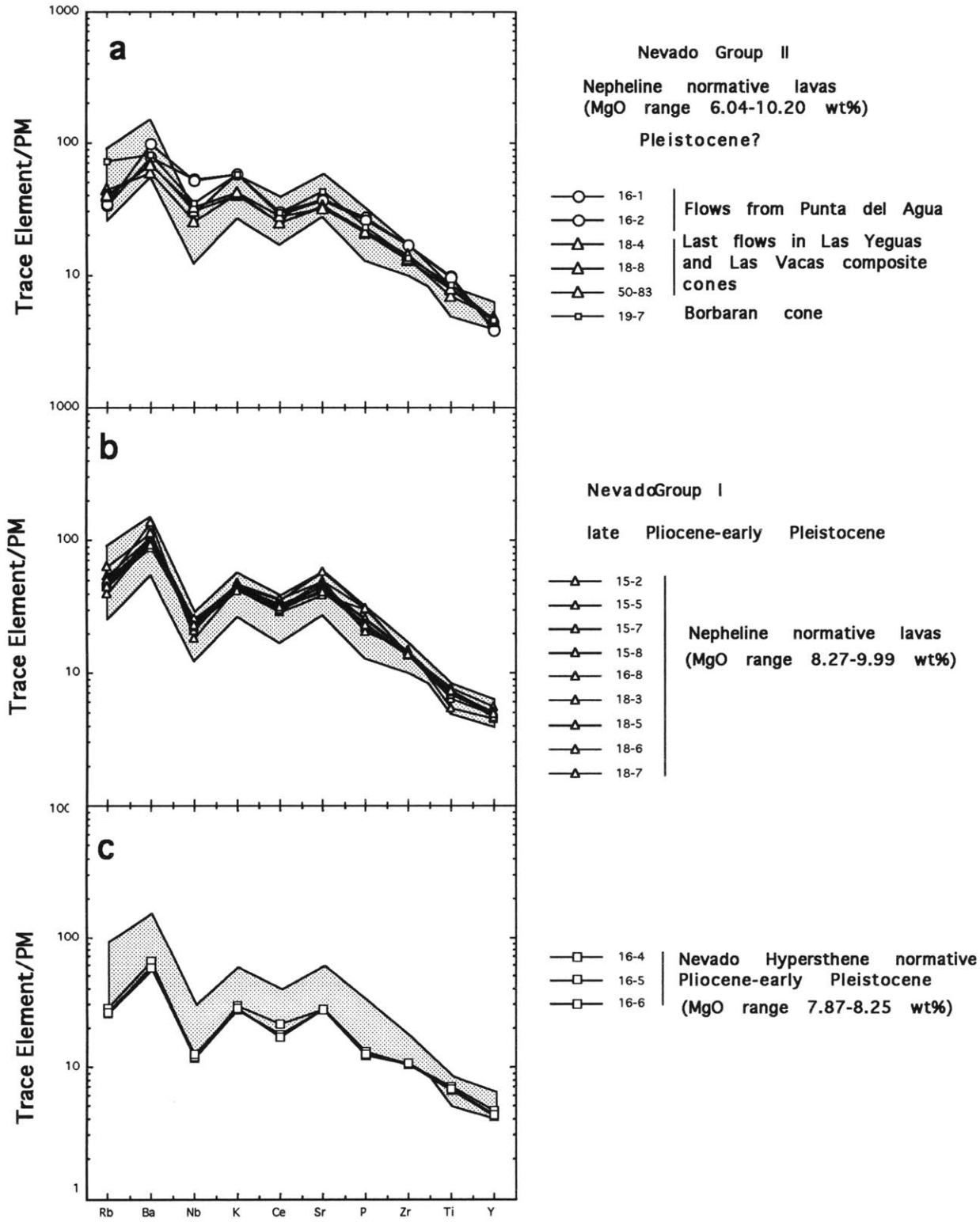

Figure 39: Primitive mantle normalized diagram for Nevado area basalts. Shaded area represents range in composition of Nevado Group I basalts (MgO range 5.91-12.57 wt%). This figure shows from c to a a temporal change in the composition of the Nevado lavas with an increase in incompatible element abundances from Hy-normative to Ne-normative (Group I) lavas at similar MgO content, during the Pliocene to early Pleistocene, and a decrease in the arc signature (Ba/Nb) from Group I to Group II lavas during the Pleistocene.

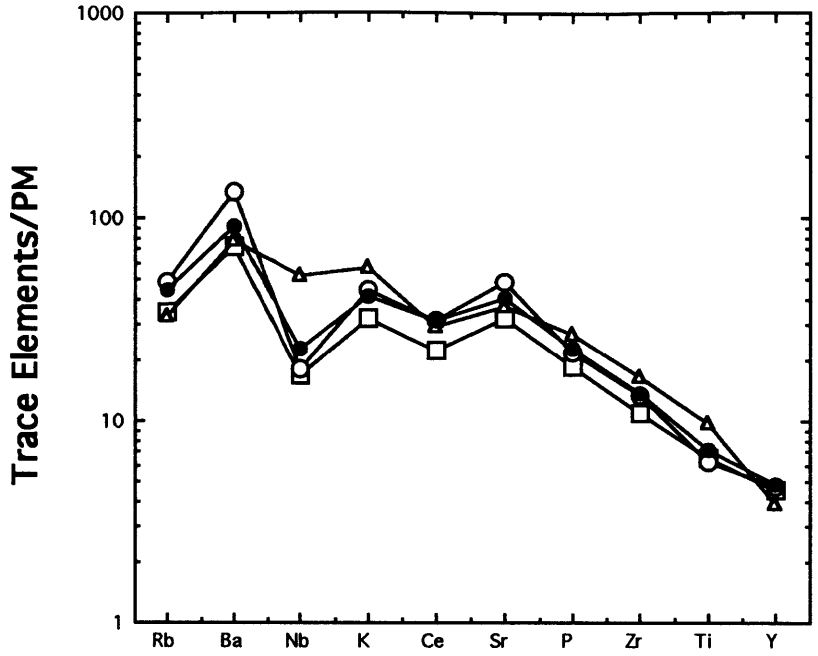

Sample	Stratigraphic age	87Sr/86Sr	143Nd/144Nd	208Pb/204Pb	Ba/Nb	MgO wt%
15-5	Pliocene-Pleistocene	0.704208	0.512779	38.350	71.92	8.80
18-7	Pliocene-Pleistocene	0.703903	0.512823	38.384	38.61	8.28
15-4	Pleistocene	0.703997		38.35	41.95	9.29
16-1	Pleistocene?	0.703981	0.512829	38.222	14.22	7.09

Figure 40: Primitive Mantle normalized diagram for Nevado area basalts analysed for Sr, Nd and Pb isotopic ratios. The diagram and table show no clear correlation between trace element abundance, Ba/Nb ratios or assigned age and isotopic composition. Although no clear correlation exist, sample 16-1 (Group II) is clearly different from the rest of the samples (Group I).

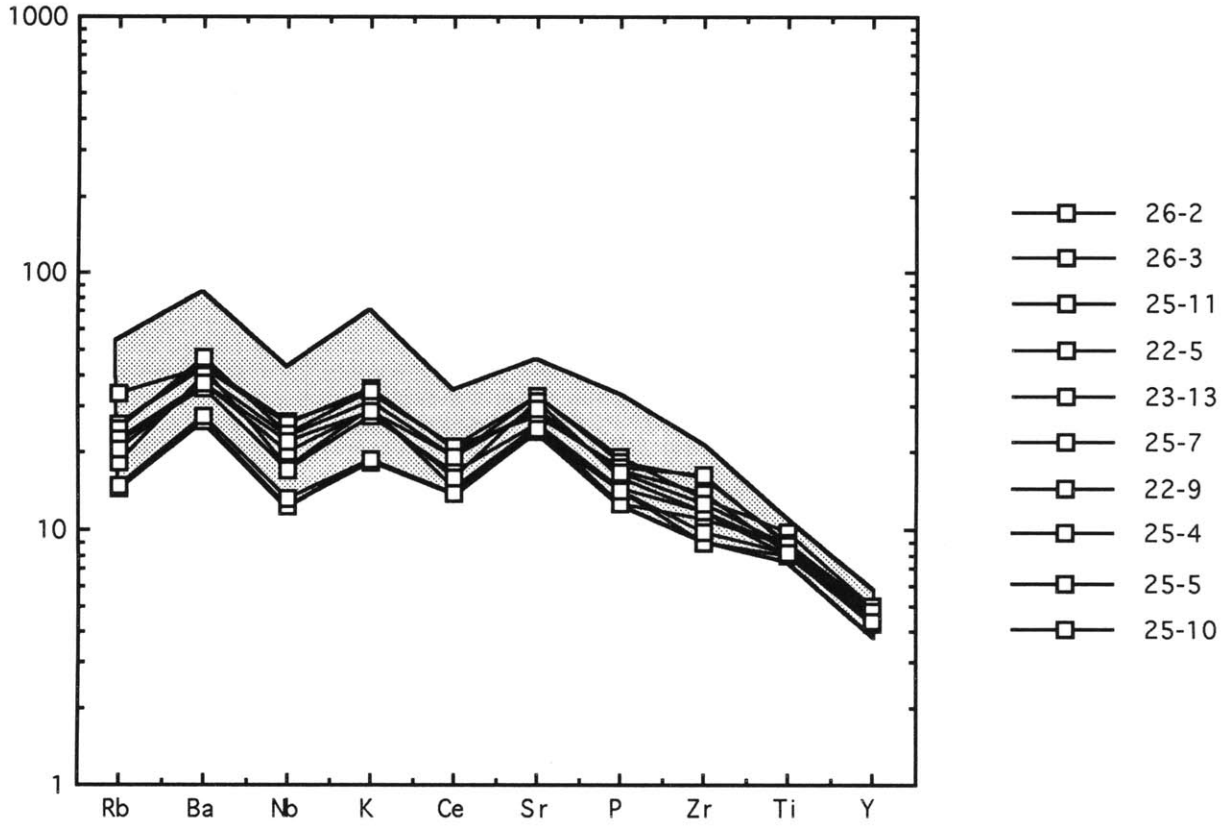

Figure 41: Primitive mantle normalized diagram for los Volcanes area basalts. Shaded area represent all the range in composition of Los Volcanes basalts (MgO range 4.65-9.5 wt%). The diagram shows data for older samples (MgO range 6.31-8.33 wt%) (Pleistocene assigned age) which have lower trace element abundance than the rest of the samples in this area with younger age (Holocene assigned age)

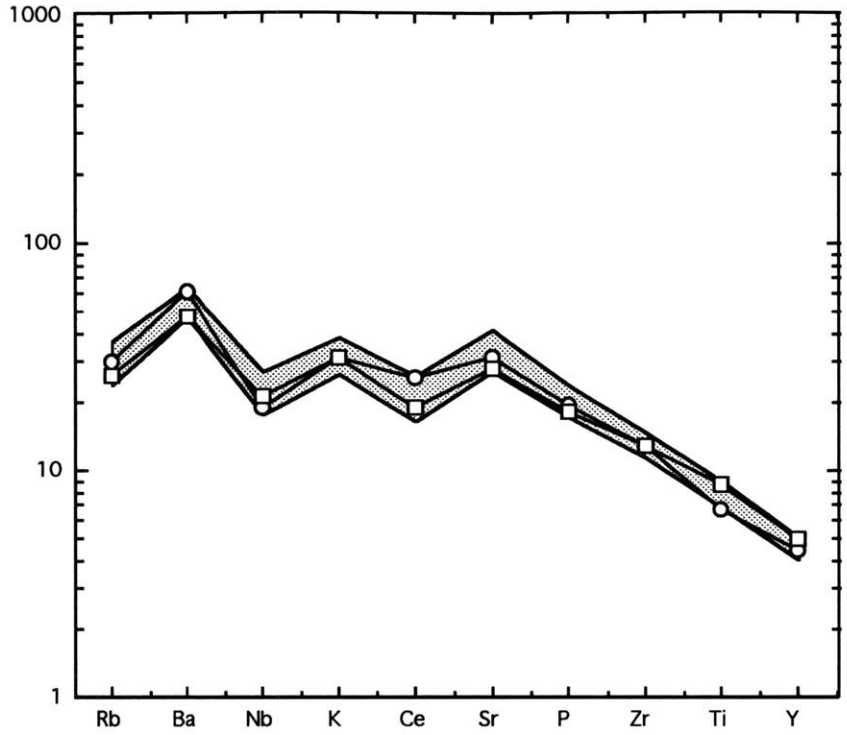

Sample	Stratigraphic age	87Sr/86Sr	143Nd/144Nd	208Pb/204Pb	Ba/Nb	MgO wt%
—o— 21-7	Pliocene-Pleistocene	0.704116	0.512766	38.387	31.56	9.88
—□— 21-1	Late Pleistocene - Early Holocene	0.704024	0.512777	38.269	21.84	6.52

Figure 42: Primitive mantle normalized diagram for Llancanelo area basalts analyzed for isotopic ratios. Shaded area represents the range in composition of Llancanelo area basalts. Although there is no significant variation in trace element abundance with age, the older sample have higher Sr , Pb and lower Nd isotopic composition and higher Ba/Nb ratios than the younger flow.

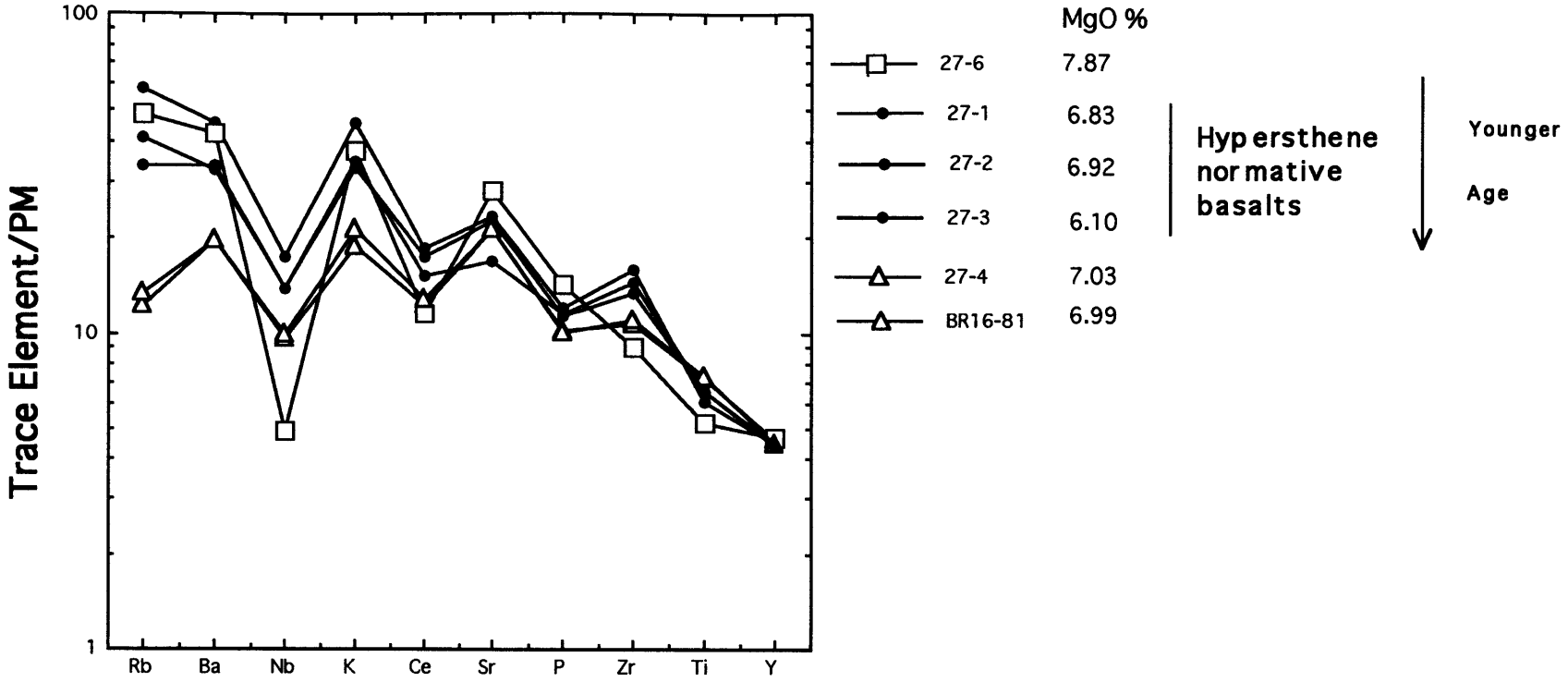

Sample	Stratigraphic age	87Sr/86Sr	143Nd/144Nd	208Pb/204Pb	Ba/Nb	MgO wt%
27-6	Late Pleistocene - Early Holocene (Older)	0.704130		38.371	85.27	7.87
27-4	Late Pleistocene - Early Holocene (Younger)	0.703769	0.512847	38.321	19.94	7.03

Figure 43: Primitive normalized diagram for Buta Ranquil volcano lavas. In contrast to the others areas Buta Ranquil younger lavas show lower trace element abundance than older lavas. On the other hand, Buta Ranquil basalts display Ba/Nb ratios and Sr and Pb isotopic composition that diminish in younger lavas. Hyperstene normative basalts in this volcanoe (at difference with hypersthene normative basalts from Nevado area) show higher trace element abundance.

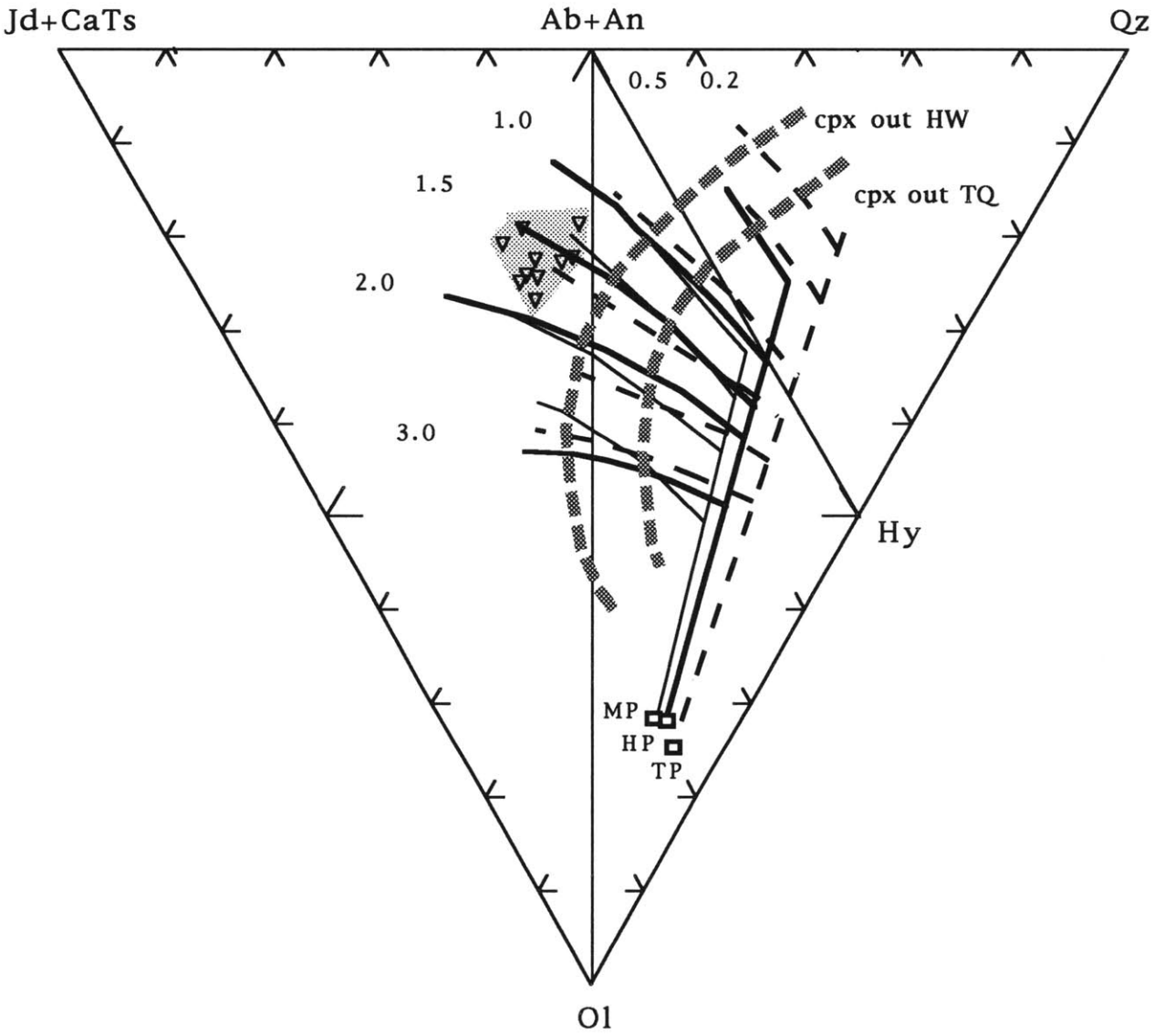

Figure 44: Projection of primitive alkaline lavas from Nevado field onto the plane Ol-Qz-Jd+CaTs, following the algorithms of Green (1970). Shown for comparison the isobaric partial melts obtained experimentally by Fallon and Green (1988) forn Hawaiian Pyrolite (HP), Tinaquillo Lherzolite (TP), and Morb Pyrolite. The primitive alkaline lavas plot between 1.5 and 2.0 GPa.

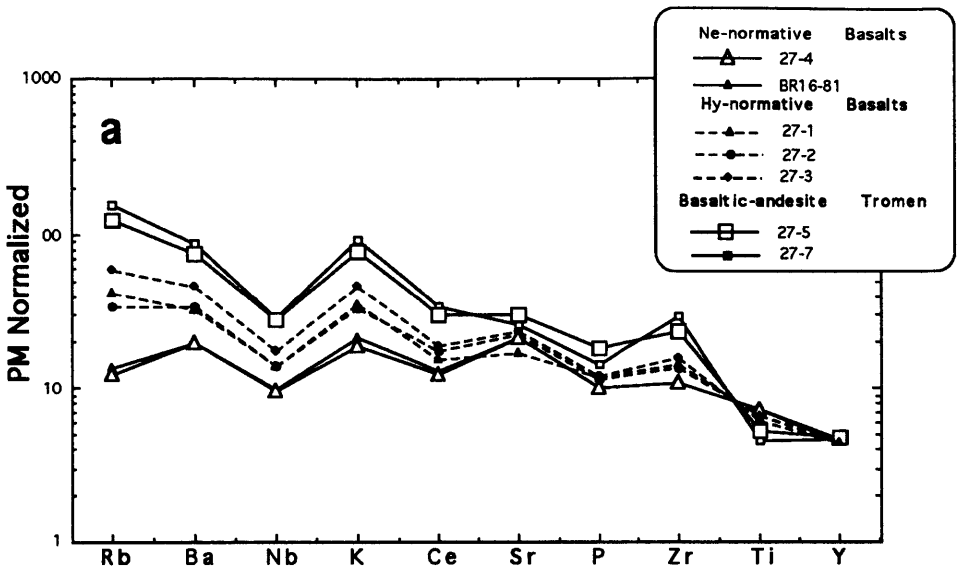

Figure 45: The hypersthene normative lavas from Buta Ranquil can be explained by mixing between the nepheline basalts (4-27 or BR-16) and the basltic andesites from Vn. Tromen (5-27 or 7-27). a) Primitive mantle normalize abundance pattern for Buta Ranquil hy-normative and ne-normative lavas and for Tromen basaltic andesites. b, c and d) Show the differences between the calculated and the observed composition with the allowed residuals for the three hy-normative lavas from Buta Ranquil. MgO, Al2O3, Ni, Cr, Zn, Sr, Rb and Ba display differences, which in some cases are larger than the allowed residual, indicating fractionation of olivine and/or plagioclase.

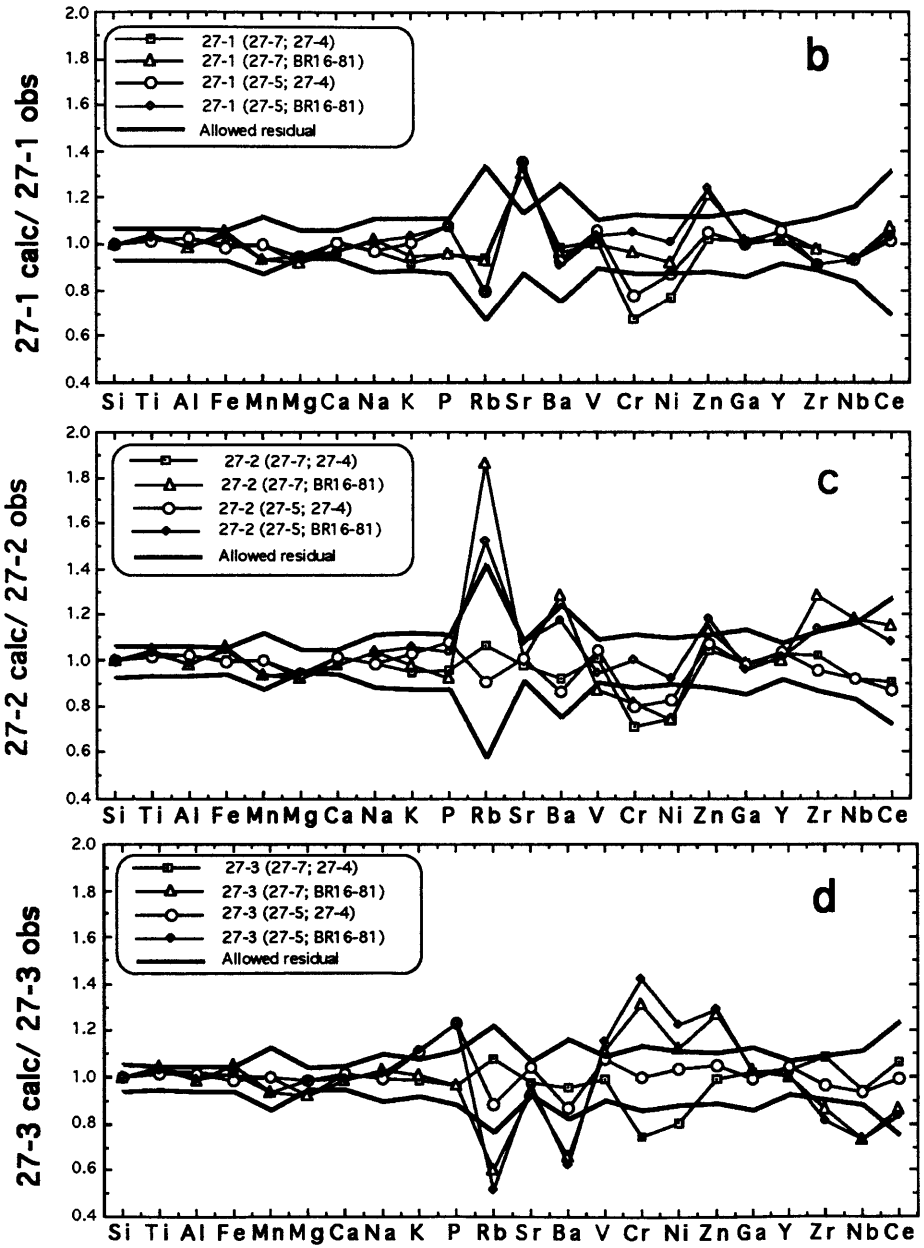

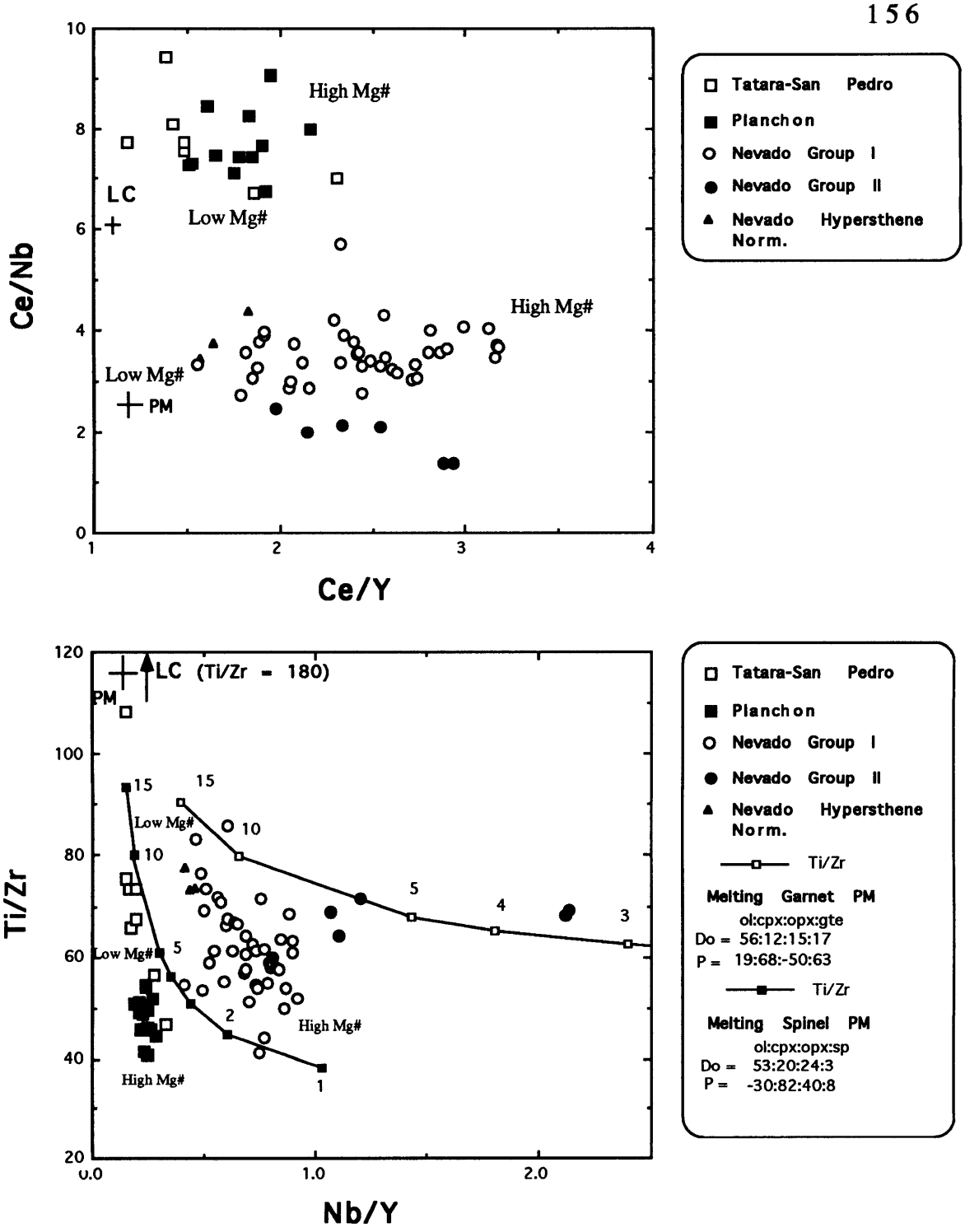

Figure 46: Ti/Zr versus Nb/Y and Ce/Nb versus Ce/Y for lavas with Mg# > 60. These plots clearly distinguish between Nevado Group I and Group II. Group II have almost constant Ti/Zr, high Nb/Y and low arc signature (low Ce/Nb at Ce/Y similar to Group I). These differences correlate with the isotopic ratios (see Figure 37), with Group II lower in Sr and Pb and higher in Nd isotopic ratios than Group I. These differences between Group I and Group II lavas can be explained by melting of two different sources. Group II is consistent with low extent of melting (batch melting) from a mantle source with garnet as a residual phase. The inverse correlation of Ti/Zr and Mg# in Group I lavas is not consistent with a simple melting model

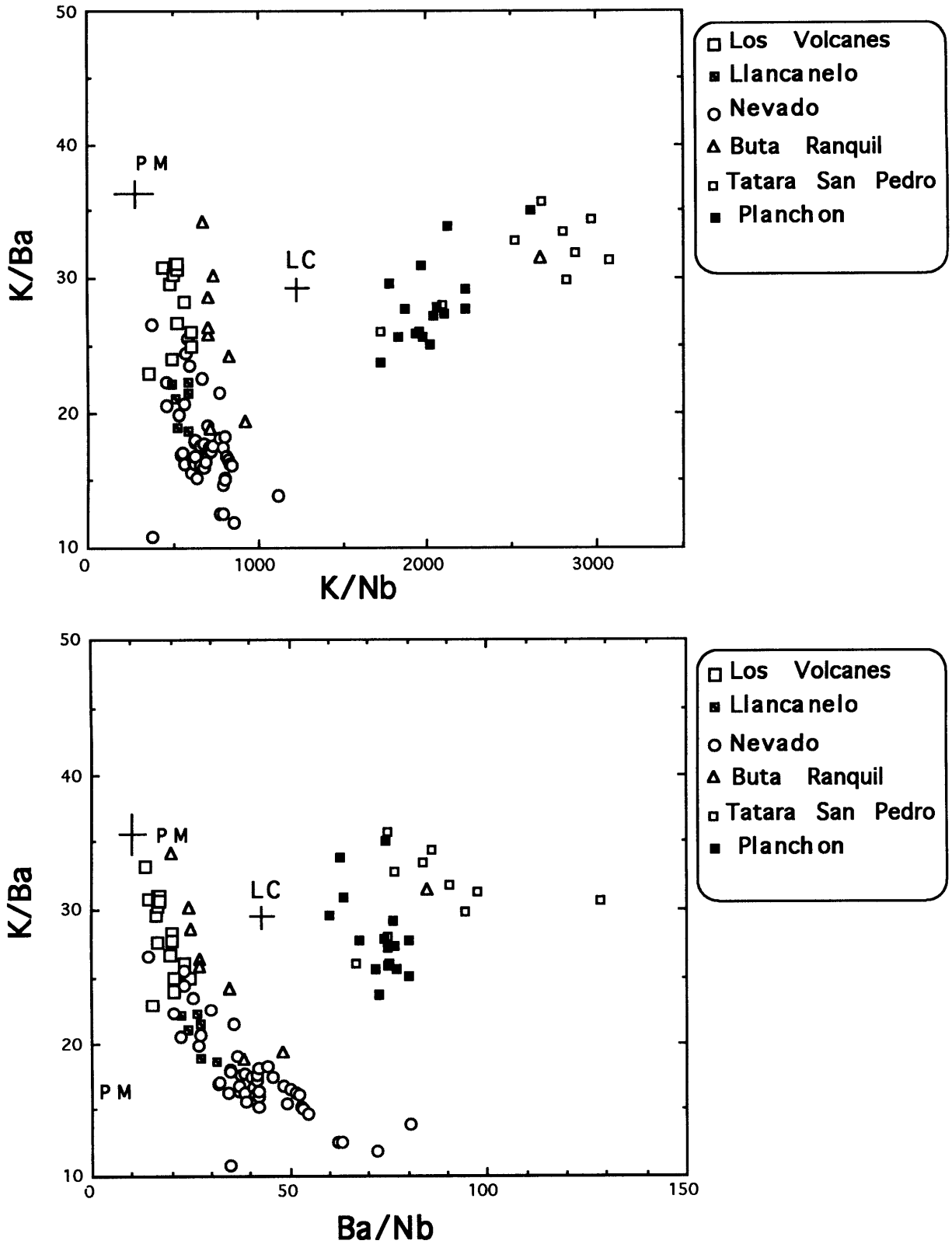

Figure 47: K/Ba versus K/Nb and Ba/Nb for the primitive (>7MgO) lavas from the volcanic front and back-arc. The figures show the inverse correlation between K/Ba ratios and the arc signature for the alkaline lavas. In contrast, K/Ba ratios correlate positively with K/Nb and negatively with Ba/Nb in the volcanic front. PM and LC represent the abundance ratios for primitive mantle and lower crust, respectively.

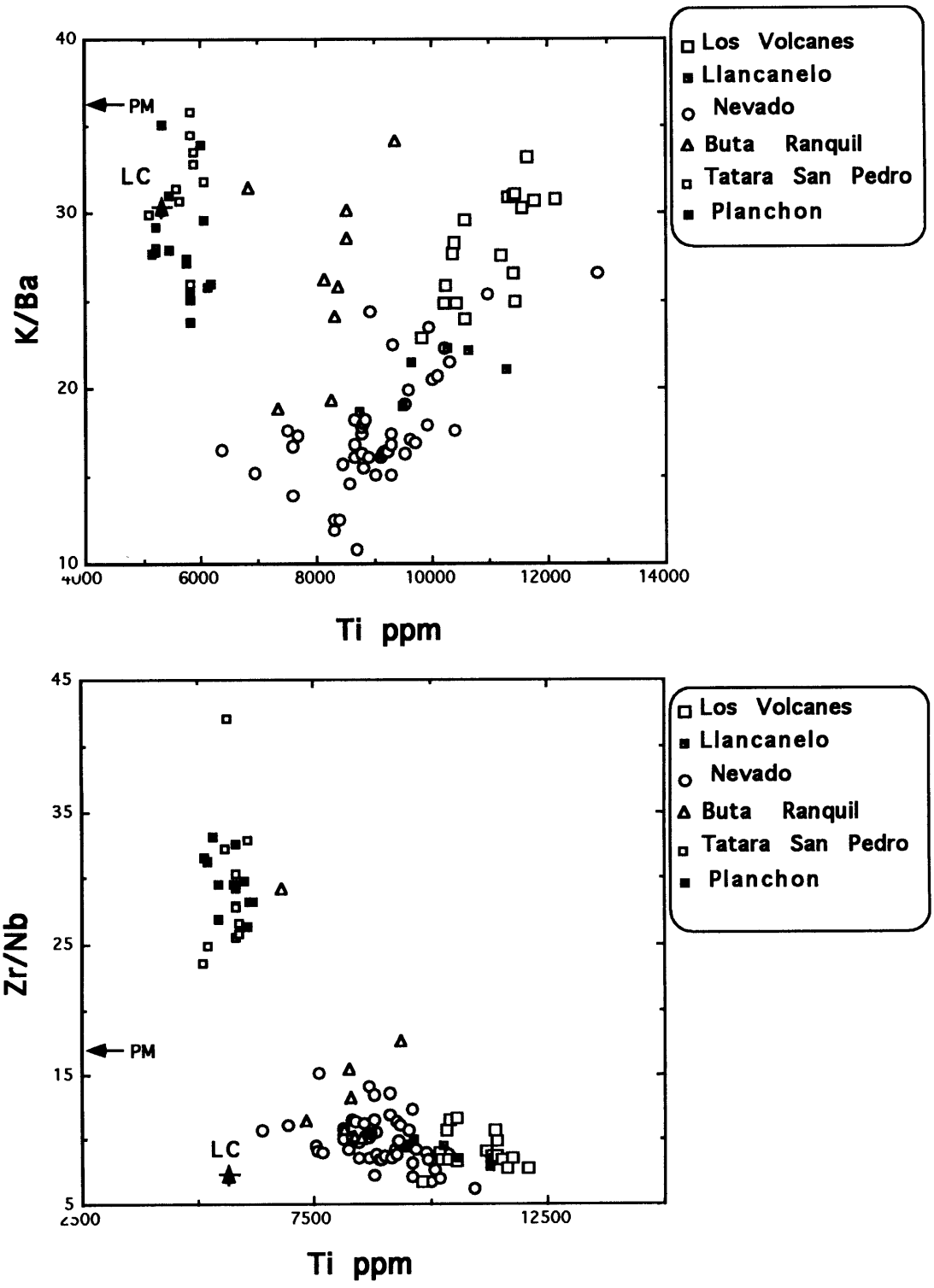

Figure 48: K/Ba and Zr/Nb versus Ti for the primitive (>7MgO) lavas from the volcanic front and back-arc. In the alkaline lavas K/Ba ratios increase and Zr/Nb ratios decrease as Ti content decreases. In the volcanic front lavas Zr/Nb or K/Ba ratios do not correlate with Ti. PM and LC represent the abundance ratios for primitive mantle and lower crust, respectively.

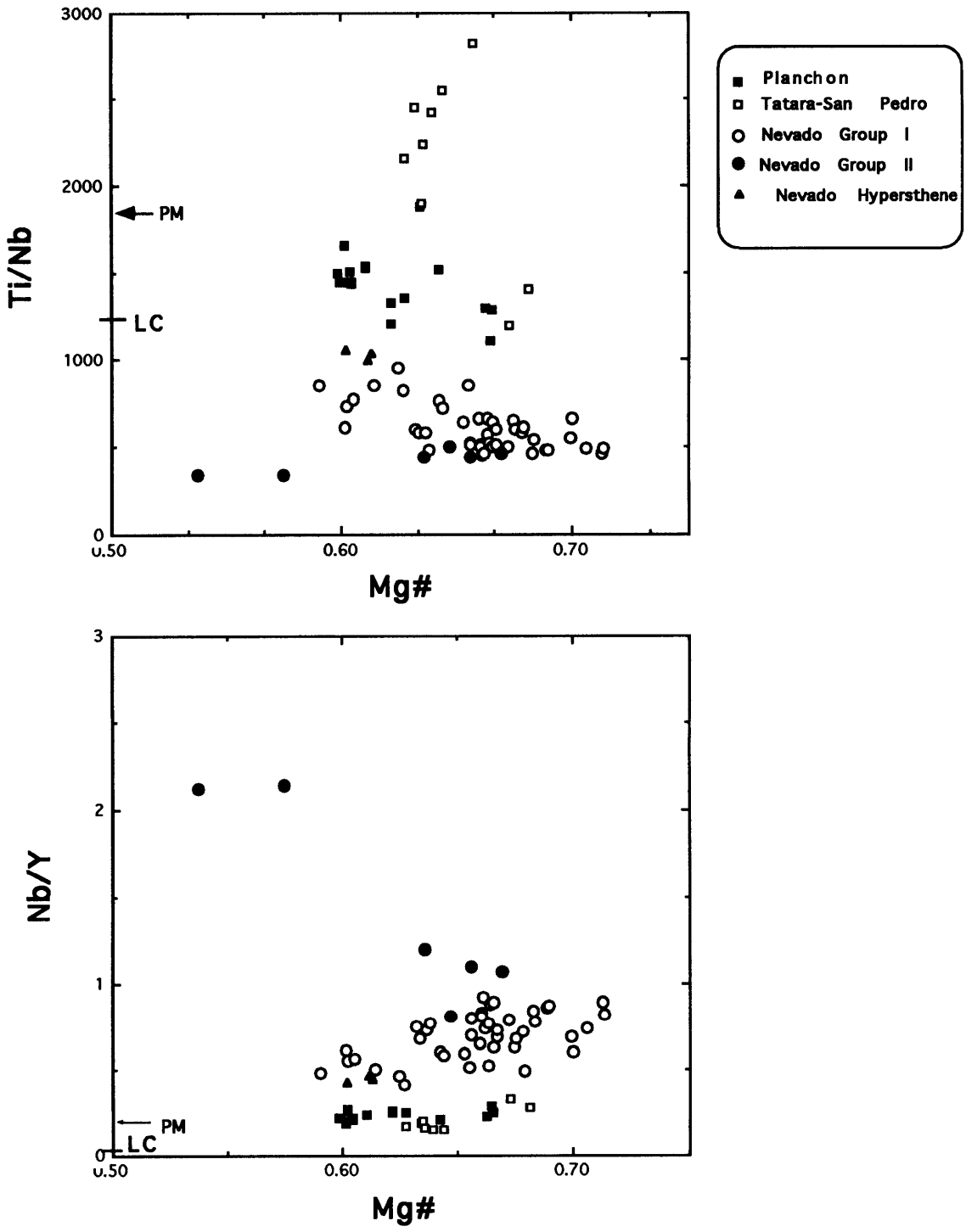

Figure 49: Ti/Nb and Nb/Y versus Mg# for the primitive (>7MgO) lavas from the volcanic front and Nevado area. The increase of Nb/Y and decrease of Ti/Nb ratios with increasing Mg# for Nevado Group I and the volcanic front lavas (Planchon) could not be explained by melting, crystal fractionation or crustal contamination. PM and LC represent the abundance ratios for primitive mantle and lower crust, respectively.

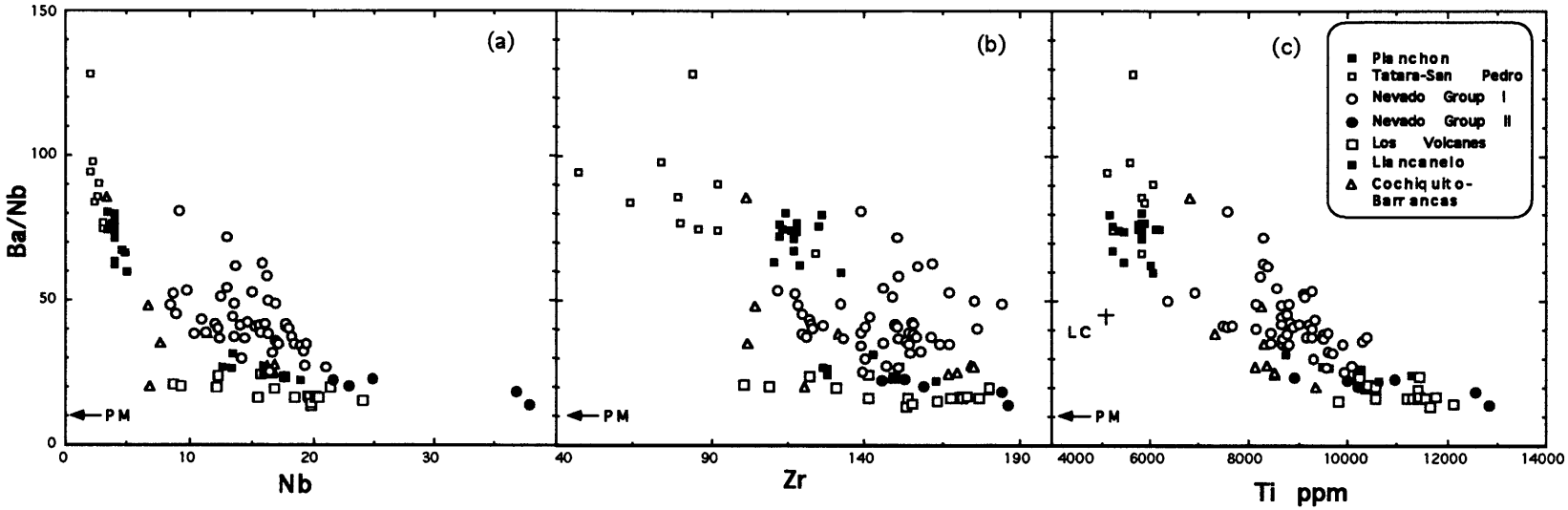

Figure 50: Ba/Nb ratios versus Nb, Zr and Ti (HFSE) for primitive lavas (MgO>7) from the volcanic front and back arc. This figure shows an inverse correlation between the flux of fluids coming from the slab (Ba/Nb), and the extent of melting (indicated by Ti abundance). In contrast, Nevado Group I lavas have higher Ba/Nb than Los Volcanes, Llancanelo lavas, but the basalts overlap in Nb and Zr content. Moreover, lavas from the Volcanic front (Planchon) with higher Ba/Nb abundance ratios overlap in Zr content with lavas from the back arc This variation is in disagreement for correlation between the increasing slab input (Ba/Nb) and increasing degree of melting toward the volcanic front.

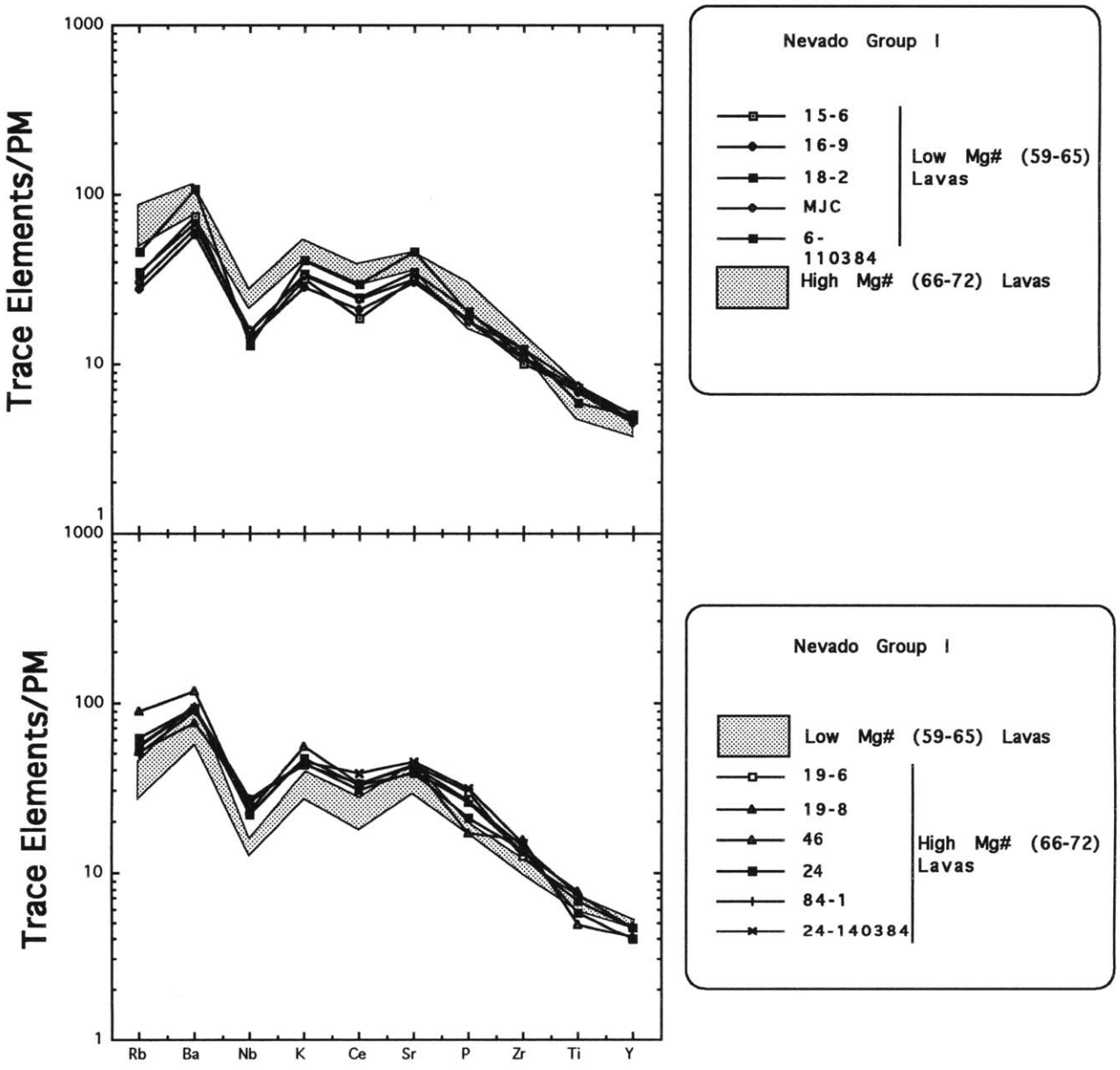

Figure 51: Primitive mantle normalized abundance pattern for Nevado Group I. The figure shows that the lavas with high Mg# range to higher highly incompatible elements abundance (except Ba and Sr) than low Mg# lavas. In contrast, in the High Mg# lavas the middle incompatible elements like Ti and Y range to lower abundances than in the low Mg# lavas.

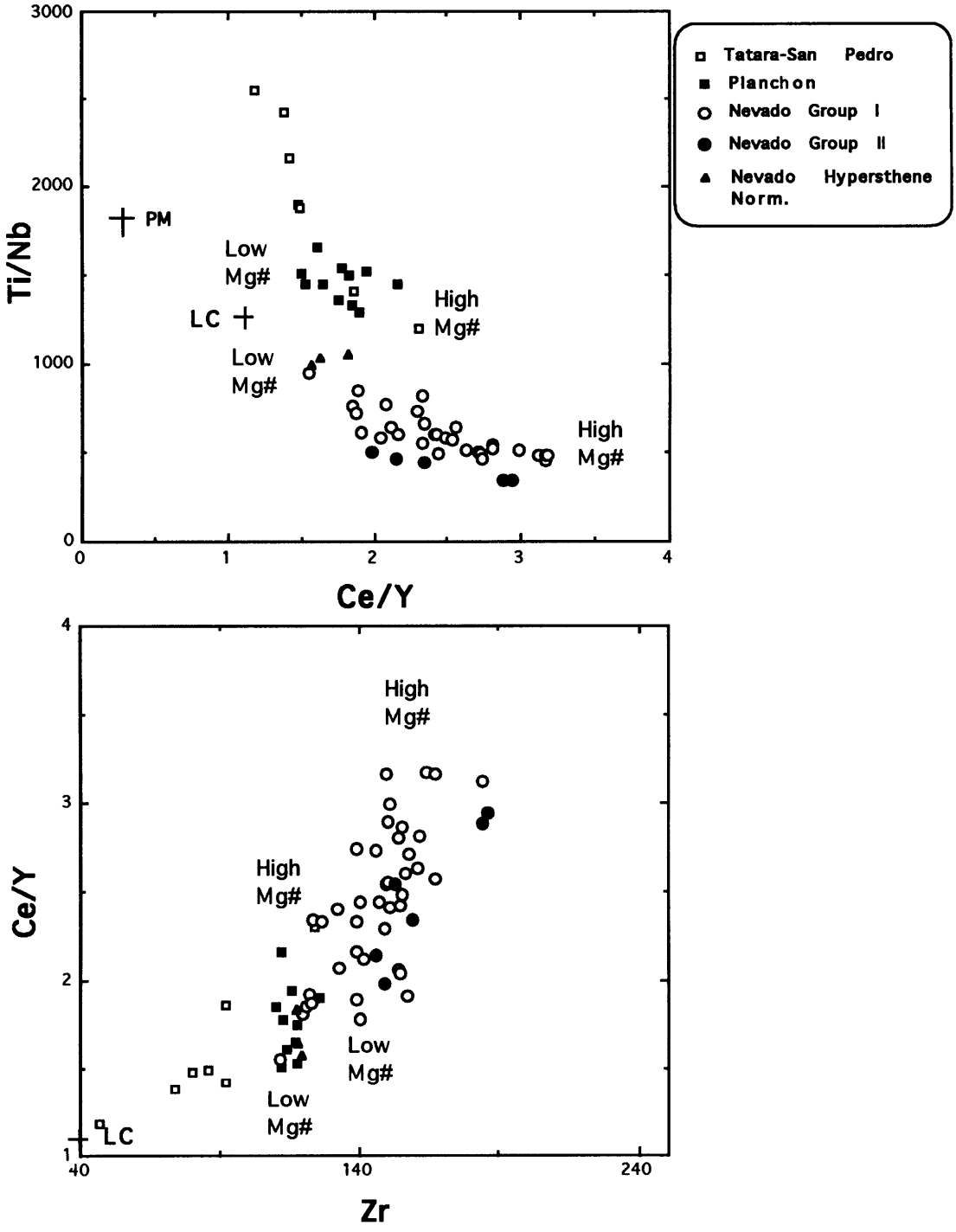

Figure 52: Ti/Nb versus Ce/Y and Ce/Y versus Zr for primitive basalts (>7% MgO) from the volcanic front and Nevado area. Ti/Nb versus Ce/Y not only separate Nevado Group I from Group II but also show that Group I or Planchon could not be explained by melting, fractional crystallization or crustal contamination (see also figures 46, 49, 51). One extreme of GroupI has high Mg#, Ce, Nb, P and Zr and low Y and Ti, and the other extreme has low Mg#, Ce, Nb, P and Zr and high Ti and Y. Also, the variation in abundance for the same element between both extremes is bigger for the most incompatible elements. For example, Ce and Nb display bigger increase from low to high Mg# than Zr. In this way, we observe a small variation in Zr for strong variation in Ce/Y in Nevado Group I and Planchon lavas. PM and LC represent the abundance ratios for primitive mantle and lower crust respectively

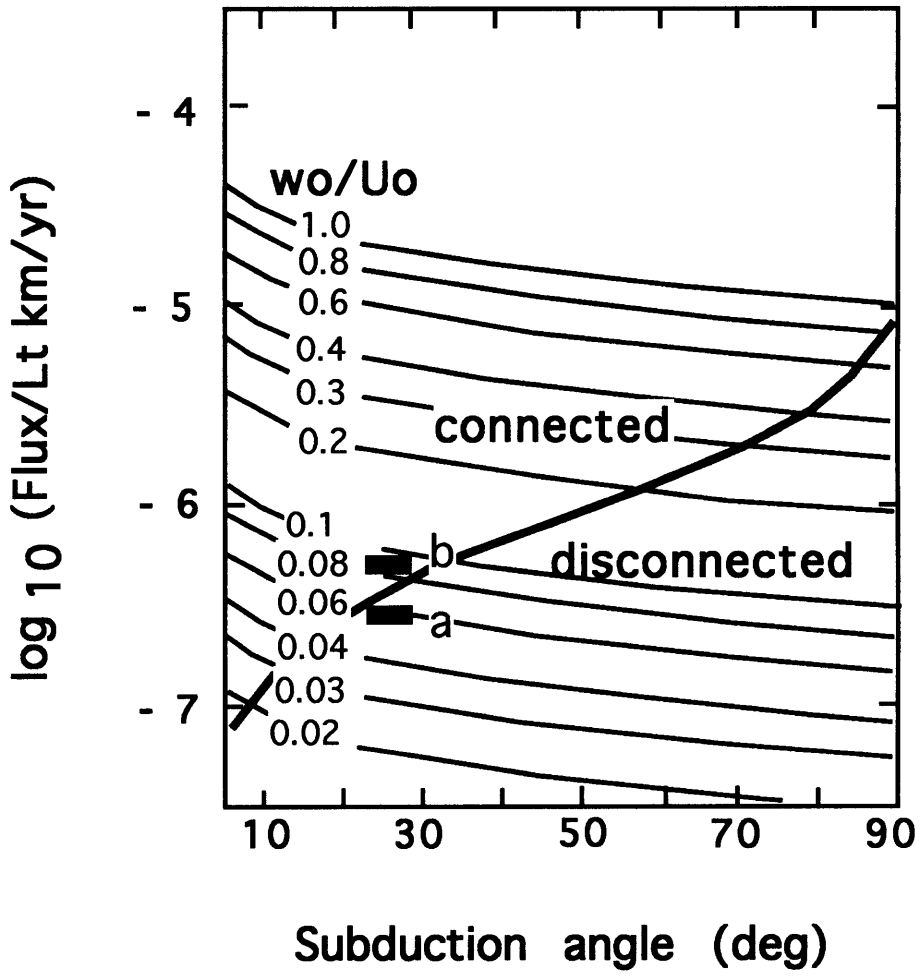

Figure 53: Volcanic arc melt flux (per length of arc, $km^2\ yr^{-1}$) normalized by Lt (length scale) as a function of subduction angle and wo/Uo (Spiegelman and McKenzie, 1987). Dark area shows data from northern SVZ Andes. Position (a) indicates the present subduction velocity ($\approx$ 10 cm/yr), with a disconnected back arc. Position (b) indicates the possible condition for the late Pliocene with slower velocity ($\approx$ 7 cm/yr), with a connected back arc.

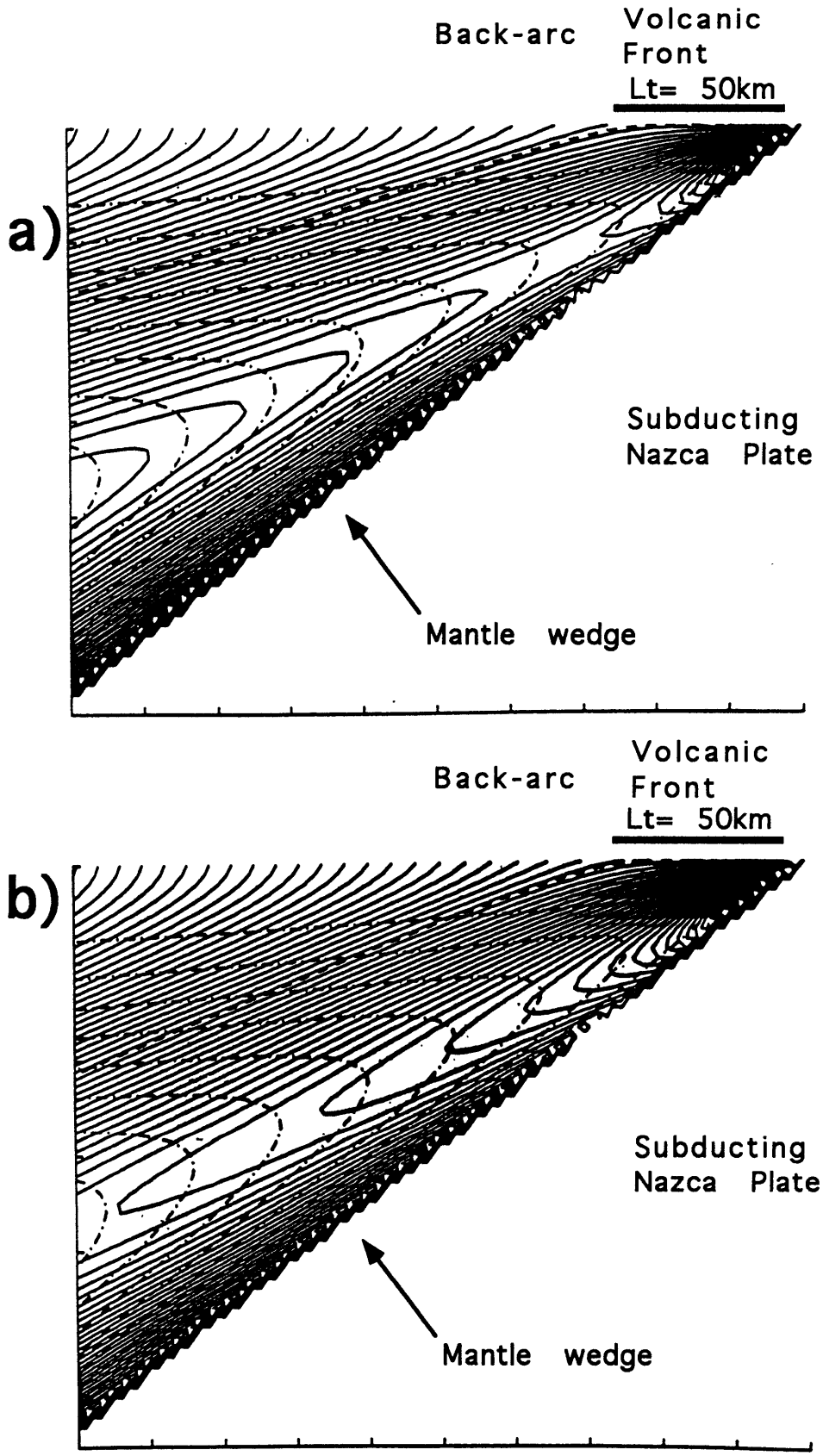

Figure 54: Fluid and matrix streamlines calculated for the Andean subduction zone at the latitude 36° S using the analytical solution from Spiegelman and McKenzie (1987). Figure (a) indicates the present condition of subduction, with velocity ≈ 10 cm/yr, producing a disconnected back arc. Figure (b) indicates the possible condition for the late Pliocene with slow subduction velocity (≈ 7 cm/yr), generating a connected back arc.See text for explanation. Dash-dot lines = matrix streamlines, solid lines = fluid streamlines